University of Sussex

Statistical characterization of galaxies in groups and isolated galaxies.

Luminosity Function

José Antonio Vázquez Mata

Submitted for the degree of Doctor of Philosophy

University of Sussex

May 2016

UNIVERSITY OF SUSSEX

José Antonio Vázquez Mata, Doctor of Philosophy

Statistical characterization of galaxies in groups and isolated galaxies. Luminosity Function

Summary

Evolution of galaxies is one of the most important topics in astronomy to understand how the universe has been evolving. In particular, galaxy groups are important because they are the observable equivalent of dark matter (DM) haloes, and thus offer a direct insight into the physics that has occurred in the DM haloes in the Universe up to the present day.

Isolated galaxies are crucial for studying intrinsic and secular processes able to affect the structure, morphology, and dynamics of galaxies for obtaining clear relationships and correlations to be confronted with the model predictions.

The main goal of this work is to characterize the GAMA G^3Cv1 galaxy groups catalogue and the $UNAM-KIAS$ catalogue of isolated galaxies by one of the most important statistical studies, the galaxy Luminosity Function (LF), that helps to constrain the models of formation and evolution of galaxies.

LFs have been estimated for galaxies in groups and isolated galaxies. The LF for groups has been characterized by the physical properties of the groups (mass and velocity dispersion), the photometry (colour), the morphological type and eleven wavelengths from the far infra-red to the ultra violet.

The LF estimated for the isolated galaxies is characterized by morphology and the colour in the five SDSS bands. The results obtained constrain more effectively the formation and evolution models of the universe than previous samples. The differences between both catalogues are presented in the conclusions.

Additionally, the galaxy morphology is one of the no well understood problems in the galaxy evolution process to support the hierarchical model of formation of large objects. In this work, a classification based on the colour and concentration of light was considered. However, due to the low resolution of the images, the confidence of this classification was only $\sim$60%.

Acknowledgements

First of all, I would like to express my deepest appreciation to my main supervisor Dr Jon Loveday for all the academic and friendly support, during the last years. He has been my guide during this intense process and has also given me the motivation to continue, due to his support for my participation in conferences and observation runs at the most amazing places: Australia, Hawaii and China. I would also like to say a big thank you to Dr Seb Oliver for his encouragement and advices in the most important moments. Thank you to my collaborator Dr Peder Norberg for his support in the last step of this work.

Thank you to my friend and collaborator Dr Hector Hernández-Toledo for his support and time; he forced me to move forwards in the hardest of all times.

The present work is dedicated to my family, for their support in all my madness, and specially for their patience during this time of my life. Thank you very much because without you I would not be here. I love you mum (Mrs Maribel), dad (Mr Tomás) and sister (Verónica).

I want to thank all my aunts, uncles, cousins, godparents for being all the time with me, even though miles away, and cheering me up: Zuco, Fernando, Lourdes, Carmen, Arturo, Oliva, America, Alma and those who unfortunately are no longer on this world.

Thank you to my friends in Brighton. Without you my life would not have been the same, from the amazing parties to the most difficult moments we went through. Fortunately, the list of wonderful people I met is very long, but particularly I want to mention those from whom I learned a lot of things, either academically or for the meanings of life. Thank you so much dear Marcos, Carlos C, Jo, Fanny, Olga, Penny, Alma & Luigi, Sevi, Adir, Marieke, Roman for being my first family in Brighton. Your role was critical for me to continue my life in this country. Thank you to the Mexican and international gang, Gabriel & Marina, Martina, Rebecca, Jenny & Andy, Steven L, Eva E, Ricardo G,

Ana Solórzano, Ana Mendoza & Juan, Claudia R, Ivonne, Mary, Salvador, Rick, Miguel, Barak, Thalia, Paula, Katherina, Ana Barros, Bibe, Jaime & Lilia Juarez, John & Veronica Lovejoy, Siska, Mark, Ilona, Wan, Jose, Fabrizio, Das, Andrea R, Pedro N, German, Bjo, Liliana, Michelle P, Tania M, Claudia Ferreiro, Edgar, Gustavo, Emil, Julieta, Javi, Yuriko, Patrick, Alex, Carlos V, Carlos & Hannah, Teresita, Anne-Lise, Julie, Aline.

A special thank you, to you, my friends, because we have cried, laughed, danced, shared a good wine and travelled, I never felt alone with you; we grew older and better every day. I love you and I will never forget you, because you are now part of my life and I consider you part of my family too: Citlalli, Maria, Claire & Tessa, Casandra, Emyr, Luis, Michelle, Mateja, Vanessa, Adrian, Erika, Nicky, Rodolfo, Silvia, Eugenia, Isabel, Mar, Alberto, Erika H, Raul, Alba.

What would my time at University be without great people around? Very dull. But I had excellent officemates, and astronomy friends. Thank you very much everyone but specially thank you to Sorour, Charlotte, Gemma, Naomi, Peter, Leonidas, Nicola, Sahar, Samane, Kexin, Luca, Chris, Leon, Will, Oskar, Guido, Steven, Alex, Daniel, Hannah, Dave, Benoit, Sam, Scott, Ridwan for all your support and genuine friendship.

I have been very lucky to meet awesome students. Thank you so much everyone but specially to Andreea, Jessica, Melina, Maria, Jussi, Marie, Alice for your friendship and support.

To my successful SIFE group: Vicky, Annie, Claire H, Nadia, Mariana, Sally's. Thank you for giving me the opportunity to participate with you. I learnt a lot about business, team work and the most important, I made good friends.

To all my friends around the world who are always in my heart and the mazing people I met in my trips. Thank you for helping me with your advices and messages from China/Australia to Hawaii. Special thanks to those being very close to me: Nahiely, Maritza, Jose, Aldo, Bernardo, Sebastian, Beatriz, Heidi, Yetli, Tania N, Salome, Rodrigo, Adriana, Fabiola, Siren, Sandra, Jorge M, Xitzel, Mirjana.

Of course, I could not forget my friends in Mexico who have always been there: Daniela,

Teresa, Jorge, Fernando, Leonardo, Rut, Tula, Mariana, Yaxkin, Paco, Hector A., Barbara, Octavio, Vladimir, Ellen, Angeles', Yvonne, Lulú.

I am very thankful to the GAMA team for accepting my collaboration in a very important project, hopefully we can continue working in the future. Thank you Michelle C, Ned T for all your advices.

Finally I want say thank you to the Mexican National Council for Science and Technology (CONACyT) scholarship scheme for giving me the opportunity to study in the UK and achieving my dreams.

Gracias, Merci, Ευχαριστώ, Danke, Thanks, Hvala, Mamnoon,
Grazie, Xie xie, Obrigado.

Contents

Chapter 1

Introduction

1.1 Prelude

The evolution of galaxies is one of the most important topics in astronomy in order to understand how the universe has been evolving up to now and make predictions for the future. During the last years, there has been significant progress in measuring the properties of galaxies in different wavelengths over the cosmic history. Large surveys with high spatial resolution images and spectroscopy information have collected millions of nearby galaxies, including galaxies in a wide range of mass, magnitude, morphology, star forming processes, in different environments from the very low dense (voids) until most dense regions (clusters).

At the same time, computing speed and new numerical methods have also improved significantly; hence the capability to make more detailed and better simulation of the universe, under the paradigm of the cold dark matter (CDM) scenario, has increased as well. Many techniques have been developed to take into account physical processes responsible for the evolution of galaxies and reproduce the observable information. Processes, such as supernovae and active galactic nucleus (AGNs) feedback, black holes, and their accretion disk have been considered into the simulations, resulting in a very close approach to observations (Somerville and Dave, 2015).

Big questions presented in the Somerville and Dave (2015) review about the cosmological models could be summarised in: i) how well do these models reproduce the observed distribution functions of galaxies, such as the luminosity function or the stellar mass function and their evolution? ii) how well do the models reproduce the global scaling relations, as the correlation between stellar mass, star formation rate (SFR), etc? iii) what do the models predict for different types of galaxies, in terms of e.g. morphology or active-passive

galaxies? iv) do the models reproduce the observed structural scaling relations, like the relation of mass with size, density and dispersion velocity?

These questions have been tested with observation and models strongly during the last decade. However, we are still limited by the observation capability of the instruments. As the measurement instruments get better, the better the data would be and the comparison with models.

The Λ CDM model predicts the hierarchical merging process that occurs between haloes of dark matter (DM) in the structure formation paradigm (e.g., Springel et al. 2005). This model supports the idea about the distribution of galaxies in space is actually strongly clustered and a significant fraction of the galaxies forms gravitationally bound multiple systems, from very populated clusters to loose groups. The assembly of galaxies over the cosmic time can be studied through the distribution of galaxy luminosities and stellar masses, observationally and theoretically (e.g., Cole et al. 2000, Somerville et al. 2001, Wolf et al. 2003). In particular, galaxy groups (2-50 galaxies approx) represent the observational part of the DM haloes, which are able to give us information about the physics in these haloes. Galaxy groups also provide a route to studying the dark matter dynamics (e.g. Robotham et al. 2008) and how galaxies populate the haloes (Robotham et al. 2010).

On the other hand, samples of galaxies that have not suffered any interaction with any other galaxy or with the environment over a Hubble time are crucial for studying intrinsic and secular processes able to affect stellar processes or the structure, morphology, and dynamics of galaxies. Homogeneous observational data for these isolated galaxies are crucial for obtaining transparent scaling relationships and correlations that can be appropriately confronted with the model predictions. The first sample of isolated galaxies was compiled by Karachentseva (1973) with an isolation criteria based on the projected separation of the galaxies on the sky. More recently, the $UNAM - KIAS$ catalogue of isolated galaxies (Hernández-Toledo et al., 2010) based in the actual space separation of galaxies, presents for the first time the opportunity to study real isolated galaxies without gravitational effects generated by any companion.

One of the most fundamental distribution of galaxies is the luminosity distribution, well known as the galaxy luminosity function (LF). The LF is an important tool to characterize statistical properties of astronomical objects. The shape of a LF depends of the physical process carried out to emit on certain wavelength; when LFs, from different galaxy populations, are compared there could be important differences, and also by integrating

the LF, we have information about the density. This density also changes according to the type of galaxies considered, cosmological environments, wavelength and redshift. On the other hand, the LF is also an important analytical tool to test the cosmological models of formation and evolution of galaxies (e.g. Benson et al. 2003).

Many authors have studied the effect of the environment on the LF. These works have been focused on the dependence of the LF on the density contrast within spheres of different radii (e.g. Hoyle et al. 2005, Park et al. 2007, Choi et al. 2007, McNaught-Roberts et al. 2014) and agree that the LF shows significant fluctuations due to large-scale structures, while the morphological fraction as a function of luminosity is relatively less sensitive and thus seems to be more universal (e.g. Sulentic et al. 2006). Strong environmental dependencies have been seen in very low dense environments (voids) and very dense clusters, (e.g. Croton et al. 2005, Tempel et al. 2009).

The LF of galaxies in low and high density environments allows us to carry out a critical test of galaxy formation models. Λ CDM models predict the existence of many low mass haloes in voids; if these haloes contain dwarf galaxies, then the LF must have a steep slope at the faint end; a feature that observations do not show. On the other extreme, at the bright end, simulations show brighter galaxies than observations. An example is presented in Fig. 1.1 where the models clearly show an excess of faint and bright galaxies. Nevertheless, models are better every day and overlap observations with a reasonable agreement, as the Virgo Consortium's Evolution and Assembly of Galaxies and their Environments (EAGLE) project Schaye et al. (2015) shows for the equivalent stellar mass function.

In this thesis, the main goal is to perform a detailed study of the LF for galaxies in opposite environments, groups and field, based on two new and unique samples of galaxies. The G^3Cv6 group catalogue (Robotham et al., 2011) compiled from the Galaxy and Mass Assembly project (GAMA; Driver et al. 2009, Driver et al. 2011) and the $UNAM-KIAS$ catalogue of isolated galaxies Hernández-Toledo et al. (2010) originated from the Sloan Digital Sky Survey (SDSS; York et al. 2000) Data Release 5 (DR5). The LFs estimated from these samples contain original data in the low mass range of galaxies using the GAMA sample and establishing new LF values that must be reproduced by models; as well as the new data extracted from the $UNAM-KIAS$ catalogue which is the first compilation of galaxies based on a 3D dimensional space.

In collaboration with Dr Jon Loveday and the GAMA team [1], the first paper (Chapter

[1] http://www.gama-survey.org/team/

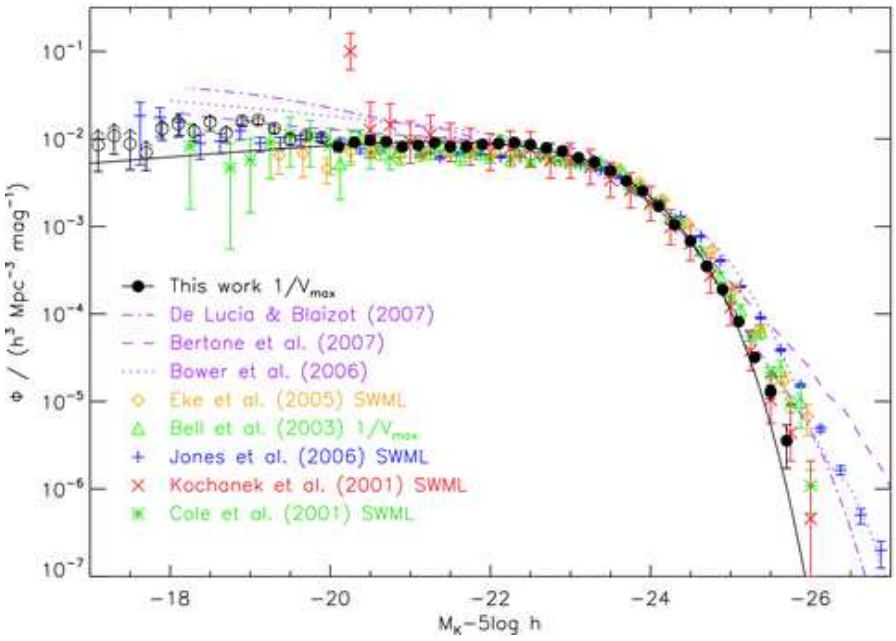

Figure 1.1: K-band LF from UKIDSS LAS comparing observations with models Smith et al. (2009)

2) focuses in the estimation of the LF of galaxies in groups in the r optical band. Using the latest version of the GAMA group catalogue (G^3Cv6), the galaxy LF was estimated and the dependence with physical and observational properties of groups and galaxies was carried out. The group properties are the mass, velocity dispersion, richness, and the galaxy properties colour and morphology. A study of the evolution of the LF with respect to the redshift is made as well.

The second paper (Chapter 3), in collaboration with Dr Héctor Hernández Toledo, Dr Aldo Puebla, Dr Ivan Lacerna and Dr Jon Loveday, characterizes statistically the $UNAM - KIAS$ catalogue, studying the LF, the stellar mass function (SMF) and the gas-to-stellar mass ratio M_{gas}/M_s. This work was carried out in the 5 SDSS passbands ($ugriz$) and compared with previous studies in the literature; but also, taking advantage of the GAMA survey, the LF was estimated for galaxies outside the grouping selection for the G^3Cv6 catalogue, since by definition, they are in the field. Another sample based on the GAMA survey has been considered, the Void galaxies sample originated by Alpaslan et al. (2013).

The third paper (Chapter 4), in collaboration with Dr Jon Loveday and the GAMA team, follows the initial study of the LF for galaxies in groups, but now this work focuses on the differences with respect to the wavelength. Since GAMA is a multi-wavelength survey,

11 bands from the near Infrared (NIR) to the ultraviolet (UV) regions, have been used to estimate the LF. Nevertheless, this work is the first attempt of a homogeneous multi-wavelength LF using the new Panchromatic Data Release (Driver et al., 2015). These data are very recent and more work is required to explore all the valuable information given in every band.

1.2 The Samples

Large spectroscopic surveys of galaxies, such as SDSS (York et al., 2000), GAMA (Driver et al. 2009, Driver et al. 2011) or the 2dF Galaxy Redshift Survey (2dFGRS; Folkes et al. 1999), are very useful to make large galaxy catalogues in different environments. Many authors have taken advantage of large galaxy surveys like the SDSS survey and have constructed galaxy group catalogues to perform multiple studies about these systems, in particular the luminosity function and the dependency with some physical properties and the environment (e.g. Zandivarez et al. 2006, Yang et al. 2009, Robotham et al. 2010).

1.2.1 GAMA

The Galaxy and Mass Assembly project (GAMA) represents a good opportunity to study statistical properties of galaxies from different perspectives following the multi-wavelength information and the high spectral completeness. GAMA is a spectroscopic survey based on the Sloan Digital Sky Survey Data Release 7 (SDSS DR7) in the second phase; GAMA-II consists of three equatorial regions, centred at 09h, 12h and 14h30m and called G09, G12 and G15 fields respectively, each of 12×5 degrees with a Petrosian magnitude limit of $r < 19.8$ mag for all the fields. This survey is complete in all regions with a completeness greater than 95% for all galaxies with up to 5 neighbours within 40¨; a detailed description can be found in Driver et al. (2011). Fig 1.2 presents the region covered by GAMA in the space and the overlapping with other samples, including the 2 GAMA southern fields (G02, G23) in the final step of observation.

The GAMA survey spectra were obtained on the Anglo-Australian Telescope (AAT) over 2008 - 2010 using 68 nights in the first phase (GAMA I). 112 000 new galaxy spectra and redshifts were acquired covering a total area of 144 deg^2. In the second phase, 110 nights were assigned over 2010-2012 to cover an area of 280 deg^2 and a total sample of 220 000 spectra.

The complete GAMA survey takes into account the overlapping of many surveys at different wavelength, from radio to x-rays, covering 24 bands.

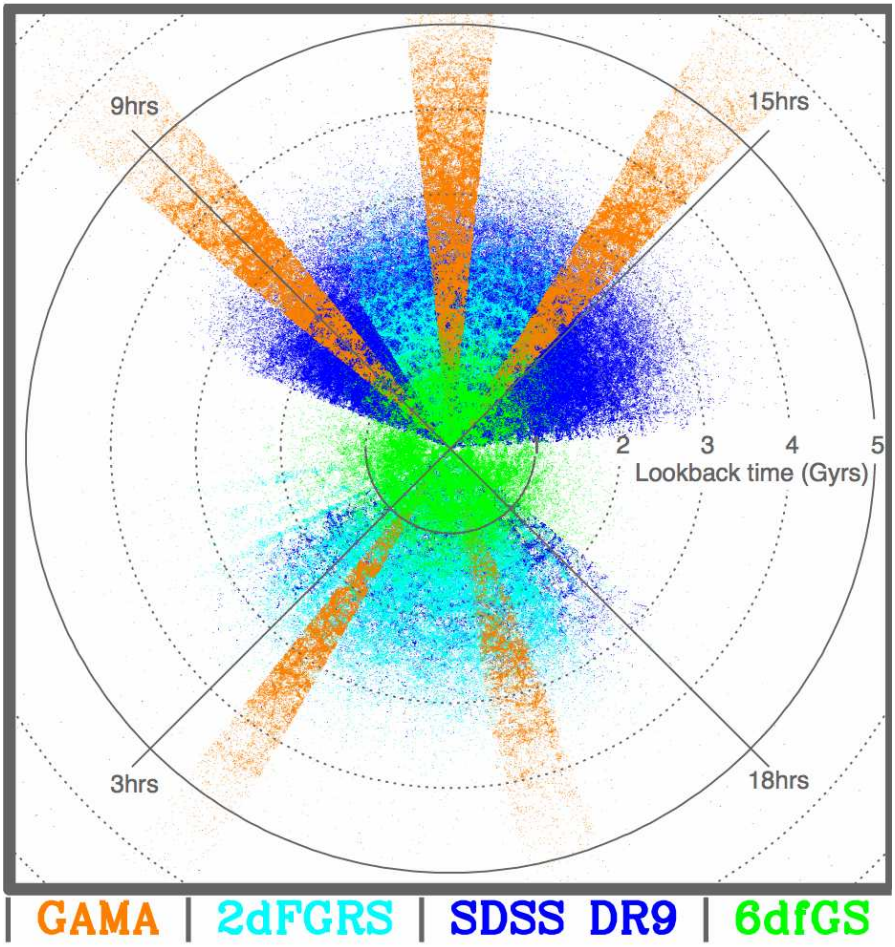

Figure 1.2: Region covered by GAMA and the overlapping with other samples (credits to Simon Driver).

One of the biggest tasks of GAMA was the measurement of redshifts from the one-dimensional spectra. This redshifting was carried out by most of the people in GAMA. These measurements were done using the GAMA version of RUNZ, code developed by Will Sutherland originally for the 2dFGRS (Driver et al., 2011). This code identifies an automatic redshift using a cross-correlation analysis and has the option for the user to estimate manually the redshift by adjusting spectra templates. The measurement of redshift was carried out immediately after the observation and repeated by other GAMA members (re-redshifting) in order to have a robust redshifts quality. A detailed explanation and errors can be found in Driver et al. (2011); an example taken from this paper (Fig. 5) is presented in Fig. 1.3 with three different redshift quality values (nQ): nQ =4 means a very high confidence redshift and can be used to do science, nQ=3 is an acceptable redshift with small doubts and can also be used for science, nQ $\leq$ 2 are redshifts not well determined mainly because of the spectrum quality where emission or absorption lines are difficult to identify, these redshift are not recommended for doing science.

However, RUNZ had a number of undesirable features and this motivated the development of a new redshifting code, AUTOZ (Baldry et al., 2014). This new code AUTOZ proved to be superior to RUNZ in every way and was used as the default for GAMA II in 2013 (for more details see Liske et al. 2015).

During phase I of GAMA, I participated in the re-redshifting process with $\sim$2000 redshifts and secondly $\sim$ 10 000 redshifts were estimated by me for the southern fields. The first redshifts were in used in a spectroscopic study in Hopkins et al. (2013) and the second results are published in Liske et al. (2015).

Robotham et al. (2011) compiled the G^3Cv1 group catalogue based on the GAMA I survey and applying a friend-of-friends (FoF) grouping algorithm. Once GAMA II was ready, this catalogue was updated using the new data to the current version (G^3Cv6). The G^3Cv6 catalogue contains a total of 23838 groups with multiplicity $\geq$2 containing 73268 galaxies, this means that a fraction of $\sim$40% of the total GAMA survey is assigned to be grouped. Most of the work presented in this thesis is based on this catalogue.

Galaxies excluded from the G^3Cv6 catalogue are considered to be in the field (isolated galaxies); these galaxies are also part of this thesis, since the local population (z $<$ 0.1) was used to compared the LF of the UNAM-KIAS catalogue of isolated galaxies.

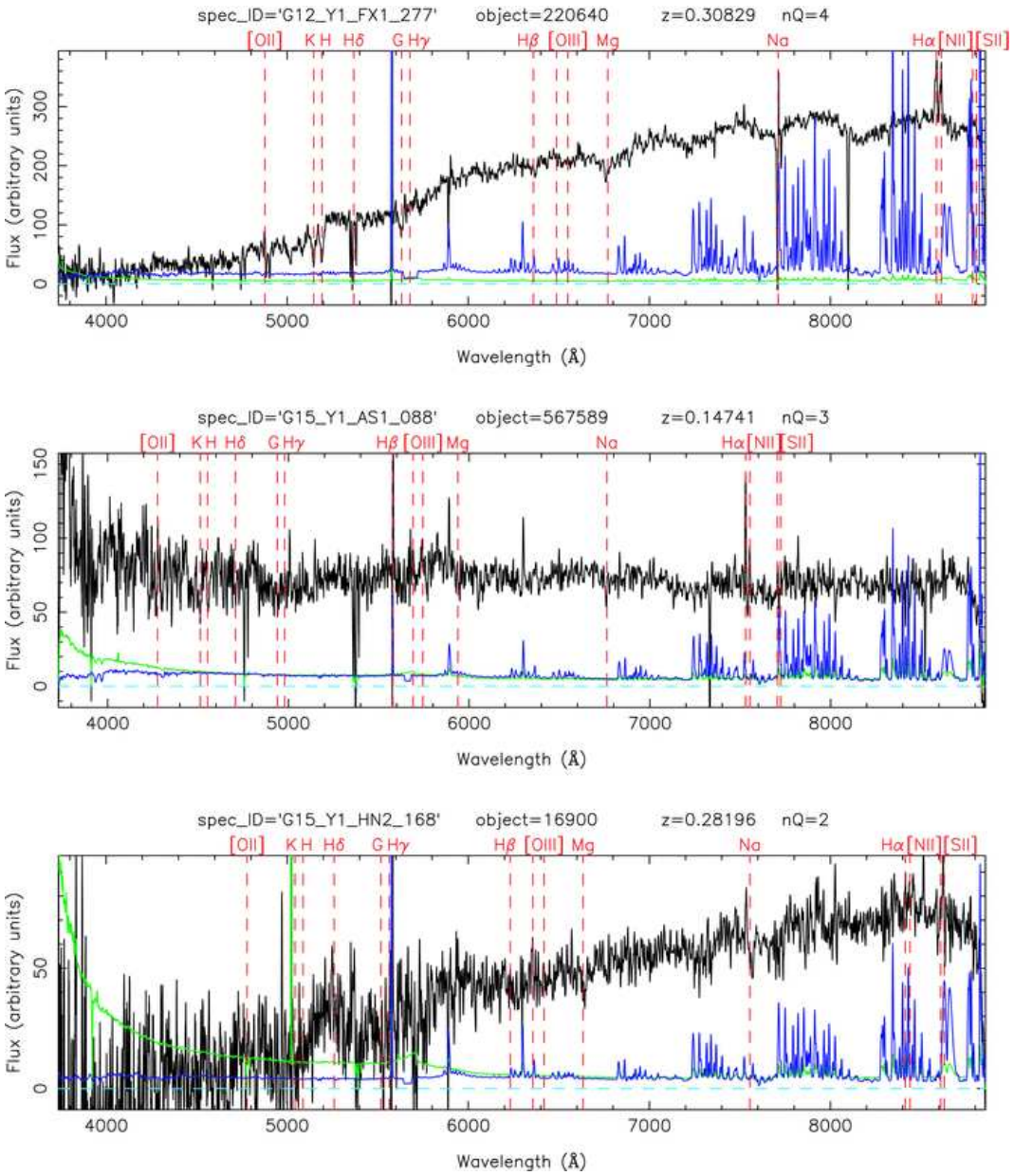

Figure 1.3: Examples of spectra with redshift quality nQ = 4 (top panel), 3 (middle panel) and 2 (bottom panel). We show the spectrum (black), the 1σ error (green) and the mean sky spectrum (blue, scaled arbitrarily with respect to the spectrum). The vertical dashed red lines mark the positions of common nebular emission and stellar absorption lines at the redshift of the galaxy. The spectra were smoothed with a boxcar of width 5 pixels (Driver et al. 2011; Fig. 5).

1.2.2 UNAM-KIAS

The UNAM-KIAS catalogue of isolated galaxies originated by the necessity of having a complete sample of these objects to study the internal processes of galaxies without external agents that can perturb the intrinsic properties.

This sample is based on the Sloan Digital Sky Survey (SDSS; York et al. 2000, Stoughton et al. 2002) covering $\sim \pi$ steradians of the northern Galactic cap in the five photometric bandpasses denoted *ugriz* centred at 3551, 4686, 6165, 7481, and 8931 Å, respectively. The large-scale structure sample, DR4plus, from the New York University Value-Added Galaxy Catalogue (NYUVAGC; Blanton et al. 2005) is used.

The isolation criteria is a modification of the Karachentseva (1973) selection, based on three parameters Hernández-Toledo et al. (2010). The first is the extinction-corrected Petrosian r-band apparent magnitude difference between a candidate galaxy and any neighbouring galaxy, Δm_r . The second is the projected separation from the nearest neighbour across the line of sight, Δd. The third is the radial velocity difference, ΔV. Given a galaxy i with apparent magnitude $m_{r,i}$ and Petrosian radius R_i, this will be considered as isolated if the separation Δd between this galaxy and a neighbouring galaxy j with magnitude $m_{r,j}$ and radius R_j satisfies that

$$\Delta d \geq 100 \times R_j \tag{1.1}$$

$$or \Delta \mathrm{V} \geq 1000 \mathrm{kms}^{-1}, \tag{1.2}$$

or the conditions

$$\Delta d < 100 \times R_j \tag{1.3}$$

$$\Delta V < 1000 \mathrm{kms}^{-1} \tag{1.4}$$

$$m_{r,j} \geq m_{r,i} + \Delta m_r, \tag{1.5}$$

for all neighbouring galaxies. Where R_j is the seeing-corrected Petrosian radius of galaxy j, measured in $i-$band using elliptical annuli to consider flattening or inclination of galaxies (Choi et al. 2007). And $\Delta m_r = 2.5$ (for more details see Hernández-Toledo et al. 2010).

This catalogue contains 1520 isolated galaxies with a detailed morphological classification with a statistical completeness of ∼80%. The Aitoff diagram in intervals of 3000 km s^{-1} are presented in Fig 1.4 and Fig 1.5 (Hernández-Toledo et al., 2010).

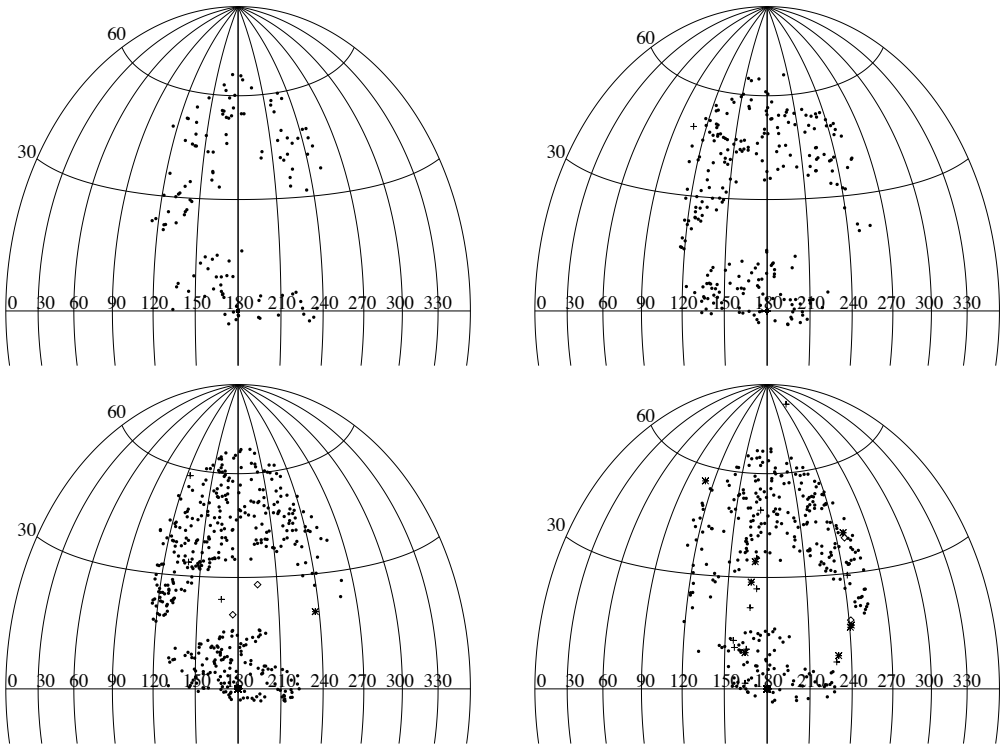

Figure 1.4: Aitoff projections in right ascension and declination showing the distribution of the UNAM-KIAS sample on the sky at 3000 km s^{-1} velocity intervals from 0 to 12000 km s^{-1}. Abell cluster cores of increasing richness classes from 0 (crosses), 1 (asterisks), 2 (rhombus) and 3 (triangles) are also indicated. (Hernández-Toledo et al., 2010).

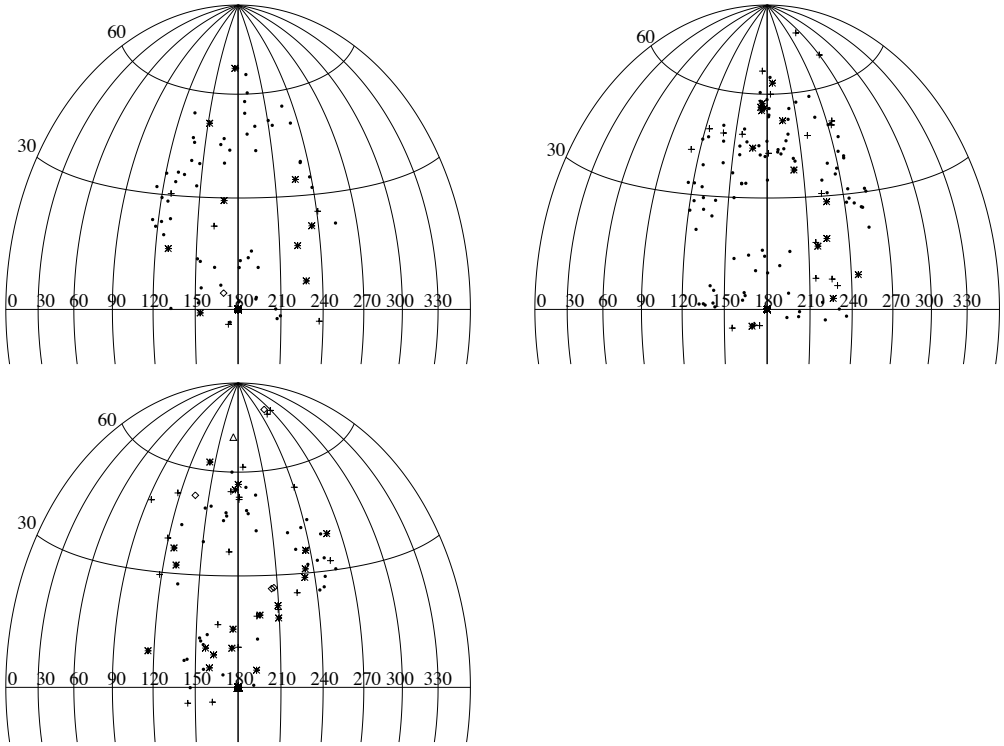

Figure 1.5: Similar to Fig 1.4 but from 12000 to 21000 km s^{-1}. (Hernández-Toledo et al., 2010).

1.3 Luminosity Function

The LF, generally represented as ϕ, is defined as the number of galaxies contained in a comoving volume (number density in Mpc^{-3}) in intervals of luminosity or absolute magnitude. The estimation of the LF is very important to discriminate between different models of formation and evolution of the universe; since the LF is one of the most important observations, models must reproduce it. The calculation of the LF started with works carried out ∼80 years ago (e.g. Pannekoek 1923, Hubble 1936). When these calculations started, people rapidly noted the lack of galaxies at the faint-end, a consequence of the magnitude limited samples which just include the brightest galaxies. This is because when we have observations made up to a determined flux, in average, we are observing brighter galaxies as the redshift increases; as we can see in Fig. 2.1. The shape for these LFs can be fitted by a Gaussian function as proposed by Hubble (1936) without taking into account the effect of faint galaxy incompleteness.

This incompleteness was first considered and taken into account by Schmidt (1968) when he estimated the LF for a sample of quasars which are much brighter than "normal" galaxies. Instead of just calculating the number density, he weights the galaxies as follows: considering the absolute magnitude for a galaxy, one estimates the maximum volume at which this galaxy can be observed to the magnitude limit; so each galaxy is weighted by dividing by this maximum volume. This method is known as $1/V_{\mathrm{max}}$; however, the $1/V_{\mathrm{max}}$ method has the disadvantage that it is sensitive to galaxy density variations. Sandage et al. (1979) (STY) developed a maximum likelihood method based on a parametric from of the LF; this method avoids the effects of density at large scales. Efstathiou et al. (1988) developed another method based on maximum likelihood where data are binned and no parametric form is required, this method is known as the stepwise maximum likelihood method (SWML).

Once the incompleteness is corrected and new large surveys came out, people realized the LF was dominated by faint galaxies, i.e. the faint-end of the LF tended to increase instead of decrease as was seen at the beginning. The LF can be well fitted by the Schechter function (Schechter, 1976),

$$\phi(L) = \phi^* \left(\frac{L}{L^*}\right)^{\alpha} \exp\left(\frac{-L}{L^*}\right), \tag{1.6}$$

or in terms of absolute magnitude

$$\phi(M) = 0.4 \ln 10 \phi^* (10^{0.4(M^*-M)})^{1+\alpha} \exp(-10^{0.4(M^*-M)}), \tag{1.7}$$

where L is the luminosity, ϕ^* is the density normalization, L^* is the characteristic luminosity at which the LF shows the turnover or "knee", α is the power law index at the faint-end (faint-end slope) and, M and M^* the corresponding absolute magnitude and the characteristic absolute magnitude.

The LF is not an universal function for all galaxies, it displays clear differences for different populations of galaxies. These differences are discussed in terms of the faint-end slopes and the knee of the function, generally associated with the Schechter parameters α and M^* respectively.

From these parameters we can infer information about physical processes in the galaxy formation, for example. When we work with a sample of galaxies with certain characteristics, the M^* parameter gives the characteristic magnitude of the sample and the value at which brighter galaxies cannot exist due to a physical process affecting the galaxy formation process, assuming no systematic errors in the selection.

Considering the cosmological point of view, the LF and other statistical studies allow us to understand the connection of the galaxy evolution and the cosmological initial conditions in the structure formation (e.g. Yoo et al. 2009). This connection is so important for the ΛCDM paradigm and also is the link between dark matter haloes and galaxies predicted and the real galaxies. To test this connection, many authors estimate the dark halo mass from luminous galaxies using different techniques like weak lensing (e.g. Mandelbaum et al. 2008, Mandelbaum et al. 2010), kinematics of galaxies (e.g. Wojtak and Mamon 2013) and galaxy clusters (e.g. Yang et al. 2012), however, uncertainties are very large and statistical studies like the LF are of great importance.

1.3.1 Luminosity function dependence on colour and morphology

As mentioned before, the LF depends on the galaxy population we are considering. When talking about morphology, these studies have been complicated due to the difficult process to classify galaxies; fortunately, everyday there are bigger samples to do more precise studies. I will describe more about morphology in the next section.

Different shapes of the LF for early and late type galaxies, and irregulars, started to be found by many authors (e.g. Holmberg 1969, Binggeli et al. 1988). Large differences suggested one should estimate individual LFs for different galaxy types; however, these samples of galaxies are very small. Marzke et al. (1998) used ~ 100 galaxies in the local universe to estimate and fit the LF using the Schechter function for early and late types, finding a dependence of the Schechter parameters with morphology. de Lapparent (2003)

made a compilation of the LF from many classified samples in a multi-wavelength study. She tries to fit the LF using a Gaussian rather than a Schechter function, since a Gaussian fits well to bright galaxies, i.e. early types. Meanwhile, for late type galaxies this fit is not very accurate. Using the method of decomposition of light to distinguish between spheroids (early) and disk (late) galaxy components for a large sample, Benson et al. 2007 find that spheroidal galaxies are less common at the faint-end, where disk galaxies dominate. Recent studies like Devereux et al. (2009), also show that spheroidal galaxies fall off at the faint end, much faster than spiral types.

Colour is an important parameter to distinguish galaxy populations, mainly the types of stars contained and indirectly the formation star rate. Using the SDSS, Blanton et al. (2001) studied the dependence of the LF with respect to colour, finding that blue galaxies are predominant at the faint-end over red galaxies, similar to that found for early and late type galaxies. This agrees with the fact that early type galaxies are associated with red colours due to an old stellar population; meanwhile, blue galaxies are associated generally with late type galaxies due to the high rate of star formation, mainly in disks where young stellar populations can be observed. Other studies similar to Baldry et al. (2004) show the same results, using the $u - r$ colour in a local sample (z up to $\sim$0.08), they find red galaxies to be brighter than blue ones and with a lower density at the faint-end compared to the blue population.

1.3.2 Luminosity function dependence with environment

Another important dependence of the LF is the environment where galaxies are found, from galaxies in voids to the most dense regions like groups or clusters. The study of galaxies in different environments is fundamental to understanding the evolution processes of galaxies, the intrinsic and external effects. Many authors started to study the LF according to the environment suggesting variations from rich clusters to low density environments (e.g. Christlein 2000, De Propris et al. 2003, Hoyle et al. 2005, Park et al. 2007, Choi et al. 2007, McNaught-Roberts et al. 2014). Croton et al. (2005), using the 2dF Galaxy Redshift Survey, estimated the LF for various environments from voids to clusters for early and late types galaxies. They find that voids are dominated by late type galaxies and are also more important at the faint-end; meanwhile clusters show a relative excess of very bright early type galaxies. Tempel et al. (2011) using the SDSS DR7, find a strong dependency of the LF for early type galaxies with the environment, whilst for late type galaxies the LF looks to be independent from the environment; this suggests similar mechanisms of

formation for this kind of galaxy.

Regarding the study at low densities, the AMIGA project started to study the luminosity characteristics for isolated galaxies, Verdes-Montenegro et al. (2005) present the parametrization of the AMIGA catalogue in the B-band, showing a good agreement with previous studies at low densities (e.g. Croton et al. 2005). Sulentic et al. (2006) made a refinement of the morphology for the AMIGA galaxies and estimated the LF for isolated galaxies in a broad range of morphological type, from pure ellipticals to distorted galaxies; they find in general the late type LF is brighter compared to early type galaxies, contrarily to the LF of galaxies in other environments.

At the other limit of densities, galaxies in groups are very important to study the distribution and dynamics of galaxies in dark haloes in the DM context. The study of the LF in groups started with works using the Hickson groups. For instance, Hunsberger et al. (1998) find a dip in the LF for groups at middle magnitudes; considering this characteristic, many authors (e.g. Lobo et al. 1997, Andreon and Pelló 2000) suggest that the bright end can be fit by a Gaussian and the faint end by a Schechter function. Miles et al. (2004) find also this dip dividing the sample into high and low X-ray bright groups. One explanation for the lack of galaxies at middle magnitudes is due to the merging process in the evolution of galaxies; this means galaxies with characteristic magnitudes (M^*) have a higher merging rate and these galaxies are transformed into more luminous objects.

Other studies consider the dependence of the LF with the group mass; for example, Eke et al. (2004) considering groups using the 2dFGRS survey, show a good fit of the Schechter function to the data; however, a different shape for mock catalogues is found, possibly due to systematic errors in the LF estimation. Densities for magnitude and volume limited group samples have been determined by Tago et al. (2010) using the SDSS and considering the richness of the groups. The largest group samples have been taken from the SDSS (e.g. Yang et al. 2009 and Zandivarez and Martínez 2011) have focused in the dependence of the LF with the group mass, finding massive and red galaxies at the centre of groups and blue galaxies in the outskirts, suggesting a physical process to stop the star formation in large scale environments. Robotham et al. (2010) studied the variation of the LF with group properties: multiplicity, virial mass and galaxy colour; they found a variation of the LF occurs just in the central region of the systems and it is strongly dependant on the position of the galaxy with respect to the virial radius.

1.3.3 Luminosity function evolution with redshift

When galaxy formation models are fit to observations, the luminosity evolution with redshift is different for every wavelength. As mentioned, the star formation rate, the dust density or temperature of gas in galaxies are different; these physical processes can evolve in different ways. For example, luminosity changes with time but at different rates for each wavelength, and consequently the colour and the LF evolve with redshift as well.

Nowadays, surveys are large enough to study these effects and evolution of the LF with redshift, however, the LF still presents the limitation due to the missing of faint galaxies as redshift increases. The bright end, or the 'knee', of the LF can be well characterized but the faint slope cannot be well estimated.

To characterize this evolution, one of the methods is the parametrization of the density and luminosity evolution as a function of redshift. Lin et al. (1999) proposed this parametrization considering the luminosity evolution parameter (Q) and the density evolution parameter (P), in this case, the Schechter parameters α, M^* and ϕ^* vary with redshift as

$$\begin{aligned} \alpha(z) &= \alpha(z_0), \\ M^*(z) &= M^*(z_0) - Q(z - z_0), \\ \phi^*(z) &= \phi^*(0)10^{0.4P_z}, \end{aligned} \tag{1.8}$$

where z_0 refers to the redshift at which magnitudes are K-corrected ($z_0 = 0.1$ for this work); evolution parameters Q and P are determined using the maximum-likelihood.

Considering the SDSS DR1 survey, Loveday (2004) finds significant evolution for galaxies in r-band. They propose that the evolution of the LF can be due to a combination of luminosity or density evolution, similar to Lin et al. (1999). Other authors have found also clear evolution of the LF (e.g. Ilbert et al. 2006, Baldry et al. 2005). More recently, Loveday et al. (2012) follow the method by Lin et al. (1999) to estimate the evolution of the GAMA LF, finding good agreement with previous works. Fig 1.6 shows this evolution for the GAMA sample (Loveday et al., 2012).

1.4 Morphology

Galaxy morphology is one of the least well understood problems in the galaxy evolution process to support the hierarchical model of formation of large objects. There are many authors trying to understand the evolution of the Hubble sequence (e.g. Fukugita et al. 2007, Nair and Abraham 2010, Delgado-Serrano et al. 2010); however, this classification

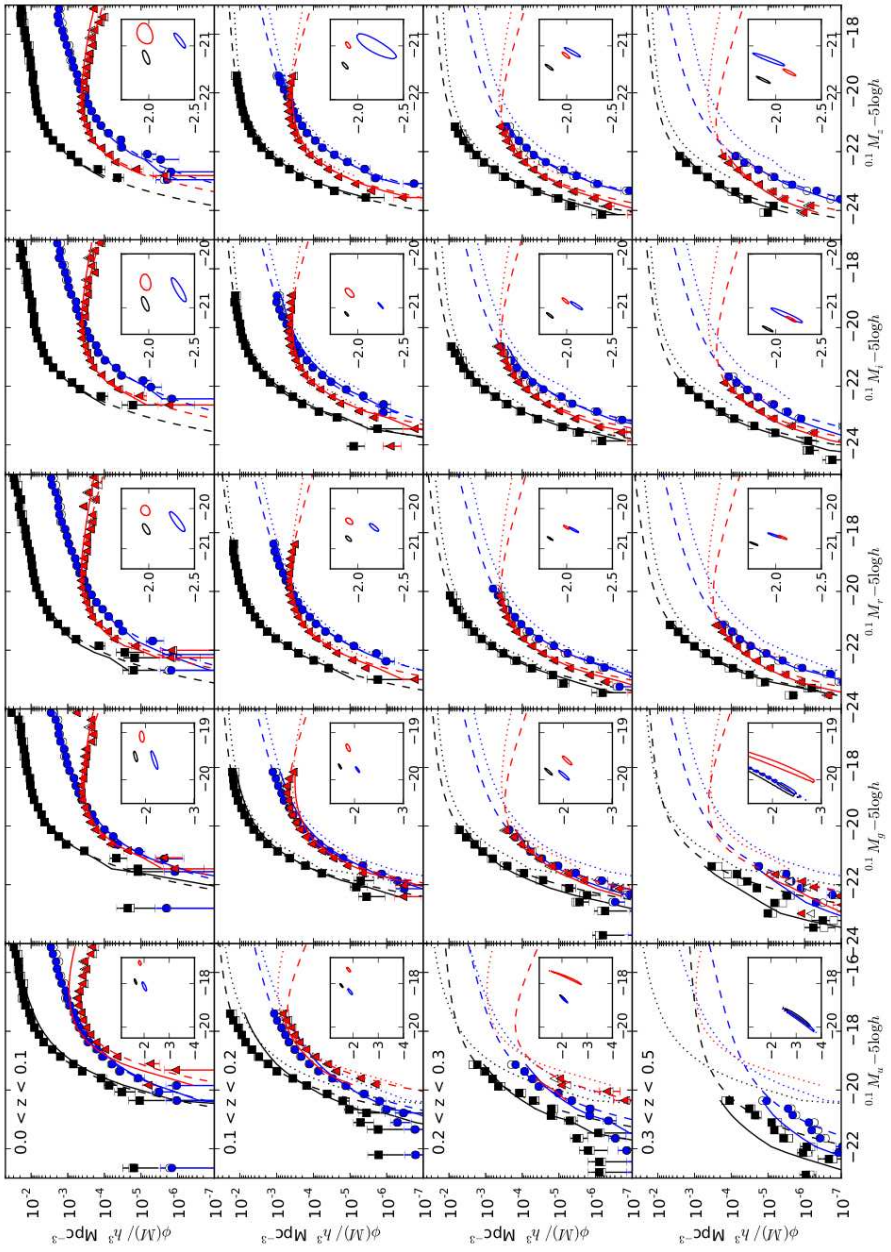

Figure 1.6: Evolution of the *ugriz* luminosity functions. The five columns show the *ugriz* LFs respectively from left to right. The four rows show the LFs in four redshift ranges increasing from top to bottom as indicated in the leftmost panels. Filled black squares show SWML estimates for combined red and blue samples, filled blue circles and red triangles show SWML LFs for the blue and red samples respectively. Open symbols show the corresponding $1/V_{max}$ estimates — in most cases these are indistinguishable from the SWML estimates. Continuous lines show the parametric evolving LF for each sample The dotted lines reproduce the parametric LF fit for each sample from the lowest redshift bin. Dashed lines show least-squares fits to the SWML estimates with α fixed at higher redshifts. The insets show the 95% likelihood contours for (M^*, lg ϕ^*) parameters obtained from these fits. LFs (but not contours) for the blue and red sample have been scaled by a factor of 0.1 to aid legibility. (Loveday et al., 2012)

is just based on the shape of the galaxies without considering any physical process, this is why many people are trying to postulate new classification of galaxies considering real physical properties more than just the shape of the objects, for example, concentration, asymmetry and clumpiness (CAS parameters; Conselice 2003) or the spin of the galaxies (e.g. Tempel and Libeskind 2013). To understand the Hubble sequence, the important task is to have well classified samples; up to now the largest classified surveys are: Nair and Abraham (2010) that classified ∼14 000 galaxies from the SDSS and the Galaxy Zoo survey (Lintott et al. 2008, Lintott et al. 2011) that in the second phase (Masters et al., 2011) provides a detailed visual classification for ∼250 000 bright galaxies in the SDSS.

For the UNAM-KIAS catalogue, a visual classification was carried out by me and collaborators in a previous work to this thesis and presented in Hernández-Toledo et al. (2010). However, for the GAMA catalogue the classification is not obvious since the GAMA sample has a median redshift of ∼0.2 with galaxies in the interval $0< z <0.5$; meanwhile the classification mentioned above is up to z∼0.05. The first classification for GAMA has been made up to z∼0.05 (Kelvin, prep) covering only ∼10% of the total sample using bulge/disk decomposition. The big challenge of classification is at higher redshift, not only because of the number of galaxies, but the resolution of the images to apply the same or different techniques. For instance the most recent and successful method of classification proposed by Huertas-Company et al. (2009) based on a Bayesian probability.

After looking for different techniques of classification to do a non-visual classification of GAMA, I adopted the classification method proposed by Park and Choi (2005), based on the light concentration and colour with confidence up to 88%, to propose a first attempt on the classification of GAMA divided in two types of galaxies, ellipticals and spirals. In order to compare the confidence of these results, a compilation of 5 classified samples is considered (Fukugita et al. 2007, Nair and Abraham 2010, the Galaxy Zoo catalogue, the UNAM-KIAS catalogue & Driver et al. 2011). The first three samples overlap with the GAMA region as seen in Fig 1.7. The UNAM-KIAS catalogue has a complementary morphology to the Nair sample and Driver et al. (2011) present a first classification for galaxies at low redshift for GAMA. A sample of 5600 classified GAMA galaxies is compiled.

The results obtained by me for the GAMA classification based on the Park and Choi (2005) method are presented in Fig 1.8 where concentration and colour gradient are plotted against $u - r$ colour; red and black dots are the elliptical and spiral galaxies according to this classification. The solid line on the bottom panel represents the separation between

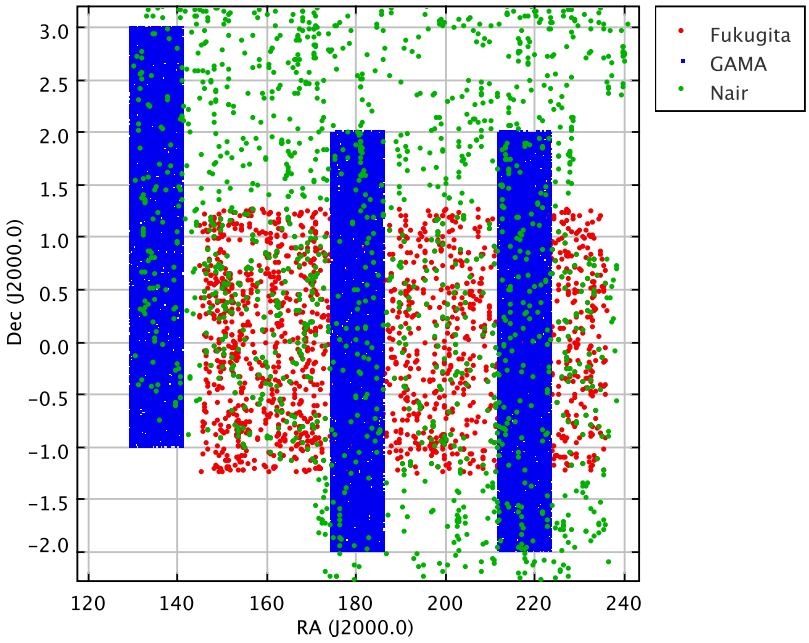

Figure 1.7: GAMA, Fukugita et al. (2007) and Nair & Abraham (2010) samples in the GAMA region

these two type of galaxies according to Park and Choi (2005). Filled circles represent the comparison sample to see where these galaxies are located in the diagram. For spiral galaxies the classification is good enough to be considered, however, for elliptical galaxies this classification does not work well; unfortunately the plot does not show clearly the elliptical galaxies, but a significant number of them are on the other side. The confidence of this classification is ∼69%, rather than the 88% expected. I divided the classification by redshift to see if the confidence changes along z but there are no significant changes; this means the same confidence level at all z and an extrapolation of this method to the total GAMA sample can be followed.

At the time when these results were ready, Kelvin et al. (2012) published the Sersic index (Sersic, 1968) GAMA catalogue. Simple classifications using the Sérsic index give a good classification at least to distinguish between spheroidal and disk shape galaxies (e.g. Barden et al. 2005). Therefore, we have made a simple classification based on this Sérsic index where galaxies are considered as spheroidals when $n > 1.9$ and disky galaxies when $n < 1.9$. Using the sample comparison sample, a confidence level of ∼78% is found.

The method of Park and Choi (2005) can be much better than the Sérsic classification,

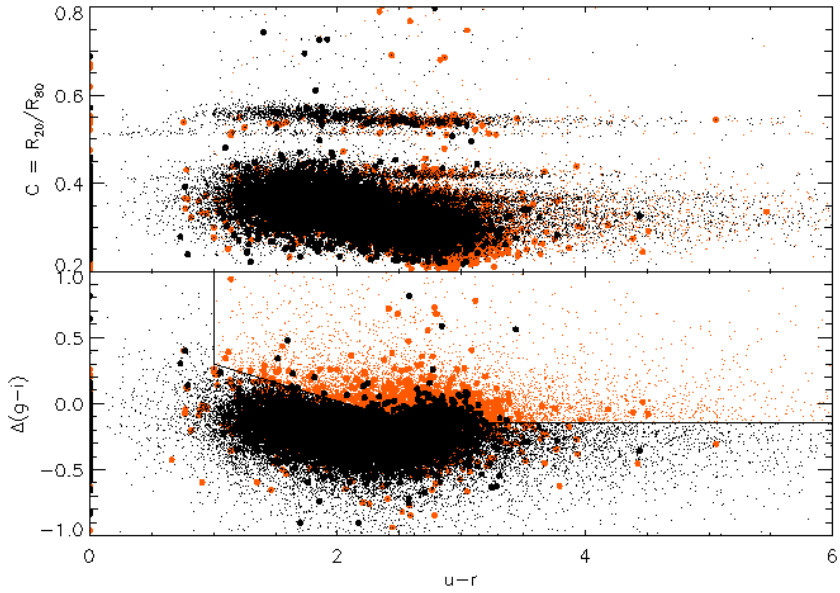

Figure 1.8: Distributions of the GAMA galaxies in the morphology training set. Top: $u-r$ colour vs. (inverse) concentration index space; bottom: $u-r$ vs. $\Delta(g-i)$ colour difference space. Red dots are elliptical types, black dots are spirals, and filled circles with same colour, the comparison sample.

but images with higher resolution are necessary. At the moment, the Sersic classification of GAMA is better (sec. 2.2.3), with a $\sim$10% higher confidence than that using the other method, this improvement is enough to consider the Sersic classification for the rest of this thesis.

1.5 Overview of the papers

In previous sections I aimed to introduce the main problems and give a general idea about the current state of the galaxy formation and evolution studies relevant to the luminosity and the environment, and the relationship with galaxy evolution models. In this work I try to answer the questions about the physical processes of the galaxies in the evolution process using the main observable measurement, the luminosity, so we can establish the most accurate values to constrain evolution models and understand the intrinsic and external physical properties of galaxies. Mainly, I extend the study of the LF to the low mass galaxies regime, where data up to now had been incomplete and the studies were low accurate. In the papers presented for this thesis, I cover as much as possible these ideas to propose real statistical relationships and differences of the LF in the most homogeneous

and spectroscopically complete samples to carry out this study.

The study of the LF and dependence with group properties is the first problem to consider, since many people have been working in this area and the credibility of our results can be easily compared with previous results but with improved results. In this sense, Paper I, focuses on the dependence of the LF on group properties, richness, velocity dispersion and mass, and also the dependence with the galaxy properties, colour and morphology. This work is based on the r-band since the GAMA sample was selected in this band and the best completeness is available in this band.

In this first paper, the first analysis was carried out with group richness, analogous to a study at different densities but on small scales; considering ungrouped galaxies, pairs, groups with 3 and 4 members and the richest groups containing more than 5 members. These limits were taken according to the richness presented in the sample, since most of the groups are dominated by pairs. We find similar results compared to Croton et al. (2005), observing changes in M^* and α as richness increases. Due to the relationship between mass and velocity dispersion, we find similar LF characteristics, comparable to the mass dependence reported by Yang et al. (2009) and Robotham et al. (2010). With respect to the colour and morphology, similar dependences are found, following the assumption that early type galaxies tend to be redder and late type galaxies bluer. These results are in agreement with those presented by Blanton et al. (2001) and Benson et al. (2007). Finally, our results are compared with mock catalogues constructed using the Millennium simulation (Springel et al., 2005); the comparison is not very accurate, mostly because of how these mock catalogues have been created (Norberg, prep).

For this paper, I did the whole study and analysis of the LF based on computational tools developed by Dr Jon Loveday but modified by myself according to my interests and needs, and many other analysis tools developed by myself throughout this work. Many suggestions and discussions were carried out with Dr Loveday and the GAMA team in different meetings with them. As the last step of this paper, it will be sent to the complete GAMA team for the latest suggestions and it will be sent to the MNRAS journal in the next couple of months.

Motivated by studying the dependence with the environment and taking advantage of my own sample of isolated galaxies (UNAM-KIAS) and the good classifications, collaborators and I characterize the UNAM-KIAS catalogue, estimating the LF in the *ugriz* bands, the stellar mass function (SMF) and the gas-to-stellar mass ratio in the second paper (Paper II). We find similar results to those reported by Sulentic et al. (2006); nevertheless, we

find an inconsistency with their results, so no straightforward comparisons can be done. This means, we are proposing completely new parameters for isolated galaxies divided by morphological type. We also consider two GAMA subsamples, one refers to galaxies considered as isolated after they were excluded in the grouping scheme (Robotham et al., 2011); the LF using this subsample matches very well with the UNAM-KIAS catalogue, just a difference in density is found due to the large difference in the number of galaxies contained in each sample. The other subsample used to compare our results is the GAMA sample of voids (Alpaslan et al., 2013); however, this subsample is selected using a volume-limited sample, meaning the lost of faint galaxies and thus information about the LF faint-end. Due to the quality of data and how the UNAM-KIAS sample was selected, we propose the most accurate LF parameters for isolated galaxies and this fact makes this paper unique. The SMF is estimated divided by colour and morphology, expected results are found comparing with other samples. Finally the gas-to-stellar mass ratio is estimated for isolated galaxies, finding higher gas fractions for these galaxies than normal disk galaxies.

This second paper started as a continuation of UNAM-KIAS catalogue study which was characterized and classified by myself in a previous work. I have estimated the LF for this sample and I did all the comparisons with other samples in the literature. I have been collaborating with other experts in their fields. I did the first estimation of the SMF; however, I was not considering important factors like completeness, so Dr. Aldo Puebla was the person in charge of this estimation and as a complement, Dr Ivan Lacerna made the estimation of the gas-to-stellar mass ratio. Dr Jon Loveday and Dr Hector Hernández-Toledo have collaborated by giving important comments and discussions.

Finally, considering that GAMA is a multi-wavelength survey, we take advantage of this fact and as a complement study to Paper I we estimated the groups LF in 11 bands from the NIR to the UV; these results are presented in the Paper III draft. In this work I study the effects of group environment on star-formation processes. However, a detailed study considering band by band is still missing for future work to investigate in-depth the physical processes occurring in these galaxies. This was a first attempt to study for the first time a homogeneous multi-wavelength LF.

References

Alpaslan, M., Robotham, A. S. G., Driver, S., Norberg, P., Baldry, I., Bauer, A. E., Bland-Hawthorn, J., Brown, M., Cluver, M., Colless, M., Foster, C., Hopkins, A., Van Kampen, E., Kelvin, L., Lara-Lopez, M. A., Liske, J., Lopez-Sanchez, A. R., Loveday, J., McNaught-Roberts, T., Merson, A., and Pimbblet, K. (2013). Galaxy And Mass Assembly (GAMA): The large scale structure of galaxies and comparison to mock universes. *ArXiv e-prints*.

Andreon, S. and Pelló, R. (2000). Near-infrared luminosity function in the Coma cluster. *A&A*, 353:479–486.

Baldry, I. K., Alpaslan, M., Bauer, A. E., Bland-Hawthorn, J., Brough, S., Cluver, M. E., Croom, S. M., Davies, L. J. M., Driver, S. P., Gunawardhana, M. L. P., Holwerda, B. W., Hopkins, A. M., Kelvin, L. S., Liske, J., López-Sánchez, Á. R., Loveday, J., Norberg, P., Peacock, J., Robotham, A. S. G., and Taylor, E. N. (2014). Galaxy And Mass Assembly (GAMA): AUTOZ spectral redshift measurements, confidence and errors. *MNRAS*, 441:2440–2451.

Baldry, I. K., Glazebrook, K., Brinkmann, J., Ivezić, Ž., Lupton, R. H., Nichol, R. C., and Szalay, A. S. (2004). Quantifying the Bimodal Color-Magnitude Distribution of Galaxies. *ApJ*, 600:681–694.

Baldry, I. K., Glazebrook, K., Budavári, T., Eisenstein, D. J., Annis, J., Bahcall, N. A., Blanton, M. R., Brinkmann, J., Csabai, I., Heckman, T. M., Lin, H., Loveday, J., Nichol, R. C., and Schneider, D. P. (2005). The Sloan Digital Sky Survey u-band Galaxy Survey: luminosity functions and evolution. *MNRAS*, 358:441–456.

Barden, M., Rix, H.-W., Somerville, R. S., Bell, E. F., Häußler, B., Peng, C. Y., Borch, A., Beckwith, S. V. W., Caldwell, J. A. R., Heymans, C., Jahnke, K., Jogee, S., McIntosh, D. H., Meisenheimer, K., Sánchez, S. F., Wisotzki, L., and Wolf, C. (2005). GEMS:

The Surface Brightness and Surface Mass Density Evolution of Disk Galaxies. *ApJ*, 635:959–981.

Benson, A. J., Džanović, D., Frenk, C. S., and Sharples, R. (2007). Luminosity and stellar mass functions of discs and spheroids in the SDSS and the supermassive black hole mass function. *MNRAS*, 379:841–866.

Benson, A. J., Frenk, C. S., Baugh, C. M., Cole, S., and Lacey, C. G. (2003). The effects of photoionization on galaxy formation - III. Environmental dependence in the luminosity function. *MNRAS*, 343:679–691.

Binggeli, B., Sandage, A., and Tammann, G. A. (1988). The luminosity function of galaxies. *ARA&A*, 26:509–560.

Blanton, M. R., Dalcanton, J., Eisenstein, D., Loveday, J., Strauss, M. A., SubbaRao, M., Weinberg, D. H., Anderson, Jr., J. E., Annis, J., Bahcall, N. A., Bernardi, M., Brinkmann, J., Brunner, R. J., Burles, S., Carey, L., Castander, F. J., Connolly, A. J., Csabai, I., Doi, M., Finkbeiner, D., Friedman, S., Frieman, J. A., Fukugita, M., Gunn, J. E., Hennessy, G. S., Hindsley, R. B., Hogg, D. W., Ichikawa, T., Ivezić, Ž., Kent, S., Knapp, G. R., Lamb, D. Q., Leger, R. F., Long, D. C., Lupton, R. H., McKay, T. A., Meiksin, A., Merelli, A., Munn, J. A., Narayanan, V., Newcomb, M., Nichol, R. C., Okamura, S., Owen, R., Pier, J. R., Pope, A., Postman, M., Quinn, T., Rockosi, C. M., Schlegel, D. J., Schneider, D. P., Shimasaku, K., Siegmund, W. A., Smee, S., Snir, Y., Stoughton, C., Stubbs, C., Szalay, A. S., Szokoly, G. P., Thakar, A. R., Tremonti, C., Tucker, D. L., Uomoto, A., Vanden Berk, D., Vogeley, M. S., Waddell, P., Yanny, B., Yasuda, N., and York, D. G. (2001). The Luminosity Function of Galaxies in SDSS Commissioning Data. *AJ*, 121:2358–2380.

Blanton, M. R., Schlegel, D. J., Strauss, M. A., Brinkmann, J., Finkbeiner, D., Fukugita, M., Gunn, J. E., Hogg, D. W., Ivezić, Ž., Knapp, G. R., Lupton, R. H., Munn, J. A., Schneider, D. P., Tegmark, M., and Zehavi, I. (2005). New York University Value-Added Galaxy Catalog: A Galaxy Catalog Based on New Public Surveys. *AJ*, 129:2562–2578.

Choi, Y.-Y., Park, C., and Vogeley, M. S. (2007). Internal and Collective Properties of Galaxies in the Sloan Digital Sky Survey. *ApJ*, 658:884–897.

Christlein, D. (2000). The Dependence of the Galaxy Luminosity Function on Environment. *ApJ*, 545:145–156.

Cole, S., Lacey, C. G., Baugh, C. M., and Frenk, C. S. (2000). Hierarchical galaxy formation. *MNRAS*, 319:168–204.

Conselice, C. J. (2003). The Relationship between Stellar Light Distributions of Galaxies and Their Formation Histories. *ApJS*, 147:1–28.

Croton, D. J., Farrar, G. R., Norberg, P., Colless, M., Peacock, J. A., Baldry, I. K., Baugh, C. M., Bland-Hawthorn, J., Bridges, T., Cannon, R., Cole, S., Collins, C., Couch, W., Dalton, G., De Propris, R., Driver, S. P., Efstathiou, G., Ellis, R. S., Frenk, C. S., Glazebrook, K., Jackson, C., Lahav, O., Lewis, I., Lumsden, S., Maddox, S., Madgwick, D., Peterson, B. A., Sutherland, W., and Taylor, K. (2005). The 2dF Galaxy Redshift Survey: luminosity functions by density environment and galaxy type. *MNRAS*, 356:1155–1167.

de Lapparent, V. (2003). Critical analysis of the luminosity functions per galaxy type measured from redshift surveys. *A&A*, 408:845–872.

De Propris, R., Colless, M., Driver, S. P., Couch, W., Peacock, J. A., Baldry, I. K., Baugh, C. M., Bland-Hawthorn, J., Bridges, T., Cannon, R., Cole, S., Collins, C., Cross, N., Dalton, G. B., Efstathiou, G., Ellis, R. S., Frenk, C. S., Glazebrook, K., Hawkins, E., Jackson, C., Lahav, O., Lewis, I., Lumsden, S., Maddox, S., Madgwick, D. S., Norberg, P., Percival, W., Peterson, B., Sutherland, W., and Taylor, K. (2003). The 2dF Galaxy Redshift Survey: the luminosity function of cluster galaxies. *MNRAS*, 342:725–737.

Delgado-Serrano, R., Hammer, F., Yang, Y. B., Puech, M., Flores, H., and Rodrigues, M. (2010). How was the Hubble sequence 6 Gyr ago? *A&A*, 509:A78.

Devereux, N., Hriljac, P., Willner, S. P., Ashby, M. L. N., and Willmer, C. N. A. (2009). The Morphological Type Dependence of K-band Luminosity Functions. In Jogee, S., Marinova, I., Hao, L., and Blanc, G. A., editors, *Galaxy Evolution: Emerging Insights and Future Challenges*, volume 419 of *Astronomical Society of the Pacific Conference Series*, page 171.

Driver, S. P., Hill, D. T., Kelvin, L. S., Robotham, A. S. G., Liske, J., Norberg, P., Baldry, I. K., Bamford, S. P., Hopkins, A. M., Loveday, J., Peacock, J. A., Andrae, E., Bland-Hawthorn, J., Brough, S., Brown, M. J. I., Cameron, E., Ching, J. H. Y., Colless, M., Conselice, C. J., Croom, S. M., Cross, N. J. G., de Propris, R., Dye, S., Drinkwater, M. J., Ellis, S., Graham, A. W., Grootes, M. W., Gunawardhana, M., Jones, D. H., van Kampen, E., Maraston, C., Nichol, R. C., Parkinson, H. R., Phillipps, S., Pimbblet, K.,

Popescu, C. C., Prescott, M., Roseboom, I. G., Sadler, E. M., Sansom, A. E., Sharp, R. G., Smith, D. J. B., Taylor, E., Thomas, D., Tuffs, R. J., Wijesinghe, D., Dunne, L., Frenk, C. S., Jarvis, M. J., Madore, B. F., Meyer, M. J., Seibert, M., Staveley-Smith, L., Sutherland, W. J., and Warren, S. J. (2011). Galaxy and Mass Assembly (GAMA): survey diagnostics and core data release. *MNRAS*, 413:971–995.

Driver, S. P., Norberg, P., Baldry, I. K., Bamford, S. P., Hopkins, A. M., Liske, J., Loveday, J., Peacock, J. A., Hill, D. T., Kelvin, L. S., Robotham, A. S. G., Cross, N. J. G., Parkinson, H. R., Prescott, M., Conselice, C. J., Dunne, L., Brough, S., Jones, H., Sharp, R. G., van Kampen, E., Oliver, S., Roseboom, I. G., Bland-Hawthorn, J., Croom, S. M., Ellis, S., Cameron, E., Cole, S., Frenk, C. S., Couch, W. J., Graham, A. W., Proctor, R., De Propris, R., Doyle, I. F., Edmondson, E. M., Nichol, R. C., Thomas, D., Eales, S. A., Jarvis, M. J., Kuijken, K., Lahav, O., Madore, B. F., Seibert, M., Meyer, M. J., Staveley-Smith, L., Phillipps, S., Popescu, C. C., Sansom, A. E., Sutherland, W. J., Tuffs, R. J., and Warren, S. J. (2009). GAMA: towards a physical understanding of galaxy formation. *Astronomy and Geophysics*, 50(5):050000–5.

Driver, S. P., Wright, A. H., Andrews, S. K., Davies, L. J., Kafle, P. R., Lange, R., Moffett, A. J., Mannering, E., Robotham, A. S. G., Vinsen, K., Alpaslan, M., Andrae, E., Baldry, I. K., Bauer, A. E., Bamford, S. P., Bland-Hawthorn, J., Bourne, N., Brough, S., Brown, M. J. I., Cluver, M. E., Croom, S., Colless, M., Conselice, C. J., da Cunha, E., De Propris, R., Drinkwater, M., Dunne, L., Eales, S., Edge, A., Frenk, C., Graham, A. W., Grootes, M., Holwerda, B. W., Hopkins, A. M., Ibar, E., van Kampen, E., Kelvin, L. S., Jarrett, T., Jones, D. H., Lara-Lopez, M. A., Lopez-Sanchez, A. R., Liske, J., Loveday, J., Maddox, S. J., Madore, B., Meyer, M., Norberg, P., Penny, S. J., Phillipps, S., Popescu, C., Tuffs, R. J., Peacock, J. A., Pimbblet, K. A., Rowlands, K., Sansom, A. E., Seibert, M., Smith, M. W. L., Sutherland, W. J., Taylor, E. N., Valiante, E., Wang, L., Wilkins, S. M., and Williams, R. (2015). Galaxy And Mass Assembly (GAMA): Panchromatic Data Release (far-UV — far-IR) and the low-z energy budget. *ArXiv e-prints*.

Efstathiou, G., Ellis, R. S., and Peterson, B. A. (1988). Analysis of a complete galaxy redshift survey. II - The field-galaxy luminosity function. *MNRAS*, 232:431–461.

Eke, V. R., Frenk, C. S., Baugh, C. M., Cole, S., Norberg, P., Peacock, J. A., Baldry, I. K., Bland-Hawthorn, J., Bridges, T., Cannon, R., Colless, M., Collins, C., Couch, W., Dalton, G., de Propris, R., Driver, S. P., Efstathiou, G., Ellis, R. S., Glazebrook,

K., Jackson, C. A., Lahav, O., Lewis, I., Lumsden, S., Maddox, S. J., Madgwick, D., Peterson, B. A., Sutherland, W., and Taylor, K. (2004). Galaxy groups in the Two-degree Field Galaxy Redshift Survey: the luminous content of the groups. *MNRAS*, 355:769–784.

Folkes, S., Ronen, S., Price, I., Lahav, O., Colless, M., Maddox, S., Deeley, K., Glazebrook, K., Bland-Hawthorn, J., Cannon, R., Cole, S., Collins, C., Couch, W., Driver, S. P., Dalton, G., Efstathiou, G., Ellis, R. S., Frenk, C. S., Kaiser, N., Lewis, I., Lumsden, S., Peacock, J., Peterson, B. A., Sutherland, W., and Taylor, K. (1999). The 2dF Galaxy Redshift Survey: spectral types and luminosity functions. *MNRAS*, 308:459–472.

Fukugita, M., Nakamura, O., Okamura, S., Yasuda, N., Barentine, J. C., Brinkmann, J., Gunn, J. E., Harvanek, M., Ichikawa, T., Lupton, R. H., Schneider, D. P., Strauss, M. A., and York, D. G. (2007). A Catalog of Morphologically Classified Galaxies from the Sloan Digital Sky Survey: North Equatorial Region. *AJ*, 134:579–593.

Hernández-Toledo, H. M., Vázquez-Mata, J. A., Martínez-Vázquez, L. A., Choi, Y.-Y., and Park, C. (2010). The UNAM-KIAS Catalog of Isolated Galaxies. *AJ*, 139:2525–2541.

Holmberg, E. (1969). A study of physical groups of galaxies. *Arkiv for Astronomi*, 5:305–343.

Hopkins, A. M., Driver, S. P., Brough, S., Owers, M. S., Bauer, A. E., Gunawardhana, M. L. P., Cluver, M. E., Colless, M., Foster, C., Lara-López, M. A., Roseboom, I., Sharp, R., Steele, O., Thomas, D., Baldry, I. K., Brown, M. J. I., Liske, J., Norberg, P., Robotham, A. S. G., Bamford, S., Bland-Hawthorn, J., Drinkwater, M. J., Loveday, J., Meyer, M., Peacock, J. A., Tuffs, R., Agius, N., Alpaslan, M., Andrae, E., Cameron, E., Cole, S., Ching, J. H. Y., Christodoulou, L., Conselice, C., Croom, S., Cross, N. J. G., De Propris, R., Delhaize, J., Dunne, L., Eales, S., Ellis, S., Frenk, C. S., Graham, A. W., Grootes, M. W., Häußler, B., Heymans, C., Hill, D., Hoyle, B., Hudson, M., Jarvis, M., Johansson, J., Jones, D. H., van Kampen, E., Kelvin, L., Kuijken, K., López-Sánchez, Á., Maddox, S., Madore, B., Maraston, C., McNaught-Roberts, T., Nichol, R. C., Oliver, S., Parkinson, H., Penny, S., Phillipps, S., Pimbblet, K. A., Ponman, T., Popescu, C. C., Prescott, M., Proctor, R., Sadler, E. M., Sansom, A. E., Seibert, M., Staveley-Smith, L., Sutherland, W., Taylor, E., Van Waerbeke, L., Vázquez-Mata, J. A., Warren, S., Wijesinghe, D. B., Wild, V., and Wilkins, S. (2013). Galaxy And Mass Assembly (GAMA): spectroscopic analysis. *MNRAS*, 430:2047–2066.

Hoyle, F., Rojas, R. R., Vogeley, M. S., and Brinkmann, J. (2005). The Luminosity Function of Void Galaxies in the Sloan Digital Sky Survey. *ApJ*, 620:618–628.

Hubble, E. (1936). The Luminosity Function of Nebulae. I. The Luminosity Function of Resolved Nebulae as Indicated by Their Brightest Stars. *ApJ*, 84:158.

Huertas-Company, M., Tasca, L., Rouan, D., Pelat, D., Kneib, J. P., Le Fèvre, O., Capak, P., Kartaltepe, J., Koekemoer, A., McCracken, H. J., Salvato, M., Sanders, D. B., and Willott, C. (2009). A robust morphological classification of high-redshift galaxies using support vector machines on seeing limited images. II. Quantifying morphological k-correction in the COSMOS field at 1 z 2: Ks band vs. I band. *A&A*, 497:743–753.

Hunsberger, S. D., Charlton, J. C., and Zaritsky, D. (1998). The Luminosity Function of Galaxies in Compact Groups. *ApJ*, 505:536–557.

Ilbert, O., Lauger, S., Tresse, L., Buat, V., Arnouts, S., Le Fèvre, O., Burgarella, D., Zucca, E., Bardelli, S., Zamorani, G., Bottini, D., Garilli, B., Le Brun, V., Maccagni, D., Picat, J.-P., Scaramella, R., Scodeggio, M., Vettolani, G., Zanichelli, A., Adami, C., Arnaboldi, M., Bolzonella, M., Cappi, A., Charlot, S., Contini, T., Foucaud, S., Franzetti, P., Gavignaud, I., Guzzo, L., Iovino, A., McCracken, H. J., Marano, B., Marinoni, C., Mathez, G., Mazure, A., Meneux, B., Merighi, R., Paltani, S., Pello, R., Pollo, A., Pozzetti, L., Radovich, M., Bondi, M., Bongiorno, A., Busarello, G., Ciliegi, P., Mellier, Y., Merluzzi, P., Ripepi, V., and Rizzo, D. (2006). The VIMOS-VLT Deep Survey. Galaxy luminosity function per morphological type up to z = 1.2. *A&A*, 453:809–815.

Karachentseva, V. E. (1973). The Catalogue of Isolated Galaxies,. *Astrofizicheskie Issledovaniia Izvestiya Spetsial'noj Astrofizicheskoj Observatorii*, 8:3–49.

Kelvin, L. (in prep). Galaxy And Mass Assembly (GAMA): ugrizYJHK Sérsic luminosity functions and the cosmic spectral energy distribution by Hubble type.

Kelvin, L. S., Driver, S. P., Robotham, A. S. G., Hill, D. T., Alpaslan, M., Baldry, I. K., Bamford, S. P., Bland-Hawthorn, J., Brough, S., Graham, A. W., Häussler, B., Hopkins, A. M., Liske, J., Loveday, J., Norberg, P., Phillipps, S., Popescu, C. C., Prescott, M., Taylor, E. N., and Tuffs, R. J. (2012). Galaxy And Mass Assembly (GAMA): Structural Investigation of Galaxies via Model Analysis. *MNRAS*, 421:1007–1039.

Lin, H., Yee, H. K. C., Carlberg, R. G., Morris, S. L., Sawicki, M., Patton, D. R., Wirth, G., and Shepherd, C. W. (1999). The CNOC2 Field Galaxy Luminosity Function. I. A Description of Luminosity Function Evolution. *ApJ*, 518:533–561.

Lintott, C., Schawinski, K., Bamford, S., Slosar, A., Land, K., Thomas, D., Edmondson, E., Masters, K., Nichol, R. C., Raddick, M. J., Szalay, A., Andreescu, D., Murray, P., and Vandenberg, J. (2011). Galaxy Zoo 1: data release of morphological classifications for nearly 900 000 galaxies. *MNRAS*, 410:166–178.

Lintott, C. J., Schawinski, K., Slosar, A., Land, K., Bamford, S., Thomas, D., Raddick, M. J., Nichol, R. C., Szalay, A., Andreescu, D., Murray, P., and Vandenberg, J. (2008). Galaxy Zoo: morphologies derived from visual inspection of galaxies from the Sloan Digital Sky Survey. *MNRAS*, 389:1179–1189.

Liske, J., Baldry, I. K., Driver, S. P., Tuffs, R. J., Alpaslan, M., Andrae, E., Brough, S., Cluver, M. E., Grootes, M. W., Gunawardhana, M. L. P., Kelvin, L. S., Loveday, J., Robotham, A. S. G., Taylor, E. N., Bamford, S. P., Bland-Hawthorn, J., Brown, M. J. I., Drinkwater, M. J., Hopkins, A. M., Meyer, M. J., Norberg, P., Peacock, J. A., Agius, N. K., Andrews, S. K., Bauer, A. E., Ching, J. H. Y., Colless, M., Conselice, C. J., Croom, S. M., Davies, L. J. M., De Propris, R., Dunne, L., Eardley, E. M., Ellis, S., Foster, C., Frenk, C. S., Häußler, B., Holwerda, B. W., Howlett, C., Ibarra, H., Jarvis, M. J., Jones, D. H., Kafle, P. R., Lacey, C. G., Lange, R., Lara-López, M. A., López-Sánchez, Á. R., Maddox, S., Madore, B. F., McNaught-Roberts, T., Moffett, A. J., Nichol, R. C., Owers, M. S., Palamara, D., Penny, S. J., Phillipps, S., Pimbblet, K. A., Popescu, C. C., Prescott, M., Proctor, R., Sadler, E. M., Sansom, A. E., Seibert, M., Sharp, R., Sutherland, W., Vázquez-Mata, J. A., van Kampen, E., Wilkins, S. M., Williams, R., and Wright, A. H. (2015). Galaxy And Mass Assembly (GAMA): end of survey report and data release 2. *MNRAS*, 452:2087–2126.

Lobo, C., Biviano, A., Durret, F., Gerbal, D., Le Fevre, O., Mazure, A., and Slezak, E. (1997). Environmental effects on the Coma cluster luminosity function. *A&A*, 317:385–392.

Loveday, J. (2004). Evolution of the galaxy luminosity function at z 0.3. *MNRAS*, 347:601–606.

Loveday, J., Norberg, P., Baldry, I. K., Driver, S. P., Hopkins, A. M., Peacock, J. A., Bamford, S. P., Liske, J., Bland-Hawthorn, J., Brough, S., Brown, M. J. I., Cameron,

E., Conselice, C. J., Croom, S. M., Frenk, C. S., Gunawardhana, M., Hill, D. T., Jones, D. H., Kelvin, L. S., Kuijken, K., Nichol, R. C., Parkinson, H. R., Phillipps, S., Pimbblet, K. A., Popescu, C. C., Prescott, M., Robotham, A. S. G., Sharp, R. G., Sutherland, W. J., Taylor, E. N., Thomas, D., Tuffs, R. J., van Kampen, E., and Wijesinghe, D. (2012). Galaxy and Mass Assembly (GAMA): ugriz galaxy luminosity functions. *MNRAS*, 420:1239–1262.

Mandelbaum, R., Seljak, U., Baldauf, T., and Smith, R. E. (2010). Precision cluster mass determination from weak lensing. *MNRAS*, 405:2078–2102.

Mandelbaum, R., Seljak, U., Hirata, C. M., Bardelli, S., Bolzonella, M., Bongiorno, A., Carollo, M., Contini, T., Cunha, C. E., Garilli, B., Iovino, A., Kampczyk, P., Kneib, J.-P., Knobel, C., Koo, D. C., Lamareille, F., Le Fèvre, O., Le Borgne, J.-F., Lilly, S. J., Maier, C., Mainieri, V., Mignoli, M., Newman, J. A., Oesch, P. A., Perez-Montero, E., Ricciardelli, E., Scodeggio, M., Silverman, J., and Tasca, L. (2008). Precision photometric redshift calibration for galaxy-galaxy weak lensing. *MNRAS*, 386:781–806.

Marzke, R. O., da Costa, L. N., Pellegrini, P. S., Willmer, C. N. A., and Geller, M. J. (1998). The Galaxy Luminosity Function at Z = 0.05: Dependence on Morphology. *ApJ*, 503:617.

Masters, K. L., Nichol, R. C., Hoyle, B., Lintott, C., Bamford, S. P., Edmondson, E. M., Fortson, L., Keel, W. C., Schawinski, K., Smith, A. M., and Thomas, D. (2011). Galaxy Zoo: bars in disc galaxies. *MNRAS*, 411:2026–2034.

McNaught-Roberts, T., Norberg, P., Baugh, C., Lacey, C., Loveday, J., Peacock, J., Baldry, I., Bland-Hawthorn, J., Brough, S., Driver, S. P., Robotham, A. S. G., and Vázquez-Mata, J. A. (2014). Galaxy And Mass Assembly (GAMA): the dependence of the galaxy luminosity function on environment, redshift and colour. *MNRAS*, 445:2125–2145.

Miles, T. A., Raychaudhury, S., Forbes, D. A., Goudfrooij, P., Ponman, T. J., and Kozhurina-Platais, V. (2004). The Group Evolution Multiwavelength Study (GEMS): bimodal luminosity functions in galaxy groups. *MNRAS*, 355:785–793.

Nair, P. B. and Abraham, R. G. (2010). A Catalog of Detailed Visual Morphological Classifications for 14,034 Galaxies in the Sloan Digital Sky Survey. *ApJS*, 186:427–456.

Norberg, P. (in prep.). Galaxy And Mass Assembly (GAMA): Preliminary global group properties from G3Cv6.

Pannekoek, A. (1923). Luminosity function and brightness for clusters and galactic clouds. , 2:5.

Park, C. and Choi, Y.-Y. (2005). Morphology Segregation of Galaxies in Color-Color Gradient Space. *ApJ*, 635:L29–L32.

Park, C., Choi, Y.-Y., Vogeley, M. S., Gott, III, J. R., Blanton, M. R., and SDSS Collaboration (2007). Environmental Dependence of Properties of Galaxies in the Sloan Digital Sky Survey. *ApJ*, 658:898–916.

Robotham, A., Phillipps, S., and De Propris, R. (2008). The Shapes of Galaxy Groups: Footballs or Frisbees? *ApJ*, 672:834–848.

Robotham, A., Phillipps, S., and de Propris, R. (2010). The variation of the galaxy luminosity function with group properties. *MNRAS*, 403:1812–1828.

Robotham, A. S. G., Norberg, P., Driver, S. P., Baldry, I. K., Bamford, S. P., Hopkins, A. M., Liske, J., Loveday, J., Merson, A., Peacock, J. A., Brough, S., Cameron, E., Conselice, C. J., Croom, S. M., Frenk, C. S., Gunawardhana, M., Hill, D. T., Jones, D. H., Kelvin, L. S., Kuijken, K., Nichol, R. C., Parkinson, H. R., Pimbblet, K. A., Phillipps, S., Popescu, C. C., Prescott, M., Sharp, R. G., Sutherland, W. J., Taylor, E. N., Thomas, D., Tuffs, R. J., van Kampen, E., and Wijesinghe, D. (2011). Galaxy and Mass Assembly (GAMA): the GAMA galaxy group catalogue (G^3Cv1). *MNRAS*, 416:2640–2668.

Sandage, A., Tammann, G. A., and Yahil, A. (1979). The velocity field of bright nearby galaxies. I - The variation of mean absolute magnitude with redshift for galaxies in a magnitude-limited sample. *ApJ*, 232:352–364.

Schaye, J., Crain, R. A., Bower, R. G., Furlong, M., Schaller, M., Theuns, T., Dalla Vecchia, C., Frenk, C. S., McCarthy, I. G., Helly, J. C., Jenkins, A., Rosas-Guevara, Y. M., White, S. D. M., Baes, M., Booth, C. M., Camps, P., Navarro, J. F., Qu, Y., Rahmati, A., Sawala, T., Thomas, P. A., and Trayford, J. (2015). The EAGLE project: simulating the evolution and assembly of galaxies and their environments. *MNRAS*, 446:521–554.

Schechter, P. (1976). An analytic expression for the luminosity function for galaxies. *ApJ*, 203:297–306.

Schmidt, M. (1968). Space Distribution and Luminosity Functions of Quasi-Stellar Radio Sources. *ApJ*, 151:393.

Sersic, J. L. (1968). *Atlas de galaxias australes*. Cordoba, Argentina: Observatorio Astronomico.

Smith, A. J., Loveday, J., and Cross, N. J. G. (2009). Luminosity and surface brightness distribution of K-band galaxies from the UKIDSS Large Area Survey. *MNRAS*, 397:868–882.

Somerville, R. S. and Dave, R. (2015). Physical models of galaxy formation in a cosmological framework. *ARA&A*, 53:51–113.

Somerville, R. S., Primack, J. R., and Faber, S. M. (2001). The nature of high-redshift galaxies. *MNRAS*, 320:504–528.

Springel, V., White, S. D. M., Jenkins, A., Frenk, C. S., Yoshida, N., Gao, L., Navarro, J., Thacker, R., Croton, D., Helly, J., Peacock, J. A., Cole, S., Thomas, P., Couchman, H., Evrard, A., Colberg, J., and Pearce, F. (2005). Simulations of the formation, evolution and clustering of galaxies and quasars. *Nature*, 435:629–636.

Stoughton, C., Lupton, R. H., Bernardi, M., Blanton, M. R., Burles, S., Castander, F. J., Connolly, A. J., Eisenstein, D. J., Frieman, J. A., Hennessy, G. S., Hindsley, R. B., Ivezić, Ž., Kent, S., Kunszt, P. Z., Lee, B. C., Meiksin, A., Munn, J. A., Newberg, H. J., Nichol, R. C., Nicinski, T., Pier, J. R., Richards, G. T., Richmond, M. W., Schlegel, D. J., Smith, J. A., Strauss, M. A., SubbaRao, M., Szalay, A. S., Thakar, A. R., Tucker, D. L., Vanden Berk, D. E., Yanny, B., Adelman, J. K., Anderson, Jr., J. E., Anderson, S. F., Annis, J., Bahcall, N. A., Bakken, J. A., Bartelmann, M., Bastian, S., Bauer, A., Berman, E., Böhringer, H., Boroski, W. N., Bracker, S., Briegel, C., Briggs, J. W., Brinkmann, J., Brunner, R., Carey, L., Carr, M. A., Chen, B., Christian, D., Colestock, P. L., Crocker, J. H., Csabai, I., Czarapata, P. C., Dalcanton, J., Davidsen, A. F., Davis, J. E., Dehnen, W., Dodelson, S., Doi, M., Dombeck, T., Donahue, M., Ellman, N., Elms, B. R., Evans, M. L., Eyer, L., Fan, X., Federwitz, G. R., Friedman, S., Fukugita, M., Gal, R., Gillespie, B., Glazebrook, K., Gray, J., Grebel, E. K., Greenawalt, B., Greene, G., Gunn, J. E., de Haas, E., Haiman, Z., Haldeman, M., Hall, P. B., Hamabe, M., Hansen, B., Harris, F. H., Harris, H., Harvanek, M.,

Hawley, S. L., Hayes, J. J. E., Heckman, T. M., Helmi, A., Henden, A., Hogan, C. J., Hogg, D. W., Holmgren, D. J., Holtzman, J., Huang, C.-H., Hull, C., Ichikawa, S.-I., Ichikawa, T., Johnston, D. E., Kauffmann, G., Kim, R. S. J., Kimball, T., Kinney, E., Klaene, M., Kleinman, S. J., Klypin, A., Knapp, G. R., Korienek, J., Krolik, J., Kron, R. G., Krzesiński, J., Lamb, D. Q., Leger, R. F., Limmongkol, S., Lindenmeyer, C., Long, D. C., Loomis, C., Loveday, J., MacKinnon, B., Mannery, E. J., Mantsch, P. M., Margon, B., McGehee, P., McKay, T. A., McLean, B., Menou, K., Merelli, A., Mo, H. J., Monet, D. G., Nakamura, O., Narayanan, V. K., Nash, T., Neilsen, Jr., E. H., Newman, P. R., Nitta, A., Odenkirchen, M., Okada, N., Okamura, S., Ostriker, J. P., Owen, R., Pauls, A. G., Peoples, J., Peterson, R. S., Petravick, D., Pope, A., Pordes, R., Postman, M., Prosapio, A., Quinn, T. R., Rechenmacher, R., Rivetta, C. H., Rix, H.-W., Rockosi, C. M., Rosner, R., Ruthmansdorfer, K., Sandford, D., Schneider, D. P., Scranton, R., Sekiguchi, M., Sergey, G., Sheth, R., Shimasaku, K., Smee, S., Snedden, S. A., Stebbins, A., Stubbs, C., Szapudi, I., Szkody, P., Szokoly, G. P., Tabachnik, S., Tsvetanov, Z., Uomoto, A., Vogeley, M. S., Voges, W., Waddell, P., Walterbos, R., Wang, S.-i., Watanabe, M., Weinberg, D. H., White, R. L., White, S. D. M., Wilhite, B., Wolfe, D., Yasuda, N., York, D. G., Zehavi, I., and Zheng, W. (2002). Sloan Digital Sky Survey: Early Data Release. *AJ*, 123:485–548.

Sulentic, J. W., Verdes-Montenegro, L., Bergond, G., Lisenfeld, U., Durbala, A., Espada, D., Garcia, E., Leon, S., Sabater, J., Verley, S., Casanova, V., and Sota, A. (2006). The AMIGA sample of isolated galaxies. II. Morphological refinement. *A&A*, 449:937–949.

Tago, E., Saar, E., Tempel, E., Einasto, J., Einasto, M., Nurmi, P., and Heinämäki, P. (2010). Groups of galaxies in the SDSS Data Release 7 . Flux- and volume-limited samples. *A&A*, 514:A102.

Tempel, E., Einasto, J., Einasto, M., Saar, E., and Tago, E. (2009). Anatomy of luminosity functions: the 2dFGRS example. *A&A*, 495:37–51.

Tempel, E. and Libeskind, N. I. (2013). Galaxy Spin Alignment in Filaments and Sheets: Observational Evidence. *ApJ*, 775:L42.

Tempel, E., Saar, E., Liivamägi, L. J., Tamm, A., Einasto, J., Einasto, M., and Müller, V. (2011). Galaxy morphology, luminosity, and environment in the SDSS DR7. *A&A*, 529:A53.

Verdes-Montenegro, L., Sulentic, J., Lisenfeld, U., Leon, S., Espada, D., Garcia, E., Sabater, J., and Verley, S. (2005). The AMIGA project. I. Optical characterization of the CIG catalog. *A&A*, 436:443–455.

Wojtak, R. and Mamon, G. A. (2013). Physical properties underlying observed kinematics of satellite galaxies. *MNRAS*, 428:2407–2417.

Wolf, C., Meisenheimer, K., Rix, H.-W., Borch, A., Dye, S., and Kleinheinrich, M. (2003). The COMBO-17 survey: Evolution of the galaxy luminosity function from 25 000 galaxies with 0.2 z 1.2. *A&A*, 401:73–98.

Yang, X., Mo, H. J., and van den Bosch, F. C. (2009). Galaxy Groups in the SDSS DR4. III. The Luminosity and Stellar Mass Functions. *ApJ*, 695:900–916.

Yang, X., Mo, H. J., van den Bosch, F. C., Zhang, Y., and Han, J. (2012). Evolution of the Galaxy-Dark Matter Connection and the Assembly of Galaxies in Dark Matter Halos. *ApJ*, 752:41.

Yoo, J., Weinberg, D. H., Tinker, J. L., Zheng, Z., and Warren, M. S. (2009). Extending Recovery of the Primordial Matter Power Spectrum. *ApJ*, 698:967–985.

York, D. G., Adelman, J., Anderson, Jr., J. E., Anderson, S. F., Annis, J., Bahcall, N. A., Bakken, J. A., Barkhouser, R., Bastian, S., Berman, E., Boroski, W. N., Bracker, S., Briegel, C., Briggs, J. W., Brinkmann, J., Brunner, R., Burles, S., Carey, L., Carr, M. A., Castander, F. J., Chen, B., Colestock, P. L., Connolly, A. J., Crocker, J. H., Csabai, I., Czarapata, P. C., Davis, J. E., Doi, M., Dombeck, T., Eisenstein, D., Ellman, N., Elms, B. R., Evans, M. L., Fan, X., Federwitz, G. R., Fiscelli, L., Friedman, S., Frieman, J. A., Fukugita, M., Gillespie, B., Gunn, J. E., Gurbani, V. K., de Haas, E., Haldeman, M., Harris, F. H., Hayes, J., Heckman, T. M., Hennessy, G. S., Hindsley, R. B., Holm, S., Holmgren, D. J., Huang, C.-h., Hull, C., Husby, D., Ichikawa, S.-I., Ichikawa, T., Ivezić, Ž., Kent, S., Kim, R. S. J., Kinney, E., Klaene, M., Kleinman, A. N., Kleinman, S., Knapp, G. R., Korienek, J., Kron, R. G., Kunszt, P. Z., Lamb, D. Q., Lee, B., Leger, R. F., Limmongkol, S., Lindenmeyer, C., Long, D. C., Loomis, C., Loveday, J., Lucinio, R., Lupton, R. H., MacKinnon, B., Mannery, E. J., Mantsch, P. M., Margon, B., McGehee, P., McKay, T. A., Meiksin, A., Merelli, A., Monet, D. G., Munn, J. A., Narayanan, V. K., Nash, T., Neilsen, E., Neswold, R., Newberg, H. J., Nichol, R. C., Nicinski, T., Nonino, M., Okada, N., Okamura, S., Ostriker, J. P., Owen, R., Pauls, A. G., Peoples, J., Peterson, R. L., Petravick, D., Pier, J. R., Pope, A.,

Pordes, R., Prosapio, A., Rechenmacher, R., Quinn, T. R., Richards, G. T., Richmond, M. W., Rivetta, C. H., Rockosi, C. M., Ruthmansdorfer, K., Sandford, D., Schlegel, D. J., Schneider, D. P., Sekiguchi, M., Sergey, G., Shimasaku, K., Siegmund, W. A., Smee, S., Smith, J. A., Snedden, S., Stone, R., Stoughton, C., Strauss, M. A., Stubbs, C., SubbaRao, M., Szalay, A. S., Szapudi, I., Szokoly, G. P., Thakar, A. R., Tremonti, C., Tucker, D. L., Uomoto, A., Vanden Berk, D., Vogeley, M. S., Waddell, P., Wang, S.-i., Watanabe, M., Weinberg, D. H., Yanny, B., Yasuda, N., and SDSS Collaboration (2000). The Sloan Digital Sky Survey: Technical Summary. *AJ*, 120:1579–1587.

Zandivarez, A. and Martínez, H. J. (2011). Luminosity function of galaxies in groups in the Sloan Digital Sky Survey Data Release 7: the dependence on mass, environment and galaxy type. *MNRAS*, 415:2553–2565.

Zandivarez, A., Martínez, H. J., and Merchán, M. E. (2006). On the Luminosity Function of Galaxies in Groups in the Sloan Digital Sky Survey. *ApJ*, 650:137–147.

Chapter 2

PaperI

Galaxy And Mass Assembly (GAMA):
Dependence of galaxy LF on host group properties

Vázquez-Mata J. A., Loveday J. et al.

We explore the luminosity function (LF) of grouped galaxies in the Galaxy and Mass Assembly (GAMA) survey. We study the dependence of the LF shape on host group properties (richness, mass and velocity dispersion) for galaxies subdivided by colour, morphology and central/satellite, and evolution of the LF over the redshift range 0–0.3. We find a correlation of the best-fit Schechter parameters with group mass and velocity dispersion, in agreement with previous work, extending the results to low mass groups ($\log M/M_\odot < 12$) for the first time. Colour and morphology are clearly related, since the luminosity functions follow the same tendency; however, the red galaxy population and the early type galaxies are likely different as a result of the edge-on dusty galaxy effects and also for the blue and late type galaxies. The LF of spiral and elliptical galaxies varies only weakly with group richness, suggesting that the main change with richness is in the elliptical/spiral ratio. Contrary to previous work, but in agreement with GALFORM mock catalogues, we find a low density of sub-L^* central galaxies. Finally, no significant differences were found in LF evolution within different mass groups. The Schechter parameters presented in this work must be considered by the models to reproduce them, since we offer new data in the low mass regime.

2.1 Introduction

The distribution of galaxies in space is strongly clustered and a large fraction of the galaxies form gravitationally bound multiple systems, from very populated clusters to loose groups, with the majority being in normal groups. The Λ-CDM model predicts the hierarchical merging process that occurs between haloes of dark matter (DM) in the structure formation paradigm (e.g. Press and Schechter 1974 and White and Rees 1978). Galaxy groups represent the observational part of the DM haloes which are able to give us information about the physics in these haloes; galaxy groups also provide a route to studying the dark matter dynamics (e.g. Robotham et al. 2008) and how galaxies populate the halos (Robotham et al., 2010). The luminosity function (LF) is a fundamental observable in terms of cosmology, giving a description of the population of galaxies in different environments, and contains valuable information about the physical processes that feature prominently in galaxy formation and evolution. The LF and its evolution provide important constraints on theories and models of galaxy formation and evolution, e.g. Benson et al. (2003).

In the last few years, many authors have concentrated on the effect of the environment on the LF. Many works have been carried out, focusing on the dependence of the LF on the density contrast within spheres of different radii (e.g. Hoyle et al. 2005, Park et al. 2007, Choi et al. 2007, McNaught-Roberts et al. 2014); these works agree that the LF shows significant fluctuations due to large-scale structures, while the morphological fraction as a function of luminosity is relatively less sensitive and thus seems to be more universal (e.g. Sulentic et al. 2006). Strong environmental dependencies have been seen from very low density environments (voids) to very dense clusters, (e.g. Croton et al. 2005, Tempel et al. 2009).

Large spectroscopic surveys of galaxies, such as GAMA (Driver et al. 2009, Driver et al. 2011) or the 2dF Galaxy Redshift Survey (2dFGRS; Colless et al. 2001) provide useful large galaxy group catalogues based on the real spatial distribution in the sky. Many authors have taken advantage of large galaxy surveys like SDSS survey (York et al., 2000) and have constructed galaxy group catalogues to explore multiple aspects of these systems, in particular the luminosity function and the dependency with some physical properties and the environment (e.g. Zandivarez et al. 2006, Yang et al. 2009, Robotham et al. 2010). Analysis in these works, explored mainly the variation of the Schechter function parameters, the characteristic magnitude M^* and the faint end slope α, for different galaxy populations, as a function of the galaxy group virial mass, multiplicity, velocity dispersion,

etc. Their results showed clear variations of M^* and α with the different group properties. Robotham et al. (2010) found clear trends for decreasing α as mass and/or multiplicity increase for early-type galaxies, while a much suppressed relation was observed for the late-type population.

In this paper, we describe the GAMA Galaxy Group Catalogue (G^3Cv6) in section 2.2, as well as completeness corrections applied to the sample and subsamples. Section 2.3 describes the method used to estimate the luminosity functions and the parametrization and evolution of the Schechter parameters with redshift. Section 2.4 shows the results and discussion of the differences between the LFs and the dependence of the Schechter parameters with the group properties. Section 2.5 presents the analysis of the LF for central and satellite galaxies. Section 2.6 shows the LF evolution results and finally Section 2.7 presents the final conclusions. Appendices present the complement mass-velocity dispersion analysis and the tests of two different mass estimators and the recovery of the real data from the the mock catalogues.

For this work, we assume the standard cosmology parameters of Ω_M=0.3, Ω_Λ=0.7 with a Hubble constant of H_0=100h km s^{-1} Mpc^{-1}.

2.2 DATA

The Galaxy and Mass Assembly project (GAMA) is a multi-wavelength spectroscopic galaxy survey based on an input catalogue described by Baldry et al. (2010). Briefly, the GAMA-II survey is based on the Sloan Digital Sky Survey Data Release 7 (SDSS DR7) and consists of three equatorial regions, each of 12 $\times$ 5 degrees centred at 09h, 12h and 14h30m, called G09, G12 and G15 respectively. The survey Petrosian magnitude limit is $r < 19.8$ mag for the three fields. This survey is complete in all regions with a completeness greater than 95% for all galaxies with up to 5 neighbours within 40¨; a detailed description can be found in Driver et al. (2011).

The GAMA Galaxy Group Catalogue (G^3Cv6) was generated using the GAMA-II spectroscopic survey and applying a friend-of-friends (FoF) grouping algorithm; the first version of this catalogue (G^3Cv1) is presented by Robotham et al. (2011) (here after AR11) using the GAMA-I survey. The G^3Cv6 (here after G^3C) catalogue contains a total of 23838 groups with multiplicity $\geq$2 containing 73268 galaxies, this means that $\sim$40% of the GAMA galaxies are assigned to groups.

Here we list and briefly summarise the main G^3C catalogue parameters as described by AR11:

- Nfof: Group multiplicity or number of galaxies contained in the group.
- GroupEdge: Fraction of the group within the survey volume, as estimated from central galaxy and the radius defined by the most distant group member, based on the projected distance from the central galaxy.
- LumBfunc: Group total r-band luminosity down to M_r - 5 $\log h$ = -14 in solar luminosities, times the functional B factor which is a function of Nfof and redshift (see AR11 section 4.4 for details) This parameter is used to estimate the group mass based on luminosity.
- VelDisp: Group velocity dispersion, corrected for the total group velocity dispersion error. This velocity dispersion is measured using the *gapper* estimator introduced by Beers et al. (1990), one advantage of this estimator is that it is unbiased, even for low multiplicity systems, and is robust to weak perturbations in group membership (see section 4.1 of AR11).
- MassProxy: Dynamical group mass estimated using the relation for a virialized system M = A $\times$ R_{50} $\times$ σ^2, where A=1 in Eq. 18 of AR11. A is the scaling factor required to create a median unbiased mass estimate of the dark halo mass and the dynamical mass; however, this is only valid for system in virial equilibrium and the parameter A must be determined considering the match with the mock catalogues (section 4.3 of AR11). R_{50} is the group radius defined by the 50th percentile group member, based on the projected distance away from the central galaxy. And σ is the group velocity dispersion.

To estimate the LFs of galaxies in groups, the G^3C catalogue is matched with the SDSS DR7 data in order to have the Petrosian and model magnitudes with their errors in all five SDSS passbands. Petrosian and model magnitudes were corrected for Galactic extinction following the dust maps of Schlegel et al. (1998).

2.2.1 Completeness

The G^3C sample is selected from the GAMA II survey with a redshift completeness of $\sim$98.5% (Liske et al., 2015), nevertheless, Loveday et al. (2012) found three sources affecting the incompleteness of the sample for GAMA I, the completeness of the input catalogue, completeness of the targets for which spectra have been obtained and the success rate of obtaining spectroscopic redshifts. We have applied the same method to correct this sample applying the updated information of GAMA II.

From each source of incompleteness, a value of completeness is associated, represented by C_{im}, C_{targ} and C_{spec} for imaging, target and spectroscopy success completeness respectively. Every galaxy has associated a weight defined as the reciprocal of the product of the three completeness. For a galaxy i, the weight W_i associated is

$$W_i = 1/(C_{im}C_{targ}C_{spec}) \tag{2.1}$$

2.2.2 K-correction and Subsamples

Since galaxies are observed at different redshifts, a correction to the intrinsic luminosity has to be applied according to the rest frame of the galaxy. All galaxies in this catalogue have been corrected by the so-called K-correction (Humason et al., 1956) using the KCORRECT v4_2 code (Blanton et al. 2003, Blanton and Roweis 2007) considering the SExtractor (Bertin and Arnouts, 1996) AUTO magnitudes reported in ApMatchedCatv06 (Hill et al., 2011). For galaxies in the most local groups ($z \leq 0.1$) we have determined K-corrections at $z_0 = 0.0$ as rest frame; however, when we divide the sample in mass bins, we consider K-corrections in a passband blue-shifted by $z_0 = 0.1$ to study evolution at higher redshifts. A superscript prefix indicates the type of correction (e.g. ${}^{0.1}M_r$).

Magnitude-selected samples always have an associated Malmquist bias because of the missing faint galaxies due to the survey magnitude limit. Tago et al. (2010) studied the consequences of these types of samples extracted from the SDSS and compared with volume-limited samples, however, they found negligible differences between them when working at low redshifts. We have selected three volume-limited subsamples from the absolute r-band magnitude vs z diagram presented in Fig. 2.1. These regions are limited in absolute magnitude by [-17.6, -19.2, -20.4] and in redshift by [0.1, 0.2, 0.3] respectively.

These subsamples are crucial to test for any difference between magnitude or volume - limited samples to study the LFs. The shape of the galaxy group LF estimated using the volume- and magnitude-limited samples presents negligible difference in the same limits of redshift. We show as reference only the corresponding LFs for the sample at $z \leq 0.1$ in Fig. 2.2. The magnitude-limited sample shows a steeper slope due to the cut of data at the faint-end in the volume-limited sample; however this can be seen as a extension to the volume-limited sample. To study the dependence on group richness, the volume-limited sample is used to avoid Malmquist bias. For the rest of this work, we have opted for the magnitude-limited sample in order to gain more galaxies, mainly at the faint end.

To study the dependence of the LFs on group properties, we have selected multiple

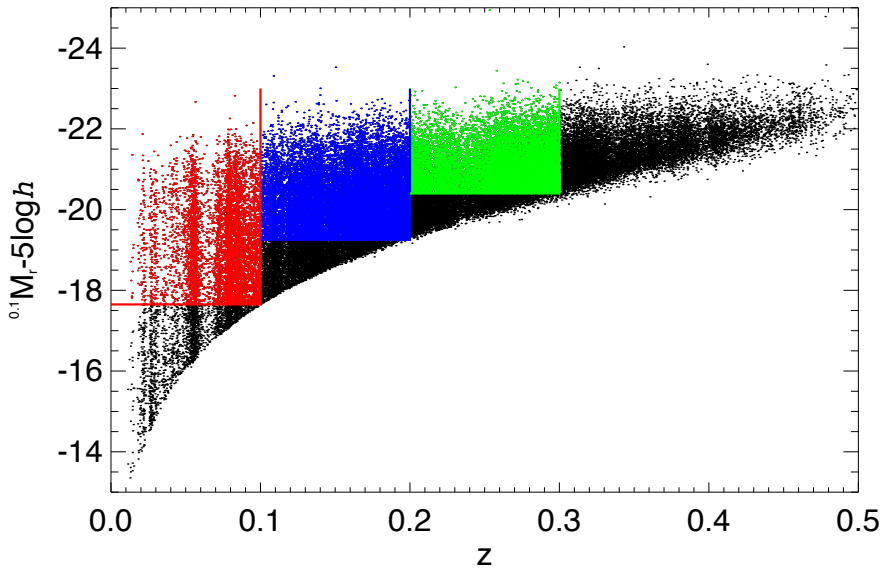

Figure 2.1: Absolute r-magnitude vs z plot for galaxies in the G^3C catalogue. Three volume-limited samples are presented in red, blue and green.

subsamples from the G^3C catalogue based on the number of group members (richness), bins of mass and bins of velocity dispersion, as well as by the galaxy colour and morphology, and a separation in central and satellite galaxies respect to the group.

2.2.3 Colour and Morphology

The G^3C catalogue is separated into red and blue galaxy populations following the method presented by Zehavi et al. (2011), considering the K-corrected $(g-r)$ model colour:

$$^{0.1}(g-r)_{model} = 0.15 - 0.03^{0.1}M_r \tag{2.2}$$

with a small change of the zero-point of 0.21 mag to 0.15 mag in order to have more equal sized subsamples. This colour cut has been well tested by Loveday et al. (2012) at all redshifts, although there is no well-defined blue population at redshifts larger than 0.2, since only the most luminous galaxies are included in our sample at high redshift.

Note that, in order to compare the results in this work with Yang et al. (2009), the colour separation criteria is modified when central and satellite galaxies are compared in Sec 5. This new criteria is followed by Yang et al. (2009) using

$$^{0.1}(g-r) = 1.022 - 0.0651x - 0.00311x^2, \tag{2.3}$$

where $x =^{0.1} M_r - 5\log h + 23.0$.

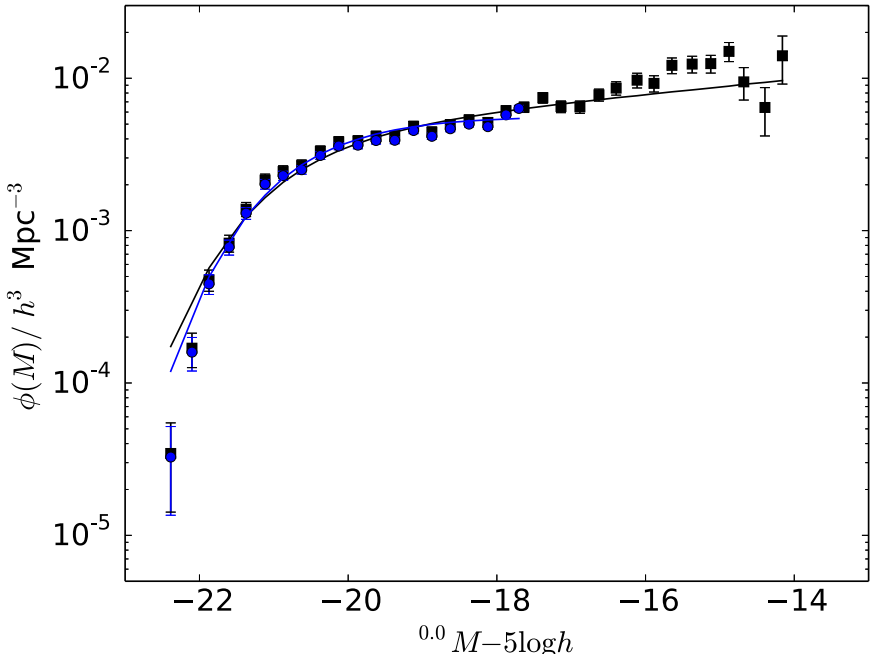

Figure 2.2: Group galaxy LF estimated using the volume-limited sample ($0.002 \leq z \leq 0.1$) in blue and the LF using a magnitude-limited sample over the same redshift range in black. Filled symbols show the non-parametric (SWML) LF and solid lines the corresponding parametric LF. Non-parametric LF is practically the same in both cases. Parametric LFs are slightly different due to data at the faint-end and consequently a steeper slope is seen at the faint-end.

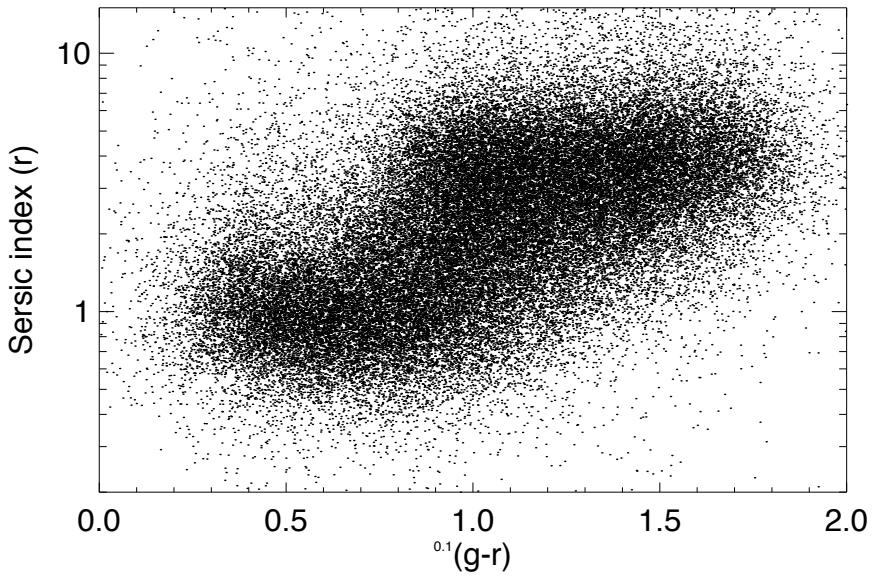

Figure 2.3: Sersic index vs (g-r) colour corrected to a rest frame of z=0.1

Since the morphology of galaxies is fundamental to understanding the behaviour of galaxies at different evolutionary epochs, we are interested in comparing the spheroidal and disky galaxy shapes with the colour. Generally, red colour is associated with galaxies containing a low fraction of dust and low star formation, i.e. early type or spheroidals, while the blue population is usually associated with star forming galaxies or late types, mainly spirals.

Many techniques have been developed to make an objective classification and also to classify hundreds of galaxies automatically (e.g. Huertas-Company et al. 2009), however, these methods work well only with high resolution images. At the moment, GAMA does not have images with enough resolution at $z \geq 0.1$. Simple methods, using the Sérsic index (Sersic, 1968), give a reliable classification at least to distinguish between spheroidal and disk shape galaxies (e.g. Barden et al. 2005). Therefore, we have made a simple classification based on the r-band Sérsic index where galaxies are considered as spheroidals when $n > 1.9$ and disky galaxies when $n < 1.9$. Many authors take the cut to be 2.5 (e.g. Barden et al. 2005); however, Kelvin et al. (2012) show in their Fig. 15, how the Sérsic index distribution in optical and NIR bands, and particularly r-band has a minimum at n=1.9. When we look at the Sérsic index vs colour diagram (Fig. 2.3) for this sample, we identify slightly this separation at 1.9.

2.3 Optical Luminosity Function

We have estimated the LFs considering two non-parametric methods, the 1/Vmax (Schmidt 1968) and stepwise maximum likelihood (SWML, Efstathiou et al. 1988). For each sub-sample considered in this work, we are taking into account a magnitude limit of r<19.8 (GAMA magnitude limit of all three fields) and 60 magnitude bins from M = -25 to M = -10 with ΔM = 0.25 are used over three redshift bins [0.002, 0.1], [0.1, 0.2], and [0.2, 0.3].

When estimating the LF over these kind of restricted redshift ranges, it is important to include just magnitude bins that are fully sampled, otherwise the LF would be underestimated in incomplete sample bins. So, the magnitude limits for each slice were set such that only complete bins are included (Loveday et al., 2012), namely

$M_{faint} < m_{faint}$ - $DM(z_{lo})$ - $K(z_{lo})$,

$M_{bright} > m_{bright}$ - $DM(z_{hi})$ - $K(z_{hi})$,

where m_{faint} and m_{bright} are the flux limits of the survey. The distance modulus is given by $DM(z)$, $K(z)$ is the K-correction for a galaxy with the median spectral energy distribution (SED) of those in the sample, and z_{lo} and z_{hi} are the limits of the redshift slice under consideration. The M_{faint} and M_{bright} denote the absolute magnitude limits of each bin. We have used Poisson errors for non-parametric LF using the 1/Vmax method and an inversion of the information matrix using the SWML method.

2.3.1 Luminosity Function Evolution

To parametrize the evolution of the galaxy luminosity function, we have followed the methods applied by Lin et al. (1999) and Loveday et al. (2012), assuming a Schechter function (Schechter, 1976) in which the characteristic magnitude M^* and galaxy density ϕ^* can vary with redshift, but not the faint-end slope (α). The Schechter function is given by

$$\phi(M) = 0.4 \ln 10 \phi^* (10^{0.4(M^*-M)})^{1+\alpha} \exp(-10^{0.4(M^*-M)}), \tag{2.4}$$

where the Schechter parameters α, M^* and ϕ^* vary with redshift as:

$$\begin{aligned} \alpha(z) &= \alpha(z_0), \\ M^*(z) &= M^*(z_0) - Q(z - z_0), \\ \phi^*(z) &= \phi^*(0) 10^{0.4 P_z}. \end{aligned} \tag{2.5}$$

The redshift z_0 is the same redshift to which magnitudes are K-corrected ($z_0 = 0.1$). Schechter parameters α, $M^*(z_0)$ and $\phi^*(0)$ and evolution parameters Q and P are determined using the maximum-likelihood method described by Lin et al. (1999). The shape

parameters α, $M^*(z_0)$ and luminosity evolution parameter Q are fitted simultaneously and independently of the other parameters, and then the number density evolution P and normalization (ϕ^*) are fitted. These parameters are fitted according to Lin et al. (1999) and Loveday et al. (2012) (see the last reference for a detailed description).

2.4 LF Results

2.4.1 Grouped and Ungrouped LF

The main goal of this work is the characterization of the LF for the galaxies in the G^3C catalogue. Nevertheless, differences between grouped and ungrouped (isolated) galaxies should be considered. We have estimated the LF for the local sample ($z < 0.1$) using the first volume-limited sample in Fig. 2.1. Fig. 2.4 shows the LFs for grouped and ungrouped galaxies in black and blue colours respectively.[1] Grouped galaxies are systematically more luminous than ungrouped ones. This agrees with previous works (e.g. Croton et al. 2005) where they find a clear increment of the number of luminous galaxies in denser environments using the 2dFGRS survey. At the faint end, isolated galaxies dominate over galaxies in groups. This effect can be explained because at the faint end, there is an overpopulation of dwarf galaxies; these types of galaxies are more predominant in isolated environments, without external perturbations (like mergers, tidal effects). If these same galaxies were part of a dense environment like a group, an imminent merger can destroy this galaxy and it would become part of another brighter system. On the other hand, this effect could also be the *nature* of these galaxies (e.g. Xu et al. 2012).

2.4.2 Dependence of the LF on mass

The mass estimation of the G^3C catalogue is based on the group velocity dispersion and radius, by AR11 (section 4.3 in their work). However, the mass estimation of the dark matter halo, where the group in contained, can be calculated following the dynamical mass, but Han et al. (2015) present a better estimator based on galaxy lensing (here after 'luminosity mass'). Appendix 2.8.2 shows a test between the dynamical and lensing methods and the halo mass from the mock galaxy catalogues used by AR11; which were taken from the Millennium DM simulation (Springel et al., 2005).

In order to investigate the LF and its dependence on mass, the G^3C catalogue was divided in 3 representative mass bins (based on the luminosity mass) to explore the low

[1] Note for a volume-limited sample, a simple estimation of the LF is enough; however the SWML is applied to be consistent with the rest of this work.

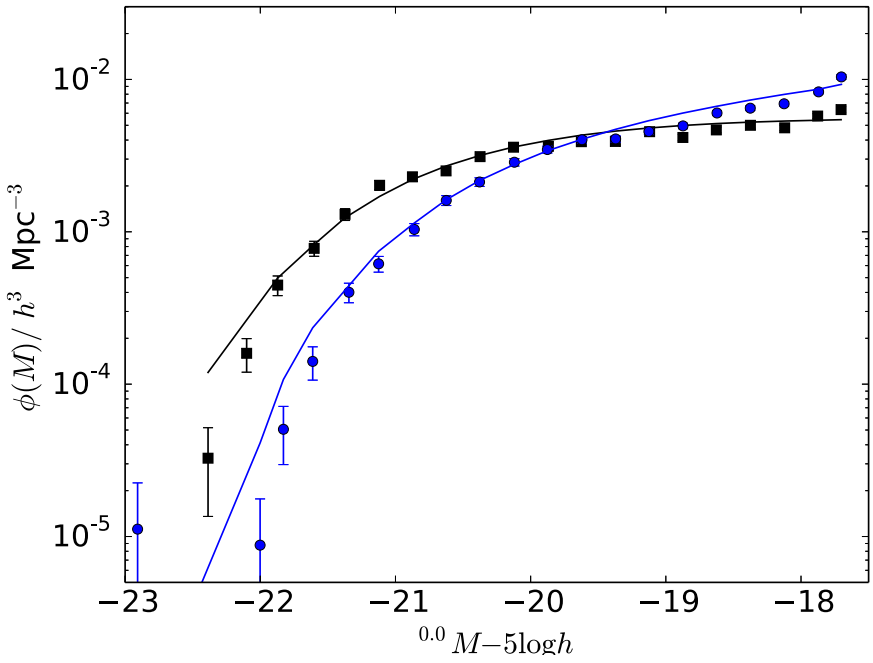

Figure 2.4: LFs are presented for grouped and ungrouped galaxies in black and blue colours respectively for a local volume-limited sample. Filled symbols show the results using the SWML method and solid lines correspond to the parametric LF.

mass, characteristic and massive galaxy groups. GAMA provides the opportunity to explore with more detail the low mass range than any other previous study; therefore, the mass limits are: $8 < \log M/M\odot \leq 12.06$ (low), $12.06 < \log M/M\odot \leq 12.70$ (middle) and $12.70 < \log M/M\odot \leq 16$ (high). These limits were set such that there is a similar number of galaxies in each bin up to z<0.1, avoiding large Poisson uncertainties at the bright end (Table 2.1).

The first row in Fig. 2.5 shows the galaxy group LFs in the three mass bins listed above up to z≤0.1. These LFs are presented from the low to high mass bin in the 2nd, 3rd and 4th column respectively.

There is a significant difference at the faint end, where even with large error bars, faint galaxies in massive groups tend to be rarer than those in groups with low mass, as the α becomes flatter at middle and high masses. On the other hand, there is a higher number of bright galaxies in the high mass bin, as there was expected and the M^* decreases at higher masses.

The corresponding Schechter fit values for α and M^* are presented in Table 2.1. Due to the overlapping of these values considering 1-σ error bars, we have estimated the number density of galaxies (n [Mpc^{-3}]) in three regions of absolute magnitudes, this test has the advantage of not assuming a parametric form, to check if there is significant difference between LFs at bright, middle and faint-end regions. Table 2.1 also presents the number density for the three intervals of mass and absolute magnitude.

We can observe differences between the number galaxy density and the mass bins as a function of the absolute magnitude (Fig. 2.6). For middle and faint-end regions n decreases as mass rises; however, at the bright-end this tendency becomes positive. These tendencies can vary according to the limits imposed. The limits, to estimate the number galaxy density, were chosen trying to separate the bright region after the M^* from the middle magnitudes and the faintest magnitudes just close to the faint end.

Since the group mass is related to the velocity dispersion and radius, there is a linear correlation between mass and velocity dispersion as seen in Fig. 2.7. Then the LF dependence on velocity dispersion is similar to the mass dependence; this analysis is presented in Appendix 2.8.1.

Colours and morphology.

LFs for blue and red galaxies in groups of different mass are shown in the second and third rows of Fig. 2.5. From the first column (all grouped galaxies) it is clear that red galaxies

Table 2.1: Number of grouped galaxies within mass bins of the local G^3Cv6 catalogue (z<0.1) and the Schechter parameters α and M^*, and the number density for the three absolute magnitude intervals.

sample	bin log$M/M\odot$	$N_{galaxies}$	α	$^{0.1}M^*$-5log h	$^{0.1}M$-5log h -23 − -21 ($n\times$10 000)	$^{0.1}M$-5log h -21 − -17 ($n\times$100)	$^{0.1}M$-5log h -17 < ($n\times$10)
All	Low mass (8-12.06)	2622	-1.29 ± 0.14	-20.45 ± 0.31	2.99 ± 0.55	8.62 ± 0.20	1.34 ± 0.08
	Middle mass (12.06-12.70)	2607	-0.81 ± 0.17	-20.34 ± 0.18	4.36 ± 0.39	3.99 ± 0.06	0.35 ± 0.03
	High mass (12.70-16)	2593	-0.91 ± 0.14	-20.71 ± 0.22	10.35 ± 0.64	2.95 ± 0.03	0.19 ± 0.02
Blue	Low mass (8-12.06)	1925	-1.41 ± 0.17	-20.16 ± 0.44	0.89 ± 0.26	6.21 ± 0.17	1.29 ± 0.01
	Middle mass (12.06-12.70)	1431	-1.09 ± 0.19	-20.33 ± 0.36	1.23 ± 0.24	3.52 ± 0.01	0.56 ± 0.05
	High mass (12.70-16)	898	-1.14 ± 0.29	-20.12 ± 0.65	1.81 ± 0.43	3.30 ± 0.01	0.64 ± 0.11
Red	Low mass (8-12.06)	679	-0.47 ± 0.55	-19.88 ± 0.31	1.76 ± 0.42	2.37 ± 0.09	0.09 ± 0.01
	Middle mass (12.06-12.70)	1155	-0.10 ± 0.35	-19.99 ± 0.17	2.43 ± 0.31	1.29 ± 0.05	0.03 ± 0.01
	High mass (12.70-16)	1675	-0.64 ± 0.18	-20.51 ± 0.20	4.83 ± 0.51	1.13 ± 0.04	0.02 ± 0.00
Spiral	Low mass (8-12.06)	1460	-1.34 ± 0.22	-20.06 ± 0.44	0.68 ± 0.23	4.82 ± 0.15	0.89 ± 0.07
	Middle mass (12.06-12.70)	1254	-1.01 ± 0.21	-20.13 ± 0.34	0.70 ± 0.17	2.91 ± 0.07	0.28 ± 0.03
	High mass (12.70-16)	987	-0.93 ± 0.33	-19.53 ± 0.40	0.90 ± 0.26	3.54 ± 0.10	0.38 ± 0.05
Ellip	Low mass (8-12.06)	560	-0.80 ± 0.54	-20.35 ± 0.48	1.04 ± 0.28	1.90 ± 0.04	0.12 ± 0.02
	Middle mass (12.06-12.70)	845	0.17 ± 0.56	-19.91 ± 0.18	2.06 ± 0.31	0.92 ± 0.05	0.02 ± 0.00
	High mass (12.70-16)	966	-0.42 ± 0.32	-20.54 ± 0.24	3.97 ± 0.49	0.66 ± 0.03	0.01 ± 0.00
Mock	Low mass (8-12.06)	3219	-1.02 ± 0.05	-20.71 ± 0.06	20.90 ± 0.56	9.98 ± 0.06	1.38 ± 0.05
	Middle mass (12.06-12.70)	1815	-1.15 ± 0.04	-20.89 ± 0.13	24.75 ± 0.81	10.37 ± 0.09	2.05 ± 0.06
	High mass (12.70-16)	2179	-1.13 ± 0.04	-20.73 ± 0.11	17.88 ± 0.73	13.71 ± 0.11	2.21 ± 0.14

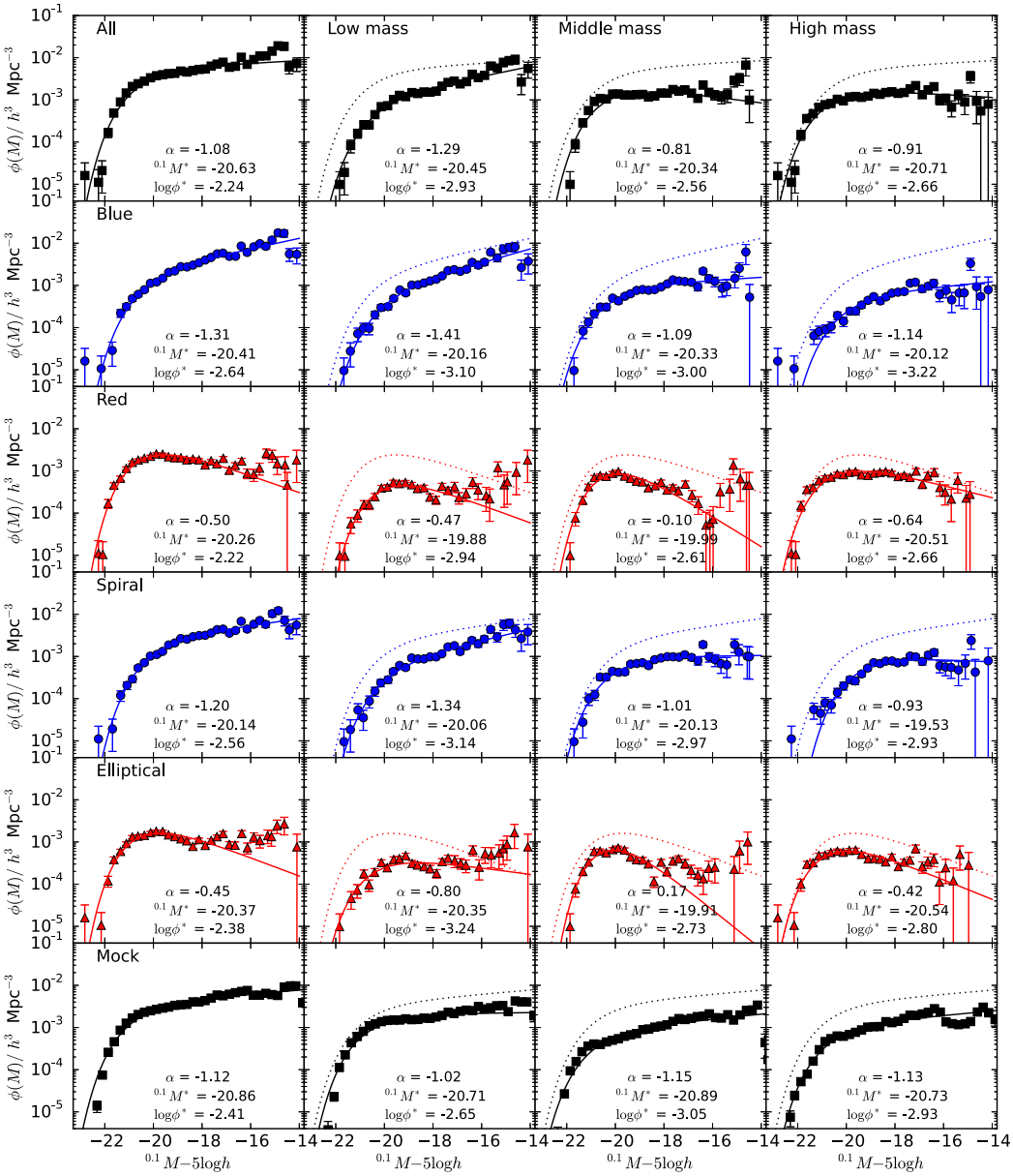

Figure 2.5: Estimation of the LF for all galaxies in groups (first column) and divided in 3 mass group bins (at $z \leq 0.1$): $8 < \log M/M\odot \leq 12.06$ (low mass; 2nd column), $12.06 < \log M/M\odot \leq 12.70$ (middle mass; 3rd column) and $12.70 < \log M/M\odot \leq 16$ (high mass; 4th column). From the top to the bottom, the galaxies in groups have been divided in blue and red colours, spiral and elliptical morphology and as a comparison the corresponding LF using the mock catalogues described in Appendix 2.8.2. The solid line corresponds to the best Schechter fit. Dotted-line show as comparison the LF in the first column for each row.

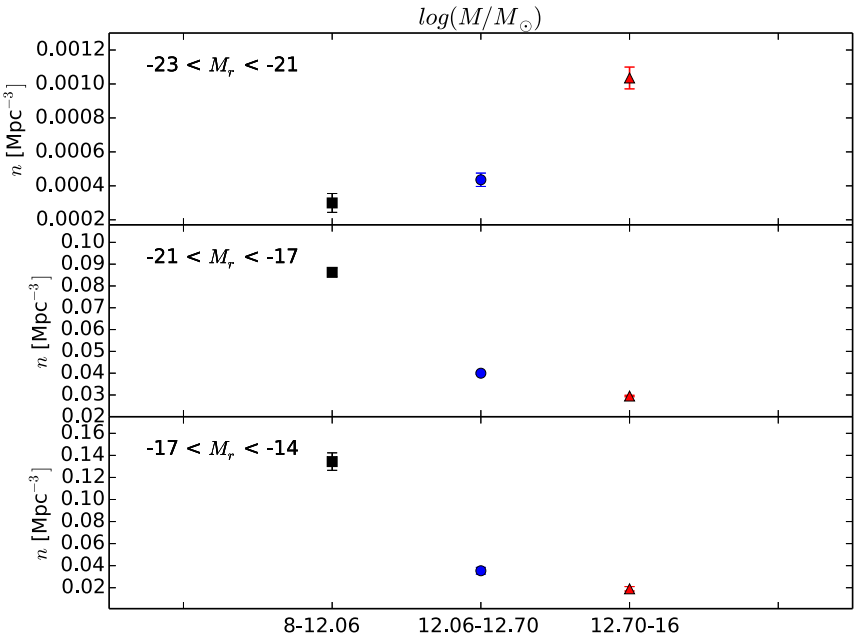

Figure 2.6: Number density ($n[Mpc^{-3}]$) of galaxies integrating the LFs over three bins of absolute magnitude [-23,-21], [-21, -17] and [-17 < -14] in descending order respectively, for the three subsamples of masses in ascending order in black, blue and red respectively.

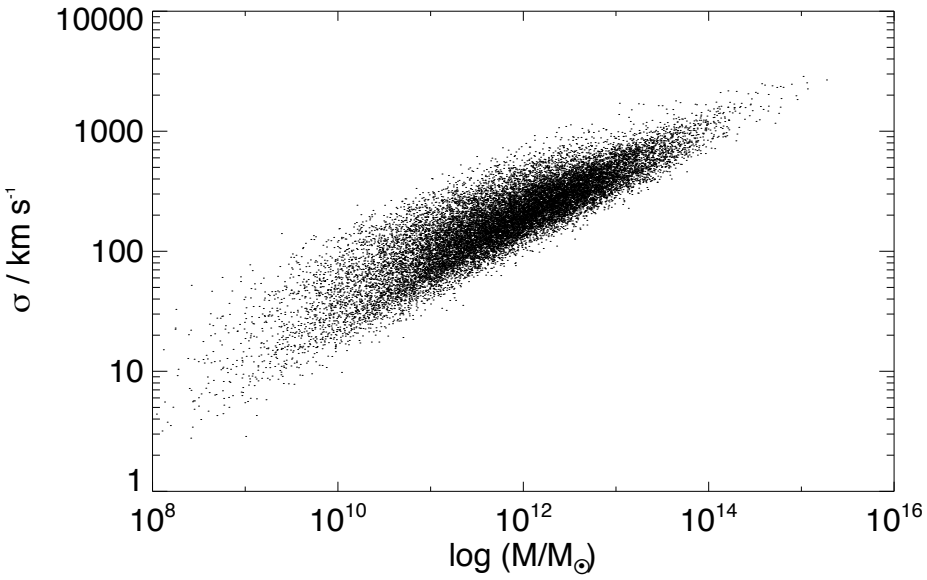

Figure 2.7: Relationship between log(σ) and log($M/M_\odot$) of groups in the G^3C catalogue

dominate over blue galaxies at the bright end and vice versa at the faint end, as reported by other authors (e.g. Yang et al. 2009). This behaviour is repeated for all the mass bins. The most obvious difference in the blue LFs is at the faint end, becoming flatter as the mass increases, meaning a lack of faint blue galaxies in massive groups. Conversely, the density of luminous red galaxies increases in massive groups. These results are presented in Table 2.1. The total LF in high mass groups is thus dominated by red galaxies. The rise in density of faint red galaxies in low and middle mass groups may partly be due to some of these objects being dust-reddened spiral galaxies, (Driver et al., 2012).

While classifying galaxies by Sersic index, as described in section 2.2.3, should be better than colour at separating ellipticals and dust-reddened spirals, the Sersic classification is just 70% reliable when comparing with a classified subsample for around 5000 galaxies, mainly from the Galaxy Zoo catalogue (Lintott et al. 2008, Lintott et al. 2011).

Fig. 2.5 presents the LFs for grouped spiral and elliptical galaxies in the 4th and 5th rows respectively. Due to the relationship between colour and morphology, these LFs follow the same tendencies found for colour. Red or early-type galaxies tend to be brighter than blue ones in most of the samples, whereas blue and late-type galaxies clearly dominate the faint end; the combination of both of them returns the total LF. We still see a faint-end turn-up in the densities of elliptical galaxies in low and middle mass groups, suggesting that this effect is not entirely due to dust-reddened spiral galaxies.

Mock catalogues

As a comparison, the bottom of Fig. 2.5 shows the corresponding LF using the mock catalogues described in Appendix 2.8.2. It is very hard to distinguish any significant difference between these LFs. The only interesting feature is presented at the faint-end in the high mass bin where there is a dip at $M_r \sim -15.5$. This could be an effect of the simulation resolution. McNaught-Roberts et al. (2014) do not present this feature due to the faintest of theirs samples are down to -17.8, so, not way to observe it. The mock LF parameters (α and M^*) agree with observations into one error bar, but at the high mass bin the agreement in much better. This test the good quality of the mock catalogues at high masses but with some unsolved issues for the low mass regime.

Comparison

Up to now, there is no similar study of the LF and the dependence with group properties, in the redshift intervals we are presenting, we can compare directly with. However, we can

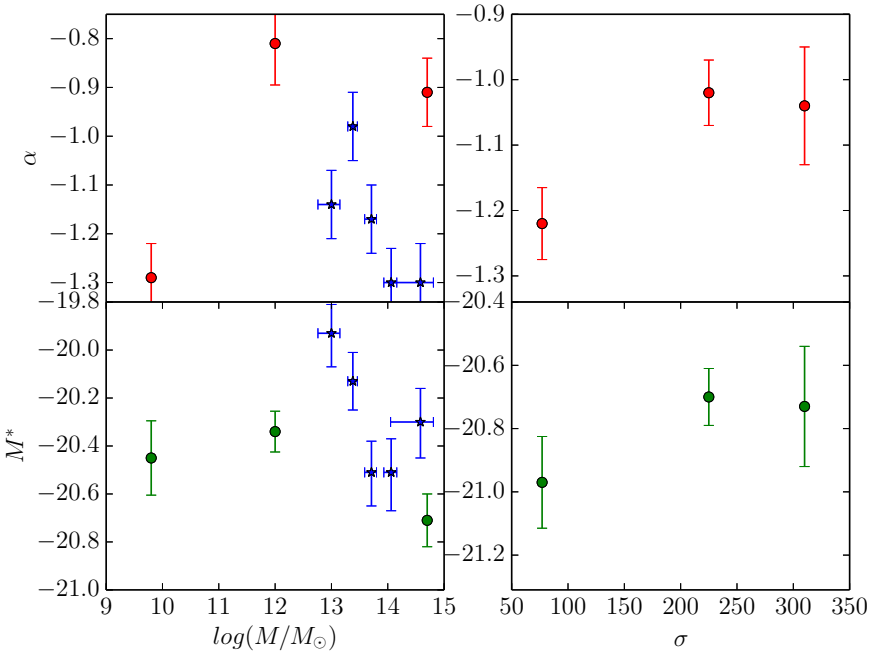

Figure 2.8: Schechter parameters α (upper panels; red dots) and M^* (lower panels; green dots) with 1-σ error bars corresponding to the interval of mass (left panels) and velocity dispersion σ (right panels) at $z < 0.1$. Blue stars shows the values found in Robotham et al. (2010).

verify the trends of the Schechter parameters (α and M^*) presented by other authors (e.g. Zandivarez et al. 2006, Robotham et al. 2010) on mass dependency of groups up to $z = 0.1$. We compare our results to Robotham et al. (2010) in Fig. 2.8 (including the velocity dispersion results); upper panels and red dots shows the relation of α with bins of mass and σ, and lower panels in green dots, the dependency of M^* with mass and σ; 1-σ error bars are plotted. Blue symbols (stars) are the results found by Robotham et al. (2010); these authors do not find a clear correlation between Schechter parameters and mass; however, there would be a negative tendency of α and M^* as mass bin increases but no clear correlation is found due to the large error bars. Nevertheless, we cannot talk about a correlation between α and mass or the velocity dispersion, but we can infer a negative tendency between M^* with both properties, mass and velocity dispersion, meaning the expected result, high luminous galaxies are located in massive groups or with high velocity dispersion. The main contribution here are the Schechter parameters (α and M^*) given at the very low mass regime.

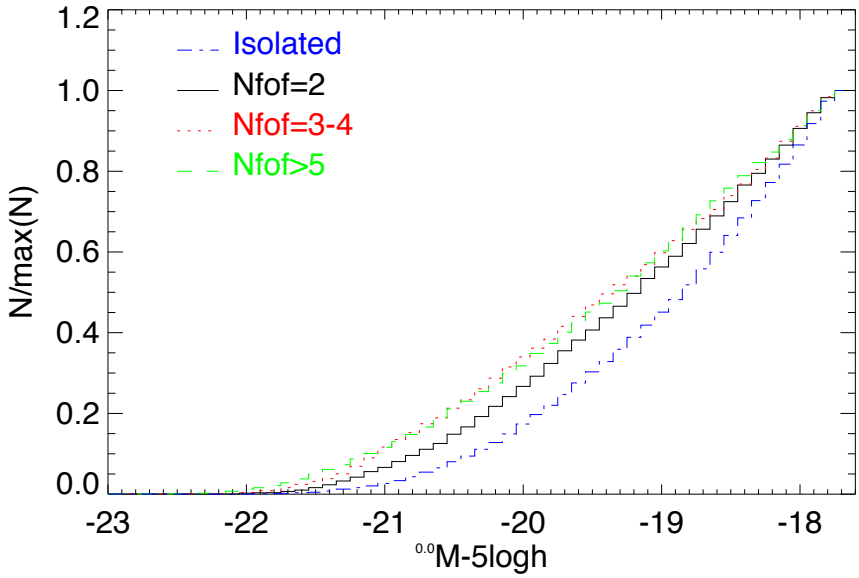

Figure 2.9: Cumulative distribution in absolute r-magnitude for galaxies in groups of richness (2, 3-4 and >5) in black, magenta and green respectively and ungrouped galaxies are presented in cyan colour.

2.4.3 Dependence on Richness

For the richness dependency of the LFs, we consider only the most local volume-selected sample (up to z ∼0.1), split into three richness bins: $N_{\rm FOF} = 2$, $N_{\rm FOF} = 3$-4 and $N_{\rm FOF} \geq 5$.

Fig. 2.9 presents the cumulative distribution of absolute r-magnitude (M_r) in richness bins, including those ungrouped galaxies. Because we are interested in observing differences in the LF at different richness, we would expect to see statistical differences in these cumulative distributions. To test these differences or similarities, we have applied the Kolmogorov-Smirnov test ($K-S$ test; Table 2.2); isolated galaxies are significantly different to the rest, nevertheless for those in the middle ($N_{\rm FOF} = 3$-4) and high ($N_{\rm FOF} > 5$) bins, the probability to come from the same distribution is ~ 0.38; meaning a insignificant difference between these distributions.

We present the relation between richness, mass and redshift for the local volume limited-sample in Fig. 2.10; the top left-hand panel does not show any clear dependence between richness in groups with z. There are some regions although, with just a few galaxies, but this is attributed to large scale structure as we can see directly from Fig. 2.1. The top right-hand panel presents $N_{\rm FOF}$ vs $\log(M/M_{\odot})$ of the groups. It is no surprise to

Table 2.2: Comparison of the M_r cumulative distribution normalized to 1. Column 2 gives the maximum distance between these distributions and Column 3 the probability of coming from the same distribution applying the $K-S$ test.

Distributions	distance	Prob
$N_{\rm FOF}=2$ – $N_{\rm FOF}=$ 3-4	0.077	5.36E-06
$N_{\rm FOF}=2$ – $N_{\rm FOF}\geq 5$	0.067	1.91E-05
$N_{\rm FOF}=$ 3-4 – $N_{\rm FOF}\geq 5$	0.026	0.44
$N_{\rm FOF}=2$ – isolated	0.117	8.54E-23

find the richest groups to be massive; but the number of groups with just 2 or 3 members covers the entire range of masses, meaning the presence of small groups with very low mass galaxies and small groups with massive galaxies. The bottom panel plots $\log(M/M_{\odot})$ vs z; there is no clear correlation between these two parameters as we would expect in a volume-limited sample.

Fig. 2.11 shows the relationship between richness and group mass. This distribution presents the number of groups for the 3 richness subsamples in mass bins, from the lowest to highest richness bin in black, magenta and green respectively. As expected, these histograms show that as groups increase in richness, they tend to be more massive; but it does not mean that poor groups cannot be massive as well.

Similar to Fig. 2.5, Fig. 2.12 presents the LFs in colours and morphology separated this time in 4 richness bins, $N_{\rm FOF}=2$, $N_{\rm FOF}=3$, $N_{\rm FOF}=4$ and $N_{\rm FOF}\geq 5$.

For every row in Fig. 2.12, the shape of the LF does not change significantly with richness, except of a systematic dispersion due to the number of galaxies in each panel. For the 2nd and 3rd rows, there is a similar number of blue and red galaxies at the bright end, meanwhile the faint end is dominated completely by the blue population, meaning a significant blue population in the group outskirts.

In terms of morphology, the spiral and elliptical LFs do not change their shape with richness. In this case is clear how the ellipticals dominate the bright end and the spirals the faint end. Bright galaxies are mainly ellipticals as expected, and since central galaxies are mostly the brightest galaxy in the group, then the central galaxies are mainly ellipticals, but not necessarily red.

When comparing the mocks LF and real data, the M^* follows the same tendency; this becomes brighter as richness increases. This means there are brighter galaxies in groups with more members or high densities as other works have showed (e.g. Croton et al.

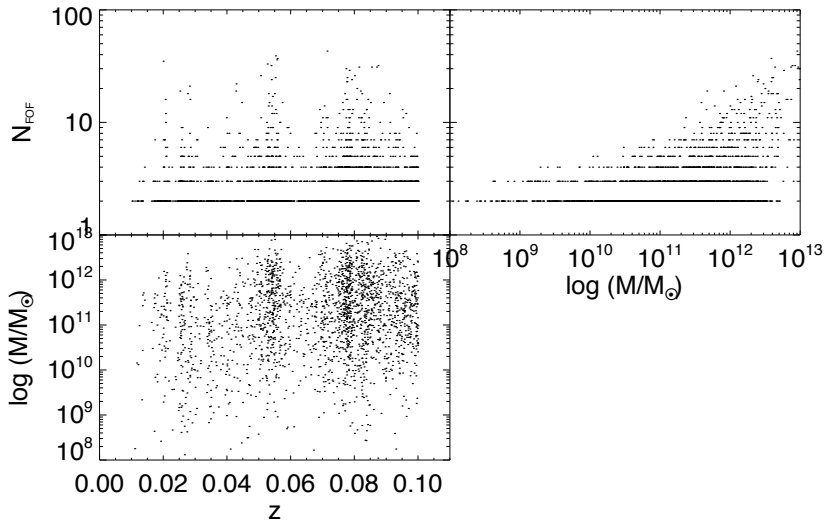

Figure 2.10: Relation between richness, mass and redshift for groups in the local volume-limited sample (z $\leq$ 0.1). Top left-hand panel shows richness-z relationship for galaxies in groups. Top right-hand panel presents the richness-log($M/M_\odot$) correlation and bottom panel the log($M/M_\odot$)-z relationship.

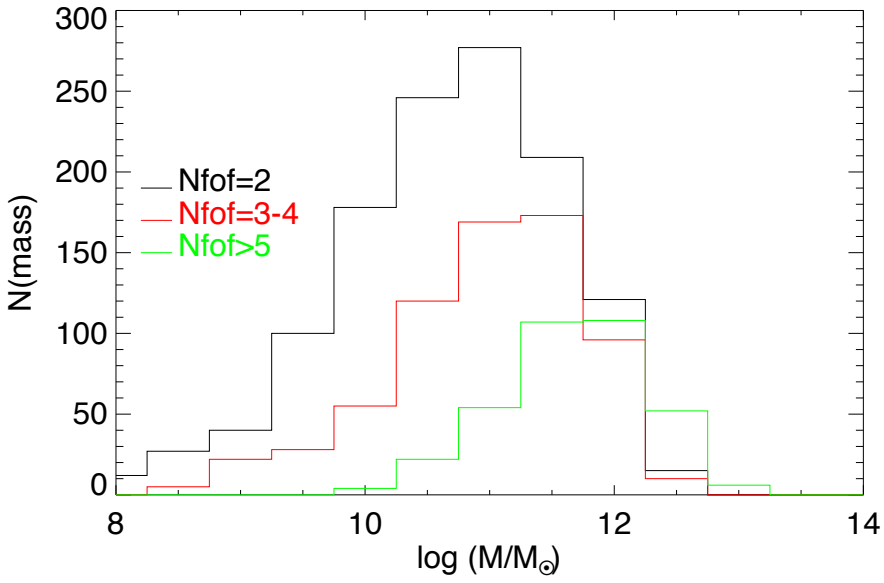

Figure 2.11: Histogram of mass in different bins of richness (number of members, Nfof) 2, 3-4 and 5 $\geq$ in black, magenta and green respectively for groups at z$\leq$0.1.

2005, McNaught-Roberts et al. 2014). α tends to be steeper as the richness increases in simulations; however this is not clear with real data where the large error bars (see Fig. 2.13) do not allow to agree to deny this tendency.

Fig. 2.13 compares the Schechter parameters α and M^* with the group richness divided by colour (2 top panels) and morphology (2 bottom panels). At the bright-end, red galaxies are mainly located in groups with richness $N_{\rm FOF} = 5$; however, for spirals is not clear even when the Schechter fit suggests the brightest spiral galaxies are contained into$N_{\rm FOF} = 4$ groups. On the other hand, α and M^* follows similar tendency between blue and the combined sample, meanwhile for red galaxies are not completely clear due to large error bars. As expected, blue galaxies dominate the LF faint-end for all richness and the bright-end is surprisingly dominated by blue galaxies at all richness.

McNaught-Roberts et al. (2014) find a tendency between α and the environment density for colours. α becomes more negative at higher densities for the red population and an apparent constant value for blue population at all richness. Even when they applied another method to define density, based on concentric spheres, Fig. 2.13 shows the same tendencies.

When comparing M^* and density, McNaught-Roberts et al. (2014) find a clear tendency, M^* becomes brighter as density increases for red and blue galaxies using the GAMA data. Looking at Fig. 2.13, the same tendency is followed either by red or blue galaxies, being less evident for the last ones. Then, the Schechter parameters follow the same tendencies in function of the density, independently of what density method is used, the group richness or concentric spheres.

For the morphology separation, there is no clear correlation between α and $N_{\rm FOF}$, in agreement with the results reported by Cuesta-Bolao and Serna (2003), even when they consider groups with $N_{\rm FOF} \geq 3$. Contrarily to colours, M^* is brighter for ellipticals, as expected following the idea that central galaxies are dominated by ellipticals.

In a very broad analysis, considering morphology, mass and richness, we find that elliptical galaxies are located in massive groups (median $\sim 5.43 \times 10^{11} M/M_{\odot}$), whereas spiral galaxies are contained in groups with lower mass with median of $\sim 1.94 \times 10^{11} M/M_{\odot}$ at the bright end of the LF ($M_r <$ -20). For the faint end ($M_r >$ -18), this fact is the same, nevertheless, differences between the medians of the two normalized distributions of mass is only about $1.1 \times 10^{11} M/M_{\odot}$ and the shift in the median with respect to the bright region is displaced to lower masses; this shows massive groups, besides contains brighter galaxies than groups with lower mass, also are dominated by elliptical galaxies. This

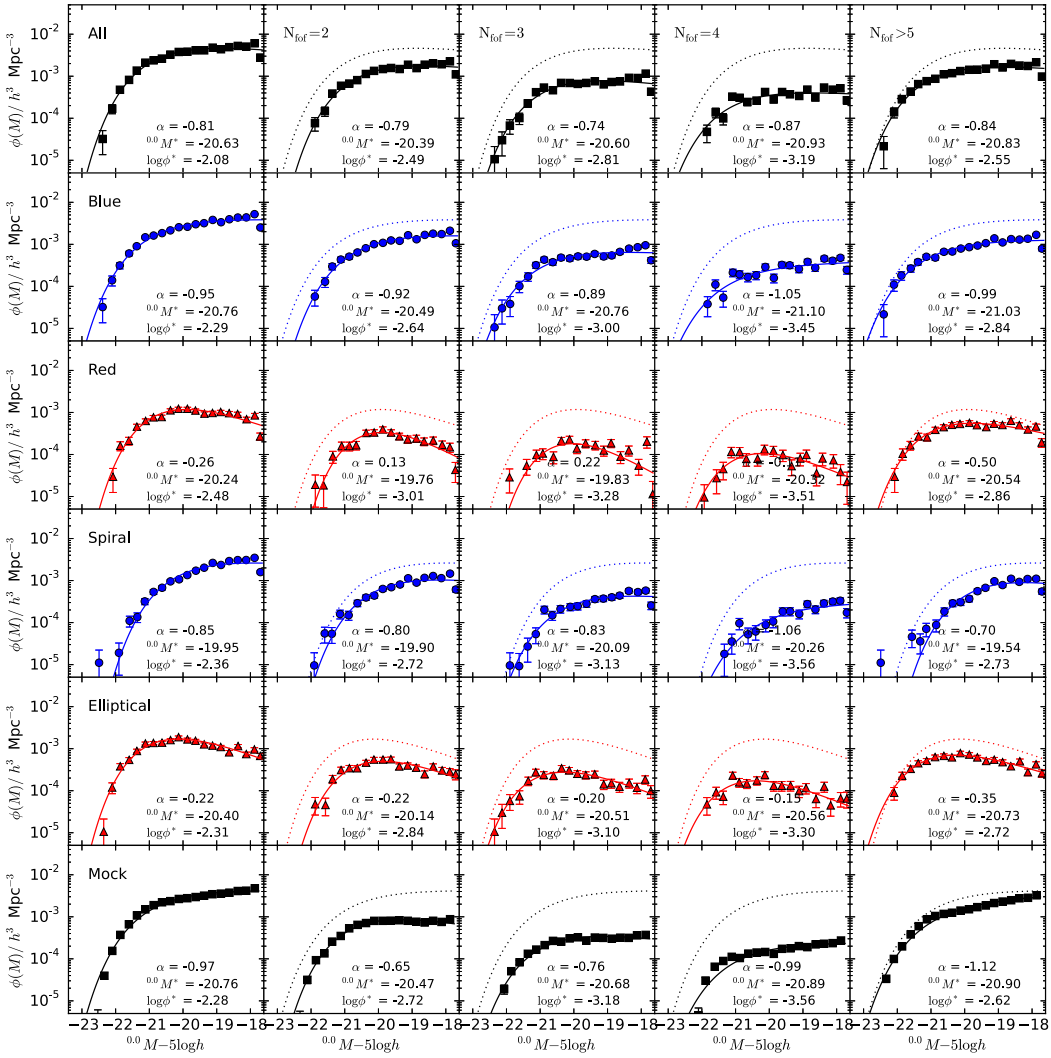

Figure 2.12: LF for all galaxies in groups (1st row), blue and red samples (2nd and 3rd rows), spiral and elliptical morphology (4th and 5th rows) and the mock catalogue in four richness bins: $N_{\rm FOF} = 2$ (2nd column), $N_{\rm FOF} = 3$ (3rd column), $N_{\rm FOF} = 4$ (4th column) and $N_{\rm FOF} \geq 5$ (5th column). As a comparison, the dotted line shows the LF from the first column for each row respectively.

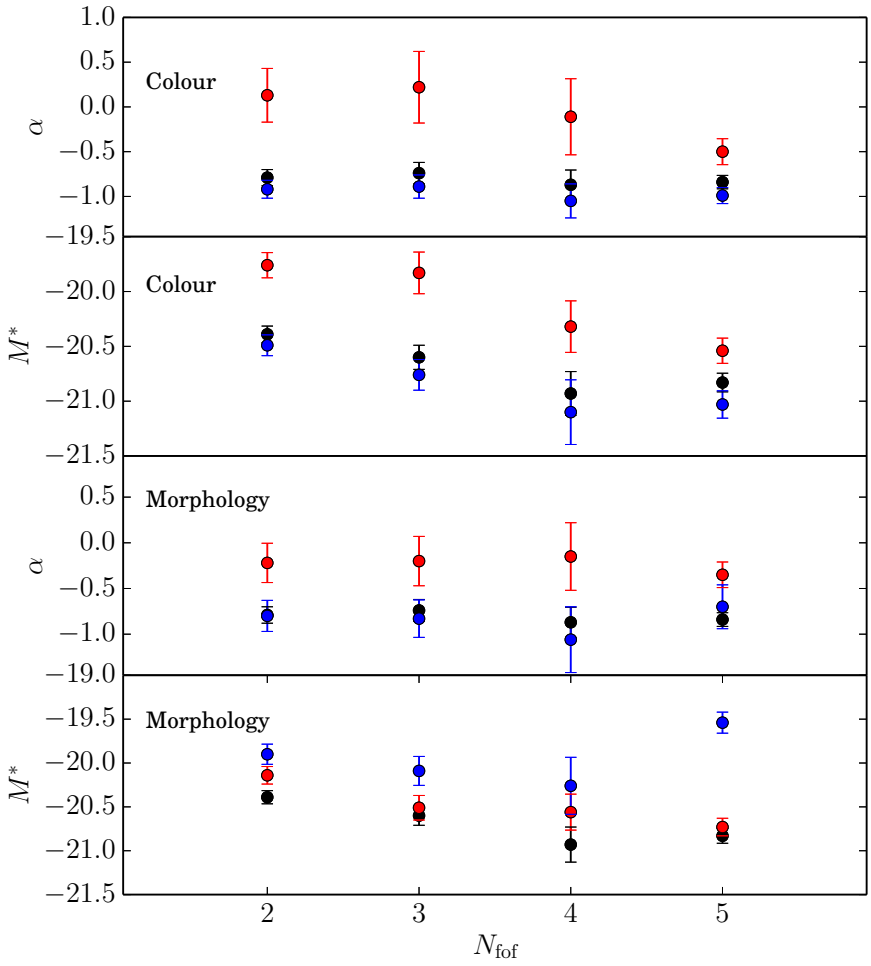

Figure 2.13: Schechter parameters α and M^* with 1-σ error bars for different $N_{\rm FOF}$ for all(black), red (elliptical) and blue (spiral) galaxies in groups in the 2 top (bottom) panels.

analysis has to be carried out with more detail considering only volume-limited samples.

2.5 Central and Satellite galaxies

Another analysis of the LF was carried out between central and satellite galaxies and their dependence with galaxy group richness. Central and satellite galaxies are divided according to AR11 (sec. 4.2.1). Briefly, AR11 select the central galaxy applying an iterative procedure, where at each step the centre of light (in the r-band) is identified and the most distance galaxy is eliminated. When there are only two galaxies remaining, the brighter galaxy will be considered as the group centre.

Fig. 2.14 shows the LFs for all grouped, central and satellite galaxies divided by colour (this separation is based on the Yang et al. (2009) colour separation), similar to previous section, up to z=0.1. The best fit for these LFs can be seen in Table 2.3. Red central galaxies dominate the bright end (M <-20) even when the M^* for red central and red satellites is the same into an error bar. There is a significant difference at the faint end where blue galaxies dominate at M >-20; however, at M ∼-17 red galaxy LF apparently arises again but this is not clear due to large error bars; as a comparison, Yang et al. (2009) results are plotted in crosses following the same colours. Yang et al. (2009) find that at the very faint end, the number of red central galaxies tends to be even bigger than the number of blue galaxies. This apparent raising can be explained if mass accretion can be truncated into small halos due to the large scale tidal field as Wang et al. (2007) find, then central galaxies in this small halos are expected to be red. Another explanation is following Ludlow et al. (2009), they find that some subhalos, present near to the large virialized progenitor halo, can lose their gas due to tidal forces and consequently star formation stops and galaxies tend to be red, more recently Wetzel et al. (2014) support this idea using SDSS groups and N-body simulations.

Yang et al. (2009) show very similar shapes for red and blue satellite galaxies LFs, this is far from our results. In Fig. 2.14, there are clearly more red satellite galaxies for magnitudes M <-20.0 and more blue satellite galaxies at M >-20.0. There is again an increment of the number of red galaxies at the faint end. This can be caused by similar reasons given for central galaxies since satellite galaxies belong to the same subhalo.

Mock catalogue results show a similar LF shape with the GAMA data more than that presented by Yang et al. (2009). A possible reason of this difference could be the separation criteria between central and satellite galaxies. AR11, as mentioned above, is based on the group luminosity, meanwhile Yang et al. (2009) separation is based on the

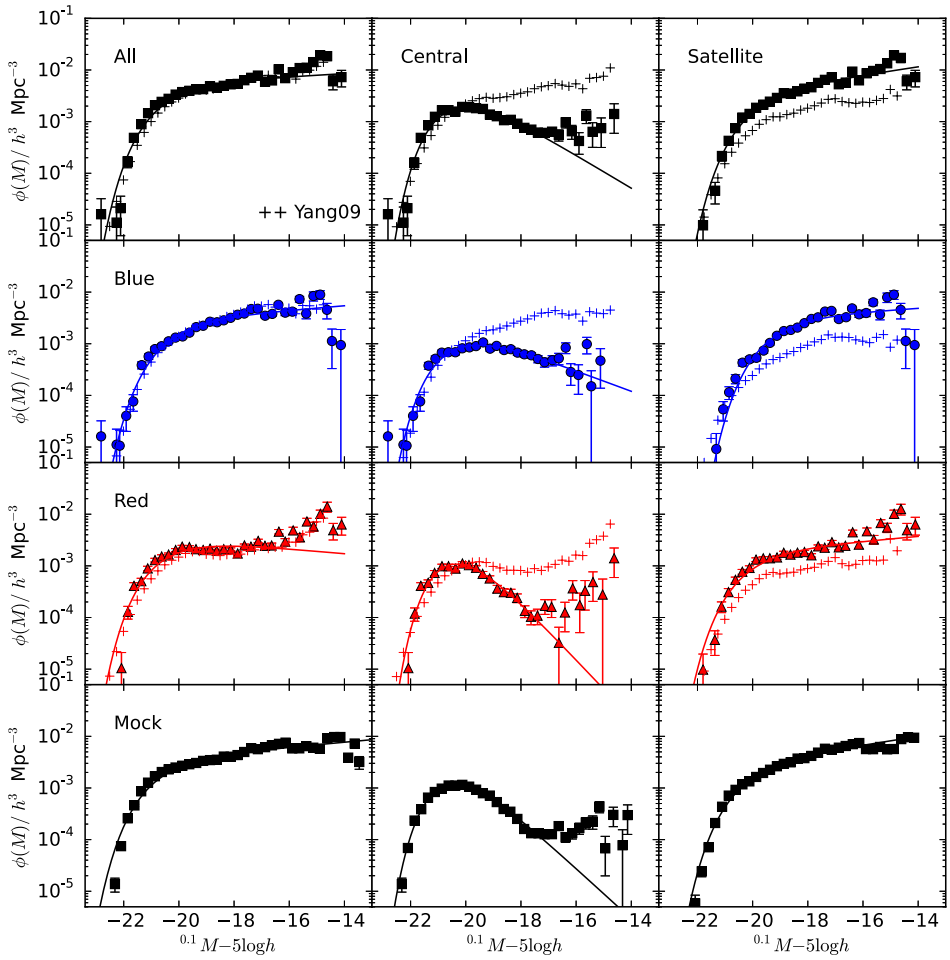

Figure 2.14: LF divided by colour, red (3rd row), blue (2nd row) and combined (1st row) for all the sample (1st column), central (2nd column) and satellite (3rd column) galaxies up to z=0.1. The mock LF is presented in the 4th row. As comparison, crosses show the LFs obtained by Yang et al. (2009) with the same colour code.

Table 2.3: The best LF fit-parameters for all, central and satellite galaxies divided by colour and compared with the mock catalogue

Galaxy	colour	α	$^{0.1}M^*$-5lg$h$	$\log \phi^*/h^3$ Mpc^{-3}
All	Combined	-1.08 ± 0.08	-20.63 ± 0.12	-2.23 ± 0.03
	Blue	-1.11 ± 0.09	-20.43 ± 0.22	-2.51 ± 0.05
	Red	-0.88 ± 0.15	-20.56 ± 0.15	-2.42 ± 0.04
	Mock	-1.12 ± 0.03	-20.86 ± 0.05	-2.41 ± 0.01
Central	Combined	-0.20 ± 0.20	-20.23 ± 0.12	-2.26 ± 0.05
	Blue	-0.50 ± 0.23	-20.30 ± 0.20	-2.63 ± 0.06
	Red	0.42 ± 0.37	-19.97 ± 0.14	-2.53 ± 0.07
	Mock	0.22 ± 0.15	-20.18 ± 0.05	-2.47 ± 0.02
Satellite	Combined	-1.20 ± 0.09	-20.06 ± 0.17	-2.39 ± 0.04
	Blue	-1.09 ± 0.15	-19.39 ± 0.25	-2.46 ± 0.06
	Red	-1.12 ± 0.16	-20.24 ± 0.22	-2.69 ± 0.06
	Mock	-1.21 ± 0.03	-20.35 ± 0.06	-2.49 ± 0.02

most massive galaxy to be the central galaxy. In spite of these authors mention, luminosity or mass based definitions, both yield indistinguishable results, there is a clear difference in this case supported by the mock catalogues.

In Fig. 2.15 we have divided central and satellite galaxies according to their group richness, $N_{\rm FOF} = 2$ (black), $N_{\rm FOF} = 3$-4 (blue) and $N_{\rm FOF} \geq 5$ (red). Similar to Fig. 2.12 in Section 2.4.3, there are more bright galaxies in rich groups than in groups with lower multiplicity and contrarily at the faint end, either for central or satellite galaxies.

2.6 Luminosity function evolution.

We estimate the evolution of the galaxy LF considering Eq. 4 (Lin et al., 1999) for the three mass bins discussed above (for the velocity dispersion analysis see Appendix 2.8.1).

Fig. 2.16 presents the evolution of the galaxy LFs separated by three mass bins (from low to high mass groups in black, blue and red respectively), in three redshift ranges [0.002, 0.1], [0.1, 0.2] and [0.2, 0.3]. The inset in the top panels shows two-σ likelihood contours for the Schechter parameters α and M^* obtained from the parametric LF. Looking at this plot, the correlation between α and M^* is clear. Insets in middle and bottom panels show M^* likelihood ratios, normalised to peak at log L = 0; α is fixed to the value at $z \leq 0.1$ according to the evolution model. The 1-σ likelihood in one dimension for the parameter

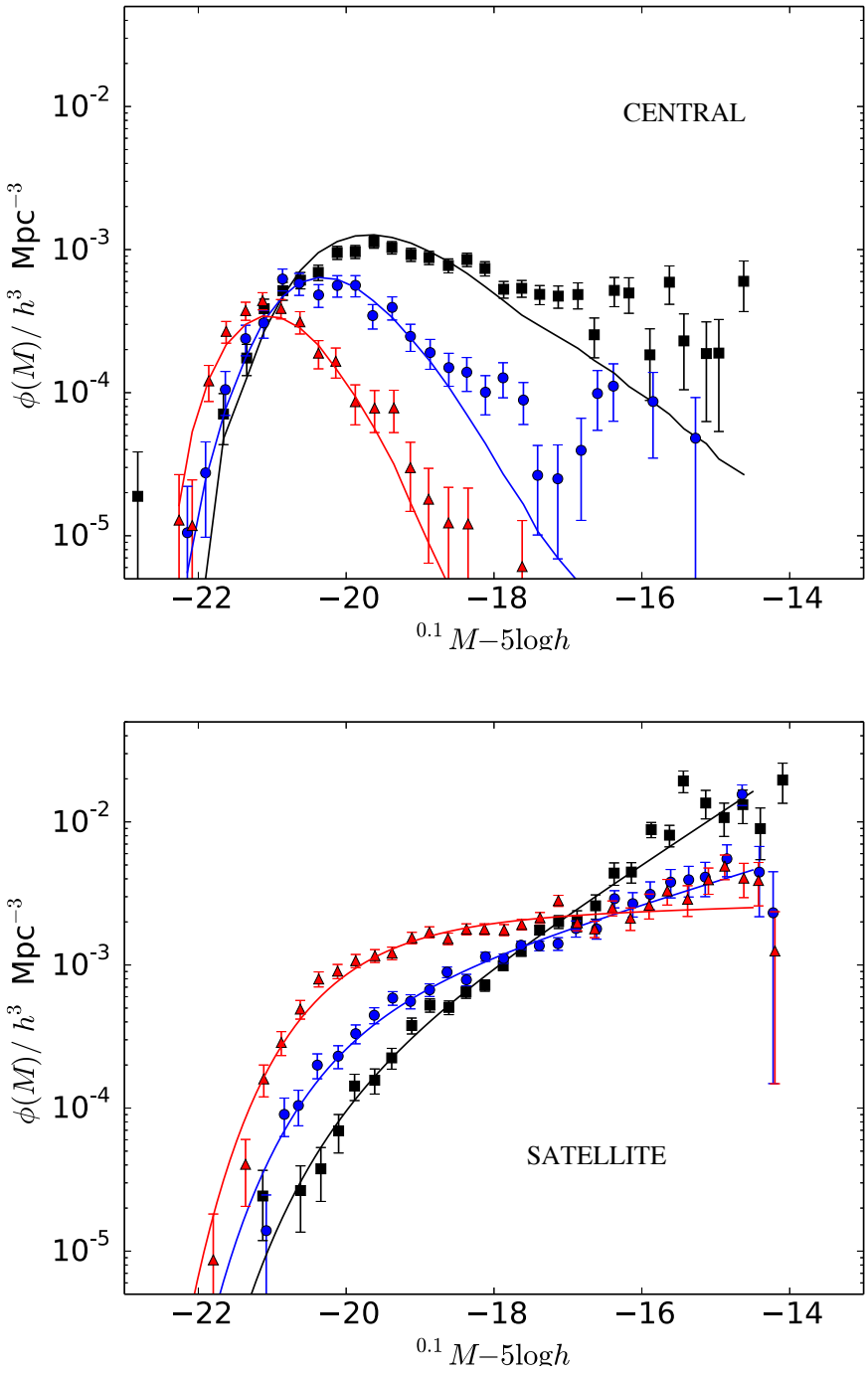

Figure 2.15: LF divided by richness $N_{\mathrm{FOF}} = 2$ (black), $N_{\mathrm{FOF}} = 3$-4 (blue) and $N_{\mathrm{FOF}} \geq 5$ (red) up to z=0.1 for central (top) and satellite (bottom) galaxies.

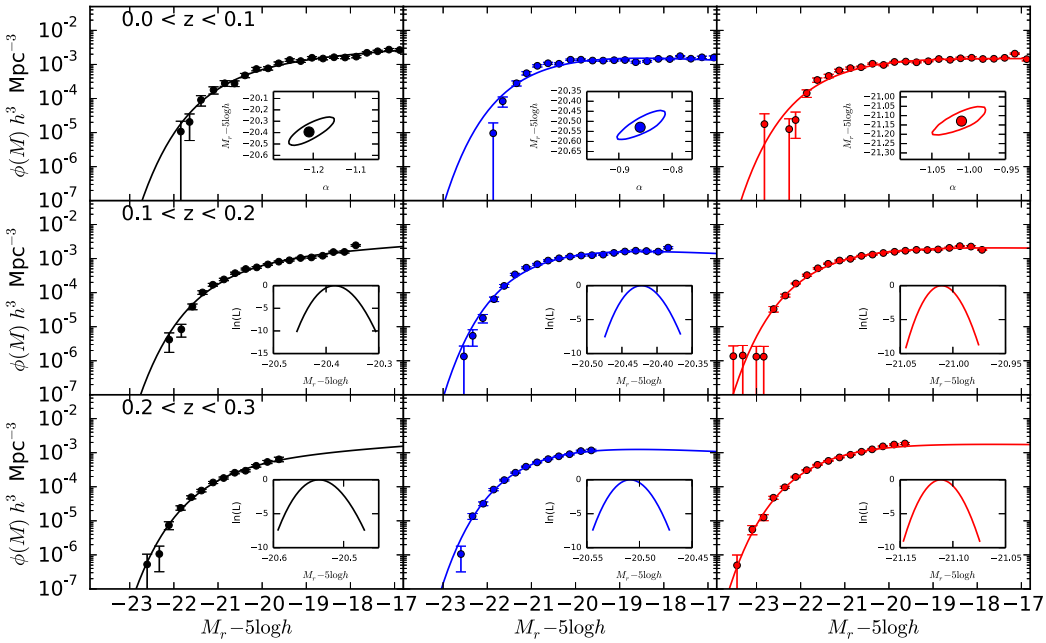

Figure 2.16: LF evolution for the three subsamples computed according to the mass of groups [8,12.06],[12.06,12.70],[12.70,16] $\log M/M\odot$ in black, blue and red respectively; for three redshift ranges [0.002, 0.1], [0.1, 0.2] and [0.2, 0.3] from the top to the bottom respectively. Filled symbols shows the SWML LF with the corresponding error bars. Solid lines are the best Schechter fit (least-squares). The inset at the top shows two-σ likelihood contours for the Schechter parameters α and M^* fitting the LF. The insets at middle and bottom show M^* likelihood ratio normalised to peak at log L = 0.

M^* is determined using the parametric fits, minimising the χ^2 for the fit.

Looking at the faint end in all cases, there are not considerable differences between the LFs, but at the bright end. Massive groups contain brighter galaxies as expected, besides, in the middle panel there is a significant increase with large error bars for the LF with high mass groups at the very bright end. On the other hand the 1-σ likelihood in one dimension shows only an overlapping of two distributions in the middle range of z at low and middle mass bins, meaning no clear statistical difference between them, meanwhile the other distributions are enough separated to indicate that there is a difference between them and then a tendency where M^* decreases with mass increasing. Schechter fit parameters are presented in Table 2.4.

In order to investigate evolutionary trends in M^*, we plot in Fig. 2.17 the 1-σ likelihood in one dimension normalised to peak at log L = 0 for the three z bins sorted from low to high in solid, dot and dashed lines; colours follow the same meaning as in Fig. 2.16. M^*

Table 2.4: Schechter parameters for evolution of the LF in three ranges of z for the three subsamples of masses. (Q and P evolution parameters are the same at any redshift)

subsample	bin $\log M/M_{\odot}$	α	$^{0.1}M^{*}$-5lg$h$	Q	P
z < 0.1					
	8-12.06	-1.21 ± 0.13	-20.33 ± 0.21	1.10 ± 0.35	-8.74 ± 0.17
	12.06-12.70	-0.83 ± 0.12	-20.41 ± 0.10	0.09 ± 0.09	-7.50 ± 0.11
	12.70-16	-0.96 ± 0.07	-20.87 ± 0.12	0.17 ± 0.17	-7.01 ± 0.08
0.1 < z < 0.2					
	8-12.06	-1.21 ± 0.13	-20.38 ± 0.08		
	12.06-12.70	-0.83 ± 0.12	-20.42 ± 0.05		
	12.70-16	-0.96 ± 0.07	-21.01 ± 0.03		
0.2 < z < 0.3					
	8-12.06	-1.21 ± 0.13	-20.53 ± 0.08		
	12.06-12.70	-0.83 ± 0.12	-20.51 ± 0.04		
	12.70-16	-0.96 ± 0.07	-21.11 ± 0.04		

gets brighter as z increases for the middle and high mass bin; however, for the low mass bin there is no clear evolutionary trend. When we compare the three mass bins together with z, M^{*} evolves in the same way for the three mass bins for the middle and high z bins, where groups tend to be brighter as the mass increases; nevertheless this feature is not present at lowest redshift . This suggests no domination of any of the mass bins in the bright region. Fig. 2.18 make this result more clear.

2.7 Conclusions

In this work we present the LF for galaxies in the GAMA group catalogue ($G^{3}Cv6$) in the r-band. The estimation of the LF for galaxies in groups and the comparison with ungrouped galaxies give us similar results to those found in Croton et al. (2005) and more recently McNaught-Roberts et al. (2014), where they find galaxies tend to be brighter as the environment density increases. At the faint-end, ungrouped galaxies dominate over the grouped galaxies, maybe because these galaxies have not suffered any external perturbation that may stop the star formation process for example. And many galaxies in groups are perhaps in the final merger phase making the system more luminous.

The $G^{3}Cv6$ was divided in three mass bins to explore the dependency of the LF with the group mass. The first result is the LF slope at the faint end becomes shallower when the

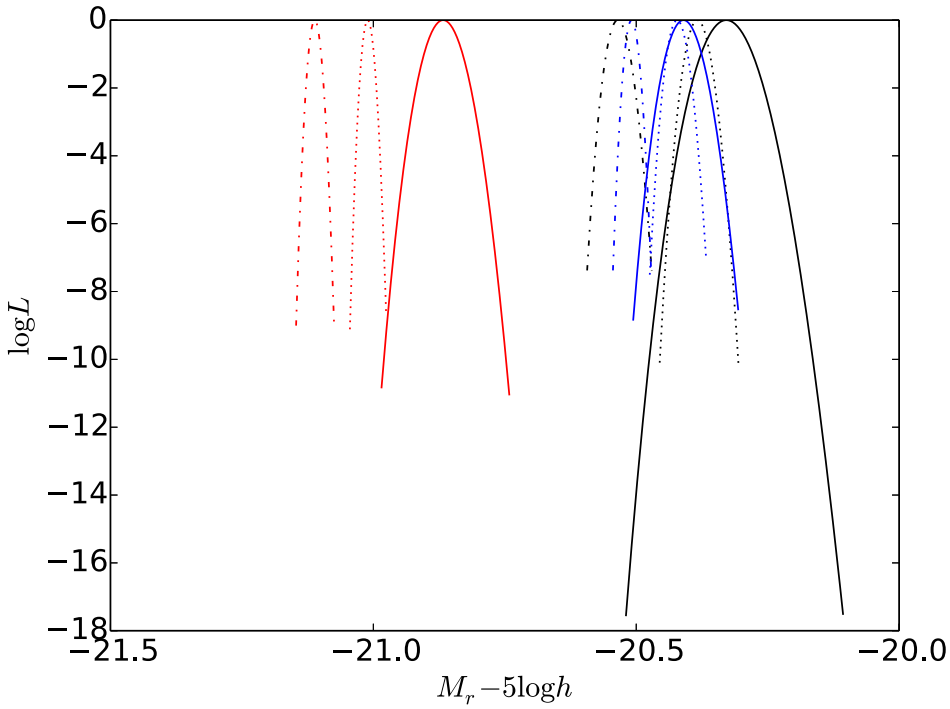

Figure 2.17: log likelihood in 1D normalised to peak at log L = 0, same insets in Fig. 2.16 plus the likelihood distribution at z=0. Solid, dot and dashed lines represent the three intervals of z in ascending order; bins: $8 < \log M/M\odot \leq 12.06$, $12.06 < \log M/M\odot \leq 12.70$ and $12.70 < \log M/M\odot \leq 16$ are shown in black, blue and red respectively.

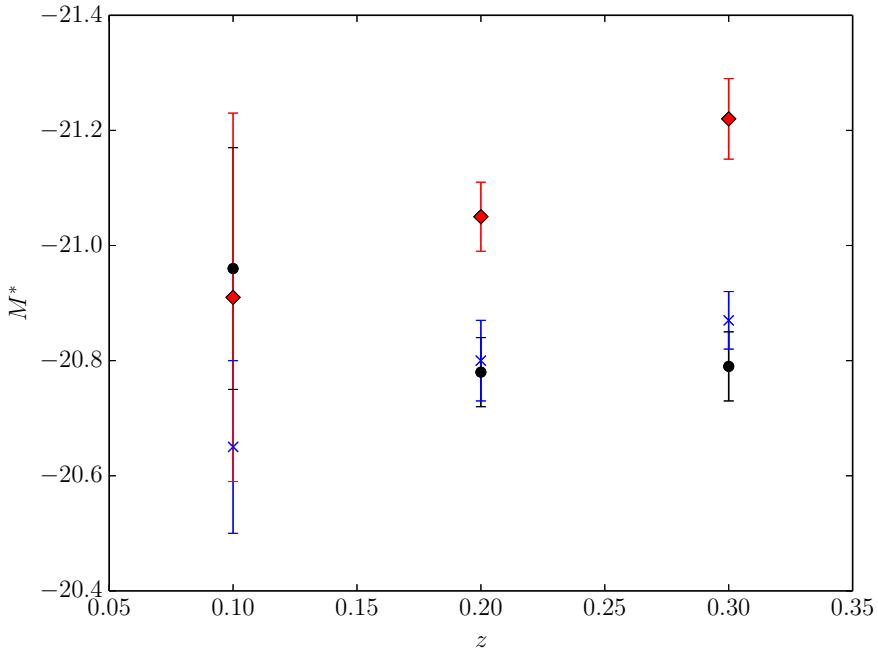

Figure 2.18: M^* vs z for the mass bins: $8 < \log M/M\odot \leq 12.06$ (black dots), $12.06 < \log M/M\odot \leq 12.70$ (blue crosses) and $12.70 < \log M/M\odot \leq 16$ (red diamonds).

mass bin increases, clearly because massive galaxies are associated to luminous galaxies, even though the total mass is estimated not only base on the luminosity, it gives a very first approximation. We cannot talk about a correlation between α and mass, but we can infer a negative tendency between M^* respect to mass, meaning the expected result, high luminous galaxies are located in massive groups, with likely high velocity dispersion. This catalogue is also separated by colour and morphology and the corresponding LF is estimated again in the mass bins. Red galaxies domain over the blue galaxies at the bright-end and vice versa at the faint-end for all the mass bins. However, the faint-end slope (α) becomes flatter as the mass increases similar to the combined sample; and on the other hand the density of massive red galaxies is higher than in the other bins. Due to the relationship between colour and morphology, the LFs divide by morphology follow the same tendencies found for colour. These LFs are tested respect to the mock catalogues. The mock LF parameters (α and M^*) agree with observations into one error bar, specially at the high mass bin, this means that the mock catalogue considered is confident at high masses but with some unsolved issues for the low mass regime.

Following the questions presented in section 1.1, the mock catalogues used here, based on the Millennium Simulation, reproduce the mainly the massive range for the group LF.

Nevertheless, these mock do not reproduce the tendencies found at the low mass bin. The Schechter parameters presented for the low mass bin are the parameters models may reproduce, since this is the first time a sample allow us to estimate the LF at very low masses.

For the velocity dispersion dependence of the LF, results are very similar to those described above for the mass dependence, with slightly differences around the M^*, due to groups with middle velocity dispersion present a lower number density of galaxies comparing to the result found in mass (e.g. Miles et al. 2004).

We compared the group properties with richness to identify any possible correlation between them using a volume-limited sample up to $z = 0.1$. However, there is no clear sign that group mass correlates with low richness, or redshift correlates with richness, just effects due to the large scale structure can be seen or the lack of rich groups at low mass as expected, but we can identify massive groups with just 2 or 3 members as shown in Fig. 2.10. Nevertheless, looking at the cumulative magnitude distribution, magnitude distributions for the middle and high richness groups are statistically very similar, meanwhile the other two magnitude distributions are clearly different. This result is reflected in the shape of the LF for middle and high richness bins which are very similar, and looking at the Schechter parameters, the faint end slope α agrees within one sigma. Our results are consistent with those reported by Marinoni et al. (2002) where galaxies are brighter in higher richness groups; also similar to the density dependence as presented by McNaught-Roberts et al. (2014).

When we divided again in colour and morphology, we found the spiral and elliptical LFs do not change their shape with richness, so the ratio of these galaxies is constant independently of the richness. Bright galaxies are mainly ellipticals as expected, and since central galaxies are mostly the brightest galaxy in the group, then the central galaxies are mainly ellipticals, but not necessarily red. We also found, there are brighter galaxies in groups with more members or high densities as other works have showed (e.g. Croton et al. 2005. α tends to be steeper as the richness increases in simulations; however this is not clear with real data where the large error bars (see Fig. 2.13) do not allow to agree to deny this tendency. Blue galaxies dominate the LF faint-end for all richness as expect; however, and the bright-end is dominated by blue galaxies at all richness. This agrees with the LF for central galaxies, where the bright end is not dominated either by blue or red galaxies. α also becomes more negative at higher densities for the red population and an apparent constant value for blue population at all richness. Meanwhile, M^* becomes

brighter as density increases for red and blue galaxies using the GAMA data.

The most important result from the central and satellite LF is the large difference between the LFs in this work and those presented by Yang et al. (2009). A possible reason of this difference could be the separation criteria between central and satellite galaxies they used based on the mass and not on luminosity. However, the mock catalogues reproduced our results. Nevertheless, a more specific study about central and satellite galaxies most be done in a future work to clarify these differences.

LF evolution over redshift is has been characterized following the method proposed by Lin et al. (1999) and the dependence on group mass and velocity dispersion. Galaxies in massive groups or those with high velocity dispersion are brighter than those in the other bins, following the idea that groups can be dominated by a very bright galaxy in the central region. In the redshift interval $0.1 < z < 0.2$, this same bright population shows a flat bright end (using the SWML method); interpretation is not clear but a possible explanation is that mentioned earlier, a population of bright AGNs. Trying to quantify the change of M^* according to the mass and velocity dispersion bin and redshift, we calculate the two-σ likelihood contours considering the M^* and α parameters, and the σ 1-dimension likelihood curves for M^* with α fixed. 1-dimension curves show clearly an increment of M^* with higher z for high and middle bins (of mass and velocity dispersion). Evolution is present in the same way for all the mass and dispersion bins.

The analysis presented in this paper was based only on the r-band. A robust analysis using the multiwavelength information in GAMA will help to understand the physical processes occurring in these groups and the relation with the results obtained here. An introduction to this work will be presented in Paper III. Paper II will analyse the LF for galaxies in low dense environments, isolated galaxies.

Acknowledgements

GAMA is a joint European-Australasian project based around a spectroscopic campaign using the Anglo-Australian Telescope. The GAMA input catalogue is based on data taken from the Sloan Digital Sky Survey and the UKIRT Infrared Deep Sky Survey. Complementary imaging of the GAMA regions is being obtained by a number of independent survey programs including GALEX MIS, VST KiDS, VISTA VIKING, WISE, Herschel-ATLAS, GMRT and ASKAP providing UV to radio coverage. GAMA is funded by the STFC (UK), the ARC (Australia), the AAO, and the participating institutions. The GAMA website is http://www.gama-survey.org/ .

JAVM was supported by the Mexican National Council for Science and Technology (CONACyT) scholarship scheme.

JAVM express his gratitude to Jon Loveday for all his constructive suggestions to improve this work.

References

Baldry, I. K., Robotham, A. S. G., Hill, D. T., Driver, S. P., Liske, J., Norberg, P., Bamford, S. P., Hopkins, A. M., Loveday, J., Peacock, J. A., Cameron, E., Croom, S. M., Cross, N. J. G., Doyle, I. F., Dye, S., Frenk, C. S., Jones, D. H., van Kampen, E., Kelvin, L. S., Nichol, R. C., Parkinson, H. R., Popescu, C. C., Prescott, M., Sharp, R. G., Sutherland, W. J., Thomas, D., and Tuffs, R. J. (2010). Galaxy And Mass Assembly (GAMA): the input catalogue and star-galaxy separation. *MNRAS*, 404:86–100.

Barden, M., Rix, H.-W., Somerville, R. S., Bell, E. F., Häußler, B., Peng, C. Y., Borch, A., Beckwith, S. V. W., Caldwell, J. A. R., Heymans, C., Jahnke, K., Jogee, S., McIntosh, D. H., Meisenheimer, K., Sánchez, S. F., Wisotzki, L., and Wolf, C. (2005). GEMS: The Surface Brightness and Surface Mass Density Evolution of Disk Galaxies. *ApJ*, 635:959–981.

Beers, T. C., Flynn, K., and Gebhardt, K. (1990). Measures of location and scale for velocities in clusters of galaxies - A robust approach. *AJ*, 100:32–46.

Benson, A. J., Frenk, C. S., Baugh, C. M., Cole, S., and Lacey, C. G. (2003). The effects of photoionization on galaxy formation - III. Environmental dependence in the luminosity function. *MNRAS*, 343:679–691.

Bertin, E. and Arnouts, S. (1996). SExtractor: Software for source extraction. *A&AS*, 117:393–404.

Blanton, M. R., Brinkmann, J., Csabai, I., Doi, M., Eisenstein, D., Fukugita, M., Gunn, J. E., Hogg, D. W., and Schlegel, D. J. (2003). Estimating Fixed-Frame Galaxy Magnitudes in the Sloan Digital Sky Survey. *AJ*, 125:2348–2360.

Blanton, M. R. and Roweis, S. (2007). K-Corrections and Filter Transformations in the Ultraviolet, Optical, and Near-Infrared. *AJ*, 133:734–754.

Bower, R. G., Benson, A. J., Malbon, R., Helly, J. C., Frenk, C. S., Baugh, C. M., Cole, S., and Lacey, C. G. (2006). Breaking the hierarchy of galaxy formation. *MNRAS*, 370:645–655.

Choi, Y.-Y., Park, C., and Vogeley, M. S. (2007). Internal and Collective Properties of Galaxies in the Sloan Digital Sky Survey. *ApJ*, 658:884–897.

Colless, M., Dalton, G., Maddox, S., Sutherland, W., Norberg, P., Cole, S., Bland-Hawthorn, J., Bridges, T., Cannon, R., Collins, C., Couch, W., Cross, N., Deeley, K., De Propris, R., Driver, S. P., Efstathiou, G., Ellis, R. S., Frenk, C. S., Glazebrook, K., Jackson, C., Lahav, O., Lewis, I., Lumsden, S., Madgwick, D., Peacock, J. A., Peterson, B. A., Price, I., Seaborne, M., and Taylor, K. (2001). The 2dF Galaxy Redshift Survey: spectra and redshifts. *MNRAS*, 328:1039–1063.

Croton, D. J., Farrar, G. R., Norberg, P., Colless, M., Peacock, J. A., Baldry, I. K., Baugh, C. M., Bland-Hawthorn, J., Bridges, T., Cannon, R., Cole, S., Collins, C., Couch, W., Dalton, G., De Propris, R., Driver, S. P., Efstathiou, G., Ellis, R. S., Frenk, C. S., Glazebrook, K., Jackson, C., Lahav, O., Lewis, I., Lumsden, S., Maddox, S., Madgwick, D., Peterson, B. A., Sutherland, W., and Taylor, K. (2005). The 2dF Galaxy Redshift Survey: luminosity functions by density environment and galaxy type. *MNRAS*, 356:1155–1167.

Cuesta-Bolao, M. J. and Serna, A. (2003). Environmental and morphological dependence of the luminosity function of galaxies. *A&A*, 405:917–930.

Driver, S. P., Hill, D. T., Kelvin, L. S., Robotham, A. S. G., Liske, J., Norberg, P., Baldry, I. K., Bamford, S. P., Hopkins, A. M., Loveday, J., Peacock, J. A., Andrae, E., Bland-Hawthorn, J., Brough, S., Brown, M. J. I., Cameron, E., Ching, J. H. Y., Colless, M., Conselice, C. J., Croom, S. M., Cross, N. J. G., de Propris, R., Dye, S., Drinkwater, M. J., Ellis, S., Graham, A. W., Grootes, M. W., Gunawardhana, M., Jones, D. H., van Kampen, E., Maraston, C., Nichol, R. C., Parkinson, H. R., Phillipps, S., Pimbblet, K., Popescu, C. C., Prescott, M., Roseboom, I. G., Sadler, E. M., Sansom, A. E., Sharp, R. G., Smith, D. J. B., Taylor, E., Thomas, D., Tuffs, R. J., Wijesinghe, D., Dunne, L., Frenk, C. S., Jarvis, M. J., Madore, B. F., Meyer, M. J., Seibert, M., Staveley-Smith, L., Sutherland, W. J., and Warren, S. J. (2011). Galaxy and Mass Assembly (GAMA): survey diagnostics and core data release. *MNRAS*, 413:971–995.

Driver, S. P., Norberg, P., Baldry, I. K., Bamford, S. P., Hopkins, A. M., Liske, J., Loveday, J., Peacock, J. A., Hill, D. T., Kelvin, L. S., Robotham, A. S. G., Cross, N. J. G., Parkinson, H. R., Prescott, M., Conselice, C. J., Dunne, L., Brough, S., Jones, H., Sharp, R. G., van Kampen, E., Oliver, S., Roseboom, I. G., Bland-Hawthorn, J., Croom, S. M., Ellis, S., Cameron, E., Cole, S., Frenk, C. S., Couch, W. J., Graham, A. W., Proctor, R., De Propris, R., Doyle, I. F., Edmondson, E. M., Nichol, R. C., Thomas, D., Eales, S. A., Jarvis, M. J., Kuijken, K., Lahav, O., Madore, B. F., Seibert, M., Meyer, M. J., Staveley-Smith, L., Phillipps, S., Popescu, C. C., Sansom, A. E., Sutherland, W. J., Tuffs, R. J., and Warren, S. J. (2009). GAMA: towards a physical understanding of galaxy formation. *Astronomy and Geophysics*, 50(5):050000–5.

Driver, S. P., Robotham, A. S. G., Kelvin, L., Alpaslan, M., Baldry, I. K., Bamford, S. P., Brough, S., Brown, M., Hopkins, A. M., Liske, J., Loveday, J., Norberg, P., Peacock, J. A., Andrae, E., Bland-Hawthorn, J., Bourne, N., Cameron, E., Colless, M., Conselice, C. J., Croom, S. M., Dunne, L., Frenk, C. S., Graham, A. W., Gunawardhana, M., Hill, D. T., Jones, D. H., Kuijken, K., Madore, B., Nichol, R. C., Parkinson, H. R., Pimbblet, K. A., Phillipps, S., Popescu, C. C., Prescott, M., Seibert, M., Sharp, R. G., Sutherland, W. J., Taylor, E. N., Thomas, D., Tuffs, R. J., van Kampen, E., Wijesinghe, D., and Wilkins, S. (2012). Galaxy And Mass Assembly (GAMA): the 0.013 z 0.1 cosmic spectral energy distribution from 0.1 μm to 1 mm. *MNRAS*, 427:3244–3264.

Efstathiou, G., Ellis, R. S., and Peterson, B. A. (1988). Analysis of a complete galaxy redshift survey. II - The field-galaxy luminosity function. *MNRAS*, 232:431–461.

Han, J., Eke, V. R., Frenk, C. S., Mandelbaum, R., Norberg, P., Schneider, M. D., Peacock, J. A., Jing, Y., Baldry, I., Bland-Hawthorn, J., Brough, S., Brown, M. J. I., Liske, J., Loveday, J., and Robotham, A. S. G. (2015). Galaxy And Mass Assembly (GAMA): the halo mass of galaxy groups from maximum-likelihood weak lensing. *MNRAS*, 446:1356–1379.

Helsdon, S. F. and Ponman, T. J. (2000). Are X-ray properties of loose groups different from those of compact groups? *MNRAS*, 319:933–938.

Hill, D. T., Kelvin, L. S., Driver, S. P., Robotham, A. S. G., Cameron, E., Cross, N., Andrae, E., Baldry, I. K., Bamford, S. P., Bland-Hawthorn, J., Brough, S., Conselice, C. J., Dye, S., Hopkins, A. M., Liske, J., Loveday, J., Norberg, P., Peacock, J. A., Croom, S. M., Frenk, C. S., Graham, A. W., Jones, D. H., Kuijken, K., Madore, B. F., Nichol, R. C., Parkinson, H. R., Phillipps, S., Pimbblet, K. A., Popescu, C. C., Prescott,

M., Seibert, M., Sharp, R. G., Sutherland, W. J., Thomas, D., Tuffs, R. J., and van Kampen, E. (2011). Galaxy and Mass Assembly: FUV, NUV, ugrizYJHK Petrosian, Kron and Sérsic photometry. *MNRAS*, 412:765–799.

Hoyle, F., Rojas, R. R., Vogeley, M. S., and Brinkmann, J. (2005). The Luminosity Function of Void Galaxies in the Sloan Digital Sky Survey. *ApJ*, 620:618–628.

Huertas-Company, M., Tasca, L., Rouan, D., Pelat, D., Kneib, J. P., Le Fèvre, O., Capak, P., Kartaltepe, J., Koekemoer, A., McCracken, H. J., Salvato, M., Sanders, D. B., and Willott, C. (2009). A robust morphological classification of high-redshift galaxies using support vector machines on seeing limited images. II. Quantifying morphological k-correction in the COSMOS field at 1 z 2: Ks band vs. I band. *A&A*, 497:743–753.

Humason, M. L., Mayall, N. U., and Sandage, A. R. (1956). Redshifts and magnitudes of extragalactic nebulae. *AJ*, 61:97–162.

Kelvin, L. S., Driver, S. P., Robotham, A. S. G., Hill, D. T., Alpaslan, M., Baldry, I. K., Bamford, S. P., Bland-Hawthorn, J., Brough, S., Graham, A. W., Häussler, B., Hopkins, A. M., Liske, J., Loveday, J., Norberg, P., Phillipps, S., Popescu, C. C., Prescott, M., Taylor, E. N., and Tuffs, R. J. (2012). Galaxy And Mass Assembly (GAMA): Structural Investigation of Galaxies via Model Analysis. *MNRAS*, 421:1007–1039.

Kim, S., Stiavelli, M., Trenti, M., Pavlovsky, C. M., Djorgovski, S. G., Scarlata, C., Stern, D., Mahabal, A., Thompson, D., Dickinson, M., Panagia, N., and Meylan, G. (2009). The Environments of High-Redshift Quasi-Stellar Objects. *ApJ*, 695:809–817.

Lin, H., Yee, H. K. C., Carlberg, R. G., Morris, S. L., Sawicki, M., Patton, D. R., Wirth, G., and Shepherd, C. W. (1999). The CNOC2 Field Galaxy Luminosity Function. I. A Description of Luminosity Function Evolution. *ApJ*, 518:533–561.

Lintott, C., Schawinski, K., Bamford, S., Slosar, A., Land, K., Thomas, D., Edmondson, E., Masters, K., Nichol, R. C., Raddick, M. J., Szalay, A., Andreescu, D., Murray, P., and Vandenberg, J. (2011). Galaxy Zoo 1: data release of morphological classifications for nearly 900 000 galaxies. *MNRAS*, 410:166–178.

Lintott, C. J., Schawinski, K., Slosar, A., Land, K., Bamford, S., Thomas, D., Raddick, M. J., Nichol, R. C., Szalay, A., Andreescu, D., Murray, P., and Vandenberg, J. (2008). Galaxy Zoo: morphologies derived from visual inspection of galaxies from the Sloan Digital Sky Survey. *MNRAS*, 389:1179–1189.

Liske, J., Baldry, I. K., Driver, S. P., Tuffs, R. J., Alpaslan, M., Andrae, E., Brough, S., Cluver, M. E., Grootes, M. W., Gunawardhana, M. L. P., Kelvin, L. S., Loveday, J., Robotham, A. S. G., Taylor, E. N., Bamford, S. P., Bland-Hawthorn, J., Brown, M. J. I., Drinkwater, M. J., Hopkins, A. M., Meyer, M. J., Norberg, P., Peacock, J. A., Agius, N. K., Andrews, S. K., Bauer, A. E., Ching, J. H. Y., Colless, M., Conselice, C. J., Croom, S. M., Davies, L. J. M., De Propris, R., Dunne, L., Eardley, E. M., Ellis, S., Foster, C., Frenk, C. S., Häußler, B., Holwerda, B. W., Howlett, C., Ibarra, H., Jarvis, M. J., Jones, D. H., Kafle, P. R., Lacey, C. G., Lange, R., Lara-López, M. A., López-Sánchez, Á. R., Maddox, S., Madore, B. F., McNaught-Roberts, T., Moffett, A. J., Nichol, R. C., Owers, M. S., Palamara, D., Penny, S. J., Phillipps, S., Pimbblet, K. A., Popescu, C. C., Prescott, M., Proctor, R., Sadler, E. M., Sansom, A. E., Seibert, M., Sharp, R., Sutherland, W., Vázquez-Mata, J. A., van Kampen, E., Wilkins, S. M., Williams, R., and Wright, A. H. (2015). Galaxy And Mass Assembly (GAMA): end of survey report and data release 2. *MNRAS*, 452:2087–2126.

Loveday, J., Norberg, P., Baldry, I. K., Driver, S. P., Hopkins, A. M., Peacock, J. A., Bamford, S. P., Liske, J., Bland-Hawthorn, J., Brough, S., Brown, M. J. I., Cameron, E., Conselice, C. J., Croom, S. M., Frenk, C. S., Gunawardhana, M., Hill, D. T., Jones, D. H., Kelvin, L. S., Kuijken, K., Nichol, R. C., Parkinson, H. R., Phillipps, S., Pimbblet, K. A., Popescu, C. C., Prescott, M., Robotham, A. S. G., Sharp, R. G., Sutherland, W. J., Taylor, E. N., Thomas, D., Tuffs, R. J., van Kampen, E., and Wijesinghe, D. (2012). Galaxy and Mass Assembly (GAMA): ugriz galaxy luminosity functions. *MNRAS*, 420:1239–1262.

Ludlow, A. D., Navarro, J. F., Springel, V., Jenkins, A., Frenk, C. S., and Helmi, A. (2009). The Unorthodox Orbits of Substructure Halos. *ApJ*, 692:931–941.

Marinoni, C., Hudson, M. J., and Giuricin, G. (2002). The Optical Luminosity Function of Virialized Systems. *ApJ*, 569:91–100.

McNaught-Roberts, T., Norberg, P., Baugh, C., Lacey, C., Loveday, J., Peacock, J., Baldry, I., Bland-Hawthorn, J., Brough, S., Driver, S. P., Robotham, A. S. G., and Vázquez-Mata, J. A. (2014). Galaxy And Mass Assembly (GAMA): the dependence of the galaxy luminosity function on environment, redshift and colour. *MNRAS*, 445:2125–2145.

Miles, T. A., Raychaudhury, S., Forbes, D. A., Goudfrooij, P., Ponman, T. J., and Kozhurina-Platais, V. (2004). The Group Evolution Multiwavelength Study (GEMS): bimodal luminosity functions in galaxy groups. *MNRAS*, 355:785–793.

Norberg, P. (in prep.). Galaxy And Mass Assembly (GAMA): Preliminary global group properties from G3Cv6.

Park, C., Choi, Y.-Y., Vogeley, M. S., Gott, III, J. R., Blanton, M. R., and SDSS Collaboration (2007). Environmental Dependence of Properties of Galaxies in the Sloan Digital Sky Survey. *ApJ*, 658:898–916.

Press, W. H. and Schechter, P. (1974). Formation of Galaxies and Clusters of Galaxies by Self-Similar Gravitational Condensation. *ApJ*, 187:425–438.

Robotham, A., Phillipps, S., and De Propris, R. (2008). The Shapes of Galaxy Groups: Footballs or Frisbees? *ApJ*, 672:834–848.

Robotham, A., Phillipps, S., and de Propris, R. (2010). The variation of the galaxy luminosity function with group properties. *MNRAS*, 403:1812–1828.

Robotham, A. S. G., Norberg, P., Driver, S. P., Baldry, I. K., Bamford, S. P., Hopkins, A. M., Liske, J., Loveday, J., Merson, A., Peacock, J. A., Brough, S., Cameron, E., Conselice, C. J., Croom, S. M., Frenk, C. S., Gunawardhana, M., Hill, D. T., Jones, D. H., Kelvin, L. S., Kuijken, K., Nichol, R. C., Parkinson, H. R., Pimbblet, K. A., Phillipps, S., Popescu, C. C., Prescott, M., Sharp, R. G., Sutherland, W. J., Taylor, E. N., Thomas, D., Tuffs, R. J., van Kampen, E., and Wijesinghe, D. (2011). Galaxy and Mass Assembly (GAMA): the GAMA galaxy group catalogue (G^3Cv1). *MNRAS*, 416:2640–2668.

Schechter, P. (1976). An analytic expression for the luminosity function for galaxies. *ApJ*, 203:297–306.

Schlegel, D. J., Finkbeiner, D. P., and Davis, M. (1998). Maps of Dust Infrared Emission for Use in Estimation of Reddening and Cosmic Microwave Background Radiation Foregrounds. *ApJ*, 500:525.

Sersic, J. L. (1968). *Atlas de galaxias australes*. Cordoba, Argentina: Observatorio Astronomico.

Springel, V., White, S. D. M., Jenkins, A., Frenk, C. S., Yoshida, N., Gao, L., Navarro, J., Thacker, R., Croton, D., Helly, J., Peacock, J. A., Cole, S., Thomas, P., Couchman, H.,

Evrard, A., Colberg, J., and Pearce, F. (2005). Simulations of the formation, evolution and clustering of galaxies and quasars. *Nature*, 435:629–636.

Sulentic, J. W., Verdes-Montenegro, L., Bergond, G., Lisenfeld, U., Durbala, A., Espada, D., Garcia, E., Leon, S., Sabater, J., Verley, S., Casanova, V., and Sota, A. (2006). The AMIGA sample of isolated galaxies. II. Morphological refinement. *A&A*, 449:937–949.

Tago, E., Saar, E., Tempel, E., Einasto, J., Einasto, M., Nurmi, P., and Heinämäki, P. (2010). Groups of galaxies in the SDSS Data Release 7 . Flux- and volume-limited samples. *A&A*, 514:A102.

Tempel, E., Einasto, J., Einasto, M., Saar, E., and Tago, E. (2009). Anatomy of luminosity functions: the 2dFGRS example. *A&A*, 495:37–51.

Wang, H. Y., Mo, H. J., and Jing, Y. P. (2007). Environmental dependence of cold dark matter halo formation. *MNRAS*, 375:633–639.

Wetzel, A. R., Tinker, J. L., Conroy, C., and Bosch, F. C. v. d. (2014). Galaxy evolution near groups and clusters: ejected satellites and the spatial extent of environmental quenching. *MNRAS*, 439:2687–2700.

White, S. D. M. and Rees, M. J. (1978). Core condensation in heavy halos - A two-stage theory for galaxy formation and clustering. *MNRAS*, 183:341–358.

Xu, C. K., Zhao, Y., Scoville, N., Capak, P., Drory, N., and Gao, Y. (2012). Major-merger Galaxy Pairs in the COSMOS FieldMass-dependent Merger Rate Evolution since z = 1. *ApJ*, 747:85.

Yang, X., Mo, H. J., and van den Bosch, F. C. (2009). Galaxy Groups in the SDSS DR4. III. The Luminosity and Stellar Mass Functions. *ApJ*, 695:900–916.

York, D. G., Adelman, J., Anderson, Jr., J. E., Anderson, S. F., Annis, J., Bahcall, N. A., Bakken, J. A., Barkhouser, R., Bastian, S., Berman, E., Boroski, W. N., Bracker, S., Briegel, C., Briggs, J. W., Brinkmann, J., Brunner, R., Burles, S., Carey, L., Carr, M. A., Castander, F. J., Chen, B., Colestock, P. L., Connolly, A. J., Crocker, J. H., Csabai, I., Czarapata, P. C., Davis, J. E., Doi, M., Dombeck, T., Eisenstein, D., Ellman, N., Elms, B. R., Evans, M. L., Fan, X., Federwitz, G. R., Fiscelli, L., Friedman, S., Frieman, J. A., Fukugita, M., Gillespie, B., Gunn, J. E., Gurbani, V. K., de Haas, E., Haldeman, M., Harris, F. H., Hayes, J., Heckman, T. M., Hennessy, G. S., Hindsley, R. B., Holm, S., Holmgren, D. J., Huang, C.-h., Hull, C., Husby, D., Ichikawa, S.-I.,

Ichikawa, T., Ivezić, Ž., Kent, S., Kim, R. S. J., Kinney, E., Klaene, M., Kleinman, A. N., Kleinman, S., Knapp, G. R., Korienek, J., Kron, R. G., Kunszt, P. Z., Lamb, D. Q., Lee, B., Leger, R. F., Limmongkol, S., Lindenmeyer, C., Long, D. C., Loomis, C., Loveday, J., Lucinio, R., Lupton, R. H., MacKinnon, B., Mannery, E. J., Mantsch, P. M., Margon, B., McGehee, P., McKay, T. A., Meiksin, A., Merelli, A., Monet, D. G., Munn, J. A., Narayanan, V. K., Nash, T., Neilsen, E., Neswold, R., Newberg, H. J., Nichol, R. C., Nicinski, T., Nonino, M., Okada, N., Okamura, S., Ostriker, J. P., Owen, R., Pauls, A. G., Peoples, J., Peterson, R. L., Petravick, D., Pier, J. R., Pope, A., Pordes, R., Prosapio, A., Rechenmacher, R., Quinn, T. R., Richards, G. T., Richmond, M. W., Rivetta, C. H., Rockosi, C. M., Ruthmansdorfer, K., Sandford, D., Schlegel, D. J., Schneider, D. P., Sekiguchi, M., Sergey, G., Shimasaku, K., Siegmund, W. A., Smee, S., Smith, J. A., Snedden, S., Stone, R., Stoughton, C., Strauss, M. A., Stubbs, C., SubbaRao, M., Szalay, A. S., Szapudi, I., Szokoly, G. P., Thakar, A. R., Tremonti, C., Tucker, D. L., Uomoto, A., Vanden Berk, D., Vogeley, M. S., Waddell, P., Wang, S.-i., Watanabe, M., Weinberg, D. H., Yanny, B., Yasuda, N., and SDSS Collaboration (2000). The Sloan Digital Sky Survey: Technical Summary. *AJ*, 120:1579–1587.

Zandivarez, A., Martínez, H. J., and Merchán, M. E. (2006). On the Luminosity Function of Galaxies in Groups in the Sloan Digital Sky Survey. *ApJ*, 650:137–147.

Zehavi, I., Zheng, Z., Weinberg, D. H., Blanton, M. R., Bahcall, N. A., Berlind, A. A., Brinkmann, J., Frieman, J. A., Gunn, J. E., Lupton, R. H., Nichol, R. C., Percival, W. J., Schneider, D. P., Skibba, R. A., Strauss, M. A., Tegmark, M., and York, D. G. (2011). Galaxy Clustering in the Completed SDSS Redshift Survey: The Dependence on Color and Luminosity. *ApJ*, 736:59.

2.8 Appendix

2.8.1 Mass and velocity dispersion complement

Sample divided by 2 mass and velocity dispersion bins

As a complement, to check the LF dependence on mass estimated in section 2.4.2 in different bins, the G^3C is divided in only two mass bins to explore the differences between these two extreme sides. In spite of the median mass group of the sample is $\log(M/M_\odot) = 11.69$, it was considered the number of galaxies distribution in function of the mass group which median is $\log(M/M_\odot) = 12.08$. The upper ($\log(M/M_\odot) = 17$) and lower

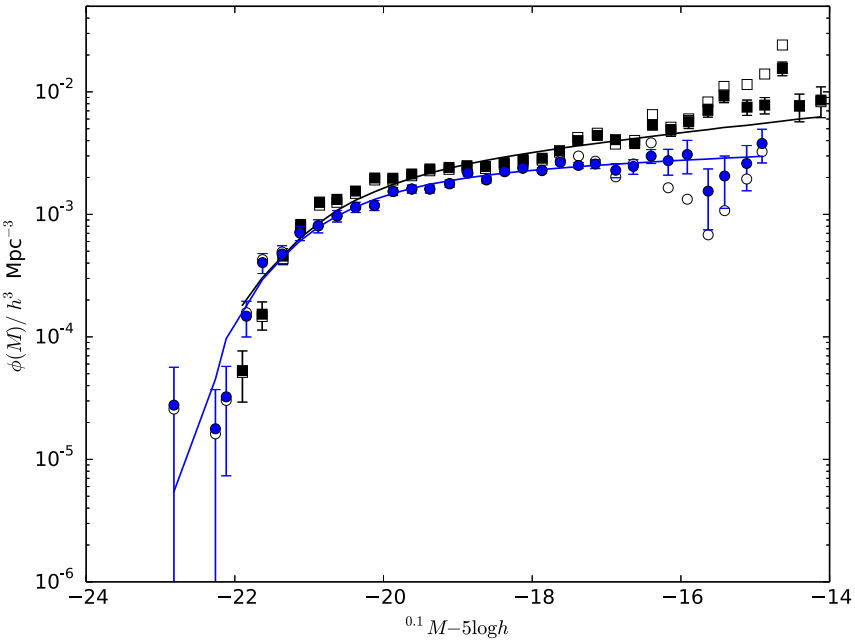

Figure 2.19: LFs from 2 bins of group masses; $8 < \log(M/M_\odot) \leq 12.08$ and $12.08 < \log(M/M_\odot) \leq 17$ presented in black and blue respectively. Symbols and lines are similar to Fig. 2.4.

($\log(M/M_\odot) = 8$) limits are chosen such as we include most of the local galaxies in the sample ($z \leq 0.1$).

Fig. 2.19 shows the LFs estimated in two mass bins; $8 < \log(M/M_\odot) \leq 12.08$ and $12.08 < \log(M/M_\odot) \leq 17$ plotted in black and blue respectively. Similar to Fig. 2.4, symbols correspond to non-parametric estimators and solid lines to the parametric estimator.

These LFs have very similar M^*, but the main difference is seen in the faint-end slopes. These values are presented in Table 2.5.

Due to the relationship between mass and velocity dispersion (Fig. 2.7), similar results are expected for the LFs dependence on velocity dispersion. The G^3C is now divided in two velocity dispersion (σ) bins: $1 < \sigma \leq 190$ km s^{-1} and 190 km s^{-1} $< \sigma$. Fig. 2.20 shows the LF for these bins, low range and high range in black and blue respectively. Differences at bright and faint end are similar to those presented above for the mass bins, where the LF is mostly affected at the faint end as well, meaning an agreement between the slopes with the mass bins. Values of the parametric LF are presented in Table 2.5.

When Fig. 2.19 and Fig. 2.20 are compared and following Fig. 2.7, these LFs are very similar considering both mass and velocity dispersion bins. The important issue

Table 2.5: α and M^* Schechter parameters fit to LFs and the dependence with 2 bins of group mass and velocity dispersion (σ).

$\log(M/M_\odot)$	α	$^{0.0}M^*$ - 5 lg h
8 - 12.08	-1.17 ± 0.02	-20.94 ± 0.06
12.08 - 17	-1.06 ± 0.03	-20.92 ± 0.09
σ (km s^{-1})	α	$^{0.0}M^*$ - 5 lg h
1 - 190	-1.18 ± 0.02	-20.97 ± 0.08
$\geq$ 190	-1.06 ± 0.02	-20.90 ± 0.08

here is to determine if the separation between the LFs at the faint end in both cases is actually large enough to talk about two different distributions of galaxies. Following Figure 18 in AR11, this separation can be explained; in this figure, richness and velocity dispersion distributions decrease as both values for these quantities increase, so when we cut the velocity dispersion distribution in two bins, there are lower groups with high velocity dispersion and consequently there are lower galaxies as well, this effect can be more observable at the faint end in Fig 2.19 and Fig. 2.20. The mass distribution peaks at middle values(Figure 18 in AR11). When we divide the mass distribution in two bins, the number of groups and galaxies in each bin are similar and we would expect LFs to be very close.

Dispersion Velocity divided in 3 bins

A similar analysis made for the dependence of mass in groups is carried out to analyse the dependence of the LF with the velocity dispersion to confirm the reliability of the differences at the faint end presented in Fig. 2.20. The G^3Cv6 catalogue is divided in three subsamples of velocity dispersion (σ) limited by [1, 155], [155, 293] and [293, 4000] kms^{-1}. These limits were chosen dividing the total distribution in three similar ranges (Table 2.6). LFs of these subsamples are presented in Fig. 2.21 where symbols are similar to Fig. 2.20 and colours, black, blue and red in ascending order of velocity dispersion, Schechter fit parameters are also showed in Table 2.6. The LF of galaxies in the middle and high range of velocity dispersion follows the same tendency at the faint end even when large error bars at highest σ range are considered; meanwhile galaxies in groups with low velocity dispersion have a higher density at faint magnitudes. At the bright end, the three LFs drop together in density and also a small difference is observed in absolute magnitude where galaxies tend to be brighter as the velocity dispersion increases; for the middle range

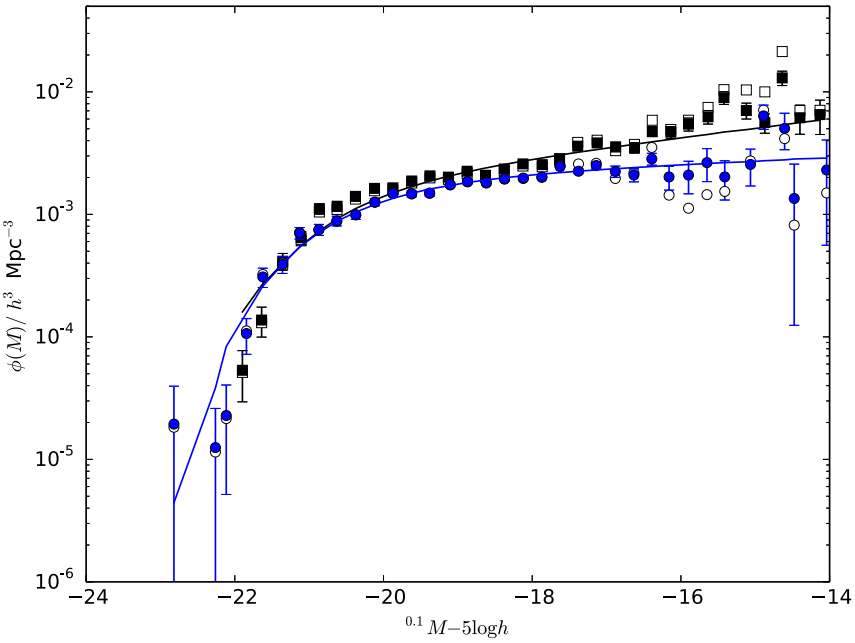

Figure 2.20: LF in 2 bins of σ; 1< $\sigma \leq$ 190 and 190 < σ km s^{-1} presented in black and blue respectively. Symbols and lines are similar to Fig. 2.4.

Table 2.6: Number of grouped galaxies within each σ bin of the G^3Cv6 catalogue and the Schechter parameters α and M^*.

σ bin $[kms^{-1}]$	$N_{galaxies}$	α	$^{0.1}M^*$-5lg$h$
$1 < \sigma < 155$	17948	-1.22 ± 0.11	-20.97 ± 0.29
$155 < \sigma < 293$	17992	-1.02 ± 0.10	-20.70 ± 0.18
$293 < \sigma < 4000$	18068	-1.04 ± 0.18	-20.73 ± 0.38

of velocity dispersion, the LF increases at the very bright end, perhaps just a statistical effect due to large error bars.

To observe carefully the differences in density, similar to Fig. 2.6, Fig. 2.22 presents the number density of galaxies ($n[Mpc^{-3}]$) in three regions of the LF, the bright end, middle magnitudes and faint end from top to lower panel. As expected, tendencies are similar to Fig. 2.6 for the upper and lower panels; middle panel differs from the tendency presented for the mass analysis. When varying the absolute magnitude interval, densities show the same tendencies; meaning an under-population of galaxies with intermediate magnitudes and σ. A similar feature has been reported previously by Miles et al. (2004) at intermediate magnitudes and X-ray dim groups (low σ). According to them a study

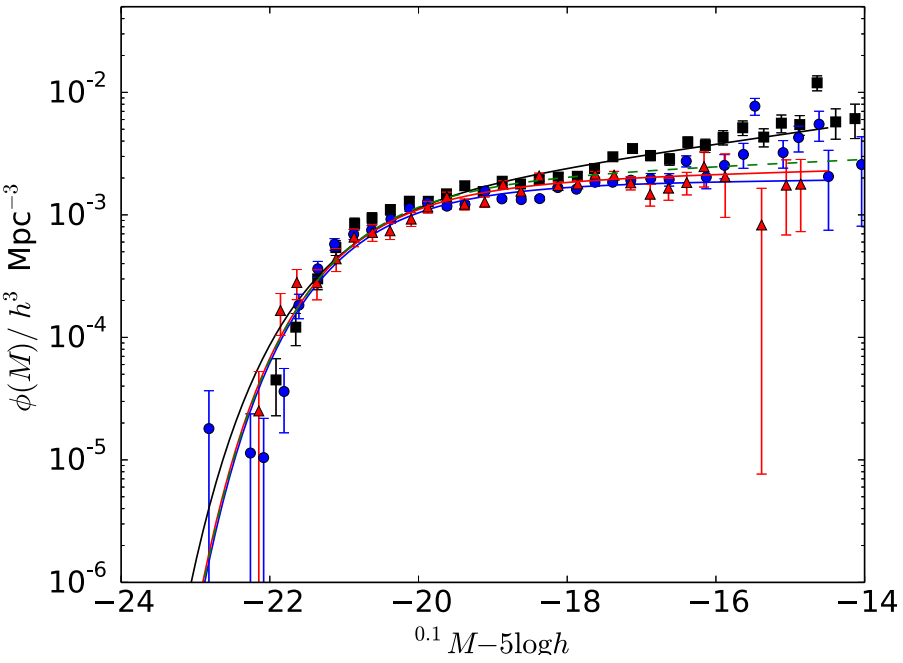

Figure 2.21: LF in 3 bins of velocity dispersion in the local Universe; $1< \sigma \leq 155$, $155< \sigma \leq 293$ and $293< \sigma$ [kms^{-1}] in black, blue and red respectively. Symbols and lines are similar to Fig. 2.4

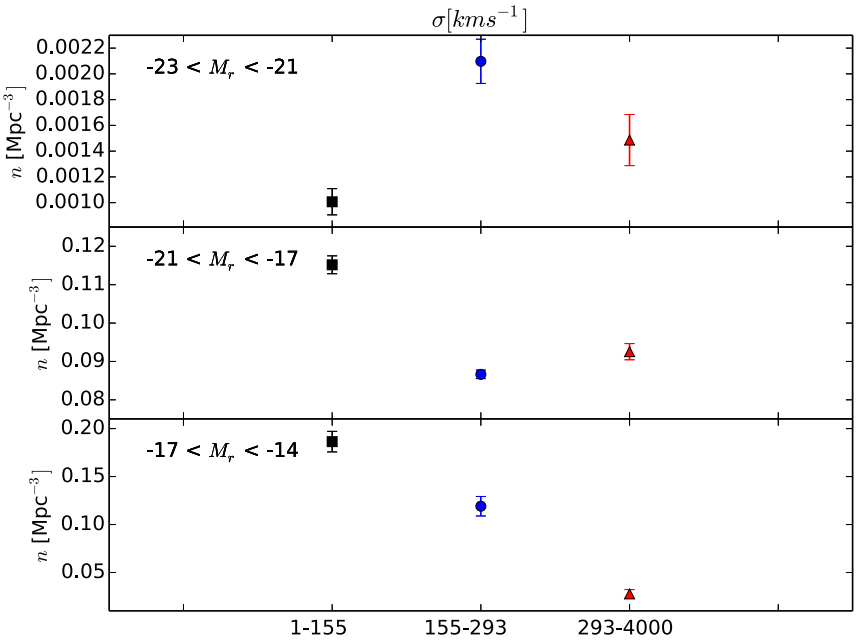

Figure 2.22: Number density ($n[Mpc^{-3}]$) of galaxies integrating the LFs over three bins of absolute magnitude [-23,-21], [-21, -17] and [-17 <] -14 in descending order respectively, for the three subsamples of σ in ascending order in black, blue and red respectively.

base on the X-rays is equivalent to one based on velocity dispersion. Based on a power-law relation between X-ray luminosity and σ (Helsdon and Ponman, 2000), Miles et al. (2004) suggest that at low σ the dynamical friction would facilitate the galaxy merging process, driving intermediate luminosity galaxies to merge and becoming in giant central galaxies. However, the dip found in this work is presented at middle σ. The big differences between Miles et al. (2004) and this work is the redshift at which the galaxies are presented. The most distant group in Miles et al. (2004) has a redshift of z=0.016, meanwhile in this section the groups are contained in a redshift of z <0.1.

LF evolution and the dependence on velocity dispersion

Fig. 2.23 presents the evolution of the galaxy LFs over the same intervals of redshift as done for the mass LF evolution, separated by three velocity dispersion bins [1, 155], [155, 293], [293, 4000] kms^{-1}, in black, blue and red respectively. The inset at the top shows again two-σ likelihood contours for the Schechter parameters α and M^* obtained from the parametric LF, and insets at middle and bottom show the 1-σ likelihood in one dimension normalised to peak at log L = 0 as α is fixed.

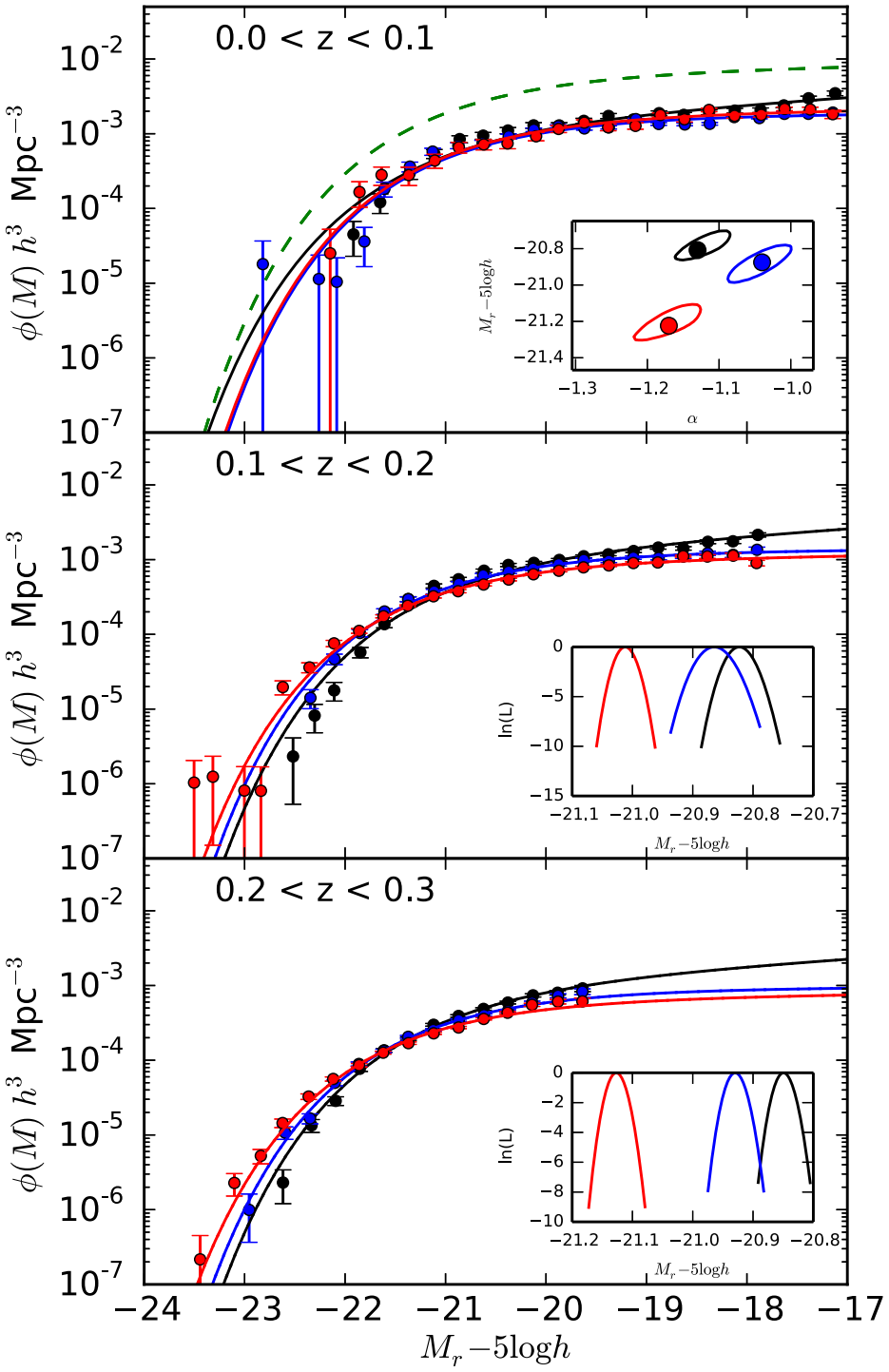

Figure 2.23: LF evolution for the subsamples computed according to the velocity dispersion of groups [1, 155], [155, 293], [293, 4000] kms^{-1} in black, blue and red respectively; for three redshift ranges [0.002, 0.1], [0.1, 0.2] and [0.2, 0.3] from the top to the bottom respectively. Symbols and lines are similar to Fig. 2.16. The inset at the top shows two-σ likelihood contours for the Schechter parameters α and M^* fitting the LF. The insets at middle and bottom show M^* likelihood ratios normalised to peak at log L = 0

Table 2.7: Schechter parameters for evolution of the LF in three ranges of z for the three subsamples of velocity dispersion.

subsample	bin σkms^{-1}	α	$^{0.1}M^*$-5lg$h$
z < 0.1			
	1-155	-1.22 ± 0.12	-20.97 ± 0.21
	155-293	-1.02 ± 0.11	-20.70 ± 0.13
	293-4000	-1.04 ± 0.18	-20.73 ± 0.27
z < 0.2			
	1-155	-1.22 ± 0.12	-20.82 ± 0.07
	155-293	-1.02 ± 0.11	-20.86 ± 0.08
	293-4000	-1.04 ± 0.18	-21.01 ± 0.05
z < 0.3			
	1-155	-1.22 ± 0.12	-20.85 ± 0.06
	155-293	-1.02 ± 0.11	-20.93 ± 0.06
	293-4000	-1.04 ± 0.18	-21.13 ± 0.07

Results are very similar to those obtained for the case of masses, due to the strong correlation between mass and velocity dispersion. A few small differences can be observed, mainly at the bright end, where galaxy population becomes brighter when the velocity dispersion increases. Note again, the large error bars of the LF at the bright end in the high mass bin and middle range of redshift. This effect can be explained by a high fraction of luminous AGNs, also predominantly massive. Table 2.7 presents the Schechter parameters of LFs in Fig. 2.23.

Likelihood insets are similar to those in Fig. 2.16, following the same tendencies with σ as well as with z (Fig. 2.24). Looking at Fig. 2.24, there are a few differences; the most significant is presented in the lowest z bin, where M^* estimated in the highest mass bin is overlapped with that one in the middle mass bin and not in the lowest mass bin as found in Fig. 2.17.

2.8.2 Comparing the mass estimators and mock catalogue predictions

The GAMA Galaxy Group Catalogue (G^3Cv6) has been extracted using the friends of friends grouping algorithm as mentioned above. The group mass has been estimated firstly using the dynamics of the system i.e. the dynamical mass; however, this estimation has to be corrected by the scaling factor A (See sec. 4.3 in AR11) to produce a halo mass

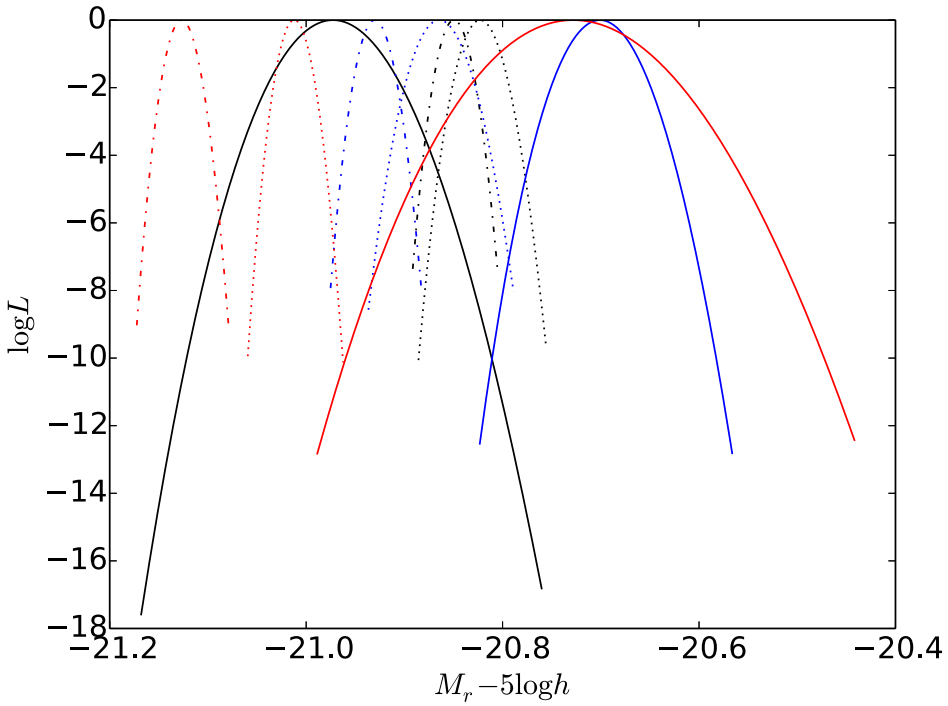

Figure 2.24: log Likelihood in 1D normalised to peak at log L = 0, same insets in Fig. 2.23 plus the distribution at z=0. Solid, dot and dashed lines represent the three intervals of z in ascending order; bins: [1, 155], [155, 293], [293, 4000] kms^{-1} in black, blue and red respectively.

comparing the best matching between FoF/halo mock groups. In this section, this quantity is simply called dynamical mass (sample i) in Table 2.8).

Han et al. (2015) apply a maximum-likelihood weak lensing analysis on the G^3Cv5 catalogue and examine how the halo mass scales with the mass observable estimators, particularly with the r-band group luminosity. In this paper the halo mass is estimated following the relation

$$M_{halo} = M_p(L_{grp}/L_0)^{\alpha_L}(\sigma_v/v_0)^{\alpha_\sigma}(1+z)^{\alpha_z} \tag{2.6}$$

where

$$\begin{aligned} \log(M_p) &= 14.15 - 0.07 \pm 0.30, \\ \alpha_L &= 0.78 + 0.02 \pm 0.29, \\ \alpha_\sigma &= 1.31 + 0.03 \pm 0.52, \\ \alpha_z &= -5.79 + 0.18 \pm 3.64, \end{aligned} \tag{2.7}$$

L_{grp} is the total luminosity of the group, $L_0 \equiv 2 \times 10^{11}\ h^{-2}L_\odot$ and $v_0 \equiv 500$ km s^{-1}. The L_{grp} is the total r-band luminosity down to M_r - 5 log h = -14 in solar luminosities. This is based on the total observed r-band flux and the fraction of light observable at the group redshift Robotham et al. (2011). In order to eliminate systematic errors, Han et al. (2015) created random catalogues to test the data. The errors presented in this equation are simply the standard deviation obtained from the model fit to these catalogues.

This is presented as sample ii) in Table 2.8.

Both methods are plotted against the other in Fig. 2.25. From this plot, it clear there is a discrepancy between both methods. So, they have to be tested against the intrinsic halo mass from the mock catalogues.

Left side of Fig. 2.26 shows the group LF divided in 3 mass bins, comparing the dynamical and luminosity halo mass estimators. Although every estimator results in a different mass distribution, the three mass bins were selected (in each distribution) containing a similar number of galaxies in each bin to avoid large Poisson bias; these samples are i) and ii) in Table 2.8 for dynamical and luminosity estimators respectively at $z \leq 0.1$. The top panel shows similar shapes for both LFs, only with a slightly difference at the bright end; this may be associated to a different number of galaxies, at these magnitudes. This effect is expected to be seen when comparing to the mock catalogue. Nevertheless, in the middle panel the LFs follow a similar shape at the bright end, but it is not clear at the faint end into large error bars. Any important difference will be notorious when comparing again with the mock catalogue. Analysing the highest mass bin, there are no differences in shape between the LFs within the large error bars presented at the bright

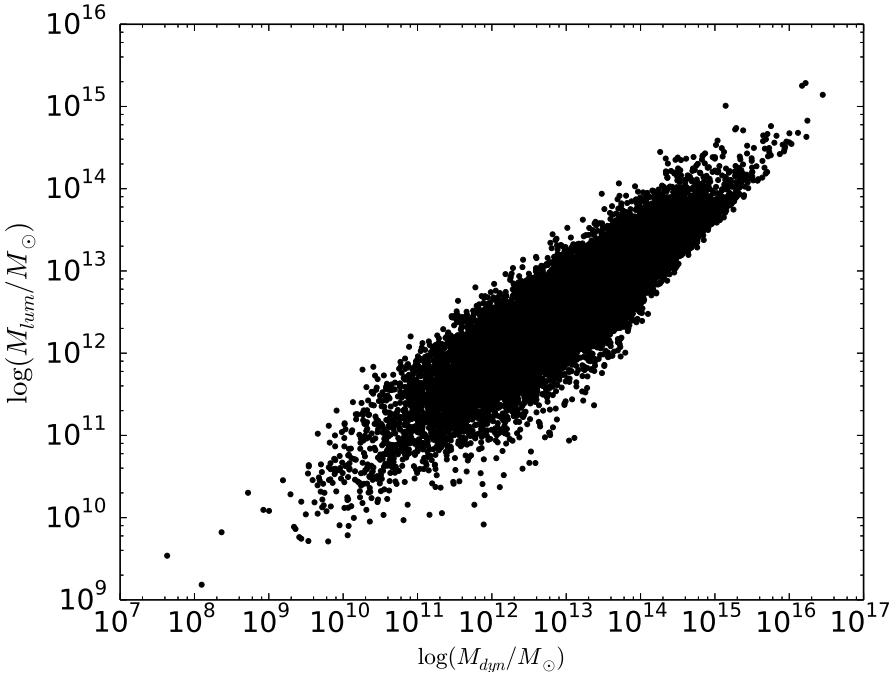

Figure 2.25: Luminosity vs dynamical halo mass estimators for the whole G^3Cv5 catalogue.

and faint ends. These differences can be confirmed looking at the right side of Fig. 2.26, where the only significant difference is shown at the bright-end for the low mass bin.

The GAMA Galaxy Group Catalogue (G^3C) has been created considering mock galaxy catalogues to test the quality and intrinsic limitations of a given group finder (AR11).

These mock galaxy catalogues used by AR11 were taken from the Millennium DM simulation (Springel et al., 2005), populated with galaxies by the GALFORM (Bower et al., 2006) semi-analytic galaxy formation recipe. The nine mock galaxy catalogues created have the exact GAMA survey geometry, with each mock extracted from the N-body simulation preserving the true angular separation between the three GAMA regions. However,

Table 2.8: $\log M/M_\odot$ limits for the three mass bins, considering the i) FoF dynamical halo mass, ii) FoF luminosity halo mass (Han et al., 2015) and iii) mock halo mass estimators.

Sample	lomass $\log M/M_\odot$	mimass $\log M/M_\odot$	himass $\log M/M_\odot$
i) FoF dyn	8 - 12.51	12.51 - 13.23	13.23 - 16
ii) FoF Lum	8 - 12.06	12.06 - 12.70	12.70 - 16
iii) Mock halo	8 - 12.91	12.91 - 13.62	13.62 - 16

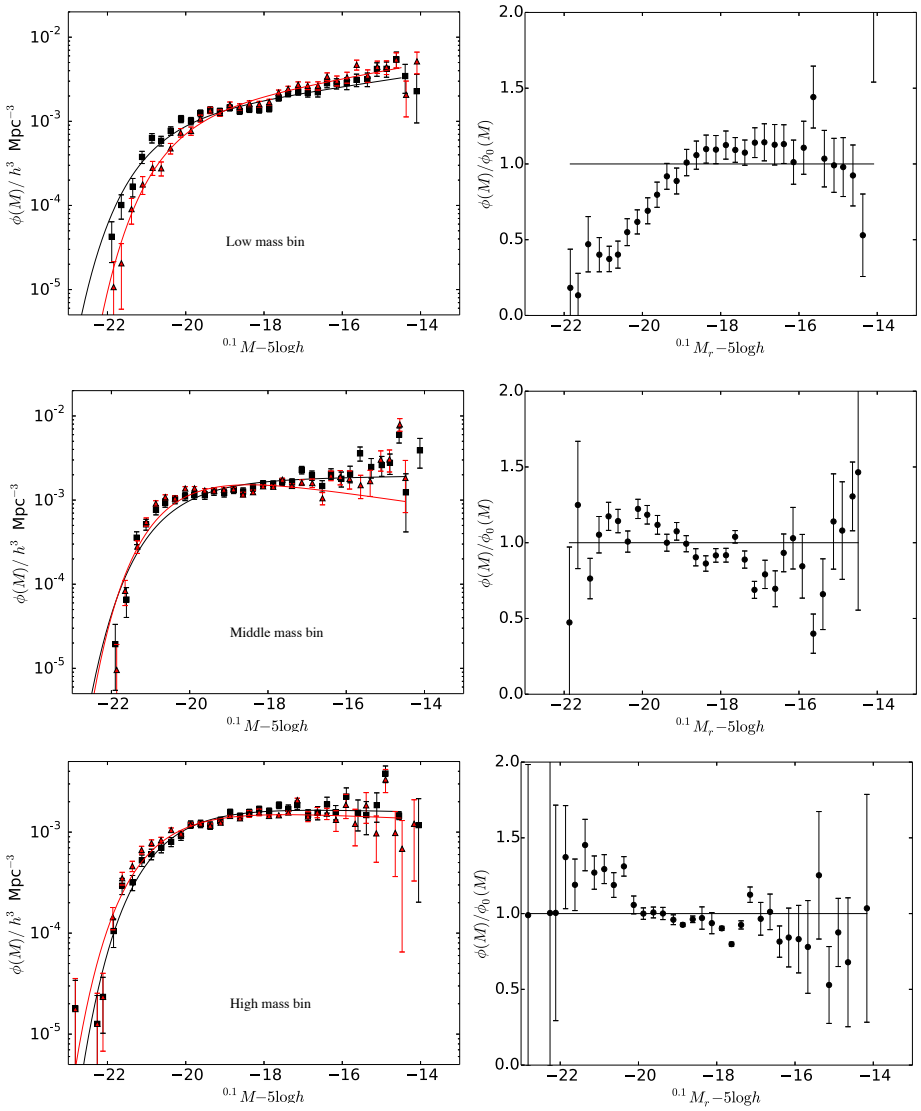

Figure 2.26: Left side, the G^3C LFs divided in three mass bins (considering the most similar number of galaxies in each bin) to compare differences between the dynamical halo mass (black) and luminosity halo mass red) estimators. From the top to the bottom, corresponding to the low, middle and high mass bins respectively for groups at $z \leq 0.1$. Right side, LF ratio of Fig. 2.26 considering the dynamical mass estimator as the reference, from the lowest mass bin (top panel) to the highest mass bin (bottom panel). Filled symbols represent the ratio between the SWML LF with an average of the errors; solid line shows the reference to the ratio=1

these mock catalogues are not totally perfect, one of the main limitations of this generation of the GAMA mock galaxy catalogue is the fact that luminosity-dependent galaxy clustering does not perfectly match the data (Kim et al., 2009), in particular in redshift space (Norberg, prep).

Sample iii in Table 2.8) contains the intrinsic groups found in the mock catalogue, containing the 9 mock catalogues together. The halo mass corresponds to the mass associated to these groups in the Millennium DM simulation. To estimate the LF for this sample, statistical effects of incompleteness associated with the GAMA sample (Loveday et al., 2012) have been ignored, since the mock catalogues are statistically complete.

The mock catalogue is also divided in three mass bins corresponding to the sample iii) in Table 2.8 to compare with the GAMA data.

Now the mock catalogue LF is compared to the G^3C LF considering the halo group mass as described above.

Left panels of Fig 2.27 show the GAMA data (using the dynamical mass estimator) to mock catalogue LF ratio for low, middle and high mass bins in the top, middle and bottom panel respectively. This corresponds to samples i) and iii) in Table 2.8. Although there is a good correlation in all the bins between the mock and GAMA catalogues, there are notorious differences between them. In the low mass bin, there are around 5% more galaxies in the mock catalogue than in G^3C for the very bright end ($M_r \sim$ -21.5); this effect is not clear at the faint end due to large error bars. There is large scatter in the middle mass bin; however, the most significant difference is presented at $M_r \sim$ -20 with an apparent excess of galaxies in the G^3C catalogue. For the high mass bin, the dispersion is less than 5%, so no important differences can be seen. The last data points at the bright end are possibly a lack of very bright galaxies in the G^3C catalogue.

Right panels of Fig 2.27 show the corresponding GAMA data (luminosity mass estimator) to mock catalogue LF ratio divided by mass bins similar to Fig 2.27. Samples ii) and iii) in Table 2.8 show the corresponding mass limits. Looking at the all mass bins, the relationship between the GAMA data and mock catalogues obeys the same tendency presented in Fig 2.27 with higher ratio differences. The bright-end in the low mass bin is dominated by the mock galaxies, being $\sim$12% more than the GAMA galaxies. In the middle mass bin the difference at $M_r \sim$ -20 is very similar to that in Fig 2.27 within large error bars, meaning a negligible difference between them. For the high mass bin there are no differences between them. These results were expected from Fig. 2.26.

Based on these results and those in Han et al. (2015), the luminosity-based mass

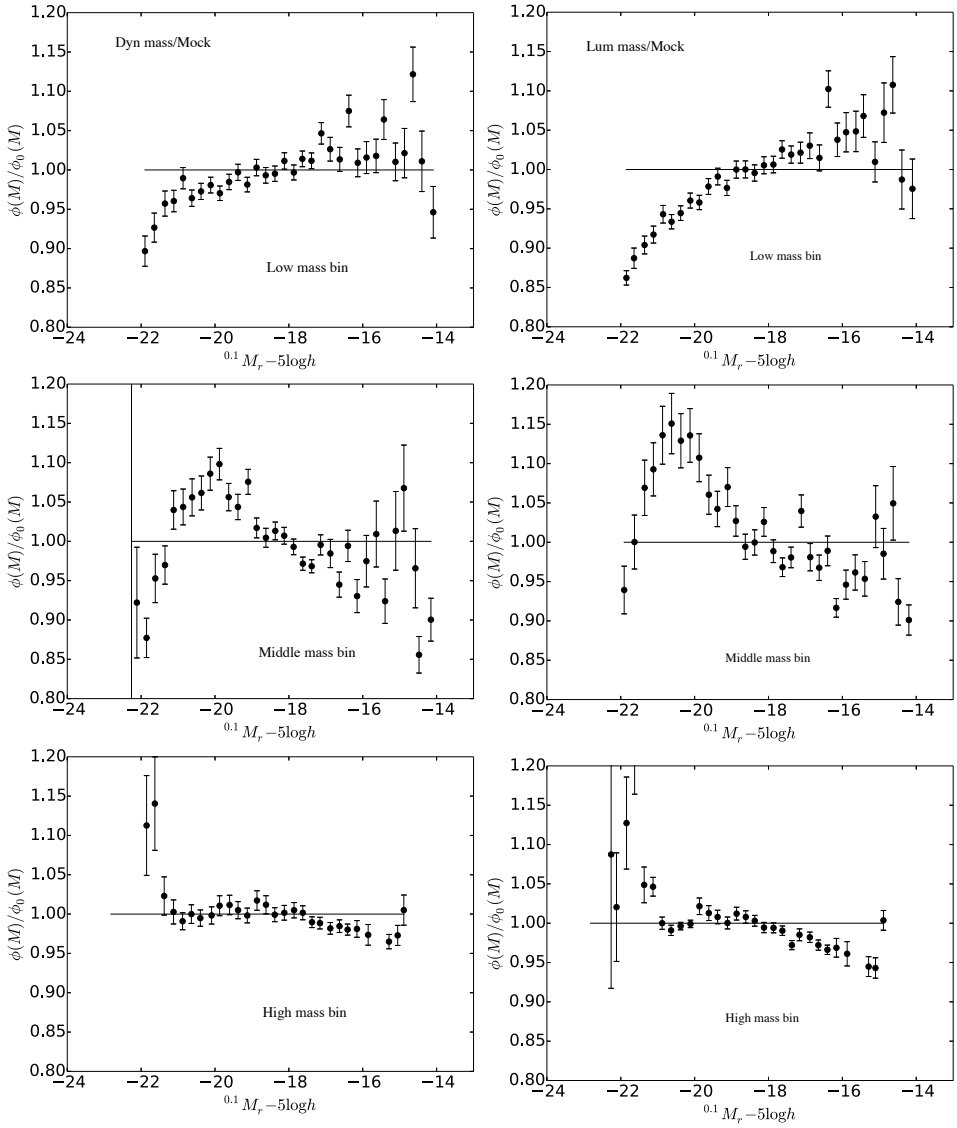

Figure 2.27: GAMA data LF and GAMA mock LF ratio for galaxies in three mass bins using the dynamical mass estimator (left panels) and the luminosity based mass (right panels), from the lowest bin (top panel) to the highest bin (bottom panel). Filled symbols represent the ratio between the SWML LF with an average of the errors; solid line shows the reference to the ratio=1.

method is the best to estimated the halo mass and this was used in this paper to separate the sample in section 2.4.2.

Chapter 3

PaperII

UNAM-KIAS Catalog of Isolated Galaxies:
The Optical Luminosity and Mass Functions.

Vázquez-Mata J. A., Lacerna I., Hernández-Toledo H., Rodriguez-Puebla A.,
Loveday J. et al.

We use the UNAM-KIAS Catalog of Isolated galaxies to calculate the galaxy luminosity and stellar mass functions as well as the gas-to-stellar mass ratio. The luminosity function was estimated for the UNAM-KIAS catalogue according to the galaxy morphology in the *ugriz* bands. We find an interesting feature in the LF shape, a dip in the middle magnitudes for all the bands, a presumably merger effect that is not well understood but that many authors have found in other work without a strong explanation. To compare the isolated galaxy LF, we also estimated the LF for two samples in low dense environments using the GAMA survey. There are significant differences of the LF with previous works for galaxies in similar environments but smaller samples. However, there is a good agreement between the UNAM-KIAS and the GAMA samples for the LF shape and the magnitude limits. We find that LF depends strongly with the number of galaxies contained in the sample. We have estimated the Schechter parameters characteristic of a statistical complete sample of isolated galaxies. These new values must be considered for other studies based on these type of galaxies. The stellar mass function agrees with our expectations and we establish the gas-to-stellar mass ratio for isolated galaxies. From the SMF, we also found that galaxies with $\log M$ $[M_{\odot}]$ $\sim$11 stop forming stars, with a few

blue galaxies in the last star formation stage, with a notable 50% of spirals. This suggest that morphology can the be last transition of isolated galaxies to become in a passive red galaxy.

3.1 Introduction

One of the most fundamental properties of a galaxy population is the luminosity distribution of galaxies, well known as the galaxy luminosity function (LF). The LF represents the number of galaxies contained in a volume in luminosity intervals, and has become an important tool to characterize statistically either stars or galaxies from large surveys. The shape of a LF depends on the physical process carried out in galaxies observed at certain wavelength, mostly related to star formation process. The density can be obtained by integrating the LF. This density also changes according to the type of galaxy considered, cosmological environments, wavelength and redshift. Statistically, the LF is a fundamental study to test the cosmological models of formation and evolution of galaxies.

The distribution of galaxy luminosities and stellar masses in the present day universe is of fundamental importance for studying the assembly of galaxies over redshift, both observationally and theoretically (e.g., Cole et al. 2000, Brinchmann and Ellis 2000, Somerville et al. 2001, Wolf et al. 2003, Croton et al. 2005, Yang et al. 2009). In addition, providing the zero redshift baseline for LF evolution, the local LF powerfully constrains much of the important physics affecting the assembly of baryons in dark matter haloes. According to the Λ Cold Dark Matter (ΛCDM) hierarchical scenario, models predict the existence of many low-mass haloes in voids or being accreted into massive haloes (White and Frenk, 1991); if these haloes are massive enough to contain dwarf galaxies, then we will have a large number of faint galaxies and the LF must have a pronounced ascending slope at the faint end. However, this steep slope is not found in observations as we showed in Paper I, where satellite galaxies dominate the LF faint end of the groups LF, however, the slope is not as steep as predicted by some cosmological models. The isolated galaxy LF can test the number and distribution of galaxies contained in haloes, far from the massive haloes acreating satellites, and give information about the intrinsic physical process of the isolated galaxies.

There have been a number of recent studies that have estimated LFs and mass functions (MFs) based on large surveys like 2dF Galaxy Redshift Survey (Folkes et al., 1999), the Sloan Digital Sky Survey (SDSS; York et al. 2000) and most recently the Galaxy and Mass Assembly survey (GAMA; Driver et al. 2009, Driver et al. 2011). Around the knee

of the LF, which represents the dominant contribution to the overall luminosity density, the agreement between the LFs from different surveys is consistent. In the optical spectrum, luminosity densities agree at typically the 20% level or better, accounting for differences in filter bandpasses and median redshift (e.g., Norberg et al. 2002, Liske et al. 2003, Blanton et al. 2003). Many authors (e.g. Croton et al. 2005; McNaught-Roberts et al. 2014) have studied the dependence of the LF with the environment and redshift, finding a correlation between the characteristic magnitude and the faint end slope with the environment. These studies are based on the galaxies contained in spheres with certain radius to associate the density.

The most recent study considering the differences of the LF according to the morphological type for isolated galaxies was carried out by Sulentic et al. (2006). They use the AMIGA sample (Verdes-Montenegro et al., 2005), a refinement of the original catalogue of isolated galaxies (KIG; Karachentseva 1973), to estimate the B-band LF.

The goal of this paper is to characterize the UNAM-KIAS Catalog of Isolated Galaxies (Hernández-Toledo et al., 2010). This catalogue is unique because it is the first compilation of isolated galaxies considering a 3D spatial distribution to warranty the isolation of the galaxies and contains almost the double number of galaxies in AMIGA. In this paper, based on the UNAM-KIAS Catalogue, we explore in detail the LFs of galaxies in the SDSS bands, from the u-band (0.35 μm) to the z-band (0.9 μm), to understand the intrinsic process carried out by the galaxies in low dense environments and to establish for the first time, reliable Schechter parameters for isolated galaxies. To understand better the physical process, we also investigate the stellar MF of galaxies with a factor of 1000 in stellar mass, using the relations between stellar mass-to-light ratio and $(g-r)$ colour from Bell et al. (2003). Fortunately, many of the UNAM-KIAS galaxies have H I and H_2 information (cold gas). Using this data we can estimate the gas-to-stellar mass fraction to check how is this fraction compare to the typical spiral galaxies in all environments; and we can estimate the halo to stellar mass fraction. These studies establish an extra test to the theoretical models as described by Rodríguez-Puebla et al. (2011) and Lacerna et al. (2014).

In section 2 we describe the samples used, the corrections applied and the selection effects. In section 3 we show the procedure to estimate the LF and the stellar MF. LF results are presented in section 4, the stellar MF in section 5 and the gas calibration in section 6. Finally, discussion and conclusions are presented in section 7.

For this work, we assume the standard cosmology parameters of Ω_M=0.3, Ω_Λ=0.7 with

a Hubble constant of H_0=100h km s^{-1} Mpc^{-1}.

3.2 THE DATA, DATA QUALITY, AND SELECTION EFFECTS

3.2.1 UNAM-KIAS

The UNAM-KIAS Catalogue of Isolated galaxies is originated from the New York University Value-Added Galaxy Catalog (NYU-VAGC; Blanton et al. 2005). The NYU-VAGC are galaxies from the SDSS (DR5; Stoughton et al. 2002) selected up to redshift $z = 0.3$. The UNAM-KIAS catalogue provides a nearly complete $13 < r < 15.2$ sample of ∼1500 isolated galaxies with accurate *ugriz* fluxes and magnitudes. Due to image quality, a uniform and detailed g-band morphological classification is established (Hernández-Toledo et al. 2010; here after HT10).

Briefly, the isolation criteria, followed by the UNAM-KIAS catalogue, was implemented from a variation on the criteria developed by Karachentseva (1973) including full redshift information. These criteria are specified by three parameters: i) the projected separation from the nearest neighbour across the line of sight, $\Delta d \geq 100 \times R_{\rm Petrosian}$; ii) the radial velocity difference, $\Delta V \geq 1000$ km s^{-1}, and if the last two are broken, a third parameter is considered, iii) the extinction-corrected Petrosian r-band apparent magnitude difference between a candidate galaxy and any neighbouring galaxy, $\Delta m_r \geq 2.5$. A detailed description of the catalogue and the selection criteria can be found in HT10.

3.2.2 GAMA

The Galaxy and Mass Assembly project (GAMA) is a multi-wavelength spectroscopic galaxy survey (Baldry et al., 2010); based on the Sloan Digital Sky Survey Data Release 7 (SDSS DR7). In the second phase, GAMA-II (Liske et al., 2015) consists of three equatorial regions, each of 12 × 5 degrees with a Petrosian magnitude limit of $r < 19.8$ mag.

Since GAMA II is a highly complete spectroscopic survey (98%) with uncertainty $\sigma_v \approx$ 50 kms^{-1}, we decided to take into account two similar samples of galaxies at low density environments to compare with the UNAM-KIAS catalogue:

I. Void galaxies sample, compiled by Alpaslan et al. (2013) applying the minimal spanning trees (MST; Iyanaga et al. 1980) method in a volume limited sample limited by z = 0.213 and M_r = 19.77. Once galaxies are classified as ungrouped, the MST method is applied and void galaxies are those that were rejected from the MST used to identify

tendrils. This void galaxies sample contains 4542 objects. Due to the small number of galaxies at very low redshift, we estimate the LF up to $z = 0.2$.

II. Isolated galaxies are defined as the galaxies ungrouped by the GAMA Galaxy Group Catalogue (G^3Cv6). This catalogue was generated applying a friend-of-friends (FoF) grouping algorithm; the first version of this catalogue (G^3Cv1) is presented by Robotham et al. (2011) using the GAMA-I survey. The G^3Cv6 catalogue contains a total of 23838 groups with multiplicity $\geq$2 containing 73268 galaxies, $\sim$40% of the whole GAMA survey. In this case, we consider galaxies with $z \leq$0.1.

3.2.3 Completeness

One of the advantages of the UNAM-KIAS catalogue is the completeness; $\sim$ 80% complete up to 15.2 r-band mag (HT10). This magnitude limit is a consequence of the selection criterion that excludes fainter galaxies to ensure they are in the limits of the parent sample. Fig. 3.1 (Fig. 17 in HT10) presents a way to estimate the completeness of the sample for the $ugiz$ bands using the V/V_{max} method (HT10 for more details). We can infer the sample completeness by finding the magnitude at which the mean value of the V/V_{max} turns drastically down (Huchra and Sargent 1973, Xu and Sulentic 1991). However, no values were reported by the authors since no well-defined cut-offs can be observed. We therefore need to consider another way to establish the sample limit for the $ugiz$ bands.

We propose to use the distributions of galaxy colours in order to assign the catalogue limiting magnitudes in the $ugiz$ bands. Fig. 4.1 shows histograms of $u-r$, $g-r$, $i-r$ and $z-r$ Petrosian colours. The vertical dashed lines indicate the 1- and 99-percentiles in each colour. The magnitude limits in the $ugiz$ bands are then given by adding the leftmost of these colours (bluest for $u-r$ and $g-r$, reddest for $i-r$ and $z-r$) to $r = 15.2$ mag. For example, only 1% of galaxies are bluer than $g-r = 0.4$ mag, and so UNAM-KIAS catalogue is 99% complete to $g = 15.6$ mag. These 99%-complete colour limits are given for each band in Table 4.1 (by design, the r-band is actually 100% complete to $r = 15.2$). These values agree accurately to the magnitude at which the $< V/V_{max} >$ turns down (Fig. 3.1). Note the large faint tail in the u-band after the apparent magnitude limit estimated. These limits have been plotted in Fig. 3.1 (dashed lines). These lines agree with the $< V/V_{max} >$ knee, so this method is a good test to find the magnitude limits for $ugiz$ bands.

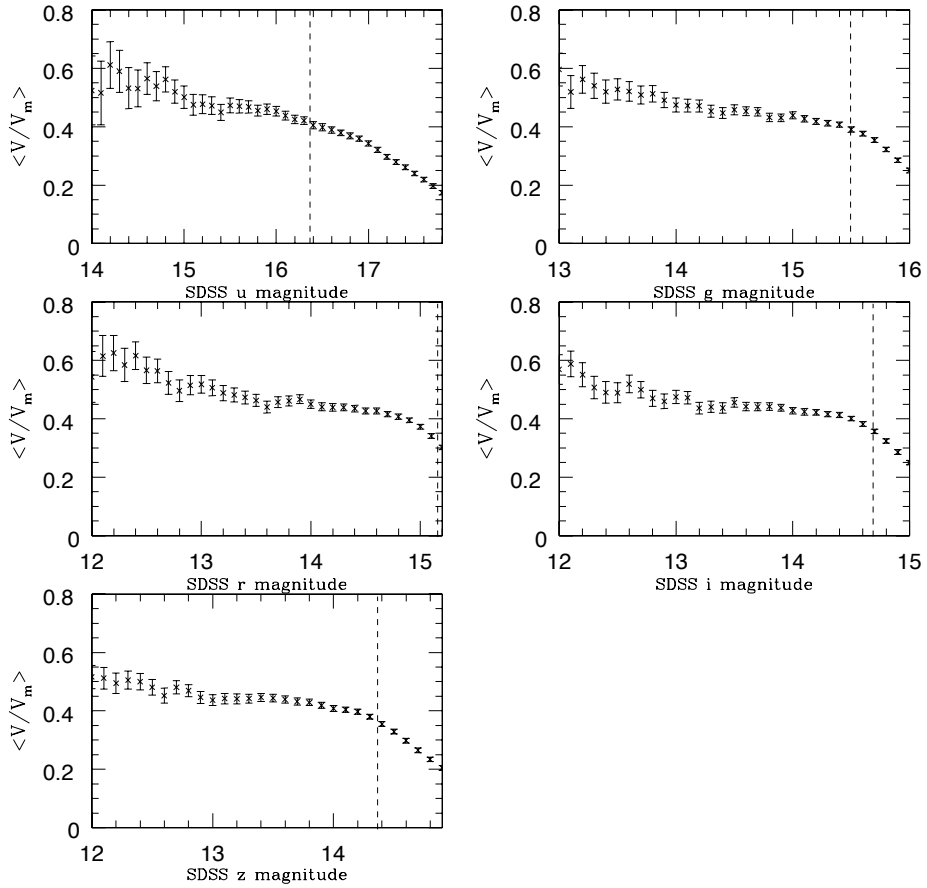

Figure 3.1: Vmax test and the completeness of the UNAM-KIAS isolated galaxy sample (Fig. 17 in HT10). Dashed lines show the magnitude limits presented in Table 4.1.

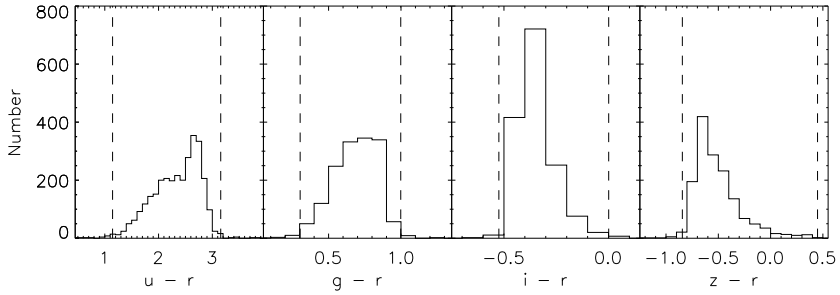

Figure 3.2: Petrosian $u-r$, $g-r$, $i-r$ and $z-r$ colour histograms in 0.1 mag bins for UNAM-KIAS galaxies. The vertical dashed lines indicate the 1- and 99-percentiles; the leftmost of which defines colour completeness in the *ugiz* bands.

Table 3.1: Magnitude limits in the *ugriz* bands, where $band-r$ corresponds to the colours of each band with respect to r and m_{faint} is the chosen faint apparent magnitude limit using the 1-percentiles in each colour distribution. The bright limit is $m_{bright} = 11.0$ mag in all bands.

band	$band-r$	m_{faint}	m_{bright}
u	1.15	16.35	11.00
g	0.30	15.50	11.00
r	0.00	15.20	11.00
i	-0.52	14.68	11.00
z	-0.84	14.36	11.00

3.2.4 K-correction

Although this is a very local sample of galaxies ($z < 0.1$), we have to consider the effect of the redshift at which galaxies are being observed. This effect is corrected by the K-correction (Humason et al., 1956); this correction is applied to the intrinsic luminosity according to the rest frame of the galaxy. This correction depends on redshift, passband and the galaxy spectral energy distribution (SED). The whole sample has been corrected using the KCORRECT V4_2 code (Blanton et al., 2003) where a rest frame of $z_0 = 0.1$ is considered.

3.2.5 H I Data

We use the information of the H I line magnitude (corrected for self-absorption) from the HyperLeda database[1] for the sample of isolated galaxies to estimate their gas mass M_{gas} content. The neutral hydrogen line magnitude in 21 cm, m_{21}, is converted into H I mass M_{HI} by using

$$\frac{M_{HI}}{M_{\odot}} = 2.36 \times 10^5 \; d_L^2 \; 10^{(17.4-m_{21})/2.5} \; , \tag{3.1}$$

where d_L is the luminosity distance in Mpc (Roberts and Haynes, 1994). The gas mass is calculated with a simple correction for helium and metals, $M_{gas} = 1.4 M_{HI}$. We found 398 isolated galaxies with the H I line information available in the HyperLeda database.

In addition, we identified five other isolated galaxies in the α40 catalogue of 21 cm H I line sources of the Arecibo Legacy Fast Arecibo L-band Feed Array (ALFALFA) survey

[1] http://leda.univ-lyon1.fr/

(Haynes et al., 2011) and 7 other isolated galaxies in the catalogue of Springob et al. (2005). In total, we estimated the gas mass for 410 isolated galaxies, ∼27% of the total UNAM-KIAS catalogue, using the 21 cm H I line.

3.3 Luminosity and Stellar Mass functions

3.3.1 LF and SMF Estimation

We estimate the galaxy luminosity function using the non-parametric $1/V_{max}$ (Schmidt 1968, Felten 1977) and the step-wise maximum likelihood (SWML, Efstathiou et al. 1988) methods. The V_{max} method has the disadvantage that it is sensitive to galaxy density variations; on the other hand, the SWML method is insensitive to density fluctuations of this type (although both methods are sensitive to density fluctuations when calculating the overall LF normalization).

The SWML method makes the assumption that the shape of the LF is independent of environment; however, there is impressive evidence against this assumption, at least in the optical (De Propris et al. 2003, Hütsi et al. 2002, McNaught-Roberts et al. 2014). In contrast, the V_{max} method does not make any a priori assumptions regarding the form of the LF.

We consider the V_{max} and SWML methods; however, both methods determine identical results within the error bars (Fig. 3.3) as found also by other authors (e.g. Cole et al. 2001, Loveday et al. 2012). Therefore, $1/V_{max}$ is used for the rest of this work, because we are considering galaxies in the same environments.

To parametrize the galaxy LF, we have assumed the standard Schechter function (Schechter, 1976):

$$\phi(M) = 0.4ln10\phi^*(10^{0.4(M^*-M)})^{1+\alpha}exp(-10^{0.4(M^*-M)}), \tag{3.2}$$

where M^* is the characteristic magnitude, ϕ^* is the galaxy density and α is the faint-end slope.

The stellar mass estimation (M_*) is not a simple task, VESPA (Tojeiro et al., 2009) is the largest database containing the mass of a large fraction of the SDSS survey. However, the isolated galaxies in the UNAM-KIAS catalogue only match up to 80% with VESPA. For this reason, stellar masses have been estimated using the M/L ratios from Bell et al. (2003), using a Kroupa (2001) initial mass function as described by Yang et al. (2009),

$$\log\left[\left(\frac{M_*}{h^{-2}M_\odot}\right)\right] = -0.306 + 1.097(g-r) - 0.10 - 0.4(^{0.0}M_r - 5\log h - 4.64). \quad (3.3)$$

Here, -4.64 is the M_r of the Sun in the AB system Blanton and Roweis (2007) and -0.10 is the term related to the initial mass function adopted.

Either for the LF or the SMF, we follow the same method based on the V_{max} method. Given a galaxy with apparent magnitude m_x in the x-band and redshift z, the absolute magnitude M_x is estimated by

$$M_x = m_x - 5\log(D_L(z)/\mathrm{Mpc}) - 25 - K(z) + Q(z), \quad (3.4)$$

where

$$D_L(z) = D_H \int_0^z \frac{1+z}{E(z)} dz, \quad (3.5)$$

$$E(z) = \frac{1}{\sqrt{\Omega_{m,0}(1+z)^3 + \Omega_{\Lambda,0}}}, \quad (3.6)$$

and

$$D_H = c/H_0. \quad (3.7)$$

$K(z)$ and $Q(z)$ are the $K-$ and evolution corrections respectively, c is the speed of light in the vacuum and H_0 the Hubble constant.

To select a galaxy to estimate the mass function, we impose the following conditions:

1) Given the apparent limit magnitude given by the survey ($m_{lim,r} = 15.2$ in SDSS), the absolute limit magnitude is estimated by

$$M_{lim,x} = m_{lim,x} - 5\log(D_L(z)/\mathrm{Mpc}) - 25 - K(z_i) + Q(z_i), \quad (3.8)$$

where z_i is the i galaxy redshift.

2) We consider all the galaxies that follow $M_{lim,x} > M_{x,i}$, otherwise the galaxy is neglected.

3) Given the apparent limit magnitude $m_{lim,x}$, the maximum distance at which the galaxy can be observed with an absolute magnitude $M_{x,i}$ is:

$$5\log(D_L(z_{max,i})/\mathrm{Mpc}) = m_{lim,x} - M_{x,i} - 25 - K(z_{max,i}) + Q(z_{max,i}), \quad (3.9)$$

4) Once we get $z_{max,i}$, we need to check that this redshift is within the observed volume $z_{vol,i}$. To estimate the maximum volume at which this galaxy can be observed (V_{max}), we follow

$$z_{max,i} < z_{vol} \text{then} V_{max,i} = \frac{\Omega_S}{3}\left[\left(\frac{D_L(z_{max,i})}{1+z_{max,i}}\right)^3 - \left(\frac{D_L(z_{min})}{1+z_{min}}\right)^3\right]$$
$$z_{max,i} > z_{vol} \text{then} V_{max,i} = \frac{\Omega_S}{3}\left[\left(\frac{D_L(z_{vol})}{1+z_{vol}}\right)^3 - \left(\frac{D_L(z_{min})}{1+z_{min}}\right)^3\right] \tag{3.10}$$

where $\Omega_S = (\pi \ / \ 180)^2 \ A$. A is the survey area in square degrees.

5) For each magnitude bin ΔM_x the luminosity function in the interval $M_x \pm \Delta M_x \ / \ 2$ is:

$$\phi(M_x) = \frac{1}{\Delta M_x}\sum_i \frac{1}{V_{max,i}} \tag{3.11}$$

and the Poisson error is given by

$$\sigma = \frac{1}{\Delta M_x}\sqrt{\sum_i \left(\frac{1}{V_{max,i}}\right)^2} \tag{3.12}$$

6) For the stellar masses, similar to equation (3.8), the completeness limit (following van den Bosch et al. 2008) is given by:

$$\log[M_{*,lim}/(h^{-2}M_\odot)] = \frac{4.852 + 2.246\log D_L(z) + 1.123\log(1+z) - 1.186z}{1 - 0.067z}, \tag{3.13}$$

Similar to the LF, for each mass bin ΔM_* the stellar mass function in the interval $M_* \pm \Delta M_* \ / \ 2$ is:

$$\phi(M_*) = \frac{1}{\Delta M_*}\sum_i \frac{1}{V_{max,i}}. \tag{3.14}$$

3.3.2 Colour and sSFR

The specific star formation rate (sSFR), defined as the star formation rate (SFR) divided by the stellar mass, has been obtained from the MPA-JHU DR7 catalogue, [2] and it is an updated version of the estimates presented in Brinchmann et al. (2004) by using a spectral synthesis fitting model.

[2] Available at http://www.mpa-garching.mpg.de/SDSS/DR7/

To separate the SMF in colour and passive/active galaxies, we follow the same method presented in Lacerna et al. (2014) based on the distribution of galaxies for different samples including the UNAM-KIAS catalogue. Galaxies can be separated in red and blue by

$$g - i = 0.16[\log(M_*)10] + 1.05, \tag{3.15}$$

and in passive/active galaxies following

$$\log(\mathrm{sSFR}) = -0.65[\log(M_*) - 10] - 10.87, \tag{3.16}$$

where M_* is in units of $h^{-2}M_\odot$ and sSFR is in units of yrs^{-1} (see Tables 4 and 5 in Lacerna et al. (2014) for the cut limits in terms of mass).

3.4 Results

Fig. 3.3 shows the LF of the UNAM-KIAS catalogue in the *ugriz* bands from top to bottom respectively. Filled symbols present the LF based on the $1/V_{max}$ method, continuous lines correspond to the best Schechter fit using the chi-square method and open symbols the SWML based LF as comparison. The corresponding Schechter parameters are presented in Table 3.2. As we expect, M^* increases from blue to red bands, as a result of the old galaxy population and the reddening of light due to the reemission of dust and gas contained in the galaxies (e.g. Blanton et al. 2005). For all of the bands, there is an unclear dip at intermediate magnitudes ($\sim$19 in the r-band), presented in both, the V_{max} and SWML estimators. This feature has been seen by other authors (e.g. Miles et al. 2004) and most recently by Moorman et al. (2015) using data from ALFALFA and SDSS. They find this feature for the global LF from ALFALFA associated with galaxies in dense regions, and also with the SDSS data, specifically using the red early type population. For the UNAM-KIAS LF, this dip is presented either for early or late type galaxies. A possible explanation is just the lack of galaxies very close to the M^*, due to, some isolated galaxies are likely recent merger products at a fixed large-scale density (Park et al., 2008) and these mergers close to the characteristic magnitude M^* may become these galaxies in brighter galaxies.

3.4.1 Early- vs. late-type galaxies

Fig. 3.4 shows the LFs divided by two broad morphological types; E and S0 are considered as early-type galaxies (red) and Sa-Sd as late-type galaxies (blue), and in black the total

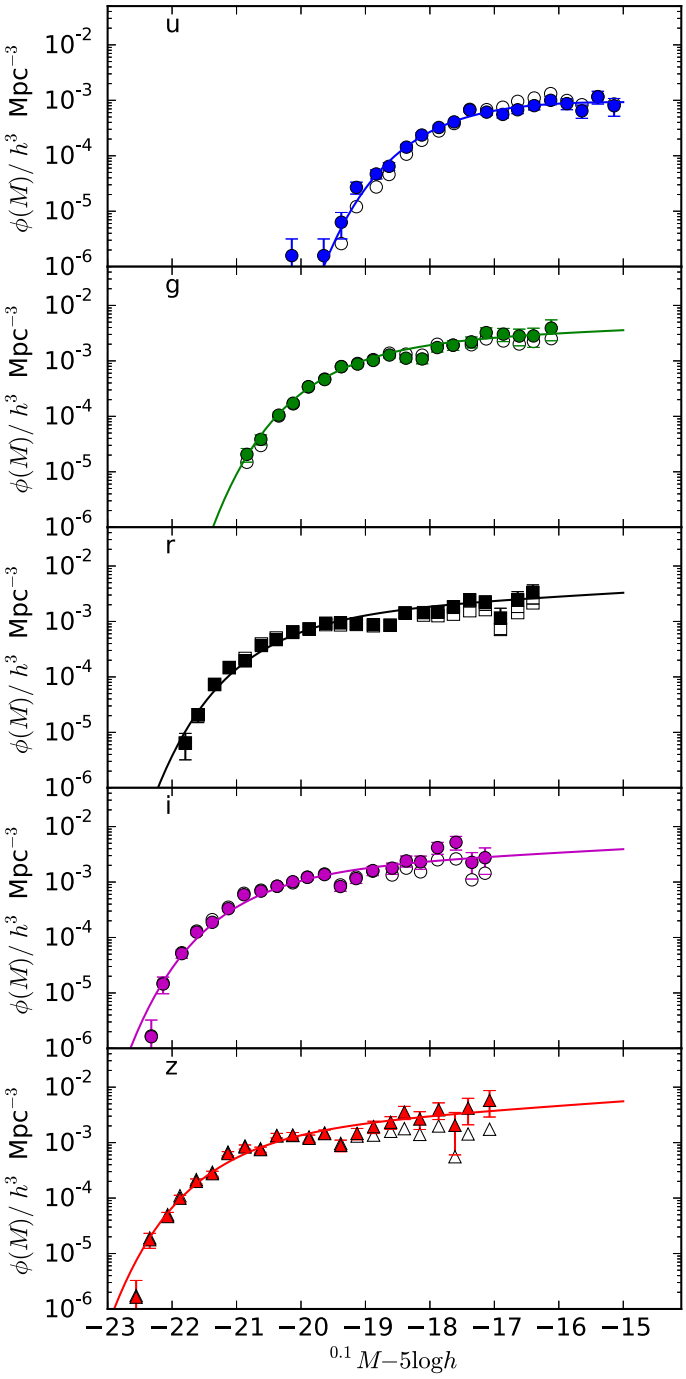

Figure 3.3: LF in the *ugriz* bands in blue, green, black, magenta and red colours, respectively. Symbols present the $1/V_{max}$ method, continuous lines correspond to the best adjust using the a chi-square method, and open symbols present the results using the SWML estimator as comparison.

Table 3.2: *ugriz* Schechter parameters.

band	α	$^{0.1}M^*$ - 5 $\log h$	$\phi^*\times$ 100 $/h^3\mathrm{Mpc}^{-3}$
u	-0.90 ± 0.25	-17.48 ± 0.13	0.14 ± 0.06
g	-1.11 ± 0.01	-19.17 ± 0.16	0.26 ± 0.07
r	-1.16 ± 0.01	-20.10 ± 0.18	0.17 ± 0.07
i	-1.15 ± 0.01	-20.51 ± 0.17	0.20 ± 0.07
z	-1.20 ± 0.01	-20.76 ± 0.19	0.21 ± 0.08

LF of the complete sample; as a comparison, the general LF in r-band from the whole SDSS is plotted in a green dotted-line. Due to the number of galaxies of each type, ∼70% late- and ∼20% early-type galaxies, the difference in density is clear between the both LFs. Contrarily to results expected for samples contained in different environments, where early-type galaxies dominate the bright-end and late-type galaxies the faint-end, we find that isolated late-type galaxies dominate over the whole range of magnitudes. This fact is consequence of the galaxies taken into account in these type of samples, in agreement with Croton et al. (2004) using galaxies in voids. Many authors have reported an excess of late-type galaxies in the field, as seen in observations (e.g. Karachentseva 1973, Loveday 1996, Hernández-Toledo et al. 2008) as well as in simulations (e.g. De Lucia et al. 2006); meanwhile early-type galaxies are mostly located in the centre of groups or clusters (e.g. Kauffmann et al. 2004).

In order to see the differences in the LFs according to the main types of galaxies, we divide the UNAM-KIAS catalogue into four subsamples: 1) E-S0/Sa, 2) Sa-Sab, 3) Sb-Sc and 4) Scd-Sd. We consider these subsamples since they contain a reasonable number of galaxies to estimate the LF. The LF is presented in Fig. 3.5 for the four subsamples in the g-band and the AMIGA LF estimated by Sulentic et al. (2006) is plotted in dotted-lines as a comparison in the B_{corr} band (Verdes-Montenegro et al., 2005) for the same morphology bins. Large error bars can be seen at the faint-end, meaning a low number of faint galaxies, consequence of the sample selection in magnitude. Similar to LF presented in Fig. 3.3, we can observe a dip at intermediate or faint magnitudes, which is weaker for very late-type galaxies, similar to what Moorman et al. (2015) report. However, for the Scd-Sd sample, there is only one point with an increment of the LF at the bright-end. This effect may just be a systematic effect from the LF estimation without the possibility to think about an AGN effect. When comparing with the AMIGA LF, the bands presented are not the

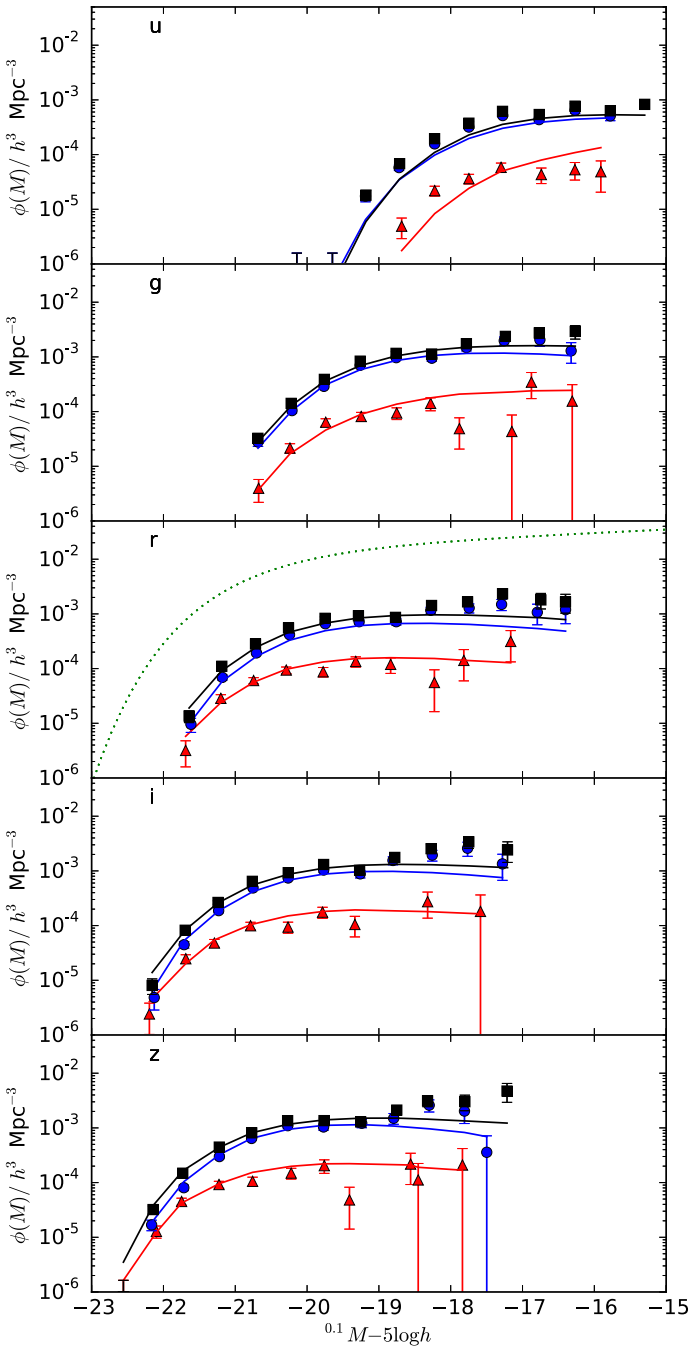

Figure 3.4: LF in the *ugriz* bands for the whole sample (black), elliptical (red) and spiral (blue) galaxies. Green dotted-line is the global SDSS LF in the r-band, plotted as comparison.

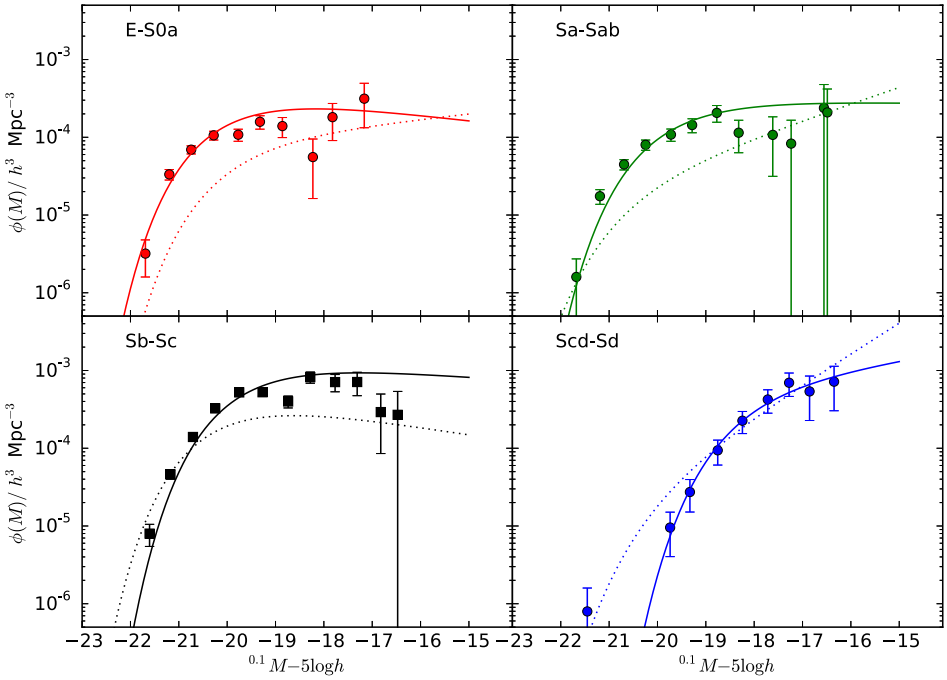

Figure 3.5: LF in the g-band for four morphology bins indicated in each panel. As a comparison, dotted-lines show the AMIGA LF (Sulentic et al., 2006) in the same bins of morphology in the B_{corr} band.

same but close enough to compare the LF shape. LF differences are clearly seen between both samples; however, the UNAM-KIAS survey is more complete and we can establish more reliable Schechter parameters. This shows also how the selection criteria affects the LF shape.

3.4.2 Comparison with other samples

Taking advantage of the complete and high data quality of the GAMA survey, we estimate the LF for two subsamples at low densities, galaxies in voids and galaxies classified as ungrouped (galaxies excluded from the G^3Cv6 catalogue). Fig. 3.6 shows the voids LF in the *ugriz* bands in blue, green, black, magenta and red colours, respectively. As comparison the global GAMA r-band LF (Loveday et al., 2012) is presented in a green dotted-line for low-redshift galaxies. The corresponding global AMIGA B-band LF (Verdes-Montenegro et al., 2005) is presented in a red dotted-line. Note, this void sample is a volume-limited sample so, there are not galaxies in the same range of magnitudes as in the UNAM-KIAS at the faint end. For this reason, we cannot compare the faint slope (α) of the voids LF to the other samples, but the M^* parameter since non bright

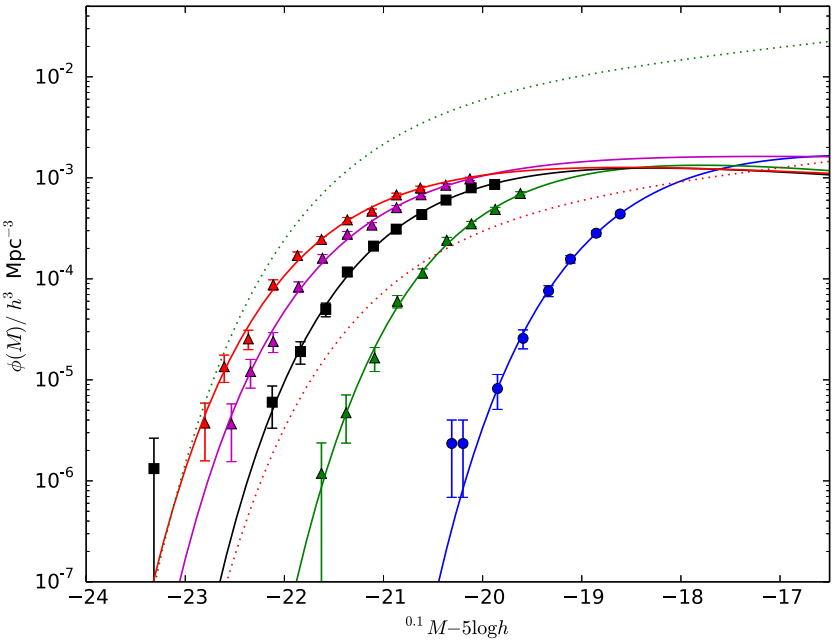

Figure 3.6: LF of the void GAMA sample in the *ugriz* bands (blue, green, black, magenta and red colours, respectively). Symbols represent the $1/V_{max}$ method. Solid lines are the best fit. As a comparison, the global GAMA r-band LF is presented in green dotted-line and the global AMIGA B-band LF in red dotted-line.

galaxy is exclude from the LF estimation in any sample. Nevertheless, there is a clear difference at the bright end, where galaxies tend to be brighter as the redder the band is as we discussed at the beginning of Sec 4.

Considering that the UNAM-KIAS catalogue is unique (besides in the SDSS bands), it is not trivial to do direct comparisons with previous works using the Johnson magnitudes. As we mentioned before, the AMIGA survey is the closest sample of isolated galaxies with which we can compare our results and also other studies such as the LF in voids by Croton et al. (2004). For this comparison, SDSS bands must be transformed into the Johnson magnitude system. The apparent magnitude in the B-band is estimated using the transformation proposed by Lupton and Ivezić (2005)

$$B = g + 0.3130 * (g - r) + 0.2271;\ \sigma = 0.0107 \tag{3.17}$$

based on stars since there are no transformation equations explicitly for galaxies; these equations must provide reasonable results for normal galaxies.[3] A transformation based

[3]www.sdss3.org/dr8/algorithms/sdssUBVRITransform.php

Table 3.3: Schechter parameters for six samples in B-band.

Sample	α	$^{0.0}M^*$ - 5 $\log h$	$\phi^*\times$ 1000 $/h^3\mathrm{Mpc}^{-3}$
UNAM-KIAS	-1.11 ± 0.01	-18.94 ± 0.16	2.60 ± 0.70
AMIGA V>1500 kms^{-1}	-0.82 ± 0.09	-19.43 ± 0.07	0.75 ± 0.06
AMIGA	-1.27 ± 0.06	-19.63 ± 0.07	0.63 ± 0.07
Croton04	-1.06 ± 0.24	-18.84 ± 0.16	1.32 ± 0.56
ungrGAMA	-1.28 ± 0.01	-19.61 ± 0.02	9.29 ± 2.45
voidsGAMA	-0.75 ± 0.23	-19.08 ± 0.09	2.63 ± 0.87

on galaxies must vary according to the galaxy type. A normal galaxy will be different to a starburst galaxy for instance. Spectral energy distribution is different for each galaxy type, so a transformation must take into account other factor apart of luminosity and colours, for example, metallicities, star formation rates or environment.

However, rather than estimating directly the B-band LF (since it may result in an over or under estimated LF due to the transformation errors), we follow the approximate correspondence between SDSS and Johnson suggested by Ilbert et al. (2005). They suggest a very close relationship between the $^{0.1}ugirz$ bands with the corresponding $UBVIR$ bands taking the average difference between absolute magnitudes; for their sample they find $\Delta(M_g - M_B) = 0.05$. For the UNAM-KIAS catalogue we find a difference of $\Delta(M_g - M_B) = 0.23$; so, for comparisons of the LF in the rest of this work (comparing with a Johnson system LF), we use

$$^{0.0}M_B^* = ^{0.1}\ M_g^* + 0.23 \tag{3.18}$$

while α and ϕ^* are the same from the g-band LF.

The AMIGA magnitude B_{corr} has been estimated following the K-correction by Giovanelli et al. (1981) based on the galaxy morphology. We have $un-corrected$ the AMIGA M^* to the same corrections in the Croton et al. (2004) sample using the inverse relation given by Verdes-Montenegro et al. (2005)

$$m_{B-corr} = b_{2dFGRS} - 0.054 \tag{3.19}$$

and expressing the absolute magnitudes in $^{0.1}M^*$ - 5log h units.

To see the differences in shape, we plot in Fig. 3.7 the Schechter parametric LF for the following samples: UNAM-KIAS, AMIGA, Croton et al. (2004), field GAMA galaxies, and void GAMA galaxies in the B-band. Schechter values are presented in Table 3.3.

UNAM-KIAS and AMIGA

This is the most important comparison for the UNAM-KIAS catalogue, since the AMIGA sample is the predecessor of this catalogue, as we mentioned before. We consider the results in Verdes-Montenegro et al. (2005) where they present the LF for a refinement of the KIG catalogue (725 galaxies) and a subsample excluding galaxies with recession velocity of V $<$ 1500 km s^{-1}. Fig. 3.7 shows the corresponding parametric LF (Table 3.3) for the UNAM-KIAS (blue) and AMIGA (green and black) samples. From the UNAM-KIAS selection criteria, most of the galaxies have recession velocities V$\geq$1000 km s^{-1}, then we should expect it to be more similar to the AMIGA LF with V $>$ 1500 km s^{-1} (green). Neither the LF shapes nor Schechter parameters are close for the two samples. M^* differences can be associated to the corrections applied to the AMIGA sample and the robust transformation to the $B-band$. At the faint-end, α is completely different for the two AMIGA samples and the UNAM-KIAS, being the last in the middle of the other values. These differences can be the result of the selection criteria. On the other hand, the UNAM-KIAS LF and Croton et al. (2004) are very similar in shape and the M^* and α parameters agree within 1 error bar, meaning a good agreement between the isolated galaxies and the lowest density estimated by Croton et al. (2004).

UNAM-KIAS and GAMA

The LF for the UNAM-KIAS (blue) and the GAMA voids (cyan) catalogues are very similar at the bright-end, where both M^* overlap in 1 error bar, meaning the same type of galaxy population mix among ellipticals and spiral galaxies as seen in Fig. 3.4. Note, the voids bright-end tends to be slightly brighter than the UNAM-KIAS. Unfortunately, the faint-end cannot be compared due to the selection cut presented in the void catalogue. Then the difference between the apparent limit magnitude (r) in GAMA (19.8) and SDSS (17.7) are not important.

When we look at the LF for ungrouped GAMA galaxies (red), the shape is very similar to the UNAM-KIAS LF, except for the faint-end. The big difference in ϕ^* between both samples could be result of the type of galaxies contained in each sample. Meanwhile the UNAM-KIAS sample contains only galaxies without interaction with other similar companion or major mergers, the ungrouped GAMA sample likely contains also interacting pairs that may affect the LF shape.

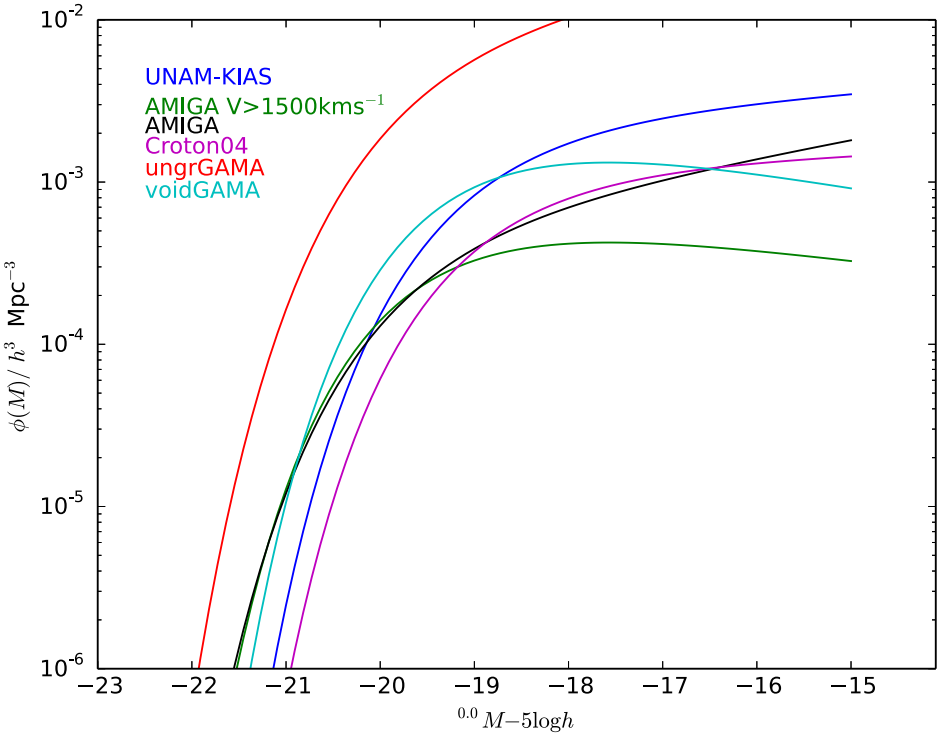

Figure 3.7: Comparison of the LF with other galaxy samples in low density environments in the B-band. 1. UNAM-KIAS catalogue is presented in blue. 2. AMIGA sample for galaxies with recession velocity V>1500 kms^{-1} in green. 3. The global AMIGA LF in black. 4. Voids sample LF from Croton et al. 2004 in magenta. 5. Ungrouped GAMA galaxy LF in red. 6. GAMA voids sample presented in cyan.

3.5 Stellar Mass Function

Fig. 3.8 presents the SMF for the UNAM-KIAS catalogue and the dependence with morphology and colour in the top panels. As we expect, elliptical galaxies show a very low SMF at low mass end, since these types of galaxies are predominately massive. Spiral galaxies dominates completely the low mass end, and from the characteristic mass ($\sim$11 $\log M$ $[M_{\odot}]$) both stellar MF are similar. This agrees with previous results (e.g. Panter et al. 2007; Baldry et al. 2008; Li and White 2009) where at low redshifts the characteristic mass of the Schechter break has been determined to be 10.6$\leq$ $\log M$ $[M_{\odot}]$ $\leq$11 for the field galaxies. This break and shape are also in agreement with the results presented by Wang and White (2012) for the more massive isolated galaxies and their respective satellite galaxies. Looking at Fig. 3.8 and the SMF in Li and White (2009), both SMF overlap at the high mass limits but not at low masses.

For the SMF and the colour, blue galaxies dominate over the red population at low masses, and at high masses, red galaxies dominate clearly the SMF. Red and blue samples are similar at $\sim$10.4 $\log M$ $[M_{\odot}]$. In this case, the steepening mentioned by Baldry et al. (2008) below 10 $\log M$ $[M_{\odot}]$, increases due to the domination of blue population at low masses.

Since we are considering galaxies with masses 9 $\leq$ $\log M$ $[M_{\odot}]$, it is not possible to observe the maximum peak proposed by different authors of the SMF (e.g. Guo et al. 2010; Moster et al. 2010, Baldry et al. 2012) that is inferred to be at 7 $\geq$ $\log M$ $[M_{\odot}]$ by Mamon et al. (2011). This peak is to explain the SMF shape and mainly the increase at low masses.

The bottom panel of Fig. 3.8 shows the SMF divided by passive (red) and active (blue) galaxies (using the specific star formation rate; sSFR). Due to the fact blue galaxies are related to the star formation process and the same for red/passive galaxies, there is an agreement with the SMF divided by colour. Passive galaxies dominate at high masses meanwhile there is a higher population of active galaxies at low masses.

We can combine the information from the SMF considering the morphology, colour and sSFR. Fig. 3.9 shows the fraction for the SMF for spirals (continuous line), blue (dashed line) and active (dashed-point line) galaxies to the total SMF

$$f_j(M_*) = \mathrm{SMF}_j(M_*)/\mathrm{SMF}_{Total}(M_*). \tag{3.20}$$

From Fig. 3.9 we can see how galaxies with $\log M$ $[M_{\odot}]$ $\sim$11 stop forming stars, with only a few of them being blue, maybe in the last star formation stage. Nevertheless,

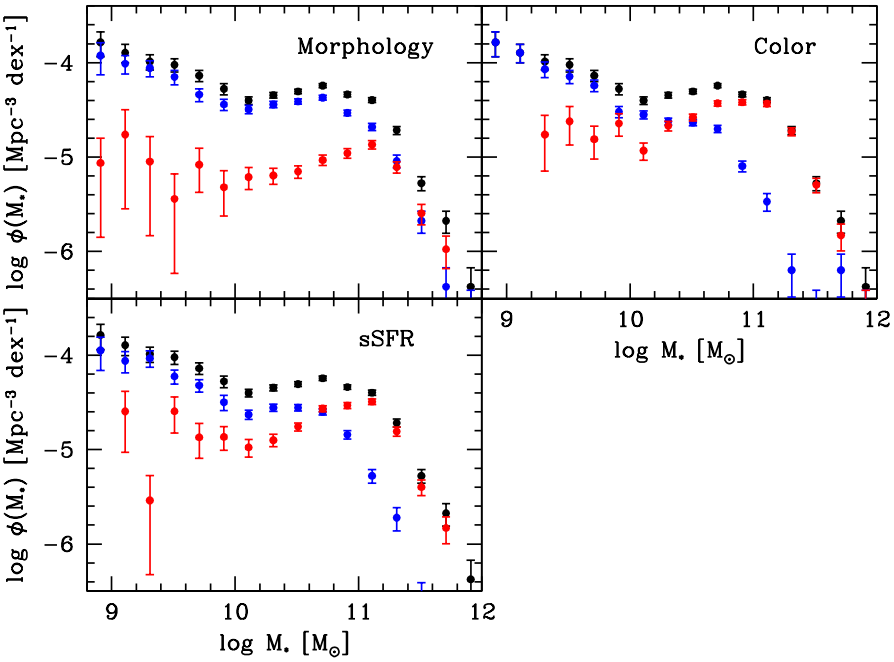

Figure 3.8: SMF by morphology, spirals (blue), ellipticals (red) and combined (black); colour (blue and red) and combined (black); and the stellar-subhalo mass relation (sSMR) separated by morphology.

galaxies with disc are still the ∼50%. In one hand, this can be the result of an overestimation of red galaxies, since an important fraction of edge-on dusty spirals are being considered in the red sample as discussed in HT10, similar to the GAMA sample discussed by Driver et al. (2012). On the other hand, this effect is presented only in the $10 \leq \log M\,[M_{\odot}] \leq 11.5$ mass interval; after a quick look at the data, there is no correlation between inclination and mass. Therefore, morphology can the be last transition of isolated galaxies to become in a passive red galaxy. This does not agree completely with Bell et al. (2012), they argue that a galaxy needs a bulge to stop its stellar formation. A more detailed analysis can be carried out in the future to confirm or deny this hypothesis

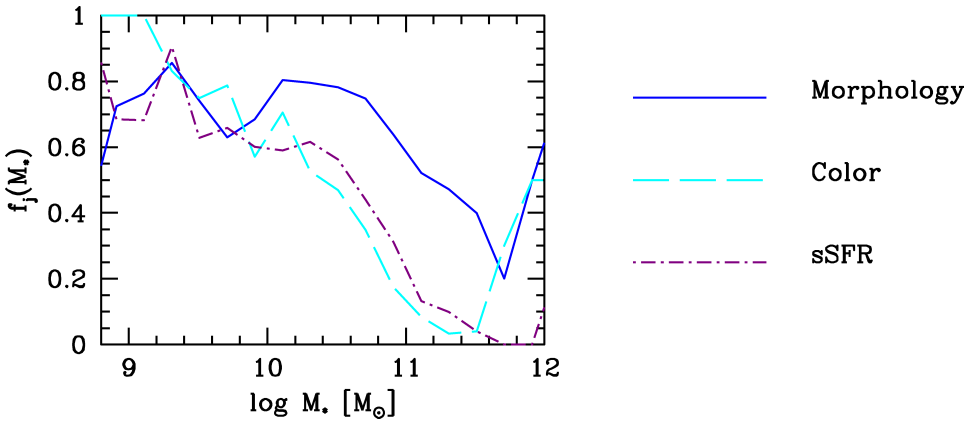

Figure 3.9: Fraction for the SMF for spirals (continuous line), blue (dashed line) and active (dashed-point line) galaxies to the total SMF.

3.6 Gas calibration

Fig. 3.10 shows the gas-to-stellar mass ratio, M_{gas}/M_s, for isolated galaxies with available information on gas content. The mean distribution of M_{gas}/M_s as a function of stellar mass M_s is shown as red open circles. This fit is given by

$$\log(M_{gas}/M_s) = -0.56\ \log(M_s) + 5.36\ , \tag{3.21}$$

where M_s is in units of $M_\odot$ ($h = 0.7$), and is shown as a blue dot-dashed line.

The solid and dotted lines are the fits of Stewart et al. (2009) and Papastergis et al. (2012) for compilations of observational data of disk galaxies, respectively. Typically, our sample of isolated galaxies has higher gas fractions than normal disk galaxies. The long-dashed line is the fit of Karachentsev and Kaisina (2013) for a sample of nearby galaxies located in extremely low density regions, which is dominated by very late-type morphologies. For a given stellar mass, the gas fraction of this fit is the lowest among those plotted in the figure. However, note that all the fits are located within the error bars of the mean distribution of isolated galaxies.

Note that the M_{gas}/M_s fraction of isolated galaxies under the Stewart et al. (2009) fit are mostly found at high stellar masses. These galaxies could be identified as early type, where the amount of gas is much smaller than galaxies with disks. Lacerna et al. (2014) estimated the M_{gas}/M_s fraction for central galaxies in different environments, including the UNAM-KIAS galaxies (only galaxies contained in the Yang et al. (2007) catalogue). They estimated the M_{gas}/M_s fraction for active and passive galaxies, finding no dependence between the M_{gas}/M_s fraction and the sSMR. A more detailed analysis of these galaxies would be necessary to agree or deny these results.

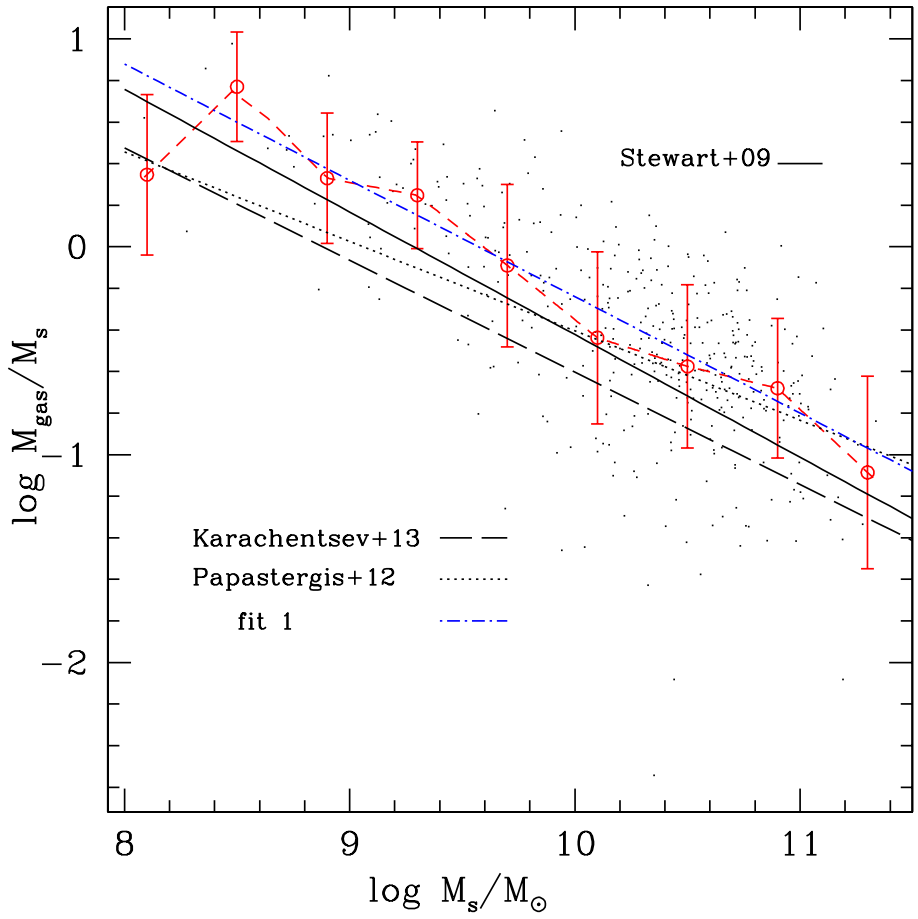

Figure 3.10: Gas-to-stellar mass ratio, M_{gas}/M_s, for the isolated galaxies as a function of M_s (dotted points), where M_{gas} is calculated using a correction for helium and metals. The mean distribution is shown as red open circles (connected by a red short-dashed line). Error bars correspond to the standard deviation. The fit to this data set is shown as a blue dot-dashed line (see the text for details). As a comparison, the solid line corresponds to the equation (1) of Stewart et al. (2009). In addition, the dotted and long-dashed lines are the fit of Papastergis et al. (2012) and Karachentsev and Kaisina (2013) for observational estimates using H I mass, respectively.

3.7 Discussion and Conclusion

The UNAM-KIAS sample is a magnitude limited sample with a completeness up to $\sim$ 80 % spectroscopy complete sample. These characteristics allow us to have a more reliable isolation of galaxies in space, more than just projected separations. Another advantage of the UNAM-KIAS catalogue is the well defined morphology; image quality gives the necessary tools to extract lots of information about the structural galaxy components to distinguish between one or another morphological type.

The main goal of this work is the characterization of the UNAM-KIAS sample through the statistical studies: LF, SMF and the gas-to-stellar mass ratio. However, we focused more on establishing the best Schechter values to fit the LF and the characteristic LF signs for galaxies in low dense environments.

There is no surprise that the fact that M^* is brighter from blue to red bands for isolated galaxies, since this is a natural consequence in observations. However, we find an interesting feature in the LF shape, an unclear dip presented at middle magnitudes; this feature has been also observed by Miles et al. (2004) for galaxies in groups. A possible explanation is the lack of galaxies at these magnitudes due to recent merger activity suffered by isolated galaxies (Park et al., 2008) with characteristic magnitudes; this also could explain from another point of view the large amount of galaxies with clear signs of distortion in the sample. Typically, author like Reda et al. (2004) and Smith et al. (2004), find that luminous isolated galaxies show an excess of dwarf companions $\sim$5 magnitudes fainter, causing signs of distortions in the host galaxy. Most recently by Moorman et al. (2015) found the same feature using data from ALFALFA and SDSS; however, they do not give a explanation for it.

The LF is $\sim$1 mag fainter than the global SDSS LF; so, no that bright isolated galaxies can be found and massive isolated galaxies may be difficult to identify. When the LF is separated by elliptical and spiral galaxies, it is clear that the spiral galaxy population dominates over the elliptical galaxies for all bands; nevertheless, at the bright end of the LF, both populations have similar M^*, contrarily to Sulentic et al. (2006) that finds spiral galaxies are brighter than ellipticals. Other differences found, with respect to Sulentic et al. (2006) work, are when we divided the sample in 4 morphology bins where no evidence of dependence with the characteristic magnitude is seen, only the very late type galaxies are fainter more than 1 mag. The LFs are completely different to those presented by Sulentic et al. (2006) presumably by the correction they apply to the magnitudes. However, we agree with them when looking at elliptical galaxies as fossil ellipticals,

since these galaxies would have to be brighter than the population from which a possible merger can be produced (resulting in an elliptical galaxy) and also for the modest luminosities of the elliptical population. the other possibility of these differences can be the result of the selection criteria, since AMIGA is based only on a 2D selection criteria.

Using the GAMA survey, the LF was estimated in two low density environments, voids and ungrouped galaxies. This survey is the second best survey to compare our results because of the spectroscopic completeness and the size of the sample. Unfortunately, the voids sample was selected as a volume-limited sample, throwing away the faintest galaxies and consequently information about the faint-end, but with important contribution at the bright end. This sample agrees with the LF shape at the bright end with the UNAM-KIAS catalogue, meaning a brightness cut of galaxies in very and not very low density environments. When the comparison is made with the Croton et al. (2004) sample, differences at the bright end are bout 0.5 mag; this may be an effect caused by the band transformation and any other corrections assumed. The ungrouped GAMA galaxies sample contains around 120 000 galaxies, being 2 orders of magnitude larger; when comparing with the rest of the samples, the LF shape is very similar to that of the UNAM-KIAS, but with a higher density and a faint slope steeper.

Comparing mainly the UNAM-KIAS, AMIGA and ungrouped GAMA samples, we can see clearly that the LF varies according to the size of the sample and when larger the sample, more reliable the results are, as mentioned by McNaught-Roberts et al. (2014). In terms of density, this work is providing more reliable information of isolated galaxies, since it agrees with many of the studies carried out in low densities. The Schechter parameters estimated can be considered as the parameters to be reproduced by the models or other comparison with density.

The stellar MF presents similar results, where spiral galaxies dominate at low mass but at massive values, elliptical and spiral galaxies have the same characteristic mass; this is unclear when we look at the results divided by colour, where red galaxies dominate completely the massive range, meaning a red population of disky galaxies. The characteristic mass for the UNAM-KIAS catalogue is $\sim 11 \leq \log M\ [M_{\odot}]$ in agreement with the values determined for galaxies in the field to be $10.6 \leq \log M\ [M_{\odot}] \leq 11$. Red and blue samples are similar at $\sim 10.4 \log M\ [M_{\odot}]$. In this case, the steepening mentioned by Baldry et al. (2008) below 10 $\log M\ [M_{\odot}]$, increases due to the domination of blue population at low masses. Passive galaxies dominate at high masses meanwhile active galaxies at low masses.

Combining all this information, we found that galaxies with $\log M\ [M_{\odot}] \sim 11$ stop

forming stars, with only a few of them being blue, maybe in the last star formation stage. In addition, galaxies with disc are still the ∼50%. This break the idea that galaxies need a bulge to turn off completely. This suggest that morphology can the be last transition of isolated galaxies to become in a passive red galaxy.

Finally the gas-to-stellar mass ratio (M_{gas}/M_s) is presented for isolated galaxies an the characteristic tendency is presented. this agrees with other works based on disky type galaxies. This study, however, needs a deeper analysis and try to estimated the baryonic mass LF. And also, the possible estimation of the halo mass based on this ratios as described by Rodríguez-Puebla et al. (2011).

Acknowledgements

GAMA is a joint European-Australasian project based around a spectroscopic campaign using the Anglo-Australian Telescope. The GAMA input catalogue is based on data taken from the Sloan Digital Sky Survey and the UKIRT Infrared Deep Sky Survey. Complementary imaging of the GAMA regions is being obtained by a number of independent survey programs including GALEX MIS, VST KiDS, VISTA VIKING, WISE, Herschel-ATLAS, GMRT and ASKAP providing UV to radio coverage. GAMA is funded by the STFC (UK), the ARC (Australia), the AAO, and the participating institutions. The GAMA website is http://www.gama-survey.org/ .

JAVM was supported by the Mexican National Council for Science and Technology (CONACyT) scholarship scheme.

References

Alpaslan, M., Robotham, A. S. G., Driver, S., Norberg, P., Baldry, I., Bauer, A. E., Bland-Hawthorn, J., Brown, M., Cluver, M., Colless, M., Foster, C., Hopkins, A., Van Kampen, E., Kelvin, L., Lara-Lopez, M. A., Liske, J., Lopez-Sanchez, A. R., Loveday, J., McNaught-Roberts, T., Merson, A., and Pimbblet, K. (2013). Galaxy And Mass Assembly (GAMA): The large scale structure of galaxies and comparison to mock universes. *ArXiv e-prints*.

Baldry, I. K., Driver, S. P., Loveday, J., Taylor, E. N., Kelvin, L. S., Liske, J., Norberg, P., Robotham, A. S. G., Brough, S., Hopkins, A. M., Bamford, S. P., Peacock, J. A., Bland-Hawthorn, J., Conselice, C. J., Croom, S. M., Jones, D. H., Parkinson, H. R., Popescu, C. C., Prescott, M., Sharp, R. G., and Tuffs, R. J. (2012). Galaxy And Mass Assembly (GAMA): the galaxy stellar mass function at z 0.06. *MNRAS*, 421:621–634.

Baldry, I. K., Glazebrook, K., and Driver, S. P. (2008). On the galaxy stellar mass function, the mass-metallicity relation and the implied baryonic mass function. *MNRAS*, 388:945–959.

Baldry, I. K., Robotham, A. S. G., Hill, D. T., Driver, S. P., Liske, J., Norberg, P., Bamford, S. P., Hopkins, A. M., Loveday, J., Peacock, J. A., Cameron, E., Croom, S. M., Cross, N. J. G., Doyle, I. F., Dye, S., Frenk, C. S., Jones, D. H., van Kampen, E., Kelvin, L. S., Nichol, R. C., Parkinson, H. R., Popescu, C. C., Prescott, M., Sharp, R. G., Sutherland, W. J., Thomas, D., and Tuffs, R. J. (2010). Galaxy And Mass Assembly (GAMA): the input catalogue and star-galaxy separation. *MNRAS*, 404:86–100.

Bell, E. F., McIntosh, D. H., Katz, N., and Weinberg, M. D. (2003). The Optical and Near-Infrared Properties of Galaxies. I. Luminosity and Stellar Mass Functions. *ApJS*, 149:289–312.

Bell, E. F., van der Wel, A., Papovich, C., Kocevski, D., Lotz, J., McIntosh, D. H., Kartaltepe, J., Faber, S. M., Ferguson, H., Koekemoer, A., Grogin, N., Wuyts, S., Cheung, E., Conselice, C. J., Dekel, A., Dunlop, J. S., Giavalisco, M., Herrington, J., Koo, D. C., McGrath, E. J., de Mello, D., Rix, H.-W., Robaina, A. R., and Williams, C. C. (2012). What Turns Galaxies Off? The Different Morphologies of Star-forming and Quiescent Galaxies since z ˜ 2 from CANDELS. *ApJ*, 753:167.

Blanton, M. R., Brinkmann, J., Csabai, I., Doi, M., Eisenstein, D., Fukugita, M., Gunn, J. E., Hogg, D. W., and Schlegel, D. J. (2003). Estimating Fixed-Frame Galaxy Magnitudes in the Sloan Digital Sky Survey. *AJ*, 125:2348–2360.

Blanton, M. R. and Roweis, S. (2007). K-Corrections and Filter Transformations in the Ultraviolet, Optical, and Near-Infrared. *AJ*, 133:734–754.

Blanton, M. R., Schlegel, D. J., Strauss, M. A., Brinkmann, J., Finkbeiner, D., Fukugita, M., Gunn, J. E., Hogg, D. W., Ivezić, Ž., Knapp, G. R., Lupton, R. H., Munn, J. A., Schneider, D. P., Tegmark, M., and Zehavi, I. (2005). New York University Value-Added Galaxy Catalog: A Galaxy Catalog Based on New Public Surveys. *AJ*, 129:2562–2578.

Brinchmann, J., Charlot, S., White, S. D. M., Tremonti, C., Kauffmann, G., Heckman, T., and Brinkmann, J. (2004). The physical properties of star-forming galaxies in the low-redshift Universe. *MNRAS*, 351:1151–1179.

Brinchmann, J. and Ellis, R. S. (2000). The Mass Assembly and Star Formation Characteristics of Field Galaxies of Known Morphology. *ApJ*, 536:L77–L80.

Cole, S., Lacey, C. G., Baugh, C. M., and Frenk, C. S. (2000). Hierarchical galaxy formation. *MNRAS*, 319:168–204.

Cole, S., Norberg, P., Baugh, C. M., Frenk, C. S., Bland-Hawthorn, J., Bridges, T., Cannon, R., Colless, M., Collins, C., Couch, W., Cross, N., Dalton, G., De Propris, R., Driver, S. P., Efstathiou, G., Ellis, R. S., Glazebrook, K., Jackson, C., Lahav, O., Lewis, I., Lumsden, S., Maddox, S., Madgwick, D., Peacock, J. A., Peterson, B. A., Sutherland, W., and Taylor, K. (2001). The 2dF galaxy redshift survey: near-infrared galaxy luminosity functions. *MNRAS*, 326:255–273.

Croton, D. J., Farrar, G. R., Norberg, P., Colless, M., Peacock, J. A., Baldry, I. K., Baugh, C. M., Bland-Hawthorn, J., Bridges, T., Cannon, R., Cole, S., Collins, C., Couch, W., Dalton, G., De Propris, R., Driver, S. P., Efstathiou, G., Ellis, R. S.,

Frenk, C. S., Glazebrook, K., Jackson, C., Lahav, O., Lewis, I., Lumsden, S., Maddox, S., Madgwick, D., Peterson, B. A., Sutherland, W., and Taylor, K. (2005). The 2dF Galaxy Redshift Survey: luminosity functions by density environment and galaxy type. *MNRAS*, 356:1155–1167.

Croton, D. J., Gaztañaga, E., Baugh, C. M., Norberg, P., Colless, M., Baldry, I. K., Bland-Hawthorn, J., Bridges, T., Cannon, R., Cole, S., Collins, C., Couch, W., Dalton, G., De Propris, R., Driver, S. P., Efstathiou, G., Ellis, R. S., Frenk, C. S., Glazebrook, K., Jackson, C., Lahav, O., Lewis, I., Lumsden, S., Maddox, S., Madgwick, D., Peacock, J. A., Peterson, B. A., Sutherland, W., and Taylor, K. (2004). The 2dF Galaxy Redshift Survey: higher-order galaxy correlation functions. *MNRAS*, 352:1232–1244.

De Lucia, G., Springel, V., White, S. D. M., Croton, D., and Kauffmann, G. (2006). The formation history of elliptical galaxies. *MNRAS*, 366:499–509.

De Propris, R., Colless, M., Driver, S. P., Couch, W., Peacock, J. A., Baldry, I. K., Baugh, C. M., Bland-Hawthorn, J., Bridges, T., Cannon, R., Cole, S., Collins, C., Cross, N., Dalton, G. B., Efstathiou, G., Ellis, R. S., Frenk, C. S., Glazebrook, K., Hawkins, E., Jackson, C., Lahav, O., Lewis, I., Lumsden, S., Maddox, S., Madgwick, D. S., Norberg, P., Percival, W., Peterson, B., Sutherland, W., and Taylor, K. (2003). The 2dF Galaxy Redshift Survey: the luminosity function of cluster galaxies. *MNRAS*, 342:725–737.

Driver, S. P., Hill, D. T., Kelvin, L. S., Robotham, A. S. G., Liske, J., Norberg, P., Baldry, I. K., Bamford, S. P., Hopkins, A. M., Loveday, J., Peacock, J. A., Andrae, E., Bland-Hawthorn, J., Brough, S., Brown, M. J. I., Cameron, E., Ching, J. H. Y., Colless, M., Conselice, C. J., Croom, S. M., Cross, N. J. G., de Propris, R., Dye, S., Drinkwater, M. J., Ellis, S., Graham, A. W., Grootes, M. W., Gunawardhana, M., Jones, D. H., van Kampen, E., Maraston, C., Nichol, R. C., Parkinson, H. R., Phillipps, S., Pimbblet, K., Popescu, C. C., Prescott, M., Roseboom, I. G., Sadler, E. M., Sansom, A. E., Sharp, R. G., Smith, D. J. B., Taylor, E., Thomas, D., Tuffs, R. J., Wijesinghe, D., Dunne, L., Frenk, C. S., Jarvis, M. J., Madore, B. F., Meyer, M. J., Seibert, M., Staveley-Smith, L., Sutherland, W. J., and Warren, S. J. (2011). Galaxy and Mass Assembly (GAMA): survey diagnostics and core data release. *MNRAS*, 413:971–995.

Driver, S. P., Norberg, P., Baldry, I. K., Bamford, S. P., Hopkins, A. M., Liske, J., Loveday, J., Peacock, J. A., Hill, D. T., Kelvin, L. S., Robotham, A. S. G., Cross, N. J. G., Parkinson, H. R., Prescott, M., Conselice, C. J., Dunne, L., Brough, S., Jones, H., Sharp, R. G., van Kampen, E., Oliver, S., Roseboom, I. G., Bland-Hawthorn, J.,

Croom, S. M., Ellis, S., Cameron, E., Cole, S., Frenk, C. S., Couch, W. J., Graham, A. W., Proctor, R., De Propris, R., Doyle, I. F., Edmondson, E. M., Nichol, R. C., Thomas, D., Eales, S. A., Jarvis, M. J., Kuijken, K., Lahav, O., Madore, B. F., Seibert, M., Meyer, M. J., Staveley-Smith, L., Phillipps, S., Popescu, C. C., Sansom, A. E., Sutherland, W. J., Tuffs, R. J., and Warren, S. J. (2009). GAMA: towards a physical understanding of galaxy formation. *Astronomy and Geophysics*, 50(5):050000–5.

Driver, S. P., Robotham, A. S. G., Kelvin, L., Alpaslan, M., Baldry, I. K., Bamford, S. P., Brough, S., Brown, M., Hopkins, A. M., Liske, J., Loveday, J., Norberg, P., Peacock, J. A., Andrae, E., Bland-Hawthorn, J., Bourne, N., Cameron, E., Colless, M., Conselice, C. J., Croom, S. M., Dunne, L., Frenk, C. S., Graham, A. W., Gunawardhana, M., Hill, D. T., Jones, D. H., Kuijken, K., Madore, B., Nichol, R. C., Parkinson, H. R., Pimbblet, K. A., Phillipps, S., Popescu, C. C., Prescott, M., Seibert, M., Sharp, R. G., Sutherland, W. J., Taylor, E. N., Thomas, D., Tuffs, R. J., van Kampen, E., Wijesinghe, D., and Wilkins, S. (2012). Galaxy And Mass Assembly (GAMA): the 0.013 z 0.1 cosmic spectral energy distribution from 0.1 μm to 1 mm. *MNRAS*, 427:3244–3264.

Efstathiou, G., Ellis, R. S., and Peterson, B. A. (1988). Analysis of a complete galaxy redshift survey. II - The field-galaxy luminosity function. *MNRAS*, 232:431–461.

Felten, J. E. (1977). Study of the luminosity function for field galaxies. *AJ*, 82:861–878.

Folkes, S., Ronen, S., Price, I., Lahav, O., Colless, M., Maddox, S., Deeley, K., Glazebrook, K., Bland-Hawthorn, J., Cannon, R., Cole, S., Collins, C., Couch, W., Driver, S. P., Dalton, G., Efstathiou, G., Ellis, R. S., Frenk, C. S., Kaiser, N., Lewis, I., Lumsden, S., Peacock, J., Peterson, B. A., Sutherland, W., and Taylor, K. (1999). The 2dF Galaxy Redshift Survey: spectral types and luminosity functions. *MNRAS*, 308:459–472.

Giovanelli, R., Haynes, M. P., and Chincarini, G. L. (1981). The H I content of galaxies in the Hercules supercluster Evidence for sweeping. *ApJ*, 247:383–402.

Haynes, M. P., Giovanelli, R., Martin, A. M., Hess, K. M., Saintonge, A., Adams, E. A. K., Hallenbeck, G., Hoffman, G. L., Huang, S., Kent, B. R., Koopmann, R. A., Papastergis, E., Stierwalt, S., Balonek, T. J., Craig, D. W., Higdon, S. J. U., Kornreich, D. A., Miller, J. R., O'Donoghue, A. A., Olowin, R. P., Rosenberg, J. L., Spekkens, K., Troischt, P., and Wilcots, E. M. (2011). The Arecibo Legacy Fast ALFA Survey: The α.40 H I Source Catalog, Its Characteristics and Their Impact on the Derivation of the H I Mass Function. *AJ*, 142:170.

Hernández-Toledo, H. M., Vázquez-Mata, J. A., Martínez-Vázquez, L. A., Avila Reese, V., Méndez-Hernández, H., Ortega-Esbrí, S., and Núñez, J. P. M. (2008). A Morphological Re-Evaluation of Galaxies in Common from the Catalog of Isolated Galaxies and the Sloan Digital Sky Survey (DR6). *AJ*, 136:2115–2135.

Hernández-Toledo, H. M., Vázquez-Mata, J. A., Martínez-Vázquez, L. A., Choi, Y.-Y., and Park, C. (2010). The UNAM-KIAS Catalog of Isolated Galaxies. *AJ*, 139:2525–2541.

Huchra, J. and Sargent, W. L. W. (1973). The space density of the Markarian galaxies including a region of the south galactic hemisphere. *ApJ*, 186:433–443.

Humason, M. L., Mayall, N. U., and Sandage, A. R. (1956). Redshifts and magnitudes of extragalactic nebulae. *AJ*, 61:97–162.

Hütsi, G., Einasto, J., Tucker, D. L., Saar, E., Einasto, M., Müller, V., Heinämäki, P., and Allam, S. S. (2002). Luminosity function and density field of the Sloan and Las Campanas Redshift Survey. *ArXiv Astrophysics e-prints*.

Ilbert, O., Tresse, L., Zucca, E., Bardelli, S., Arnouts, S., Zamorani, G., Pozzetti, L., Bottini, D., Garilli, B., Le Brun, V., Le Fèvre, O., Maccagni, D., Picat, J.-P., Scaramella, R., Scodeggio, M., Vettolani, G., Zanichelli, A., Adami, C., Arnaboldi, M., Bolzonella, M., Cappi, A., Charlot, S., Contini, T., Foucaud, S., Franzetti, P., Gavignaud, I., Guzzo, L., Iovino, A., McCracken, H. J., Marano, B., Marinoni, C., Mathez, G., Mazure, A., Meneux, B., Merighi, R., Paltani, S., Pello, R., Pollo, A., Radovich, M., Bondi, M., Bongiorno, A., Busarello, G., Ciliegi, P., Lamareille, F., Mellier, Y., Merluzzi, P., Ripepi, V., and Rizzo, D. (2005). The VIMOS-VLT deep survey. Evolution of the galaxy luminosity function up to z = 2 in first epoch data. *A&A*, 439:863–876.

Karachentsev, I. D. and Kaisina, E. I. (2013). Star Formation Properties in the Local Volume Galaxies via Hα and Far-ultraviolet Fluxes. *AJ*, 146:46.

Karachentseva, V. E. (1973). The Catalogue of Isolated Galaxies,. *Astrofizicheskie Issledovaniia Izvestiya Spetsial'noj Astrofizicheskoj Observatorii*, 8:3–49.

Kauffmann, G., White, S. D. M., Heckman, T. M., Ménard, B., Brinchmann, J., Charlot, S., Tremonti, C., and Brinkmann, J. (2004). The environmental dependence of the relations between stellar mass, structure, star formation and nuclear activity in galaxies. *MNRAS*, 353:713–731.

Kroupa, P. (2001). On the variation of the initial mass function. *MNRAS*, 322:231–246.

Lacerna, I., Rodríguez-Puebla, A., Avila-Reese, V., and Hernández-Toledo, H. M. (2014). Central Galaxies in Different Environments: Do They have Similar Properties? *ApJ*, 788:29.

Li, C. and White, S. D. M. (2009). The distribution of stellar mass in the low-redshift Universe. *MNRAS*, 398:2177–2187.

Liske, J., Baldry, I. K., Driver, S. P., Tuffs, R. J., Alpaslan, M., Andrae, E., Brough, S., Cluver, M. E., Grootes, M. W., Gunawardhana, M. L. P., Kelvin, L. S., Loveday, J., Robotham, A. S. G., Taylor, E. N., Bamford, S. P., Bland-Hawthorn, J., Brown, M. J. I., Drinkwater, M. J., Hopkins, A. M., Meyer, M. J., Norberg, P., Peacock, J. A., Agius, N. K., Andrews, S. K., Bauer, A. E., Ching, J. H. Y., Colless, M., Conselice, C. J., Croom, S. M., Davies, L. J. M., De Propris, R., Dunne, L., Eardley, E. M., Ellis, S., Foster, C., Frenk, C. S., Häußler, B., Holwerda, B. W., Howlett, C., Ibarra, H., Jarvis, M. J., Jones, D. H., Kafle, P. R., Lacey, C. G., Lange, R., Lara-López, M. A., López-Sánchez, Á. R., Maddox, S., Madore, B. F., McNaught-Roberts, T., Moffett, A. J., Nichol, R. C., Owers, M. S., Palamara, D., Penny, S. J., Phillipps, S., Pimbblet, K. A., Popescu, C. C., Prescott, M., Proctor, R., Sadler, E. M., Sansom, A. E., Seibert, M., Sharp, R., Sutherland, W., Vázquez-Mata, J. A., van Kampen, E., Wilkins, S. M., Williams, R., and Wright, A. H. (2015). Galaxy And Mass Assembly (GAMA): end of survey report and data release 2. *MNRAS*, 452:2087–2126.

Liske, J., Lemon, D. J., Driver, S. P., Cross, N. J. G., and Couch, W. J. (2003). The Millennium Galaxy Catalogue: 16 $=\mathrm{B}_{MGC}$ 24 galaxy counts and the calibration of the local galaxy luminosity function. *MNRAS*, 344:307–324.

Loveday, J. (1996). The APM Bright Galaxy Catalogue. *MNRAS*, 278:1025–1048.

Loveday, J., Norberg, P., Baldry, I. K., Driver, S. P., Hopkins, A. M., Peacock, J. A., Bamford, S. P., Liske, J., Bland-Hawthorn, J., Brough, S., Brown, M. J. I., Cameron, E., Conselice, C. J., Croom, S. M., Frenk, C. S., Gunawardhana, M., Hill, D. T., Jones, D. H., Kelvin, L. S., Kuijken, K., Nichol, R. C., Parkinson, H. R., Phillipps, S., Pimbblet, K. A., Popescu, C. C., Prescott, M., Robotham, A. S. G., Sharp, R. G., Sutherland, W. J., Taylor, E. N., Thomas, D., Tuffs, R. J., van Kampen, E., and Wijesinghe, D. (2012). Galaxy and Mass Assembly (GAMA): ugriz galaxy luminosity functions. *MNRAS*, 420:1239–1262.

Lupton, R. and Ivezić, Ž. (2005). Experience with SDSS: the Promise and Perils of Large Surveys. In Seidelmann, P. K. and Monet, A. K. B., editors, *Astrometry in the Age of the Next Generation of Large Telescopes*, volume 338 of *Astronomical Society of the Pacific Conference Series*, page 151.

McNaught-Roberts, T., Norberg, P., Baugh, C., Lacey, C., Loveday, J., Peacock, J., Baldry, I., Bland-Hawthorn, J., Brough, S., Driver, S. P., Robotham, A. S. G., and Vázquez-Mata, J. A. (2014). Galaxy And Mass Assembly (GAMA): the dependence of the galaxy luminosity function on environment, redshift and colour. *MNRAS*, 445:2125–2145.

Miles, T. A., Raychaudhury, S., Forbes, D. A., Goudfrooij, P., Ponman, T. J., and Kozhurina-Platais, V. (2004). The Group Evolution Multiwavelength Study (GEMS): bimodal luminosity functions in galaxy groups. *MNRAS*, 355:785–793.

Moorman, C. M., Vogeley, M. S., Hoyle, F., Pan, D. C., Haynes, M. P., and Giovanelli, R. (2015). The Optical Luminosity Function of Void Galaxies in the SDSS and ALFALFA Surveys. *ArXiv e-prints*.

Norberg, P., Cole, S., Baugh, C. M., Frenk, C. S., Baldry, I., Bland-Hawthorn, J., Bridges, T., Cannon, R., Colless, M., Collins, C., Couch, W., Cross, N. J. G., Dalton, G., De Propris, R., Driver, S. P., Efstathiou, G., Ellis, R. S., Glazebrook, K., Jackson, C., Lahav, O., Lewis, I., Lumsden, S., Maddox, S., Madgwick, D., Peacock, J. A., Peterson, B. A., Sutherland, W., Taylor, K., and 2DFGRS Team (2002). The 2dF Galaxy Redshift Survey: the b_J-band galaxy luminosity function and survey selection function. *MNRAS*, 336:907–931.

Panter, B., Jimenez, R., Heavens, A. F., and Charlot, S. (2007). The star formation histories of galaxies in the Sloan Digital Sky Survey. *MNRAS*, 378:1550–1564.

Papastergis, E., Cattaneo, A., Huang, S., Giovanelli, R., and Haynes, M. P. (2012). A Direct Measurement of the Baryonic Mass Function of Galaxies and Implications for the Galactic Baryon Fraction. *ApJ*, 759:138.

Park, C., Gott, III, J. R., and Choi, Y.-Y. (2008). Transformation of Morphology and Luminosity Classes of the SDSS Galaxies. *ApJ*, 674:784–796.

Reda, F. M., Forbes, D. A., Beasley, M. A., O'Sullivan, E. J., and Goudfrooij, P. (2004). The photometric properties of isolated early-type galaxies. *MNRAS*, 354:851–869.

Roberts, M. S. and Haynes, M. P. (1994). Physical Parameters along the Hubble Sequence. *ARA&A*, 32:115–152.

Robotham, A. S. G., Norberg, P., Driver, S. P., Baldry, I. K., Bamford, S. P., Hopkins, A. M., Liske, J., Loveday, J., Merson, A., Peacock, J. A., Brough, S., Cameron, E., Conselice, C. J., Croom, S. M., Frenk, C. S., Gunawardhana, M., Hill, D. T., Jones, D. H., Kelvin, L. S., Kuijken, K., Nichol, R. C., Parkinson, H. R., Pimbblet, K. A., Phillipps, S., Popescu, C. C., Prescott, M., Sharp, R. G., Sutherland, W. J., Taylor, E. N., Thomas, D., Tuffs, R. J., van Kampen, E., and Wijesinghe, D. (2011). Galaxy and Mass Assembly (GAMA): the GAMA galaxy group catalogue (G^3Cv1). *MNRAS*, 416:2640–2668.

Rodríguez-Puebla, A., Avila-Reese, V., Firmani, C., and Colín, P. (2011). On the stellar and baryonic mass fractions of central blue and red galaxies. , 47:235–253.

Schechter, P. (1976). An analytic expression for the luminosity function for galaxies. *ApJ*, 203:297–306.

Schmidt, M. (1968). Space Distribution and Luminosity Functions of Quasi-Stellar Radio Sources. *ApJ*, 151:393.

Smith, R. M., Martínez, V. J., and Graham, M. J. (2004). A Sample of Field Ellipticals. *ApJ*, 617:1017–1021.

Somerville, R. S., Primack, J. R., and Faber, S. M. (2001). The nature of high-redshift galaxies. *MNRAS*, 320:504–528.

Springob, C. M., Haynes, M. P., Giovanelli, R., and Kent, B. R. (2005). A Digital Archive of H I 21 Centimeter Line Spectra of Optically Targeted Galaxies. *ApJS*, 160:149–162.

Stewart, K. R., Bullock, J. S., Barton, E. J., and Wechsler, R. H. (2009). Galaxy Mergers and Dark Matter Halo Mergers in ΛCDM: Mass, Redshift, and Mass-Ratio Dependence. *ApJ*, 702:1005–1015.

Stoughton, C., Lupton, R. H., Bernardi, M., Blanton, M. R., Burles, S., Castander, F. J., Connolly, A. J., Eisenstein, D. J., Frieman, J. A., Hennessy, G. S., Hindsley, R. B., Ivezić, Ž., Kent, S., Kunszt, P. Z., Lee, B. C., Meiksin, A., Munn, J. A., Newberg, H. J., Nichol, R. C., Nicinski, T., Pier, J. R., Richards, G. T., Richmond, M. W., Schlegel, D. J., Smith, J. A., Strauss, M. A., SubbaRao, M., Szalay, A. S., Thakar, A. R., Tucker, D. L., Vanden Berk, D. E., Yanny, B., Adelman, J. K., Anderson, Jr.,

J. E., Anderson, S. F., Annis, J., Bahcall, N. A., Bakken, J. A., Bartelmann, M., Bastian, S., Bauer, A., Berman, E., Böhringer, H., Boroski, W. N., Bracker, S., Briegel, C., Briggs, J. W., Brinkmann, J., Brunner, R., Carey, L., Carr, M. A., Chen, B., Christian, D., Colestock, P. L., Crocker, J. H., Csabai, I., Czarapata, P. C., Dalcanton, J., Davidsen, A. F., Davis, J. E., Dehnen, W., Dodelson, S., Doi, M., Dombeck, T., Donahue, M., Ellman, N., Elms, B. R., Evans, M. L., Eyer, L., Fan, X., Federwitz, G. R., Friedman, S., Fukugita, M., Gal, R., Gillespie, B., Glazebrook, K., Gray, J., Grebel, E. K., Greenawalt, B., Greene, G., Gunn, J. E., de Haas, E., Haiman, Z., Haldeman, M., Hall, P. B., Hamabe, M., Hansen, B., Harris, F. H., Harris, H., Harvanek, M., Hawley, S. L., Hayes, J. J. E., Heckman, T. M., Helmi, A., Henden, A., Hogan, C. J., Hogg, D. W., Holmgren, D. J., Holtzman, J., Huang, C.-H., Hull, C., Ichikawa, S.-I., Ichikawa, T., Johnston, D. E., Kauffmann, G., Kim, R. S. J., Kimball, T., Kinney, E., Klaene, M., Kleinman, S. J., Klypin, A., Knapp, G. R., Korienek, J., Krolik, J., Kron, R. G., Krzesiński, J., Lamb, D. Q., Leger, R. F., Limmongkol, S., Lindenmeyer, C., Long, D. C., Loomis, C., Loveday, J., MacKinnon, B., Mannery, E. J., Mantsch, P. M., Margon, B., McGehee, P., McKay, T. A., McLean, B., Menou, K., Merelli, A., Mo, H. J., Monet, D. G., Nakamura, O., Narayanan, V. K., Nash, T., Neilsen, Jr., E. H., Newman, P. R., Nitta, A., Odenkirchen, M., Okada, N., Okamura, S., Ostriker, J. P., Owen, R., Pauls, A. G., Peoples, J., Peterson, R. S., Petravick, D., Pope, A., Pordes, R., Postman, M., Prosapio, A., Quinn, T. R., Rechenmacher, R., Rivetta, C. H., Rix, H.-W., Rockosi, C. M., Rosner, R., Ruthmansdorfer, K., Sandford, D., Schneider, D. P., Scranton, R., Sekiguchi, M., Sergey, G., Sheth, R., Shimasaku, K., Smee, S., Snedden, S. A., Stebbins, A., Stubbs, C., Szapudi, I., Szkody, P., Szokoly, G. P., Tabachnik, S., Tsvetanov, Z., Uomoto, A., Vogeley, M. S., Voges, W., Waddell, P., Walterbos, R., Wang, S.-i., Watanabe, M., Weinberg, D. H., White, R. L., White, S. D. M., Wilhite, B., Wolfe, D., Yasuda, N., York, D. G., Zehavi, I., and Zheng, W. (2002). Sloan Digital Sky Survey: Early Data Release. *AJ*, 123:485–548.

Sulentic, J. W., Verdes-Montenegro, L., Bergond, G., Lisenfeld, U., Durbala, A., Espada, D., Garcia, E., Leon, S., Sabater, J., Verley, S., Casanova, V., and Sota, A. (2006). The AMIGA sample of isolated galaxies. II. Morphological refinement. *A&A*, 449:937–949.

Tojeiro, R., Wilkins, S., Heavens, A. F., Panter, B., and Jimenez, R. (2009). A Public Catalog of Stellar Masses, Star Formation and Metallicity Histories, and Dust Content from the Sloan Digital Sky Survey using VESPA. *ApJS*, 185:1–19.

van den Bosch, F. C., Aquino, D., Yang, X., Mo, H. J., Pasquali, A., McIntosh, D. H., Weinmann, S. M., and Kang, X. (2008). The importance of satellite quenching for the build-up of the red sequence of present-day galaxies. *MNRAS*, 387:79–91.

Verdes-Montenegro, L., Sulentic, J., Lisenfeld, U., Leon, S., Espada, D., Garcia, E., Sabater, J., and Verley, S. (2005). The AMIGA project. I. Optical characterization of the CIG catalog. *A&A*, 436:443–455.

Wang, W. and White, S. D. M. (2012). Satellite abundances around bright isolated galaxies. *MNRAS*, 424:2574–2598.

White, S. D. M. and Frenk, C. S. (1991). Galaxy formation through hierarchical clustering. *ApJ*, 379:52–79.

Wolf, C., Meisenheimer, K., Rix, H.-W., Borch, A., Dye, S., and Kleinheinrich, M. (2003). The COMBO-17 survey: Evolution of the galaxy luminosity function from 25 000 galaxies with 0.2 z 1.2. *A&A*, 401:73–98.

Xu, C. and Sulentic, J. W. (1991). Infrared emission in paired galaxies. II - Luminosity functions and far-infrared properties. *ApJ*, 374:407–430.

Yang, X., Mo, H. J., and van den Bosch, F. C. (2009). Galaxy Groups in the SDSS DR4. III. The Luminosity and Stellar Mass Functions. *ApJ*, 695:900–916.

Yang, X., Mo, H. J., van den Bosch, F. C., Pasquali, A., Li, C., and Barden, M. (2007). Galaxy Groups in the SDSS DR4. I. The Catalog and Basic Properties. *ApJ*, 671:153–170.

York, D. G., Adelman, J., Anderson, Jr., J. E., Anderson, S. F., Annis, J., Bahcall, N. A., Bakken, J. A., Barkhouser, R., Bastian, S., Berman, E., Boroski, W. N., Bracker, S., Briegel, C., Briggs, J. W., Brinkmann, J., Brunner, R., Burles, S., Carey, L., Carr, M. A., Castander, F. J., Chen, B., Colestock, P. L., Connolly, A. J., Crocker, J. H., Csabai, I., Czarapata, P. C., Davis, J. E., Doi, M., Dombeck, T., Eisenstein, D., Ellman, N., Elms, B. R., Evans, M. L., Fan, X., Federwitz, G. R., Fiscelli, L., Friedman, S., Frieman, J. A., Fukugita, M., Gillespie, B., Gunn, J. E., Gurbani, V. K., de Haas, E., Haldeman, M., Harris, F. H., Hayes, J., Heckman, T. M., Hennessy, G. S., Hindsley, R. B., Holm, S., Holmgren, D. J., Huang, C.-h., Hull, C., Husby, D., Ichikawa, S.-I., Ichikawa, T., Ivezić, Ž., Kent, S., Kim, R. S. J., Kinney, E., Klaene, M., Kleinman, A. N., Kleinman, S., Knapp, G. R., Korienek, J., Kron, R. G., Kunszt, P. Z., Lamb,

D. Q., Lee, B., Leger, R. F., Limmongkol, S., Lindenmeyer, C., Long, D. C., Loomis, C., Loveday, J., Lucinio, R., Lupton, R. H., MacKinnon, B., Mannery, E. J., Mantsch, P. M., Margon, B., McGehee, P., McKay, T. A., Meiksin, A., Merelli, A., Monet, D. G., Munn, J. A., Narayanan, V. K., Nash, T., Neilsen, E., Neswold, R., Newberg, H. J., Nichol, R. C., Nicinski, T., Nonino, M., Okada, N., Okamura, S., Ostriker, J. P., Owen, R., Pauls, A. G., Peoples, J., Peterson, R. L., Petravick, D., Pier, J. R., Pope, A., Pordes, R., Prosapio, A., Rechenmacher, R., Quinn, T. R., Richards, G. T., Richmond, M. W., Rivetta, C. H., Rockosi, C. M., Ruthmansdorfer, K., Sandford, D., Schlegel, D. J., Schneider, D. P., Sekiguchi, M., Sergey, G., Shimasaku, K., Siegmund, W. A., Smee, S., Smith, J. A., Snedden, S., Stone, R., Stoughton, C., Strauss, M. A., Stubbs, C., SubbaRao, M., Szalay, A. S., Szapudi, I., Szokoly, G. P., Thakar, A. R., Tremonti, C., Tucker, D. L., Uomoto, A., Vanden Berk, D., Vogeley, M. S., Waddell, P., Wang, S.-i., Watanabe, M., Weinberg, D. H., Yanny, B., Yasuda, N., and SDSS Collaboration (2000). The Sloan Digital Sky Survey: Technical Summary. *AJ*, 120:1579–1587.

Chapter 4

PaperIII

Galaxy And Mass Assembly:
The multiwavelength LF of galaxies in groups

Vázquez-Mata J. A., Loveday J. et al.

Using the Galaxy and Mass Assembly (GAMA) survey, we explore the multiwavelength luminosity function (LF) of galaxies in groups. Considering the GAMA Galaxy Group Catalogue (G^3Cv6), the galaxy luminosity function for these galaxies was estimated and we compare the dependence of the LF shape in 11 wavelengths, from the ultra violet to the near infrared, and also with the richness and mass of the groups.

We find a clear correlation of the LF bright-end with wavelength, in agreement with previous works, where bright galaxies in groups dominate at red bands whereas in blue and ultra violet bands, the bright galaxy population is found in low density environments but not in groups. This is because most of galaxies in groups are red ellipticals with low star formation activity, mainly in the central parts of rich groups.

When samples are separated in richness and mass bins, we find correlation between the Schechter parameters and wavelengths; however, no clear differences in these correlations are observed when we go to the highest richness and mass bins.

This is the first work presenting the galaxy group LF in 11 bands in a complete spectroscopic sample.

4.1 Introduction

The luminosity function (LF) started to be studied many years ago by different authors (e.g. Pannekoek 1923, Hubble 1936). This is a fundamental observable to give a description about the galaxy population in different environments and epochs, containing essential information about the physical processes carried out during the origin and evolution of galaxies in the universe. The LF is a fundamental constraint of galaxy formation and evolution models (e.g. Benson et al. 2003).

The LF has been studied for galaxies in different environments, from the very low density (voids) to the densest environments like clusters of galaxies (e.g. Park et al. 2007, Choi et al. 2007, McNaught-Roberts et al. 2014). Galaxy groups are an important clue in the study of the paradigm of hierarchical structure formation since this paradigm considers the accretion and merger of galaxy groups to form clusters (e.g. White and Rees 1978, White and Frenk 1991); following this fact and the observations, this suggests that most of the galaxies are contained in groups. There are many studies of the galaxy LF in groups, the most recent Zandivarez et al. (2006), Yang et al. (2009), Robotham et al. (2010) and Paper I.

The Group Evolution Multiwavelength Study project (GEMS; Osmond and Ponman 2004) was developed with a view to clarifying the different stages of group evolution and the ways in which this is related to galaxy properties, using optical photometry, radio and X-ray observations. This project started to do a detailed comparison of the multiwavelength properties of groups with evolution models and cosmological simulations, to understand how galaxies evolve in these environments. Unfortunately, the GEMS project only has 60 groups, not enough to make a well defined comparison with the models and simulations. In this context, the Galaxy and Mass Assembly project (GAMA; Driver et al. 2009, Driver et al. 2011) and the GAMA Galaxy Group Catalogue (G^3Cv6; Robotham et al. 2011) present the opportunity to complete the studies made by the GEMS project with better accuracy, since the G^3Cv6 catalogue contains about 23838 groups with multiplicity $\geq$2.

Multiwavelength luminosity functions might reveal the interplay between star formation, chemical evolution, and absorption and re-emission of dust within evolving galaxy populations. There are studies showing the importance of the role of the dust in galaxy evolution and the influence on the luminosities and colour of galaxies (Tuffs et al. 2004, Driver et al. 2007, Rocha et al. 2008, Tempel et al. 2010). Other studies have been focused specifically in the near and far infrared (FIR, NIR) LF (Miles et al. 2006, Guo prep), and

the ultra violet (UV) LF (Schenker et al. 2013, Jurek et al. 2013) in groups.

The motivation of this paper is to establish for the first time a homogeneous estimation of the LF in 11 bands $FUV, NUV, u, g, r, i, z, Y, J, H$ and K, and establish the characteristic Schechter parameters for these bands. Following the ideas from Paper II, establishing the dependence of the multiwavelength LF with the group mass and richness. This is a first attempt for this studies following the recent Panchromatic data presented by Driver et al. (2015). As the authors mention in private a communication, these data will be improved in a future, then the LF could be estimated in the far infrared, in the WISE (Wright et al., 2010) and Herschel bands (Eales et al., 2010).

In this paper, we describe generally the GAMA Galaxy Group Catalogue (G^3Cv6) in section 2 and the samples used in this work . Section 3 describes the correction applied to the sample. Section 4 shows the results for the LF, Sections 5 and 6 the LF and the dependence with the wavelength and the group properties. And finally, section 7 presents the conclusions.

For this paper we assume the standard cosmology parameters of Ω_M=0.3, Ω_Λ=0.7 with a Hubble constant of H_0=100h km s^{-1} Mpc^{-1}.

4.2 DATA

The Galaxy and Mass Assembly project (GAMA) is a multi-wavelength galaxy survey, with high spectral completeness, representing a good opportunity to study statistical properties of galaxies from different perspectives. GAMA is a survey based on an input catalogue described by Baldry et al. (2010), considering the Sloan Digital Sky Survey (SDSS; York et al. 2000, Abazajian et al. 2009) Data Release 6 (DR6; for the first phase) and DR7 for the second phase. The second phase (GAMA-II) consists of three equatorial regions, centred at 09h, 12h and 14h30m, called G09, G12 and G15 respectively, each of 12 $\times$ 5 degrees with a Petrosian magnitude limit of $r < 19.8$ mag for all the fields, and two non-equatorial regions G02 and G23.

Robotham et al. (2011) compiled the G^3Cv1 group catalogue based on the GAMA I survey applying a friend-of-friends (FoF) grouping algorithm. Once GAMA II was ready to be studied, the group catalogue was updated to the new data following the same algorithm (G^3Cv6). The G^3Cv6 catalogue contains a total of 23838 groups with multiplicity $\geq$2 containing 73268 galaxies, meaning a fraction of $\sim$40% of the total GAMA galaxies to be grouped.

In order to estimate the galaxy multiwavelength LF in groups, we have considered the

GAMA Panchromatic Photometry presented in Driver et al. (2015). These authors take the panchromatic imaging in the G09, G12 and G15 fields, acquired by other teams in the UV to far-IR range in 21 broad-band filters.

The Galaxy Exploration Explorer (GALEX) Medium Imaging Survey (Martin et al., 2005) has been matched with GAMA regions to obtain the ultraviolet information in the NUV and FUV bands (www.mpi-hd.mpg.de/galex-gama). GALEX-GAMA match covers between 75% and 97% of the three equatorial regions (Driver et al., 2015). The SDSS is used to get the optical bands $ugriz$ images. For the near-infrared (NIR), GAMA area is covered by the VIsta Kilodegree INfrared Galaxy survey (VIKING; a description is presented by Edge et al. 2013) in the $YJHK$ bands. For the far-infrared (FIR), the Wide-field Infrared Survey Explorer (WISE; Wright et al. 2010) and the Herschel Astrophysical Terahertz Large Area Survey (Herschel-ATLAS, Eales et al. 2010).

The idea behind the Panchromatic Photometry is to make homogeneous all the photometry from the different wavelengths; defining an aperture in a single band, and apply the same aperture at the same astrometric location with images with identical spatial sampling (Driver et al., 2015), and this is used to derive $u-K$ aperture-matched photometry. Nevertheless, this idea cannot be applied to other wavelengths outside this range due to the resolution mismatch. For the FUV and NUV bands, the GAMA GALEX catalogues described by Liske et al. (2015) is used.

4.3 Completeness and K-correction

4.3.1 Completeness

The GAMA survey is spectroscopically highly complete in the three equatorial regions (Driver et al., 2011); however, Loveday et al. (2012) and the Paper I have corrected the GAMA sample for completeness in: the input catalogue (C_{im}), selection target (C_{targ}) and the success rate for obtaining spectroscopic redshifts (C_{spec}) with good quality. In this work, these corrections are applied and weighted by the reciprocal of the product of these three completenesses

$$\mathrm{W}_i = 1/(C_{im}C_{targ}C_{spec}). \quad (4.1)$$

Table 4.1: Faint magnitude limits for the $FNugizYJHK$ bands in order to have a complete sample in each wavelength

Band	apparent magnitude limit
F	21.14
N	20.53
u	20.49
g	19.98
r	19.80
i	18.64
z	18.31
Y	18.09
J	17.87
H	17.48
K	17.34

4.3.2 Luminosity limits

The GAMA survey is a magnitude limited sample selected in the r-band, and complete at r =19.8. Nevertheless, other magnitudes are not limited by any other value but the intrinsic value corresponding to the r-band. To obtain a complete sample in the other bands, we follow the method described in Paper II; we consider the colour distributions of galaxies between the corresponding magnitude and the r magnitude. All magnitudes are taken from the Panchromatic catalogues described in Driver et al. (2015). These distributions are presented in Fig. 4.1 for the $j - r$ colours where in UV $j = FN$, in optical $j = ugiz$ and infrared $j = YJHK$ where dashed-lines represent the 1 and 99 percentile in each colour. Magnitude limits in band are given by adding the leftmost value of these colours to the sample limited value of r=19.8. Since the leftmost colour represent the 1%, so the sample will be 99% complete in each band by adding this value. Magnitude limits are presented in Table 4.1 and these limits are used to calculate and fit the LF.

4.3.3 K-correction

In spite of GAMA being a local galaxy survey, the median redshift is ∼0.2 and we have to apply a correction to the intrinsic luminosity according to the rest frame of the galaxy. We apply this correction to the whole sample, called K-correction (Humason et al., 1956) using the KCORRECT V4_2 code (Blanton et al. 2003, Blanton and Roweis 2007). In this

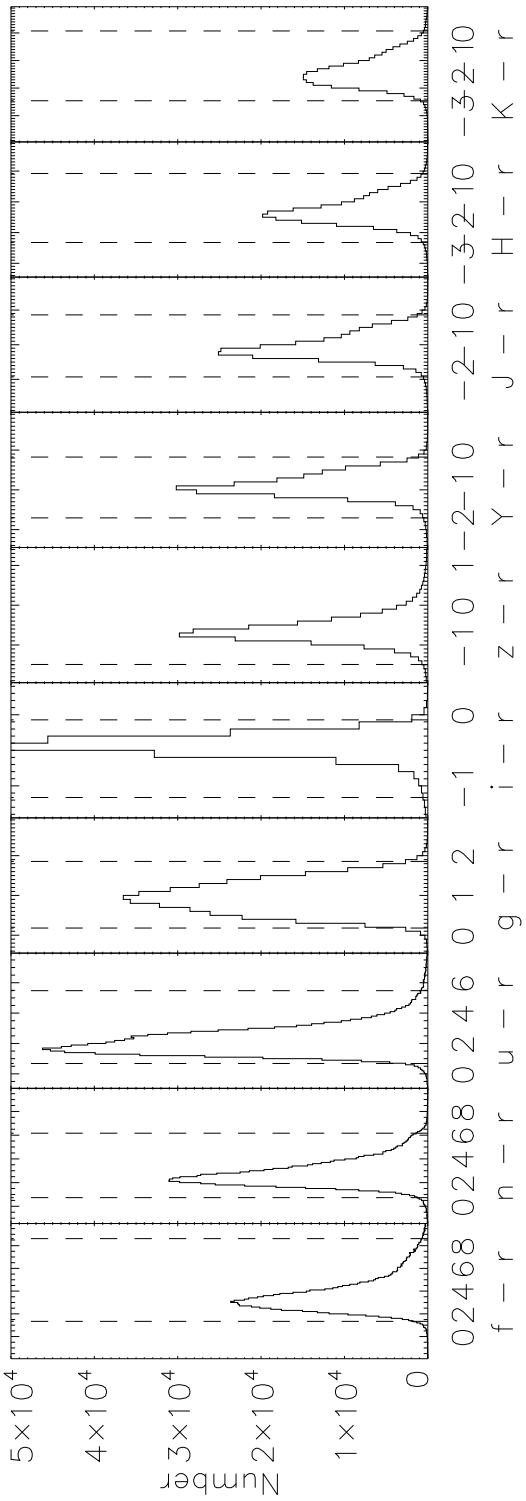

Figure 4.1: Colour histograms in 0.1 mag bins for the G^3Cv6 galaxies. The vertical dashed lines indicate the 1- and 99-percentiles; the leftmost of which defines colour completeness in the $FNugizYJHK$ bands.

work, the GAMA sample has been corrected in a passband blue-shifted by $z_0 = 0.1$, since NUV and FUV bands show large evolution for low redshift as Driver et al. (2012) describe in section 4.1.4.

4.4 Luminosity Function

Estimation of the LF was carried out using the well known non-parametric methods: the 1/Vmax (Schmidt, 1968) and the stepwise maximum likelihood (SWML, Efstathiou et al. 1988); a parametric method developed by Sandage et al. (1979) (STY) based on the maximum likelihood is also considered to estimate the LF. The $1/V_{max}$ method has the disadvantage that it is sensitive to galaxy density variations, so we prefer to work with the SWML method where we have considered ΔM = 0.25 bins. The parametric STY method avoids the effects of density at large scales and we use the standard Schechter function (Schechter, 1976),

$$\phi(M) = 0.4 \ln 10 \phi^* (10^{0.4(M^*-M)})^{1+\alpha} \exp(-10^{0.4(M^*-M)}), \tag{4.2}$$

where M is the absolute magnitude, ϕ^* is the density normalization, M* is the characteristic luminosity at which the LF shows the turnover or "knee" and α is the slope at the faint-end (see Paper I for more details). In this broad analysis, the LFs have been calculated for a local sample, with redshift $z \leq 0.1$.

Fig. 4.2 shows the LF for the 11 bands $FNugrizYJHK$ up to z =0.1; open symbols show the $1/V_{max}$ method as comparison to the SWML presented in filled symbols. Solid line shows our parametric fit using the Schechter function and dotted-lines shows the results presented in Driver et al. (2012) for the complete GAMA I survey. Note that Driver et al. (2012) estimated the LF using other magnitude limits based on the data available for GAMA I and they did not do any correction for incompleteness.

Our results agree very well with those presented by Driver et al. (2012) where M* becomes brighter as the band gets redder, as well as the results presented in Hill et al. (2010) for the $ugrizYJHK$ bands (dashed-lines) who combine data from the Millennium Galaxy Catalogue (Liske et al., 2003), SDSS and the UKIRT Infrared Deep Sky Survey Large Area Survey (Lawrence et al. 2007; Warren et al. 2007). Note, at the NIR bands, Hill et al. (2010) show LFs brighter than Driver et al. (2012) and this work. Driver et al. (2012) do not report this difference, this could be the result of any extra correction applied for the magnitudes. There is an important difference between the group LF and the global GAMA LF, this effect is observed at the bright end. In the UV bright end, the global LF

dominates over the group LF, meaning a large galaxy population of ungrouped galaxies in this region; this characteristic is observed only in the $FNugr$ bands. This means galaxies in groups do not present high star formation activity like galaxies in the field. From the i-band to the K-band, this difference at the bright end is negligible, showing that galaxies in groups are brighter in red and infrared bands meaning a decrease of star formation process and dominated with galaxies reddened by dust and gas, characteristic of elliptical type galaxies.

Snaith et al. (2011) estimated the LF for galaxies in groups in semi analytical models (SAM), they find a clear difference between the group LF and the global galaxy LF at the faint-end using the r-band; in this work we find this differences are presented for all bands. Surprisingly, the gap between the LF is larger in the UV bands, probably because faint blue galaxies are rarely present in groups but dominate the low dense environments.

4.5 Wavelength dependence with multiplicity

One of the most important properties of the groups is their multiplicity or richness (Nfof), from pairs of galaxies to large groups with ∼50 members. The LF is estimated for groups up to z =0.1 using a magnitude-limited sample, not a volume-limited sample. Paper I shows for local groups ($z \leq$0.1) volume- and magnitude- limited samples are equivalent and working with a magnitude-limited sample gives the advantage of having a larger population of groups and consequently fainter galaxies.

Appendix A shows the SWML LF and parametric LF, as well as a the log likelihood ratio test between the non- and parametric LF.

Left hand side of Fig. 4.3 shows the parametric LF for three richness bins: Nfof = 2, 3 $\leq$ Nfof $\leq$ 4 and Nfof $\geq$ 5 from the top to the bottom respectively. FNugrizYJHK bands LFs are plotted in magenta, cyan, blue, green, black, yellow, red, magenta, cyan, blue and green respectively. UV bands can be seen at the faintest magnitudes, a consequence of low emission due to low star formation processes; meanwhile, NIR bands are brighter for most of the galaxies, so it is not likely star formation processes are carried out (apart of some star burst that may be presented in the sample). Star forming or blue galaxies are present predominantly in the outskirts of the groups or in the field; so, only a small portion of galaxies in groups are blue dominant and are found mainly in groups with low richness as Fig. 4.3 suggests.

To clarify any tendency of the Schechter parameters α and M^* in these richness bins with respect to the wavelengths, we plot them together in the right hand side of Fig. 4.3.

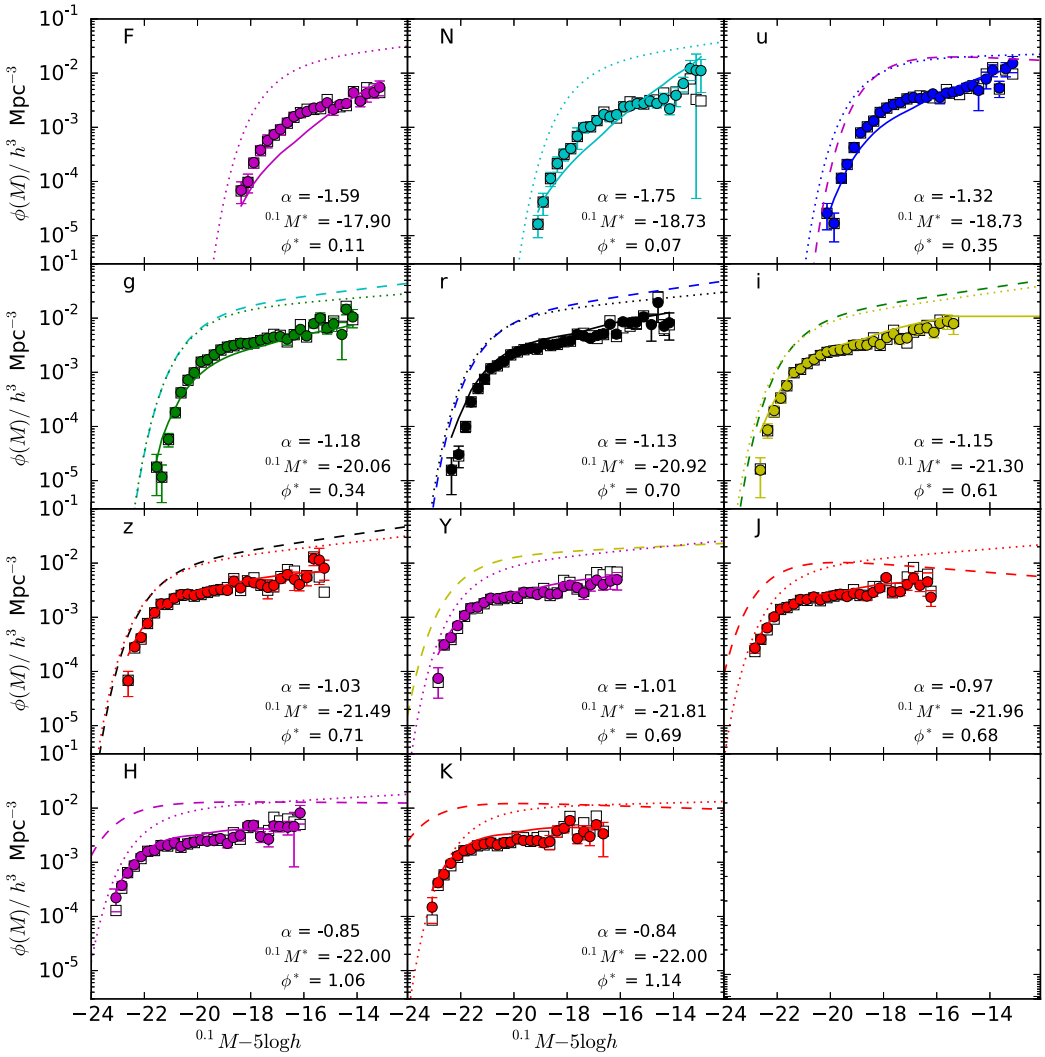

Figure 4.2: The group LF in the 11 wavelengths from the top-left panel in the FUV band to the NIR K band in the bottom-middle panel. Open symbols represent the $1/V_{max}$ method, filled symbols the SWML method and the solid line the parametric Schechter function. As comparison, dotted-lines shows the LF for the total GAMA sample estimated by Driver et al. (2012), and dashed-lines the multiwavelength LF (u-K) presented by Hill et al. (2010).

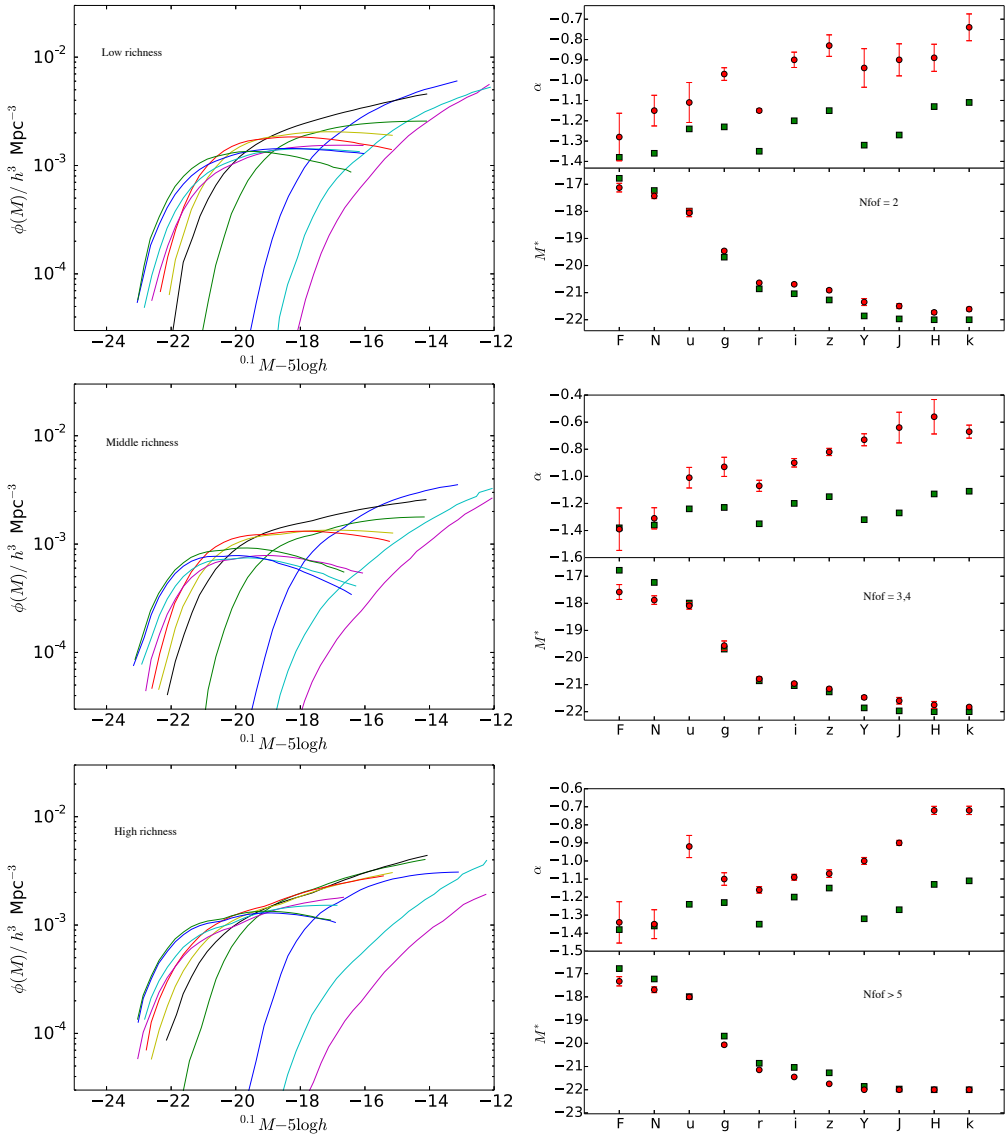

Figure 4.3: Left hand side, the group LF divided by richness, from the top (low richness bin) to the bottom (high richness bin) in the FNugrizYJHK bands in magenta, cyan, blue, green, black, yellow, red, magenta, cyan, blue and green respectively being UV bands the faintest and NIR bands the brightest. Right hand side, the Schechter parameters α and M^* in three richness bins against wavelengths. Low, middle and high richness bin are presented from the top to the bottom panel respectively in red circles and green squares show a comparison to the complete GAMA sample

Low, middle and high richness bin, are presented from the top to the bottom panel respectively in red circles with the respective error bars. Green squares are plotted as a comparison to the complete GAMA sample (Driver et al., 2012). Note that this data was k-corrected to redshift zero, making a small bias when comparing in this plots, affecting more the $FNug$ bands as these authors described.

For all of the cases, α becomes flatter as we approach the NIR bands, except for the ug bands in the middle and high richness; however, large error bars are also evident. This suggests a low UV emission from these galaxies as we expect in agreement with the M^* parameter, where there is a higher emission in the NIR bands than UV. Within the error bars, there is no strong difference between α or M^* with respect to the richness for the UV and NIR bands as there is for example in the r-band as reported in Paper I. However, for $rizY$ bands, α becomes steeper at high richness, this could be the result of a magnitude limit bias in these bands.

4.6 Wavelength dependence with mass

Another important property of the groups is their mass. G^3C catalogue has been divided in three mass bins: $8 < \log M/M\odot \leq 12.06$, $12.06 < \log M/M\odot \leq 12.70$ and $12.70 < \log M/M\odot \leq 16$. Appendix A also shows the non- and the parametric LF for each of the mass bins and the respective log-likelihood ratio test between them.

We plot, in the left hand side of Fig. 4.4, the paramtric LF for all the bands with colour similar to Fig. 4.3 from the lowest, in the top, to the highest mass bin in the bottom. From this figure it is very hard to distinguish a proper Schechter LF shape at the high mass bin for the NF bands. This support the idea that stellar formation activity is truncated in dense regions (massive groups) mainly by dynamical frictions and forces acting on galaxies stripping the gas. Then, galaxies must be observed at fainter NF magnitudes to have enough information and establish the corresponding Schechter parameter α.

Right hand side of Fig. 4.4 shows the Schechter parameters α and M^* in three mass bins with respect to the wavelengths. M^* is very similar in all cases and also with respect to the complete GAMA LF (green squares); nevertheless, it is possible to distinguish the group M^* is brighter than the global M^* at the high mass bin. This must be consequence of the bias produced by the estimation of the parametric LF. This issue could be solved by applying the joint stepwise maximum likelihood presented by Loveday et al. (2015). From g-band, group M^* becomes fainter, independently of the mass range. Surprisingly at high masses, group and global M^* for the NIR bands are basically the same; this means

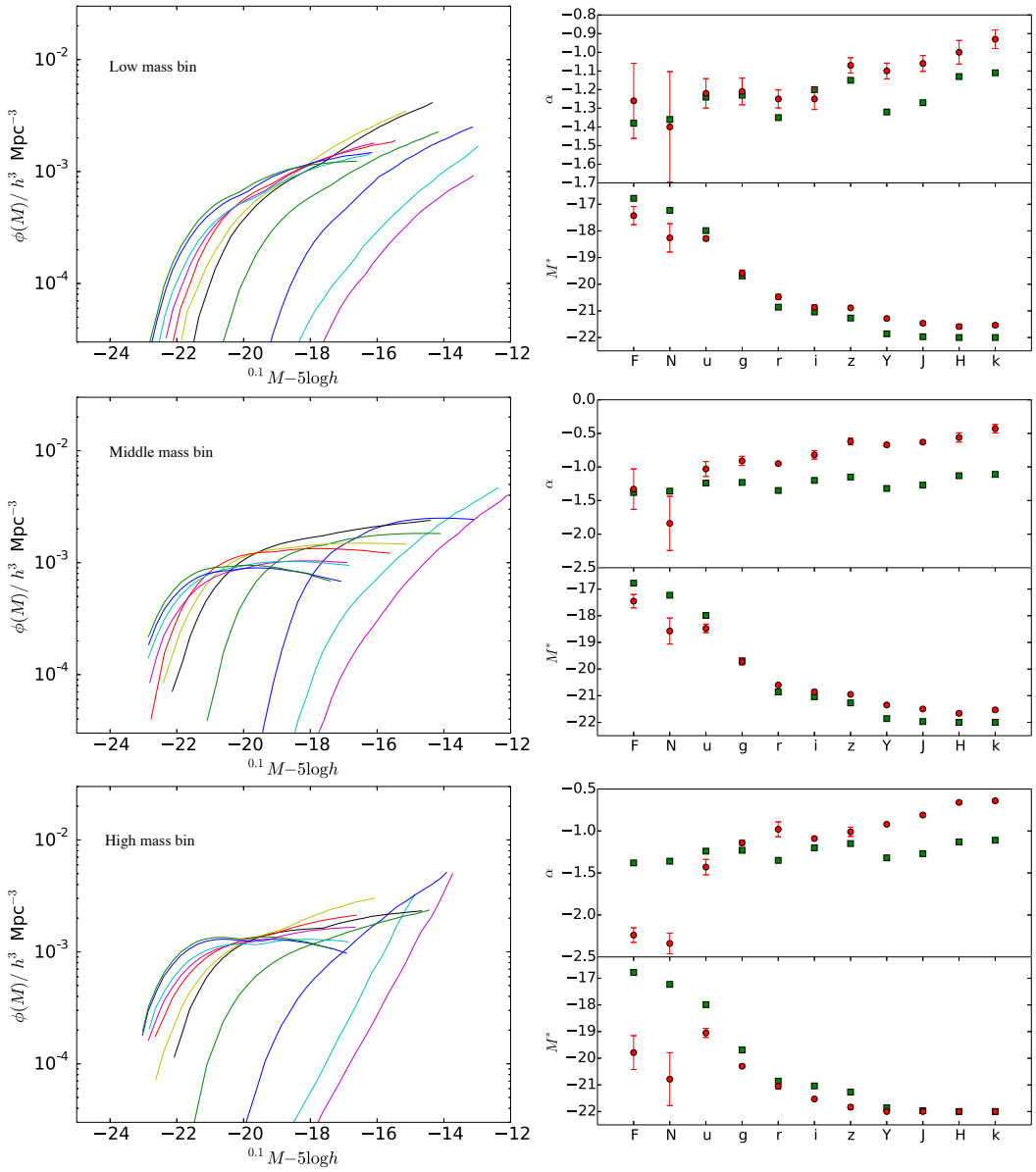

Figure 4.4: Left hand side, the group LF divided by three mass bins in the FNugrizYJHK bands in magenta, cyan, blue, green, black, yellow, red, magenta, cyan, blue and green respectively being the UV bands the faintest and NIR bands the brightest. Similar to Fig. **??**, the right hand side shows the Schechter parameters α and M^*.

massive galaxies in groups with high emission in IR, dominate the bright end of the global LF for these bands. α is also changing from the g-band where the group α is getting flatter as we move to IR bands independently of the mass bin.

4.7 Conclusions

In this work we present the first attempt to estimate the multiwavelength LF ($FNugrizYJHK$) for the G^3Cv6 catalogue based on the complete GAMA II survey covering 11 bands up to the r-Petrosian band r=19.8. Results are in agreement with previous works based on multiwavelength studies, mainly the changes in the bright and faint ends between the group LF and the global galaxy LF.

When galaxies in groups are separated by richness and mass bins, we prove as expected that galaxies in groups are dominated by the NIR emission. Early type galaxies dominate the group population, as Paper I presents; this type of galaxies are preferably red and massive with low or almost null star formation processes. This fact agrees with the low UV luminosity presents in these galaxies specially in the high mass bin, where the population is dominate by the central galaxies in groups and these galaxies tend to be large ellipticals. There are clear evidence about a correlation between the Schechter parameters respect to the richness or mass for all the wavelengths. A detailed study of these correlations between the Schechter parameters and the group properties by band is suggested in a further work. When galaxies are separated in mass group bins, the FN bands LF is badly estimated, i.e. likely due to the number of galaxies considering in the sample with the mass constrains, no FN faint galaxies are considered and this was observed in the high mass bin. This suggest a more careful study in these bands and the relation with the mass group bins.

This is the first work estimating the group LF in 11 bands and a deep study is necessary to take advantage of the whole information accessible from the GAMA survey, to identify the different stages of evolution of galaxies in groups.

Acknowledgements

GAMA is a joint European-Australasian project based around a spectroscopic campaign using the Anglo-Australian Telescope. The GAMA input catalogue is based on data taken from the Sloan Digital Sky Survey and the UKIRT Infrared Deep Sky Survey. Complementary imaging of the GAMA regions is being obtained by a number of independent survey programs including GALEX MIS, VST KiDS, VISTA VIKING, WISE, Herschel-ATLAS,

GMRT and ASKAP providing UV to radio coverage. GAMA is funded by the STFC (UK), the ARC (Australia), the AAO, and the participating institutions. The GAMA website is http://www.gama-survey.org/ .

JAVM was supported by the Mexican National Council for Science and Technology (CONACyT) scholarship scheme.

References

Abazajian, K. N., Adelman-McCarthy, J. K., Agüeros, M. A., Allam, S. S., Allende Prieto, C., An, D., Anderson, K. S. J., Anderson, S. F., Annis, J., Bahcall, N. A., and et al. (2009). The Seventh Data Release of the Sloan Digital Sky Survey. *ApJS*, 182:543–558.

Benson, A. J., Frenk, C. S., Baugh, C. M., Cole, S., and Lacey, C. G. (2003). The effects of photoionization on galaxy formation - III. Environmental dependence in the luminosity function. *MNRAS*, 343:679–691.

Blanton, M. R., Brinkmann, J., Csabai, I., Doi, M., Eisenstein, D., Fukugita, M., Gunn, J. E., Hogg, D. W., and Schlegel, D. J. (2003). Estimating Fixed-Frame Galaxy Magnitudes in the Sloan Digital Sky Survey. *AJ*, 125:2348–2360.

Blanton, M. R. and Roweis, S. (2007). K-Corrections and Filter Transformations in the Ultraviolet, Optical, and Near-Infrared. *AJ*, 133:734–754.

Choi, Y.-Y., Park, C., and Vogeley, M. S. (2007). Internal and Collective Properties of Galaxies in the Sloan Digital Sky Survey. *ApJ*, 658:884–897.

Driver, S. P., Allen, P. D., Liske, J., and Graham, A. W. (2007). The Millennium Galaxy Catalogue: The Luminosity Functions of Bulges and Disks and Their Implied Stellar Mass Densities. *ApJ*, 657:L85–L88.

Driver, S. P., Hill, D. T., Kelvin, L. S., Robotham, A. S. G., Liske, J., Norberg, P., Baldry, I. K., Bamford, S. P., Hopkins, A. M., Loveday, J., Peacock, J. A., Andrae, E., Bland-Hawthorn, J., Brough, S., Brown, M. J. I., Cameron, E., Ching, J. H. Y., Colless, M., Conselice, C. J., Croom, S. M., Cross, N. J. G., de Propris, R., Dye, S., Drinkwater, M. J., Ellis, S., Graham, A. W., Grootes, M. W., Gunawardhana, M., Jones, D. H., van Kampen, E., Maraston, C., Nichol, R. C., Parkinson, H. R., Phillipps, S., Pimbblet, K., Popescu, C. C., Prescott, M., Roseboom, I. G., Sadler, E. M., Sansom, A. E., Sharp, R. G., Smith, D. J. B., Taylor, E., Thomas, D., Tuffs, R. J., Wijesinghe, D., Dunne, L.,

Frenk, C. S., Jarvis, M. J., Madore, B. F., Meyer, M. J., Seibert, M., Staveley-Smith, L., Sutherland, W. J., and Warren, S. J. (2011). Galaxy and Mass Assembly (GAMA): survey diagnostics and core data release. *MNRAS*, 413:971–995.

Driver, S. P., Norberg, P., Baldry, I. K., Bamford, S. P., Hopkins, A. M., Liske, J., Loveday, J., Peacock, J. A., Hill, D. T., Kelvin, L. S., Robotham, A. S. G., Cross, N. J. G., Parkinson, H. R., Prescott, M., Conselice, C. J., Dunne, L., Brough, S., Jones, H., Sharp, R. G., van Kampen, E., Oliver, S., Roseboom, I. G., Bland-Hawthorn, J., Croom, S. M., Ellis, S., Cameron, E., Cole, S., Frenk, C. S., Couch, W. J., Graham, A. W., Proctor, R., De Propris, R., Doyle, I. F., Edmondson, E. M., Nichol, R. C., Thomas, D., Eales, S. A., Jarvis, M. J., Kuijken, K., Lahav, O., Madore, B. F., Seibert, M., Meyer, M. J., Staveley-Smith, L., Phillipps, S., Popescu, C. C., Sansom, A. E., Sutherland, W. J., Tuffs, R. J., and Warren, S. J. (2009). GAMA: towards a physical understanding of galaxy formation. *Astronomy and Geophysics*, 50(5):050000–5.

Driver, S. P., Robotham, A. S. G., Kelvin, L., Alpaslan, M., Baldry, I. K., Bamford, S. P., Brough, S., Brown, M., Hopkins, A. M., Liske, J., Loveday, J., Norberg, P., Peacock, J. A., Andrae, E., Bland-Hawthorn, J., Bourne, N., Cameron, E., Colless, M., Conselice, C. J., Croom, S. M., Dunne, L., Frenk, C. S., Graham, A. W., Gunawardhana, M., Hill, D. T., Jones, D. H., Kuijken, K., Madore, B., Nichol, R. C., Parkinson, H. R., Pimbblet, K. A., Phillipps, S., Popescu, C. C., Prescott, M., Seibert, M., Sharp, R. G., Sutherland, W. J., Taylor, E. N., Thomas, D., Tuffs, R. J., van Kampen, E., Wijesinghe, D., and Wilkins, S. (2012). Galaxy And Mass Assembly (GAMA): the 0.013 z 0.1 cosmic spectral energy distribution from 0.1 μm to 1 mm. *MNRAS*, 427:3244–3264.

Driver, S. P., Wright, A. H., Andrews, S. K., Davies, L. J., Kafle, P. R., Lange, R., Moffett, A. J., Mannering, E., Robotham, A. S. G., Vinsen, K., Alpaslan, M., Andrae, E., Baldry, I. K., Bauer, A. E., Bamford, S. P., Bland-Hawthorn, J., Bourne, N., Brough, S., Brown, M. J. I., Cluver, M. E., Croom, S., Colless, M., Conselice, C. J., da Cunha, E., De Propris, R., Drinkwater, M., Dunne, L., Eales, S., Edge, A., Frenk, C., Graham, A. W., Grootes, M., Holwerda, B. W., Hopkins, A. M., Ibar, E., van Kampen, E., Kelvin, L. S., Jarrett, T., Jones, D. H., Lara-Lopez, M. A., Lopez-Sanchez, A. R., Liske, J., Loveday, J., Maddox, S. J., Madore, B., Meyer, M., Norberg, P., Penny, S. J., Phillipps, S., Popescu, C., Tuffs, R. J., Peacock, J. A., Pimbblet, K. A., Rowlands, K., Sansom, A. E., Seibert, M., Smith, M. W. L., Sutherland, W. J., Taylor, E. N., Valiante, E., Wang, L., Wilkins, S. M., and Williams, R. (2015). Galaxy And Mass Assembly

(GAMA): Panchromatic Data Release (far-UV — far-IR) and the low-z energy budget. *ArXiv e-prints*.

Eales, S., Dunne, L., Clements, D., Cooray, A., de Zotti, G., Dye, S., Ivison, R., Jarvis, M., Lagache, G., Maddox, S., Negrello, M., Serjeant, S., Thompson, M. A., van Kampen, E., Amblard, A., Andreani, P., Baes, M., Beelen, A., Bendo, G. J., Benford, D., Bertoldi, F., Bock, J., Bonfield, D., Boselli, A., Bridge, C., Buat, V., Burgarella, D., Carlberg, R., Cava, A., Chanial, P., Charlot, S., Christopher, N., Coles, P., Cortese, L., Dariush, A., da Cunha, E., Dalton, G., Danese, L., Dannerbauer, H., Driver, S., Dunlop, J., Fan, L., Farrah, D., Frayer, D., Frenk, C., Geach, J., Gardner, J., Gomez, H., González-Nuevo, J., González-Solares, E., Griffin, M., Hardcastle, M., Hatziminaoglou, E., Herranz, D., Hughes, D., Ibar, E., Jeong, W.-S., Lacey, C., Lapi, A., Lawrence, A., Lee, M., Leeuw, L., Liske, J., López-Caniego, M., Müller, T., Nandra, K., Panuzzo, P., Papageorgiou, A., Patanchon, G., Peacock, J., Pearson, C., Phillipps, S., Pohlen, M., Popescu, C., Rawlings, S., Rigby, E., Rigopoulou, M., Robotham, A., Rodighiero, G., Sansom, A., Schulz, B., Scott, D., Smith, D. J. B., Sibthorpe, B., Smail, I., Stevens, J., Sutherland, W., Takeuchi, T., Tedds, J., Temi, P., Tuffs, R., Trichas, M., Vaccari, M., Valtchanov, I., van der Werf, P., Verma, A., Vieria, J., Vlahakis, C., and White, G. J. (2010). The Herschel ATLAS. *PASP*, 122:499–515.

Edge, A., Sutherland, W., Kuijken, K., Driver, S., McMahon, R., Eales, S., and Emerson, J. P. (2013). The VISTA Kilo-degree Infrared Galaxy (VIKING) Survey: Bridging the Gap between Low and High Redshift. *The Messenger*, 154:32–34.

Efstathiou, G., Ellis, R. S., and Peterson, B. A. (1988). Analysis of a complete galaxy redshift survey. II - The field-galaxy luminosity function. *MNRAS*, 232:431–461.

Guo, Q. (in prep.). Herschel-atlas/gama:how does the far-ir luminosity function depend on galaxy group properties?

Hill, D. T., Driver, S. P., Cameron, E., Cross, N., Liske, J., and Robotham, A. (2010). The ugrizYJHK luminosity distributions and densities from the combined MGC, SDSS and UKIDSS LAS data sets. *MNRAS*, 404:1215–1230.

Hubble, E. (1936). The Luminosity Function of Nebulae. I. The Luminosity Function of Resolved Nebulae as Indicated by Their Brightest Stars. *ApJ*, 84:158.

Humason, M. L., Mayall, N. U., and Sandage, A. R. (1956). Redshifts and magnitudes of extragalactic nebulae. *AJ*, 61:97–162.

Jurek, R. J., Drinkwater, M. J., Pimbblet, K., Glazebrook, K., Blake, C., Brough, S., Colless, M., Contreras, C., Couch, W., Croom, S., Croton, D., Davis, T. M., Forster, K., Gilbank, D., Gladders, M., Jelliffe, B., Li, I.-h., Madore, B., Martin, D. C., Poole, G. B., Pracy, M., Sharp, R., Wisnioski, E., Woods, D., Wyder, T. K., and Yee, H. K. C. (2013). The WiggleZ Dark Energy Survey: star formation in UV-luminous galaxies from their luminosity functions. *MNRAS*, 434:257–281.

Lawrence, A., Warren, S. J., Almaini, O., Edge, A. C., Hambly, N. C., Jameson, R. F., Lucas, P., Casali, M., Adamson, A., Dye, S., Emerson, J. P., Foucaud, S., Hewett, P., Hirst, P., Hodgkin, S. T., Irwin, M. J., Lodieu, N., McMahon, R. G., Simpson, C., Smail, I., Mortlock, D., and Folger, M. (2007). The UKIRT Infrared Deep Sky Survey (UKIDSS). *MNRAS*, 379:1599–1617.

Liske, J., Baldry, I. K., Driver, S. P., Tuffs, R. J., Alpaslan, M., Andrae, E., Brough, S., Cluver, M. E., Grootes, M. W., Gunawardhana, M. L. P., Kelvin, L. S., Loveday, J., Robotham, A. S. G., Taylor, E. N., Bamford, S. P., Bland-Hawthorn, J., Brown, M. J. I., Drinkwater, M. J., Hopkins, A. M., Meyer, M. J., Norberg, P., Peacock, J. A., Agius, N. K., Andrews, S. K., Bauer, A. E., Ching, J. H. Y., Colless, M., Conselice, C. J., Croom, S. M., Davies, L. J. M., De Propris, R., Dunne, L., Eardley, E. M., Ellis, S., Foster, C., Frenk, C. S., Häußler, B., Holwerda, B. W., Howlett, C., Ibarra, H., Jarvis, M. J., Jones, D. H., Kafle, P. R., Lacey, C. G., Lange, R., Lara-López, M. A., López-Sánchez, Á. R., Maddox, S., Madore, B. F., McNaught-Roberts, T., Moffett, A. J., Nichol, R. C., Owers, M. S., Palamara, D., Penny, S. J., Phillipps, S., Pimbblet, K. A., Popescu, C. C., Prescott, M., Proctor, R., Sadler, E. M., Sansom, A. E., Seibert, M., Sharp, R., Sutherland, W., Vázquez-Mata, J. A., van Kampen, E., Wilkins, S. M., Williams, R., and Wright, A. H. (2015). Galaxy And Mass Assembly (GAMA): end of survey report and data release 2. *MNRAS*, 452:2087–2126.

Liske, J., Lemon, D. J., Driver, S. P., Cross, N. J. G., and Couch, W. J. (2003). The Millennium Galaxy Catalogue: 16 =B$_{MGC}$ 24 galaxy counts and the calibration of the local galaxy luminosity function. *MNRAS*, 344:307–324.

Loveday, J., Norberg, P., Baldry, I. K., Bland-Hawthorn, J., Brough, S., Brown, M. J. I., Driver, S. P., Kelvin, L. S., and Phillipps, S. (2015). Galaxy and Mass Assembly (GAMA): maximum-likelihood determination of the luminosity function and its evolution. *MNRAS*, 451:1540–1552.

Loveday, J., Norberg, P., Baldry, I. K., Driver, S. P., Hopkins, A. M., Peacock, J. A., Bamford, S. P., Liske, J., Bland-Hawthorn, J., Brough, S., Brown, M. J. I., Cameron, E., Conselice, C. J., Croom, S. M., Frenk, C. S., Gunawardhana, M., Hill, D. T., Jones, D. H., Kelvin, L. S., Kuijken, K., Nichol, R. C., Parkinson, H. R., Phillipps, S., Pimbblet, K. A., Popescu, C. C., Prescott, M., Robotham, A. S. G., Sharp, R. G., Sutherland, W. J., Taylor, E. N., Thomas, D., Tuffs, R. J., van Kampen, E., and Wijesinghe, D. (2012). Galaxy and Mass Assembly (GAMA): ugriz galaxy luminosity functions. *MNRAS*, 420:1239–1262.

Martin, D. C., Fanson, J., Schiminovich, D., Morrissey, P., Friedman, P. G., Barlow, T. A., Conrow, T., Grange, R., Jelinsky, P. N., Milliard, B., Siegmund, O. H. W., Bianchi, L., Byun, Y.-I., Donas, J., Forster, K., Heckman, T. M., Lee, Y.-W., Madore, B. F., Malina, R. F., Neff, S. G., Rich, R. M., Small, T., Surber, F., Szalay, A. S., Welsh, B., and Wyder, T. K. (2005). The Galaxy Evolution Explorer: A Space Ultraviolet Survey Mission. *ApJ*, 619:L1–L6.

McNaught-Roberts, T., Norberg, P., Baugh, C., Lacey, C., Loveday, J., Peacock, J., Baldry, I., Bland-Hawthorn, J., Brough, S., Driver, S. P., Robotham, A. S. G., and Vázquez-Mata, J. A. (2014). Galaxy And Mass Assembly (GAMA): the dependence of the galaxy luminosity function on environment, redshift and colour. *MNRAS*, 445:2125–2145.

Miles, T. A., Raychaudhury, S., and Russell, P. A. (2006). The group evolution multiwavelength study: the near-infrared luminosity function of nearby galaxy groups. *MNRAS*, 373:1461–1469.

Osmond, J. P. F. and Ponman, T. J. (2004). The GEMS project: X-ray analysis and statistical properties of the group sample. *MNRAS*, 350:1511–1535.

Pannekoek, A. (1923). Luminosity function and brightness for clusters and galactic clouds. , 2:5.

Park, C., Choi, Y.-Y., Vogeley, M. S., Gott, III, J. R., Blanton, M. R., and SDSS Collaboration (2007). Environmental Dependence of Properties of Galaxies in the Sloan Digital Sky Survey. *ApJ*, 658:898–916.

Robotham, A., Phillipps, S., and de Propris, R. (2010). The variation of the galaxy luminosity function with group properties. *MNRAS*, 403:1812–1828. 163

Robotham, A. S. G., Norberg, P., Driver, S. P., Baldry, I. K., Bamford, S. P., Hopkins, A. M., Liske, J., Loveday, J., Merson, A., Peacock, J. A., Brough, S., Cameron, E., Conselice, C. J., Croom, S. M., Frenk, C. S., Gunawardhana, M., Hill, D. T., Jones, D. H., Kelvin, L. S., Kuijken, K., Nichol, R. C., Parkinson, H. R., Pimbblet, K. A., Phillipps, S., Popescu, C. C., Prescott, M., Sharp, R. G., Sutherland, W. J., Taylor, E. N., Thomas, D., Tuffs, R. J., van Kampen, E., and Wijesinghe, D. (2011). Galaxy and Mass Assembly (GAMA): the GAMA galaxy group catalogue (G^3Cv1). *MNRAS*, 416:2640–2668.

Rocha, M., Jonsson, P., Primack, J. R., and Cox, T. J. (2008). Dust attenuation in hydrodynamic simulations of spiral galaxies. *MNRAS*, 383:1281–1291.

Sandage, A., Tammann, G. A., and Yahil, A. (1979). The velocity field of bright nearby galaxies. I - The variation of mean absolute magnitude with redshift for galaxies in a magnitude-limited sample. *ApJ*, 232:352–364.

Schechter, P. (1976). An analytic expression for the luminosity function for galaxies. *ApJ*, 203:297–306.

Schenker, M. A., Robertson, B. E., Ellis, R. S., Ono, Y., McLure, R. J., Dunlop, J. S., Koekemoer, A., Bowler, R. A. A., Ouchi, M., Curtis-Lake, E., Rogers, A. B., Schneider, E., Charlot, S., Stark, D. P., Furlanetto, S. R., and Cirasuolo, M. (2013). The UV Luminosity Function of Star-forming Galaxies via Dropout Selection at Redshifts z ˜ 7 and 8 from the 2012 Ultra Deep Field Campaign. *ApJ*, 768:196.

Schmidt, M. (1968). Space Distribution and Luminosity Functions of Quasi-Stellar Radio Sources. *ApJ*, 151:393.

Snaith, O. N., Gibson, B. K., Brook, C. B., Courty, S., Sánchez-Blázquez, P., Kawata, D., Knebe, A., and Sales, L. V. (2011). A comparison of galaxy group luminosity functions from semi-analytic models. *MNRAS*, 415:2798–2811.

Tempel, E., Tamm, A., and Tenjes, P. (2010). Dust-corrected surface photometry of M 31 from Spitzer far-infrared observations. *A&A*, 509:A91.

Tuffs, R. J., Popescu, C. C., Völk, H. J., Kylafis, N. D., and Dopita, M. A. (2004). Modelling the spectral energy distribution of galaxies. III. Attenuation of stellar light in spiral galaxies. *A&A*, 419:821–835.

Warren, S. J., Hambly, N. C., Dye, S., Almaini, O., Cross, N. J. G., Edge, A. C., Foucaud, S., Hewett, P. C., Hodgkin, S. T., Irwin, M. J., Jameson, R. F., Lawrence, A., Lucas, P. W., Adamson, A. J., Bandyopadhyay, R. M., Bryant, J., Collins, R. S., Davis, C. J., Dunlop, J. S., Emerson, J. P., Evans, D. W., Gonzales-Solares, E. A., Hirst, P., Jarvis, M. J., Kendall, T. R., Kerr, T. H., Leggett, S. K., Lewis, J. R., Mann, R. G., McLure, R. J., McMahon, R. G., Mortlock, D. J., Rawlings, M. G., Read, M. A., Riello, M., Simpson, C., Smith, D. J. B., Sutorius, E. T. W., Targett, T. A., and Varricatt, W. P. (2007). The United Kingdom Infrared Telescope Infrared Deep Sky Survey First Data Release. *MNRAS*, 375:213–226.

White, S. D. M. and Frenk, C. S. (1991). Galaxy formation through hierarchical clustering. *ApJ*, 379:52–79.

White, S. D. M. and Rees, M. J. (1978). Core condensation in heavy halos - A two-stage theory for galaxy formation and clustering. *MNRAS*, 183:341–358.

Wright, E. L., Eisenhardt, P. R. M., Mainzer, A. K., Ressler, M. E., Cutri, R. M., Jarrett, T., Kirkpatrick, J. D., Padgett, D., McMillan, R. S., Skrutskie, M., Stanford, S. A., Cohen, M., Walker, R. G., Mather, J. C., Leisawitz, D., Gautier, III, T. N., McLean, I., Benford, D., Lonsdale, C. J., Blain, A., Mendez, B., Irace, W. R., Duval, V., Liu, F., Royer, D., Heinrichsen, I., Howard, J., Shannon, M., Kendall, M., Walsh, A. L., Larsen, M., Cardon, J. G., Schick, S., Schwalm, M., Abid, M., Fabinsky, B., Naes, L., and Tsai, C.-W. (2010). The Wide-field Infrared Survey Explorer (WISE): Mission Description and Initial On-orbit Performance. *AJ*, 140:1868–1881.

Yang, X., Mo, H. J., and van den Bosch, F. C. (2009). Galaxy Groups in the SDSS DR4. III. The Luminosity and Stellar Mass Functions. *ApJ*, 695:900–916.

York, D. G., Adelman, J., Anderson, Jr., J. E., Anderson, S. F., Annis, J., Bahcall, N. A., Bakken, J. A., Barkhouser, R., Bastian, S., Berman, E., Boroski, W. N., Bracker, S., Briegel, C., Briggs, J. W., Brinkmann, J., Brunner, R., Burles, S., Carey, L., Carr, M. A., Castander, F. J., Chen, B., Colestock, P. L., Connolly, A. J., Crocker, J. H., Csabai, I., Czarapata, P. C., Davis, J. E., Doi, M., Dombeck, T., Eisenstein, D., Ellman, N., Elms, B. R., Evans, M. L., Fan, X., Federwitz, G. R., Fiscelli, L., Friedman, S., Frieman, J. A., Fukugita, M., Gillespie, B., Gunn, J. E., Gurbani, V. K., de Haas, E., Haldeman, M., Harris, F. H., Hayes, J., Heckman, T. M., Hennessy, G. S., Hindsley, R. B., Holm, S., Holmgren, D. J., Huang, C.-h., Hull, C., Husby, D., Ichikawa, S.-I., Ichikawa, T., Ivezić, Ž., Kent, S., Kim, R. S. J., Kinney, E., Klaene, M., Kleinman,

A. N., Kleinman, S., Knapp, G. R., Korienek, J., Kron, R. G., Kunszt, P. Z., Lamb, D. Q., Lee, B., Leger, R. F., Limmongkol, S., Lindenmeyer, C., Long, D. C., Loomis, C., Loveday, J., Lucinio, R., Lupton, R. H., MacKinnon, B., Mannery, E. J., Mantsch, P. M., Margon, B., McGehee, P., McKay, T. A., Meiksin, A., Merelli, A., Monet, D. G., Munn, J. A., Narayanan, V. K., Nash, T., Neilsen, E., Neswold, R., Newberg, H. J., Nichol, R. C., Nicinski, T., Nonino, M., Okada, N., Okamura, S., Ostriker, J. P., Owen, R., Pauls, A. G., Peoples, J., Peterson, R. L., Petravick, D., Pier, J. R., Pope, A., Pordes, R., Prosapio, A., Rechenmacher, R., Quinn, T. R., Richards, G. T., Richmond, M. W., Rivetta, C. H., Rockosi, C. M., Ruthmansdorfer, K., Sandford, D., Schlegel, D. J., Schneider, D. P., Sekiguchi, M., Sergey, G., Shimasaku, K., Siegmund, W. A., Smee, S., Smith, J. A., Snedden, S., Stone, R., Stoughton, C., Strauss, M. A., Stubbs, C., SubbaRao, M., Szalay, A. S., Szapudi, I., Szokoly, G. P., Thakar, A. R., Tremonti, C., Tucker, D. L., Uomoto, A., Vanden Berk, D., Vogeley, M. S., Waddell, P., Wang, S.-i., Watanabe, M., Weinberg, D. H., Yanny, B., Yasuda, N., and SDSS Collaboration (2000). The Sloan Digital Sky Survey: Technical Summary. *AJ*, 120:1579–1587.

Zandivarez, A., Martínez, H. J., and Merchán, M. E. (2006). On the Luminosity Function of Galaxies in Groups in the Sloan Digital Sky Survey. *ApJ*, 650:137–147.

4.8 Appendix

4.8.1 SWML and STY LF

Figures 4.5, 4.6 and 4.7, similar to Fig. 4.2, show the LF estimated in the low, middle and high richness bins respectively from UV to NIR. Filled circles represent the non-parametric SWML LF and solid lines the corresponding parametric LF. For most of the bands the fit is really close to data; however, at the faint end, data are very noisy and the parametric fit does not adjust very well. Looking at the F band, fits are not close to data perhaps for the large error bars at the bright and faint ends. From these plots, we conclude that taking the parametric LFs is enough to make comparisons between LFs. The corresponding Schechter parameters are presented in Table 4.3.

To test the LF fit, we apply the log-likelihood ratio test to the results. Table 4.2 shows the log likelihood ratio, the degrees of freedom and the empirical probability. From this table we can confirm the good fitting for most of the wavelengths; however, according to the probabilities found, *gr* bands are the worst, mainly in the low bin. Nevertheless,

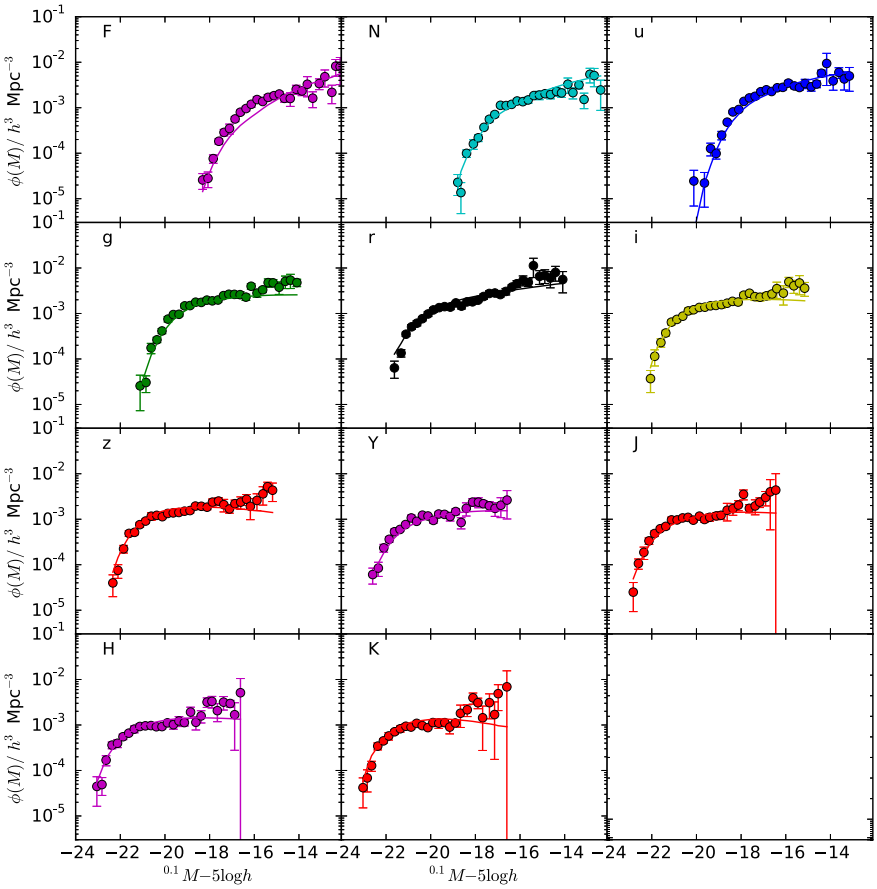

Figure 4.5: The LF estimated for groups with Nfof=2 in the 11 wavelengths from the top-left panel in the FUV band to the NIR K band in the bottom-middle panel. Filled circles present the SWML LF and the solid line the parametric LF (Schechter function).

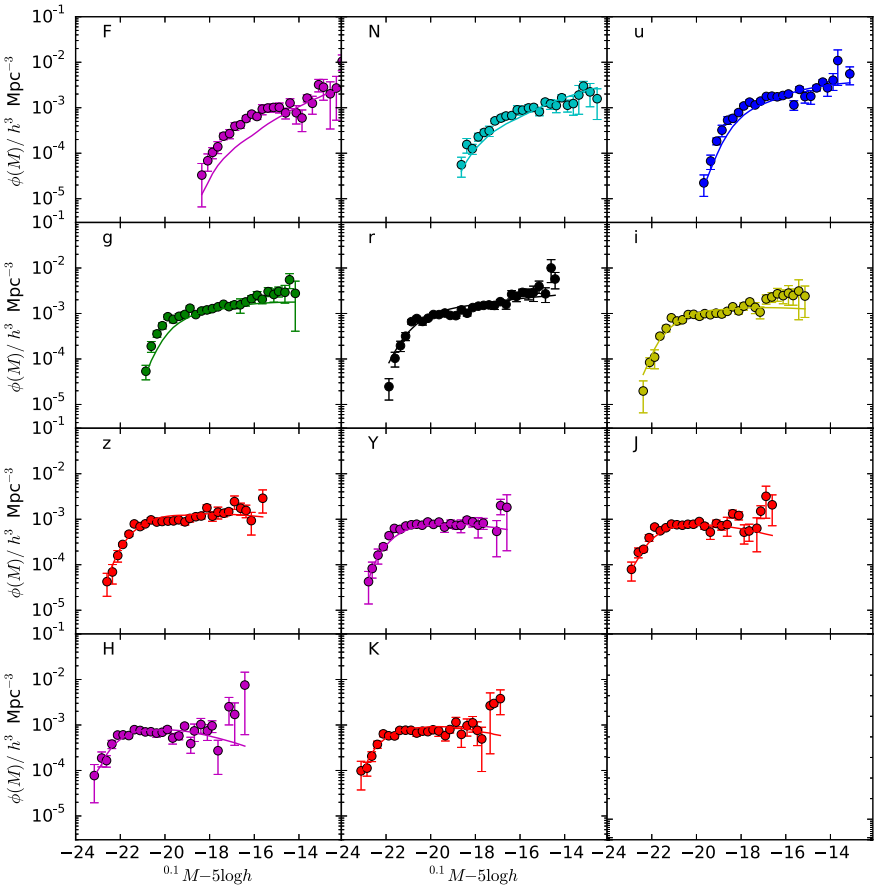

Figure 4.6: The LF estimated for groups with Nfof=3,4 in the 11 wavelengths from the top-left panel in the FUV band to the NIR K band in the bottom-middle panel. Filled circles present the SWML LF and the solid line the parametric LF (Schechter function).

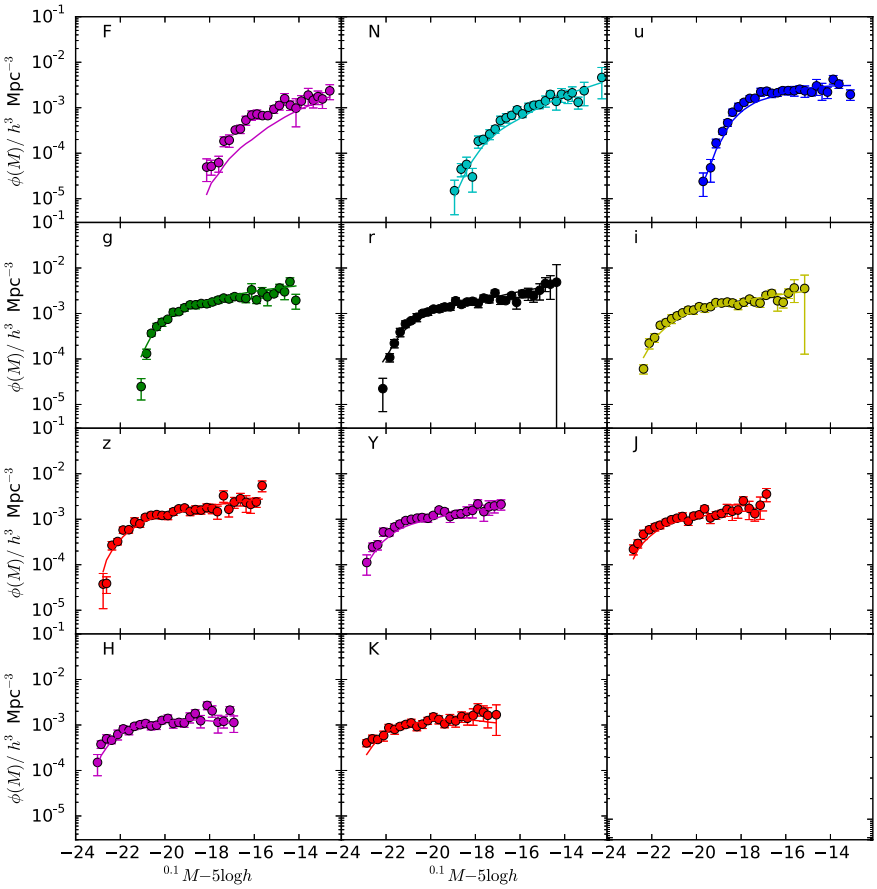

Figure 4.7: The LF estimated for groups with Nfof≥5 in the 11 wavelengths from the top-left panel in the FUV band to the NIR K band in the bottom-middle panel. Filled circles present the SWML LF and the solid line the parametric LF (Schechter function).

combining the results from the plots and the table, we can use the parametric LF to make tests using the group properties and wavelengths.

We have also estimated the LF for all the 11 wavelengths in these three mass bins. Figures 4.8, 4.9 and 4.10 show the non-parametric LF as red circles (SWML) and the parametric LF as a solid line for the mass bins. Most of the LFs are well fitted by the Schechter function; nevertheless, FUV band does not show a good fit by the Schechter function, but a different shape is observed. Contrarily to the good fit in all richness bins, the high mass bin shows a poor fit to the non-parametric LF. A systematic error with the normalization can be the reason of this bad fit; so, no accurate conclusions can be obtained from this high mass bin. However, another method, like the joint stepwise maximum likelihood (SWML) presented by Loveday et al. (2015), could be applied in a future work. In the meantime, the corresponding Schechter parameters are presented in Table 4.5.

Similar to Table 4.2, Table 4.4 show the corresponding log-likelihood ratio test for the LF in mass bins. No important discrepancies can seen between the non- and parametric LF, except for the *ur* bands in the lowest bin. Both results, the plots and this table are enough to carry on with the comparative study of the LF considering mass bins.

Table 4.2: log likelihood ratio test results applied to the SWML LF and the parametric fit for the $FNugizYJHK$ bands in the richness bins

Band	log likelihood ratio	degrees of freedom	prob	log likelihood ratio	degrees of freedom	prob	log likelihood ratio	degrees of freedom	prob
	Nfof = 2			Nfof = 3, 4			Nfof $\geq$ 5		
F	-29.76	24.0	7.44e-05	-26.92	22.0	1.74e-04	-18.32	23.0	3.55e-02
N	-23.80	26.0	5.99e-03	-26.92	22.0	1.74e-04	-22.49	25.0	8.37e-03
u	-105.52	27.0	1.94e-30	-58.22	24.0	4.16e-14	-27.12	23.0	2.49e-04
g	-31.05	26.0	8.67e-05	-53.57	26.0	8.11e-12	-23.44	27.0	1.02e-02
r	-62.16	28.0	4.21e-14	-57.75	29.0	2.81e-12	-38.64	29.0	2.88e-06
i	-27.50	25.0	4.92e-04	-36.43	26.0	2.52e-06	-21.96	27.0	2.11e-02
z	-22.90	26.0	9.61e-03	-27.67	26.0	6.87e-04	-26.11	27.0	2.49e-03
Y	-19.89	23.0	1.62e-02	-13.05	24.0	3.48e-01	-10.28	23.0	6.08e-01
J	-19.15	24.0	3.22e-02	-18.42	23.0	3.38e-02	-14.94	21.0	9.45e-02
H	-19.64	25.0	3.45e-02	-21.69	23.0	6.22e-03	-14.80	22.0	1.28e-01
K	-24.54	24.0	1.863-03	-17.95	23.0	4.22e-02	-13.41	21.0	1.77e-01

Table 4.3: Schechter parameters for the parametric LFs in richness bins

band	*alpha*	M^*	ϕ^*
	lorich		
F	-1.28 ± 0.12	-17.12 ± 0.16	2.44E-03 ± 5.50E-04
N	-1.15 ± 0.08	-17.43 ± 0.10	3.49E-03 ± 5.76E-04
u	-1.11 ± 0.10	-18.06 ± 0.14	4.78E-03 ± 1.75E-03
g	-0.97 ± 0.03	-19.46 ± 0.05	3.41E-03 ± 2.99E-04
r	-1.15 ± 0.01	-20.64 ± 0.03	2.08E-03 ± 1.76E-04
i	-0.90 ± 0.04	-20.69 ± 0.04	3.55E-03 ± 4.13E-04
z	-0.83 ± 0.05	-20.91 ± 0.06	3.79E-03 ± 4.50E-04
Y	-0.94 ± 0.10	-21.35 ± 0.13	2.34E-03 ± 4.91E-04
J	-0.90 ± 0.08	-21.50 ± 0.09	2.47E-03 ± 3.59E-04
H	-0.89 ± 0.07	-21.73 ± 0.07	2.51E-03 ± 3.51E-04
K	-0.74 ± 0.07	-21.61 ± 0.07	3.25E-03 ± 4.32E-04
	mirich		
F	-1.39 ± 0.16	-17.58 ± 0.27	6.15E-04 ± 3.26E-04
N	-1.31 ± 0.08	-17.88 ± 0.16	8.38E-04 ± 2.75E-04
u	-1.01 ± 0.08	-18.09 ± 0.12	4.47E-03 ± 1.21E-03
g	-0.93 ± 0.07	-19.56 ± 0.17	3.07E-03 ± 6.92E-04
r	-1.07 ± 0.04	-20.79 ± 0.08	1.93E-03 ± 3.04E-04
i	-0.90 ± 0.03	-20.96 ± 0.06	2.47E-03 ± 3.38E-04
z	-0.82 ± 0.03	-21.16 ± 0.06	3.23E-03 ± 4.90E-04
Y	-0.73 ± 0.04	-21.47 ± 0.07	2.25E-03 ± 3.65E-04
J	-0.64 ± 0.11	-21.60 ± 0.12	2.50E-03 ± 5.97E-04
H	-0.56 ± 0.13	-21.75 ± 0.13	3.19E-03 ± 7.38E-04
K	-0.67 ± 0.05	-21.83 ± 0.04	2.93E-03 ± 3.74E-04
	hirich		
F	-1.34 ± 0.11	-17.33 ± 0.20	6.99E-04 ± 2.57E-04
N	-1.35 ± 0.08	-17.69 ± 0.12	9.34E-04 ± 2.27E-04
u	-0.92 ± 0.06	-18.00 ± 0.06	5.50E-03 ± 1.63E-03
g	-1.10 ± 0.03	-20.06 ± 0.06	2.77E-03 ± 6.70E-04
r	-1.16 ± 0.02	-21.14 ± 0.04	1.85E-03 ± 3.86E-04
i	-1.09 ± 0.02	-21.45 ± 0.03	2.18E-03 ± 3.86E-04
z	-1.07 ± 0.02	-21.75 ± 0.03	2.25E-03 ± 3.65E-04
Y	-1.00 ± 0.02	-22.00 ± 0.00	2.28E-03 ± 3.49E-04
J	-0.90 ± 0.01	-22.00 ± 0.00	3.05E-03 ± 4.80E-04
H	-0.72 ± 0.02	-22.00 ± 0.00	4.66E-03 ± 7.15E-04
K	-0.72 ± 0.02	-22.00 ± 0.00	4.63E-03 ± 6.50E-04

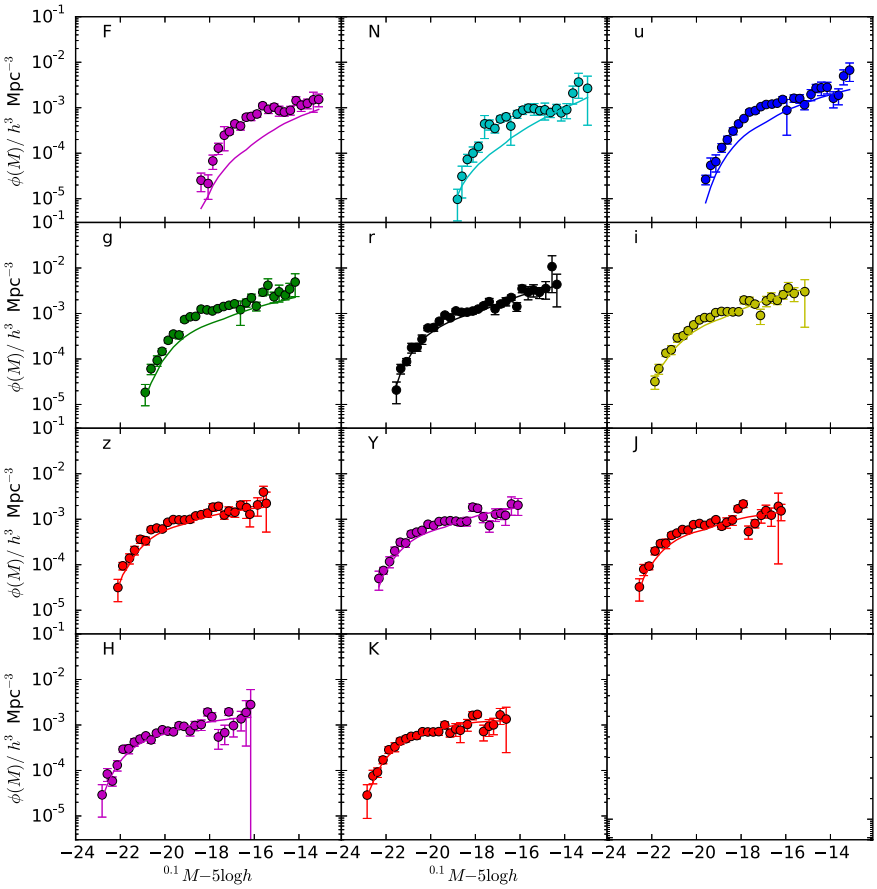

Figure 4.8: The LF estimated for groups in the bin $8 < \log M/M\odot \leq 12.06$ in the 11 wavelengths from the top-left panel in the FUV band to the NIR K band in the bottom-middle panel. Filled circles present the SWML LF and the solid line the parametric LF (Schechter function).

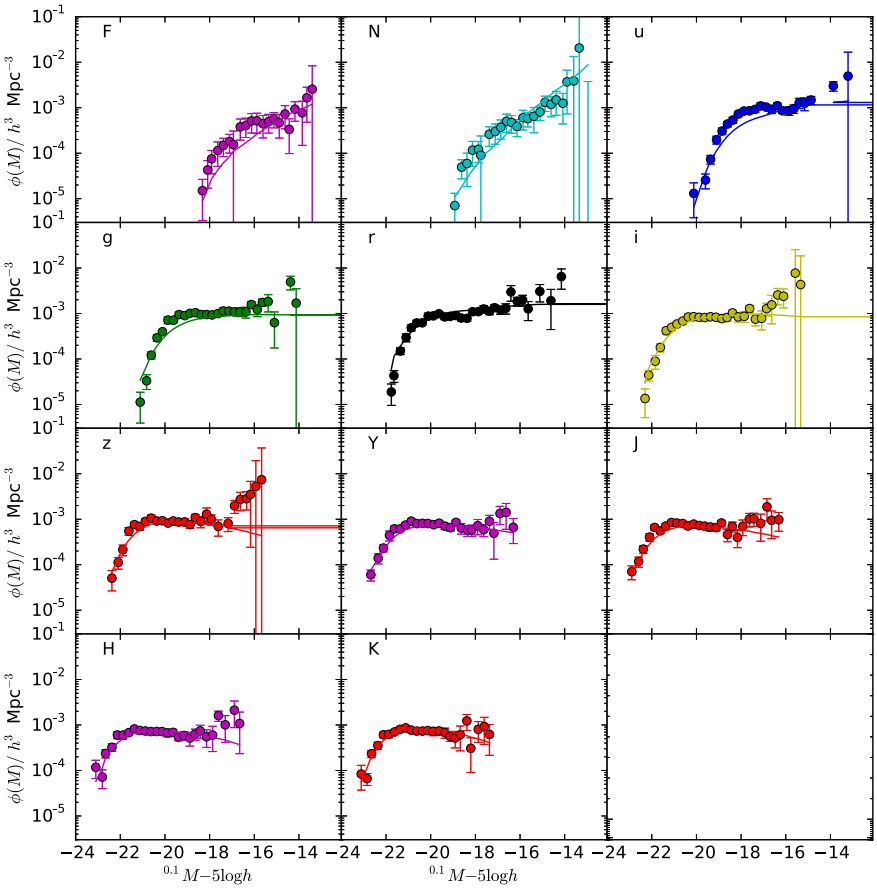

Figure 4.9: The LF estimated for groups in the bin $12.06 < \log M/M\odot \leq 12.70$ in the 11 wavelengths from the top-left panel in the FUV band to the NIR K band in the bottom-middle panel. Filled circles present the SWML LF and the solid line the parametric LF (Schechter function).

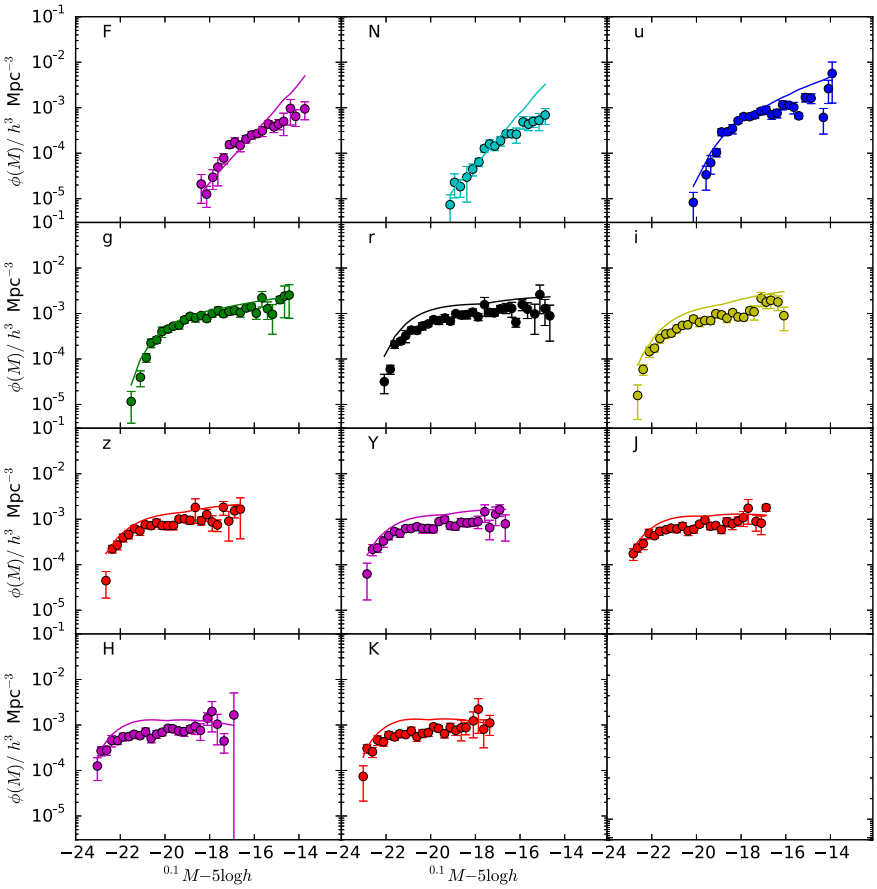

Figure 4.10: The LF estimated for groups in the bin $12.70 < \log M/M\odot \leq 16$ in the 11 wavelengths from the top-left panel in the FUV band to the NIR K band in the bottom-middle panel. Filled circles present the SWML LF and the solid line the parametric LF (Schechter function).

Table 4.4: log likelihood ratio test results applied to the SWML LF and the parametric fit for the $FNugizYJHK$ bands in the mass bins

Band	log likelihood ratio	degrees of freedom	prob	log likelihood ratio	degrees of freedom	prob	log likelihood ratio	degrees of freedom	prob
	$8<\log M/M_\odot \leq 12.06$			$12.06<\log M/M_\odot \leq 12.70$			$12.70<\log M/M_\odot \leq 16$		
F	-41.79	23	8.28E-09	-11.76	23	4.31E-01	-12.39	15	5.30E-02
N	-31.16	25	4.98E-05	-21.95	24	7.85E-03	-12.69	20	1.87E-01
u	-117.28	26	1.82E-35	-23.85	24	2.75E-03	-20.12	23	1.44E-02
g	-44.63	25	3.78E-09	-25.36	27	3.75E-03	-17.78	27	1.25E-01
r	-59.14	28	4.60E-13	-29.85	29	6.73E-04	-22.63	26	1.10E-02
i	-34.46	26	9.53E-06	-32.90	27	4.35E-05	-13.16	25	3.90E-01
z	-22.05	26	1.48E-02	-32.04	27	7.50E-05	-10.82	24	6.00E-01
Y	-23.36	24	3.62E-03	-16.61	24	9.97E-02	-14.53	22	1.43E-01
J	-26.81	24	4.80E-04	-14.33	22	1.55E-01	-19.25	21	1.13E-02
H	-27.92	24	2.41E-04	-12.90	23	3.10E-01	-16.97	21	3.67E-02
K	-24.79	24	1.60E-03	-7.72	20	7.50E-01	-17.02	21	3.59E-02

Table 4.5: Schechter parameters for the parametric LFs for mass bins

band	*alpha*	M^*	ϕ^*
	lomass		
F	-1.26 ± 0.20	-17.42 ± 0.34	0.59E-03 ± 3.20E-04
N	-1.39 ± 0.29	-18.26 ± 0.53	0.36E-03 ± 3.67E-04
u	-1.22 ± 0.08	-18.28 ± 0.08	1.25E-03 ± 2.18E-04
g	-1.21 ± 0.07	-19.58 ± 0.11	1.01E-03 ± 1.85E-04
r	-1.25 ± 0.05	-20.47 ± 0.09	1.32E-03 ± 1.76E-04
i	-1.25 ± 0.06	-20.86 ± 0.09	1.21E-03 ± 2.24E-04
z	-1.07 ± 0.04	-20.88 ± 0.06	1.63E-03 ± 2.37E-04
Y	-1.10 ± 0.04	-21.28 ± 0.06	1.50E-03 ± 2.19E-04
J	-1.06 ± 0.04	-21.46 ± 0.06	1.38E-03 ± 2.14E-04
H	-0.99 ± 0.06	-21.58 ± 0.08	1.87E-03 ± 4.44E-04
K	-0.93 ± 0.05	-21.53 ± 0.06	2.16E-03 ± 2.87E-04
	mimass		
F	-1.33 ± 0.30	-17.45 ± 0.25	6.37E-04 ± 3.23E-04
N	-1.84 ± 0.40	-18.57 ± 0.49	2.41E-04 ± 2.91E-04
u	-0.03 ± 0.11	-18.47 ± 0.15	1.47E-03 ± 4.26E-04
g	-0.91 ± 0.07	-19.73 ± 0.11	1.66E-03 ± 3.09E-04
r	-0.95 ± 0.02	-20.60 ± 0.03	2.67E-03 ± 2.61E-04
i	-0.82 ± 0.06	-20.86 ± 0.08	2.54E-03 ± 3.50E-04
z	-0.62 ± 0.05	-20.95 ± 0.04	3.34E-03 ± 2.28E-04
Y	-0.67 ± 0.03	-21.35 ± 0.05	2.88E-03 ± 2.67E-04
J	-0.63 ± 0.02	-21.49 ± 0.03	2.85E-03 ± 2.38E-04
H	-0.56 ± 0.07	-21.66 ± 0.07	3.47E-03 ± 3.72E-04
K	-0.43 ± 0.06	-21.53 ± 0.05	4.57E-03 ± 3.48E-04
	himass		
F	-2.24 ± 0.08	-19.78 ± 0.64	1.13E-05 ± 1.53E-05
N	-2.34 ± 0.12	-20.78 ± 0.99	5.00E-06 ± 1.37E-05
u	-1.43 ± 0.09	-19.05 ± 0.16	9.61E-04 ± 3.48E-04
g	-1.14 ± 0.03	-20.30 ± 0.04	1.28E-03 ± 1.94E-04
r	-0.98 ± 0.08	-21.05 ± 0.10	3.30E-03 ± 7.88E-04
i	-1.09 ± 0.02	-21.53 ± 0.07	2.53E-03 ± 2.52E-04
z	-1.01 ± 0.05	-21.83 ± 0.08	2.59E-03 ± 3.62E-04
Y	-0.92 ± 0.01	-22.00 ± 0.00	3.22E-03 ± 2.30E-04
J	-0.81 ± 0.02	-22.00 ± 0.00	3.91E-03 ± 3.21E-04
H	-0.66 ± 0.02	-22.00 ± 0.00	5.99E-03 ± 5.08E-04
K	-0.64 ± 0.02	-22.00 ± 0.00	6.24E-03 ± 5.35E-04

Chapter 5

Conclusion

In this thesis I have made a deep analysis about the luminosity function for galaxies in two different environments, groups and isolated; where I established the most accurate values of the Schechter parameter fits associated mainly with different group properties. These parameters will help to better constrain evolution models and thereby improving our understanding of the intrinsic and external physical properties of galaxies. In the chapters presented in this thesis, I cover as much as possible, the ideas presented in the introduction; to test (or confirm) any relationship and difference between the LF and the galaxy samples, based on two of the most homogeneous and spectroscopically complete samples available: the GAMA (Driver et al., 2009) and UNAM-KIAS (Hernández-Toledo et al., 2010).

In Section 1.3.2 I described the previous studies on the LF dependence with environment, where I pointed out that one of the main problems is the sample completeness at low luminosity or equivalently mass. Chapter 2 presents the galaxy LF for the GAMA group catalogue (G^3Cv6) in the r-band. For the first time the LF analysis was carried out using a complete groups sample with group mass down to 10^{10} $M_\odot$ (previous works are made only down to 10^{12} $M_\odot$; e.g. Yang et al. 2009).

I estimated the LF for galaxies in groups and ungrouped galaxies (those that were excluded from the FoF grouping algorithm) and I found galaxies tend to be brighter in groups. At the faint-end, ungrouped galaxies dominate over the grouped galaxies, one explanation could be because these galaxies have not suffered any external perturbation to merge and form brighter systems as can occur in dense regions. This result is in agreement with previous works (e.g. Croton et al. 2005, McNaught-Roberts et al. 2014).

In order to find the LF dependence with group mass, the G^3Cv6 was divided in three mass bins. I found the LF slope at the faint end becomes shallower when the mass bin increases, possibly because massive groups contain predominantly massive galaxies and

in consequence the most luminous too. I cannot talk about a correlation between α and group mass, but do infer a negative tendency between M^* with respect to mass, resulting in the expected result, that highly luminous galaxies are located in massive groups, with likely high velocity dispersion. With this result, I am extending this possible correlation three orders of magnitude to lower mass than that found by Robotham et al. (2010), who used groups with mass higher than 10^{13} $M_{\odot}$.

As described in Section 1.3.1, separation by colour and morphology are important to distinguish galaxies by their evolutionary stage, mainly related with the star formation rate. In this sense, this catalogue was also separated by colour and morphology and the corresponding LF is estimated, separated again in the same group mass bins. Red galaxies dominate over the blue galaxies at the bright-end and vice versa at the faint-end, for all mass bins. However, for red galaxies, the faint-end slope (α) becomes flatter as the mass increases similar to the combined sample; also,the density of massive red galaxies is higher than in the other bins. Due to the relationship between colour and morphology, the LFs divided by morphology follow the same tendencies found for colour. These results are in agreement with previous works (e.g. Blanton et al. 2001, Baldry et al. 2004) at masses $> 10^{13}$ $M_{\odot}$. More specifically, Robotham et al. (2010) report α becomes steeper as a function of group mass either for blue or red galaxies. In this work red galaxies confirm this tendency to lower mass groups ($> 10^{8}$ $M_{\odot}$) and disagree with the blue population. This discrepancy is likely due to low luminosity limits. The amount of low mass and faint galaxies is higher than in previous works. From this work, α becomes flatter as a function of group mass for blue galaxies. This clearly means low mass groups contain more fainter (and blue) galaxies than massive ones. These systems are still forming stars and possibly they have not had time to produce galaxy mergers. As the group mass increases, these faint galaxies are less likely because they have merged and the star formation rate decreased moving the galaxies to the red sequence. On the other hand M^* agree with Robotham et al. (2010) for both populations when extended to lower group mass.

Following the questions presented in section 1.1, I tested the mock catalogues, based on the Millennium Simulation (Springel et al., 2005), to reproduce the LF from observations. The mock LF parameters (α and M^*) agree with observations within one error bar in the high mass bin, meaning that the mock catalogues considered are partialy reliable at high masses but with some unsolved issues for the low mass regime. Unfortunately, at present, there is still no information from these mock catalogues to test the LF according to colour, but this will be an important analysis once the new data come out, in order to check how

well the models reproduce the star formation rate, mainly at low group mass limits.

Following a similar analysis made by Robotham et al. (2010) on the LF dependence with the group multiplicity, I compared the LF with the group richness to identify any possible correlation. First of all, there is no clear sign that group mass correlates with richness; though as expected, effects due to large scale structure can be seen on the lack of rich groups at low mass. However, we can identify massive groups with only 2 or 3 members. Looking at the cumulative magnitude distribution, magnitude distributions for the middle and high richness groups are statistically very similar, meanwhile the low richness distribution is clearly different. This result is reflected in the shape of the LF for middle and high richness bins which are very similar, and looking at the Schechter parameters, the faint end slope α agrees within one sigma. Our results are consistent with those reported by Marinoni et al. (2002) where galaxies are brighter in higher richness groups; also similar to the density dependence as presented by McNaught-Roberts et al. (2014).

I also looked at colour and morphology, and group richness. In this context, spiral and elliptical galaxy LFs do not change their shape with richness, meaning the ratio between these galaxies is constant, independent of the richness. Bright galaxies are mainly ellipticals as expected, and since central galaxies are mostly the brightest galaxy in the group, it follows that the central galaxies are mainly ellipticals, but not necessarily red. There are brighter galaxies in groups with more members or high densities, as other works have shown (e.g. Croton et al. 2005). The parameter α tends to be steeper as the richness increases in simulations; however this is not clear with observational data, where the large error bars do not allow one to confirm or deny this tendency. Blue galaxies dominate the LF faint-end for all richness bins as expected; and the bright-end is also dominated by blue galaxies at all richness (according to the M^*). This agrees with the LF for central galaxies, where the bright end is not dominated either by blue or red galaxies. α also becomes more negative at higher densities for the red population and an apparent constant value for blue population at all richness. Meanwhile, M^* becomes brighter as density increases for red and blue galaxies using the GAMA data.

I found a large discrepancy between the results presented by Yang et al. (2009) (using a SDSS based group catalogue) mainly for the central galaxy LF at the faint-end. Their population of central galaxies is one order of magnitude higher than what I found at the faint-end, in spite of the total LF being the same within one error bar. A possible reason for this difference could be the separation criteria between the central and satellite galaxies

they used based on mass and not luminosity. However, the mock catalogues reproduced our results. Nevertheless, a more specific study about central and satellite galaxies should be done in a future work to clarify this difference.

As described in Section 1.3.3, the LF evolution with cosmic time has been studied carefully using the recent large galaxy samples to understand the star formation process at different stages of the universe. Under this motivation, the LF evolution over redshift was characterized along with its dependence on group mass. Galaxies in massive groups are brighter than the rest, since groups can be dominated by a very bright galaxy in the central region. To try and to quantify the change of M^* according to the mass and redshift, I calculated the two- and one-σ likelihood considering the M^* and α parameters. 1-dimensioned curves show clearly an increment of M^* with higher z for high and middle bins (of mass and velocity dispersion). Evolution is presented in the same way for all the mass bins, so not differences in evolution ar shown for different mass bins.

In conclusion, in the first paper, I extended the LF studies carried out by previous authors, between the LF and the group properties, for low mass groups down to 10^8 $M_\odot$. I also found some discrepancies with previous works that need to be investigated further with additional data to minimise the uncertainties. This is the first time that the LF has been studied with respect to all of the group properties mentioned using the same sample, so the possible systematic errors cancel out when comparing between two more group properties.

Motivated by studying the dependence of the LF with the environment, in Chapter 3 I analysed the LF for isolated galaxies separated by morphology in the *ugriz* bands. Additionally, I also studied the stellar mass function and the gas-to-stellar mass ratio, taking advantage of the isolated galaxies sample UNAM-KIAS. This sample was well characterized by I and other collaborators in a previous work to this thesis.

The first analysis was the estimation of the galaxy LF in the 5 bands. There was no surprise the fact that M^* is brighter from blue to red bands for isolated galaxies, since this is a natural consequence in observations. I found an unclear dip presented at middle magnitudes in the LF; this feature had also been observed by Miles et al. (2004) for galaxies in groups. The most plausible explanation is the lack of galaxies at these magnitudes due to recent merger activity. This could also explain the large number of galaxies with clear signs of distortion in the sample. This feature has also been reported using the ALFALFA (Haynes et al., 2011) and SDSS (York et al., 2000) data. Some studies have found luminous isolated galaxies show an excess of dwarf companions $\sim$5 magnitudes fainter, causing

signs of distortions in the host galaxy (e.g. Reda et al. 2004, Smith et al. 2004). However, the final results and a deeper analysis is required to explain this anomalous feature.

In general I find the LF for isolated galaxies is ∼1 mag fainter than the global SDSS LF, meaning the lack of very bright isolated galaxies or in other words, massive isolated galaxies, compared with galaxies at higher densities as found in Chapter 2. In terms of morphology, the spiral galaxy LF dominates over the elliptical LF for all bands. I found, at the bright end of the LF, both populations have similar M^*, contray to Sulentic et al. (2006), using the AMIGA sample (Verdes-Montenegro et al., 2005), who finds spiral galaxies are brighter than ellipticals. This could be due to different classification methods applied. When the sample is divided in 4 morphology bins, there is no evidence of dependence with the characteristic magnitude, only the very late type galaxies are fainter by more than 1 mag. This result does not agree with the AMIGA studies and also the LFs are completely different to those they present. Presumably these differences are the result of the selection criteria and the correction applied to the magnitudes.

In order to test my results with other samples in similar environments, I took a couple of GAMA subsasmples. Due to the way every sample is selected, the results can vary. Based on the voids-GAMA sample, I found the LF shape at the bright-end is the same compared with my results. Only slight differences of 0.5 mag at the bright-end are found when comparing with the Croton et al. (2004) voids samples, meanwhile the shape remains the same. Taking the ungrouped GAMA galaxies sample, α is steeper than mine, maybe because that sample contains galaxies not associated with groups rather than completely isolated. In conclusion, my results are in agreement with other studies made at low densities but not with the most similar sample (AMIGA). As described in Section 1.2.2, the UNAM-KIAS sample presents advantages over other samples like AMIGA. Then the results found here are more reliable and can be taken with more confidence. A similar test (like that applied to galaxies in groups) of the LF based on mass must be studied for these galaxies in order to check their evolution stage.

Looking at the stellar MF, spiral galaxies dominate at low mass but at higher mass, elliptical and spiral galaxies have the same characteristic mass; this is unclear when we look at the results divided by colour, where red galaxies completely dominate the massive range, meaning a red population of disky galaxies. I found the characteristic mass for the UNAM-KIAS catalogue to be $\log M\ [M_\odot] \sim 11$. This is in agreement with the values determined for galaxies in the field to be $10.6 \leq \log M\ [M_\odot] \leq 11$. When we divided the sample in passive and active galaxies, passive galaxies dominate at high masses while active

galaxies dominate at low masses. Combining all this information, we can infer galaxies with $\log M\ [M_{\odot}] \sim$11 stop forming stars, with only a few of them being blue, maybe in the last star formation stage. In addition, galaxies with disc are still the $\sim$50% of the sample at this mass bin. This breaks the idea that galaxies need a bulge to turn off completely. This suggests that morphology can the be last transition of isolated galaxies to become in a passive red galaxy.

In last part of Chapter 3 the gas-to-stellar mass ratio (M_{gas}/M_s) is presented for isolated galaxies and the characteristic tendency is presented. This agrees with other works based on disk type galaxies. This study, however, requires further analysis to try to estimate the baryonic mass LF and possibly the estimation of the halo mass based on this ratio (M_{gas}/M_s) as described by Rodríguez-Puebla et al. (2011).

Finally we present the first attempt to study the multi-wavelength LF in the $FNugriz\ YJHK$ bands for the G^3Cv6 catalogue based on the first time complete Panchromatic GAMA survey (M_r=19.8) covering 21 bands. The first estimation of the LF (based on 11 bands) is in agreement with previous works based on multi-wavelength studies. This is the first work estimating the group LF in 11 bands where we investigate the effects of group environment on star-formation processes. As expected, we find a good correlation between the Schechter parameters α and $M^{\star}$ with respect to the wavelengths when we considere the total galaxy group LF and the LF in three different richness and mass bins. However, further analysis is necessary to investigate the LF in each band in order to determine the exact source of the differences found in this paper and also to take advantage of the whole information accessible from the GAMA survey. These kinds of studies can give us valuable information about the star formation rate in these galaxies and groups.

Groups have been studied in detail by many authors and there have been many attempts to have a reliable LF. Based on this information, evolution models have tried to predict and match this function, coming from observations. Environment effects are crucial to have a better picture of the galaxy evolution, nevertheless, isolated galaxies still need to be explored. New, larger and complete catalogues are needed to have confident results, not only of the LF, but also about the intrinsic physical processes happening inside these structures. In this thesis I have improved the LF analysis based on a more confident sample, but there remains some open questions about the nature of these systems. Observations in multi-wavelengths are crucial to understand the total baryonic content and the stellar activity for example. With everyday, galaxy surveys are larger and more information can be extracted to confirm or deny ideas behind our knowledge about the

Universe's evolution. This thesis utilised new information given by two of these surveys (GAMA and SDSS), to explore groups at lower mass than previous studies and also to explore a new sample of isolated galaxies.